ZfK – 592

PROCEEDINGS

of the XV-th International Symposium on Nuclear Physics

– Nuclear Fission –

organized by
Technical University of Dresden
November 11–15, 1985 in Gaussig (GDR)

edited by
D. Seeliger, K. Seidel and H. Märten

April 1986

Postanschrift: Akademie der Wissenschaften der DDR
Zentralinstitut für Kernforschung Rossendorf
Postschließfach 19
Dresden
8051
Deutsche Demokratische Republik

Diese Publikation wurde in der Abteilung Information des Zentralinstitutes für Kernforschung hergestellt

III-12-12 J 1432/

AKADEMIE DER WISSENSCHAFTEN DER DDR

ZENTRALINSTITUT FÜR KERNFORSCHUNG

ROSSENDORF BEI DRESDEN

ZfK - 592

PROCEEDINGS

of the XV-th International Symposium

on Nuclear Physics

- Nuclear Fission -

organized by

Technical University of Dresden

November 11 - 15, 1985 in Gaussig (GDR)

edited by

D. Seeliger, K. Seidel and H. Märten

April 1986

Editorial Note

In preparing this material for press, the editors have compiled and paginated the original manuscripts as submitted by the authors. Some of the papers which didn't meet the requirements stated in the 2nd announcement have been accepted after re-typing and editor proof.
Authors are themselves responsible for obtaining necessary permissions to reproduce copyright material from other sources.

Dear Colleagues!

On the behalf of the Rector of the Technical University Dresden and as the chairman of the organizing commitee I like to welcome you at the

XVth International Symposium on Nuclear Physics

in Gaussig.

About 15 years have been passed since the first small symposium on neutron induced reactions held here in the same room. In this time every year scientists from many countries met here for small symposia on topics like

- neutron induced reactions,
- nuclear reaction mechanisms,
- nuclear theory,
- neutron generators etc.

In this year our meeting is mainly dealing with nuclear fission. It is one of the most extensively studied nuclear processes which remains an interisting field for investigations.
Nuclear fission as a strongly collective process plays a principal role for the understanding of the dynamics in nuclear many-particle systems.
The study of fission dynamics are also stimulated by investigations of heavy ion collisions.
Nuclear fission is of practical importance for nuclear energetics specifically.
Moreover, the prompt neutron spectrum and the average number of neutrons from the spontaneous fission of Cf-252 and the U-235 fission cross section are some of the admitted nuclear standards widely used as reference data in nuclear measurements.
Organizing a meeting on nuclear fission in this time we had also in mind that the IAEA stopped the organization of the well-established International Symposia on Physics and Chemistry of Fission several years ago. On the other hand, many scientists, especially at the INDC, expressed the real need of meetings on nuclear fission.
Last not least, it seems that the work carried out at the Technical University Dresden on absolute measurements of fast-fission cross-sections, fission neutron spectra, and fissioning resonances could be a justification for a meeting on nuclear fission here.
We are very glad that so much distinguished scientists from many countries followed our invitation to Gaussig.
I hope that you will have a pleasant stay and many interesting scientific and cultural impressions here. With your help the XVth Nuclear Physics Symposium is certain to be a success!

D. Seeliger

LIST OF PARTICIPANTS

Albert, D.	ZfK Rossendorf	GDR
Klenkov, D.V.	INRNE Sofia	BULGARIA
Klfruth, T.	TU Dresden	GDR
Flambaum, V.V.	INP Novosibirsk	USSR
Gippner, P.	ZfK Rossendorf	GDR
Gohs, U.	TU Dresden	GDR
Hehl, T.	TU Dresden	GDR
Herbach, C.U.	TU Dresden	GDR
Hermsdorf, D.	TU Dresden	GDR
Ignatiuk, A.V.	PEI Obninsk	USSR
Jacobs, E.	NPL Genf	BELGIUM
Janeva, W.	INRNE Sofia	BULGARIA
Kalka, H.	TU Dresden	GDR
Karacsony	KU Debrecen	HUNGARIA
Knitter, H.-H.	CEEN Geel	BELGIUM
Kornman, A.	INP Warsaw	POLAND
Kotte, R.	ZfK Rossendorf	GDR
Lajtai, A.	CRIP Budapest	HUNGARIA
Lemmer, M.	IAEA Vienna	AUSTRIA
Mädler, P.	JINR Dubna	USSR
Märten, H.	TU Dresden	GDR
Meister, A.	TU Dresden	GDR
Mendez, R.L.	INR Havana	CUBA
Merla, K.	TU Dresden	GDR
Nagy, S.	KU Debrecen	HUNGARIA
Nguyen Hoai Chan	JINR Dubna	USSR
Neubert, W.	ZfK Rossendorf	GDR
Ortlepp, H.B.	ZfK Rossendorf	GDR
Pausch, G.	TU Dresden	GDR
Piessens, M.	NPL Genf	BELGIUM
Pilz, W.	ZfK Rossendorf	GDR
Pilz, W.	TU Dresden	GDR
Raics, P.	KU Debrecen	HUNGARIA
Richter, D.	TU Dresden	GDR
Seeliger, D.	TU Dresden	GDR
Seidel, K.	TU Dresden	GDR
Shpakov, V.I.	RI Leningrad	USSR
Soldatov, A.S.	PEI Obninsk	USSR
Stavisski, J.J.	INR Moskau	USSR
Theobald, J.	TH Darmstadt	FRG
Töpfer, M.	TU Dresden	GDR
Trzcinski, A.	INP Warsaw	POLAND
Unholzer, S.	TU Dresden	GDR
Wagemans, C.	CEN MOL	BELGIUM
Wasson, O.	NBS Gaithersburg	USA
Zaika, N.I.	INR Kiev	USSR

TABLE OF CONTENS

Page

I. SPONTANEOUS FISSION OF CF-252

On the Mechanism of Fission Neutron Emission 1
H. Märten, D. Richter, D. Seeliger, W. Neubert

Simultaneous Investigation of Fission Fragments and Neutrons in $^{252}Cf(S,F)$ 18
.. Budtz-Jørgensen and H.-H. Knitter

Experimental Study of Correlations of Energy and Angular Distributions of Cf-252 Spontaneous Fission Neutrons 25
O.I. Batenkov, A.B. Blinov, M.V. Blinov, S.N. Smirnov

Study of the Relationships between the Characteristics of Mass, Energy, and Neutron Multiplicity Distributions at the ^{252}Cf Spontaneous Fission 29
I.D. Alkhazov, V.D. Dmitriev, A.V. Kuznetsov, S.S. Kovalenko, K.A. Petrzhak, B.F. Petrov, L.Z. Malkin, V.I. Shpacov

Low Mass Fragments from ^{252}Cf Spontaneous Fission 35
H.-G. Ortlepp, R. Kotte, F. Stary

Experimental Arrangement for the Measurement of Correlations between Fission Products and Neutrons 39
H. Märten, D. Richter, D. Seeliger, W.D. Fromm, W. Neubert

II. NEUTRON-INDUCED FISSION

Multiparameter Measurements on Charged Particle Associated Fission of ^{236}U 43
J.P. Theobald

Triton and Alpha Emission in the Ternary Fission of the Actinides 53
C. Wagemans, P. D'Hondt, P. Schillebeeckx, R. Brissot

Resonance Parameters of Pu-239 in the Resolved and Unresolved Resonance Region 58
N. Janeva

Measurement of the Mean-Square Charge Radii of Neutron Resonance States in Uranium Nuclei 65
A. Meister, S. Mittag, L.B. Pikelner, W. Pilz, D. Seeliger, K. Seidel

Mean-Square Radii of the ^{236}U Nucleus in Excited States with Different Fission Widths 70
A. Meister, S. Mittag, L.B. Pikelner, W. Pilz, D. Seeliger, K. Seidel

Temperature Shift of Neutron Resonances 74
V.K. Ignatovich, A. Meister, S. Mittag, W. Pilz, D. Seeliger, K. Seidel

Сечение деления ^{243}Am в области порога (n,n'f). 78
А.А. Говердовский, Б.Д. Кузьминов, В.Ф. Митрофанов, А.И. Сергачёв

III. PHOTON-INDUCED FISSION

Экспериментальное излучение подбарьерной структуры сечения фотоделения ^{232}Th 82
A.C. Солдатов, З.А. Александрова, Г.Н. Смиренкин, М.З. Тараско

Выход и сечение фотоделения ^{231}Pa 88
A.C. Солдатов, В.Е. Рудников, З.А. Александрова, Г.Н. Смиренкин

Photon Induced Fission of ^{232}Th with 12 and 20 MeV Bremsstrahlung 92
M. Piessens, E. Jacobs, D.De Frenne, A.De Clercq, M. Verboven, G.De Smet

Emission of ^{3}H and ^{4}He Particles in the Photofission of Actinides 96
M. Verboven, E. Jacobs, P.D'Hondt, A.De Clercq, D.De Frenne, M. Piessens and G.De Smet

IV. CHARGED-PARTICLE-INDUCED FISSION, HEAVY-ION REACTIONS THEORY

Odd Harmonics in the Angular Distribution of Fission Fragments 100
V.V. Flambaum

Исследования по физике деления на мезонной фабрике ИЯИ АН СССР 108
Ю.Я. Стависский

Linear Momentum Transfer to Residual Nuclei Leading to Fission 114
L.A. Androuenko, A.A. Kotov, L.A. Vaishnene, W. Neubert

Catapult Mechanism for Fast Particle Emission after Scission 117
P. Mädler

Polar Particle Emission in Spontaneous Fission 121
B. Milek, R. Reif, J. Revai

Fragment Mass Distributions in Heavy-Ion Reactions Leading to Composite Systems with Z = 108 122
P. Gippner, K.D. Schilling, W. Seidel, F. Stary, E. Will, H. Sodan, S.M. Lukyanov, G.G. Chubarian, V.S. Salamatin and Yu.E. Penionzhkevich

Alpha-Fragment Correlation Measurements in the Reaction ^{12}C (85 MeV) + ^{232}Th 127
Nguyen Hoai Chau, W. Agustyniak, C. Borcea and M. Lewitowicz

V. MEASUREMENTS OF FISSION CROSS SECTIONS

Recent Fission Cross Section Standards Measurements 130
O.A. Wasson

Absolute Measurements of the ^{235}U Induced Fission Cross Section at the Neutron Energy of 1,88 MeV 140
I.D. Alkhazov, V.D. Dmitriev, V.A. Kalinin, S.S. Kovalenko, V.I. Kutuzov, V.N. Kuzmin, Yu.A. Nemilov, B.F. Petrov, L.M. Solin, V.I. Shpakov

Application of Magnet Analysis in the Time Correlation Assotiated Particle Method 146
V.A. Kalinin, S.S. Kovalenko, V.N. Kuzmin, Yu.A. Nemilov, L.M. Solin, V.I. Shpakov, A.V. Fomichev

Absolute Fission Cross-Section Measurement of Pu-239 at 4.8, 8.65 and 18.8 MeV and of U-235 at 4.45 and 18.8 MeV Neutron Energy 152
C.M. Herbach, K. Merla, G. Musiol, H.G. Ortlepp, G. Pausch
I.L. Alkhazov, L.V. Drapchinsky, E.A. Ganza, S.S. Kovalenko, O.I. Kostochkin, S.M. Solovjev, V.I. Shpakov

Identification of Associated Particles in the TCAPM Fission Cross Section Measurements at the IANDEM Accelerator of the CINR Rossendorf 156
H.G. Ortlepp, C.M. Herbach, K. Merla, G. Musiol, G. Pausch

CAMAC Data Acquisition System and Data Analysis in TCAPM Fission Cross-Section Measurements at the Tandem Accelerator of the CINR Rossendorf 160
G. Pausch, W.D. Fromm, C.M. Herbach, K. Merla, G. Musiol, H.G. Ortlepp

^{6}Li Glass Spectrometer for Low Energy Fission Neutrons 164
A. Lajtai, J. Kecskemeti

Emploing of Gadolinium Loaded Large Liquid Scintillation Counters for Research of Neutron Multiplicity Distribution in Separate Channels of Reactions 168
I.D. Alkhazov, A.V. Daniel, V.D. Dmitriev, V.N. Dushin, S.S. Kovalenko, K.A. Petrzhak, A.V. Kuznetsov, L.Z. Malkin B.F. Petrov, V.I. Shpakov

VI. NEUTRON INTERACTIONS WITH NUCLEI

Изомерное отношение и сечение реакции $^{237}Np(n,2n)$ 173
А.В. Игнатюк, Н.В. Корнилов, В.М. Маслов, А.Б. Пащенко

Measurement of the Total Proton Emission Cross Section of Neutron Induced Reaction on ^{60}Ni at 18.5 MeV 181
A. Korman, B. Marianski, J. Rondio, K. Czerski

Two Target DSAM Following the (n,n'γ) Reaction with Fast Reactor Neutrons 184
M. Georgieva, D. Elenkov, G. Toumbev

Low Background Telescopic System for Study of (n,α) Reactions on Light Nuclei 188
A. Trzcinski, S. Burzynski, K.M. Rusek, I.M. Turkiewicz

ON THE MECHANISM OF FISSION NEUTRON EMISSION

H. Märten, D. Richter, D. Seeliger
Technische Universität Dresden, Sektion Physik, DDR-8027, Dresden, Mommsenstraße 13

W. Neubert
Zentralinstitut für Kernforschung Rossendorf, DDR-8051 Dresden, PF 19

Abstract

This review represents the present knowledge of the mechanism of prompt fission neutron emission. Starting with a brief fission process characterization related with neutron emission, possible emission mechanisms are discussed. It is emphasized that the experimental study of special mechanisms, i.e. scission neutron emission processes, requires a sufficiently correct description of emission probabilities on the base of the main mechanism, i.e. the evaporation from fully accelerated fragments.
Adequate statistical-model approaches have to account for the complexity of nuclear fission reflected by an intricate fragment distribution.
The present picture of scission neutron emission is not clarified neither experimentally nor theoretically. Deduced data are contradictory and depend on the used analysis procedures often involving rough discriptions of evaporated-neutron distributions.
The contribution of two secondary mechanisms of fission neutron emission, i.e. the neutron evaporation during fragment acceleration and neutron emission due to the decay of ^{5}He after ternary fission, is estimated.
We summarize the recent progress of the theoretical description of fission neutron spectra in the framework of statistical models considering the standard spectrum of ^{252}Cf(sf) neutrons especially.
The main experimental basis for the study of fission neutron emission is the accurate measurement of emission probabilities as a function of emission energy and angle (at least) as well as fragment parameters (mass number ratio and kinetic energy).
The present status is evaluated.

1. Introduction

Fission neutron emission was found and roughly explained in 1939, i.e. a short time after the discovery of nuclear fission (Ref. 1 and references therein). Stimulated by urgent nuclear data needs for practical purposes, prompt neutron spectra from different fission reactions have been measured. They could be described assuming neutron evaporation from fully accelerated fragments on the base of rather simple statistical models[2-4]. Early measurements of angular correlations between fission fragments and promptly emitted neutrons[5-7] corroborated the stated supposition as the main emission mechanism.
In connection with Bohr's and Wheeler's hypothesis that "hydrodynamical" distortions appearing at scission might cause a special emission component, i.e. the so-called scission neutrons, several groups carried out more detailed investigations of the mechanism of fission neutron emission on the base of different methods of angular-correlation measurements[8-20]. Deduced characteristics of scission neutrons are contradictory and appear to be dependent on the description of the main component (see chapter 3). Scission neutron emission was studied in the framework of different models[21-25] including diabatic effects close to scission. This illustrates the connection with fission dynamics and, therefore, the difficulty of such investigations.

Inspite of the recent progress in the theoretical description of prompt fission neutron emission on the base of complex statistical models (cf. chapter 4) the full picture of fission neutron emission is not clear. We try to show contradictions of experimental and theoretical results and to give outlooks for further studies. We emphasize the requirements to be met in experiment and theory.

As recommended by an IAEA Consultants' Meeting[26] concerning the standard neutron spectrum from ^{252}Cf(sf) the investigation of neutron emission in fission by the measurement of multiple-differential emission probabilities is very important for the clarification of open fundamental problems of the mechanism as well as for practical purposes like the development of models.

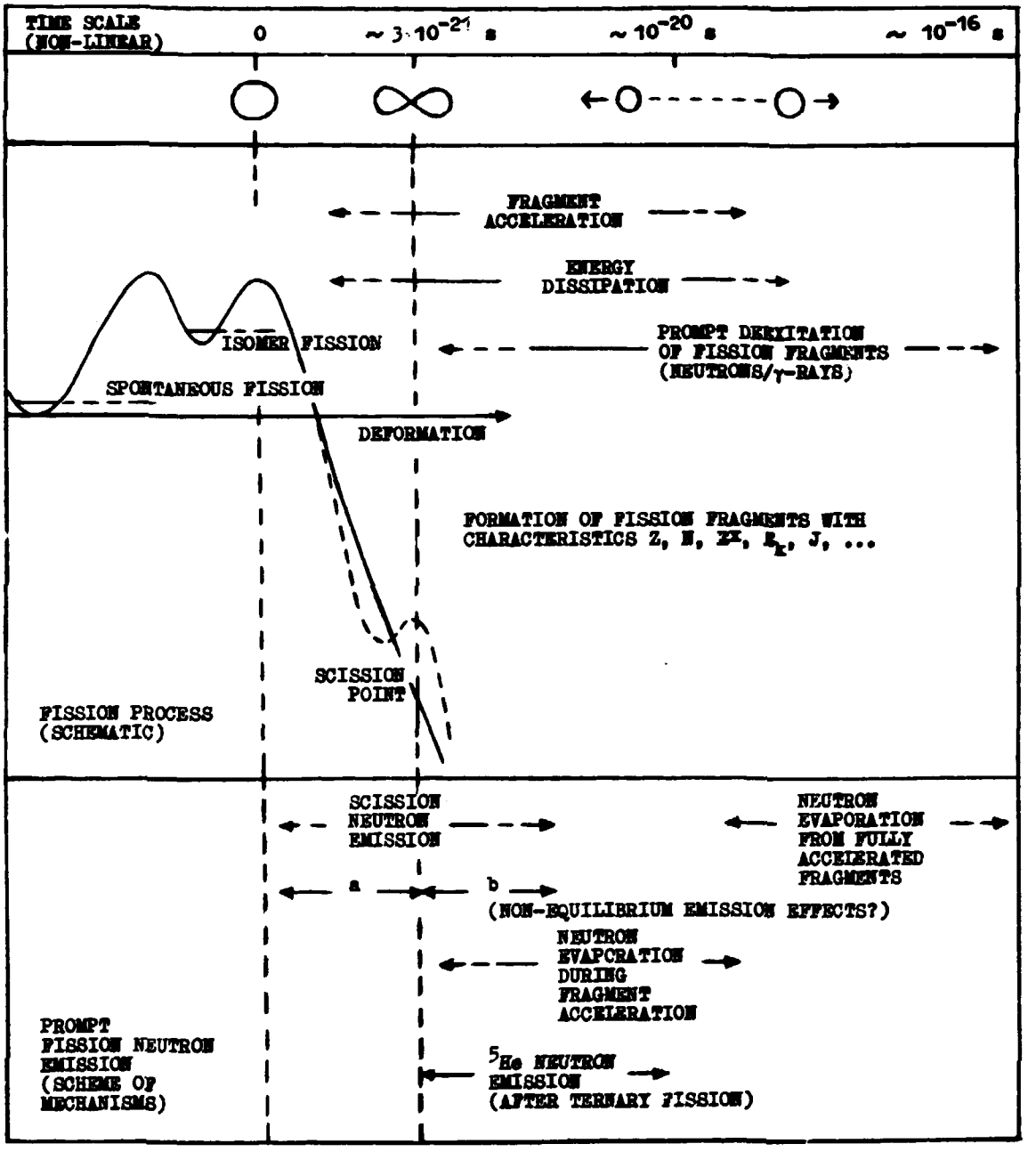

Fig. 1
Scheme of the fission process including possible mechanisms of prompt neutron emission

2. Time evolution in fission and possible mechanisms of prompt neutron emission

The understanding of prompt fission neutron emission requires some basic problems to be solved:

i) diabatic single-particle excitation due to rapid changes of deformation (descent from the saddle point to scission point, snapping-in of the fragment neck end after scission),

ii) dissipation of excess deformation (at scission) into intrinsic excitation (main source of fragment excitation),

iii) correlation of fragment excitation with the scission configuration which defines a complex fragment probability distribution as a function of nucleon numbers N and Z (A=Z+N), total kinetic energy TKE, excitation energy E^x, angular momentum I, etc.,
iv) neutron emission models for different mechanisms.

Fission dynamics have been treated in the framework of different kinds of models. One extreme, the adiabatic model, excludes excitation at scission[27]. Assuming that the energy at scission is shared among all degrees of freedom according to the laws of thermal equilibrium, one deals with the other extreme (statistical model)[28], i.e. strong single-particle excitation during the descent from saddle point to scission point (viscous transition). Several intermediate models have been proposed[29-33]. They account for the coupling of the fission mode to different collective degrees of freedom and/or intrinsic degrees of freedom. The assumptions made are different and partly contrary. However, all these models are suited to describe the general features of nuclear fission, but it is not possible to obtain a sufficiently quantitative agreement with experimental data on fragment distributions. In any case, the consideration of shell effects is of fundamental importance for the understanding of fission and, specifically, the diversity of scission configurations. The shell energies of complementary fragments define the ratio of their excess deformation at scission and, therefore, the value of their final excitation energy (see below). Different studies[22,23,34-36] of single particle excitation due to the rapid change of nuclear potential resulted in the qualitative conclusion that this appearance should be considerable. Nevertheless, quantitative estimations are quite uncertain. Further, it is likely that the degree of single-particle excitation is correlated with the scission configuration defined by elongation (TKE) and mass asymmetry (A_L / A_H) mainly.
The dissipation occuring during the descent from saddle point to scission can be of different types (one-body or two-body dissipation). Negele et al.[30] studied the evolution of the fissioning system by the use of the time-dependent-Hartree-Fock (TDHF) method. The transition time between saddle point and scission was found to be in the order of some 10^{-21}s ($\sim 3 \cdot 10^{-21}$s, cf. scheme). The corresponding rapid change of deformation might give rise to a considerable single-particle excitation and, consequently, "scission neutron" emission[22,23]. Mädler[25] studied the fast-particle emission in the framework of TDHF for scissioning nuclear systems (catapult mechanism) recently. Nevertheless, all hitherto published theoretical treatments of scission neutron emission give some first clues for an understanding and are far from a reliable description of energy and angular distributions.
Ternary fission is connected with the preferred release of neutron-enriched light nuclei due to the neutron excess in the neck of the scissioning nucleus[27]. Cheifetz et al.[31] found that about 11 % of alpha-particles from ^{252}Cf(sf) are originally emitted as n-unstable ^{5}He nuclei decaying in an alpha-particle and a neutron with a half-life of about $8 \cdot 10^{-22}$s. Such neutrons are predominantly directed in the equatorial plane obviously (see paragraph 5.1.).
Two simultaneous processes occuring after scission within some 10^{-20}s are of special interest: the fragment acceleration in the Coulomb field and the dissipation of excess fragment deformation energy into intrinsic excitation.
Neutron emission can occur in this time. The corresponding energy and angular distribution is dependent on time obviously. Neutron evaporation during fragment acceleration was investigated[39-41] on the base of arbitrary assumptions concerning the excitation energy as a function of time. The study of post-scission dynamics by Samanta et al.[42] resulted in an estimation of the dissipated energy depending on time (one-body friction). This was the base of a new calculation (see paragraph 5.2.). Further, it can be suggested that non-equilibrium neutron emission might occur within about 10^{-20}s after scission, but this mechanism seems to be of much lower order of magnitude than in particle-induced nuclear reactions. Speaking in terms of the exciton model[43], the exciton number of a

fragment during its excitation should be less than the average one and much higher than 1. A value close to 10 was roughly estimated from experimental data on the high-energy "end" of fission neutron spectra[44,45] (cf. paragraph 6.).
The main mechanism of fission neutron emission, i.e. neutron evaporation from the fully accelerated fragments, comes into action after the excitation of the originally strongly deformed fragments ($\gtrsim 10^{-20}$s). The main sources of fragment excitation energy[46] are

- the excess fragment deformation at scission E_D,
- the "velocity" of collective degrees of freedom at scission,
- a contribution due to diabatic single-particle excitation before scission as already discussed,
- (in the case of induced fission) the excess excitation energy at the saddle point of the fission barrier ("heat" energy divided among the complementary fragments according to thermodynamics).

E_D contributes to the fragment excitation energy E^x mainly. It is strongly dependent on shell effects[32,46,47] which are a function of nucleon numbers on the other hand. The saw-tooth curve of $\overline{E^x}(A)$ which is typical for low-energy fission of actinides is a consequence. Hence, the average numbers and average energies of the de-excitation products, i. e. neutrons and γ-rays mainly, are similar functions of A. The total excitation energy $\overline{E^x_{total}} = \overline{E^x_1} + \overline{E^x_2}$ of the complementary fragments is

$$\overline{E^x_{total}}\left(\frac{A_1}{A_2}, TKE\right) = \overline{Q}\left(\frac{A_1}{A_2}\right) + E^x_{CN} - \overline{TKE} \qquad (1)$$

(Q - energy release for the given mass split, E^x_{CN} - excitation energy of the fissioning compound nucleus). The ratio $\overline{E^x_1}$ / $\overline{E^x_2}$ (see Fig. 2) demonstrates the shell influence for different scission configurations defined by A_1 / A_2 and TKE (asymmetry and elongation respectively).

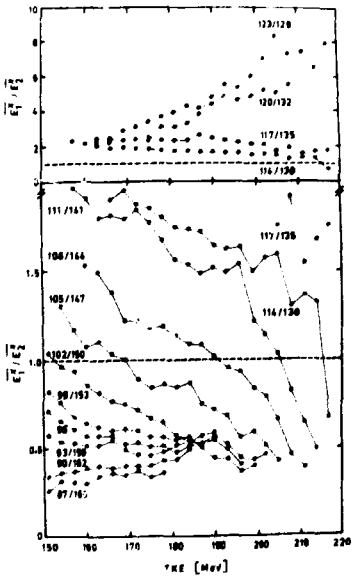

Fig. 2
The ratio of the excitation energies of complementary fragments deduced from experimental data on multiplicities and average emission energies of prompt neutrons and γ-rays[49] as a function of mass number ratio (parameter) and TKE.
The Fig. was taken from Ref. 51.

The excitation energy distributions of complementary fragments deduced from experimental data on neutron multiplicity and γ-emission[48,49] (cf. Fig. 2) can be assumed to have nearly identical width[49]

$$\sigma^2_{E^x}(A_1, TKE) \approx \sigma^2_{E^x}(A_2, TKE) \qquad (2)$$

The theoretical description of neutron evaporation from fully accelerated fragments

requires the application of a statistical-model approach. As reviewed in Ref. 50, several attempts considering the complexity of fragment configurations up to a certain degree are known from literature (cf. paragraph 4.2.).
In fact, all the fission neutron components mentioned above are superposed. Only the ^{5}He neutron emission can be investigated by means of α-n-coincidence measurements separately[38].
Neutron evaporation from fully accelerated fragments is the predominant one. As outlined above, this main component has to be attributed to a diversity of fragment configurations covering excitation energies up to about 50 MeV[50]. Consequently, an experimental study of secondary components like scission neutrons is very difficult and have to be based on accurate measurements of multiple-differential emission probabilities of fission neutrons and a detailed theoretical description of the main component. These requirements will be founded in paragraph 4. more clearly.

3. Scission neutrons - fiction or reality?

Scission neutron emission might be interpreted as an extreme case of ternary fission[52]. The yields of light charged particles are well-known (in total nearly 3.10^{-3} per fission). As emphasized above, scission neutrons cannot be separated experimentally. The theory[21-25] concedes the possibility of scission neutron emission, but doesn't allow to estimate the order of magnitude of the yield.
The average energy and the yield of scission neutrons deduced from experimental data cover the ranges 1.65 to 3.4 MeV and 5 to 25 %, respectively[8-20] (cf. review in Ref. 50). The dependence of the scission neutron yield on TKE obtained by different authors exhibits strong contradictions (Fig. 3).

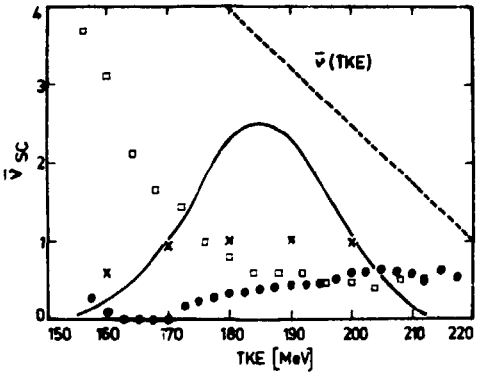

Fig. 3
The scission neutron yield $\bar{\nu}_{sc}$ versus TKE (• - Ref. 19, x - Ref. 13, ¤ - Ref. 18) for ^{252}Cf(sf) (dashed line - total neutron yield, continuous line - fragment yield).

The analysis of the quoted works has been based on rather rough approximations for the description of the center-of-mass (CMS) neutron spectra (evaporation component).
The non-adequate theoretical treatment of the main fission neutron component gives rise to systematic errors in the analysis of scission neutron data. Therefore, one has to question the truth of earlier data. It is indicated that scission neutron yields higher than about 10 % should be understood as "fiction". New results and outlooks are presented below.

4. Statistical-model approach to fission neutron emission

4.1. Basic principles

Calculations of fission neutron emission probabilities considering all possible emission mechanisms are infeasible at present. It was emphasized above that the description of

the main mechanism, i.e. evaporation from fully accelerated fission fragments, is a complex task due to the necessary consideration of many characteristics of fission and fission neutron emission:

i) complex fragment distribution as discussed in paragraph 2, item (iii), i.e. $P(E^x, I, A, Z, TKE)$ depending on the characteristics of the fissioning nucleus,
ii) cascade neutron emission from highly-excited, neutron-enriched fragments in competition to γ-emission.

The fragment distribution P cannot be derived from fission theory completely and/or with sufficient accuracy (cf. Ref. 32). Therefore, one has to consider experimental data and/or special assumptions.
The CMS spectrum $\varphi(\varepsilon)$ is calculated in the framework of either the Weisskopf formalism[56] (without P(I) consideration) or the Hauser-Feshbach theory[57]. In any case, the level density $\rho(U,I')$ of the residual nucleus with excitation energy U and angular momentum I' and the transition probabilities, i.e. the inverse cross section σ_c of compound-nucleus formation or the transmission coefficients respectively, have to be taken into account. Using the Weisskopf ansatz one can approximately consider the influence of the spin distribution on spectrum shape if assuming $\rho(U,I) = \rho(U,I=0)$[58]. The emission of fission neutrons is not isotropic in the center-of-mass system (CMS) of the fragments due to the fragment spin[53]. This influence is often neglected. The average spin amounts to about (6 - 8)$\hbar$[54] yielding a CMS anisotropy close to 10 %[55].
The function $\varphi(\vartheta)$, i.e. CMS angular distribution, has been assumed to be independent on ε in Refs. 4,50 and 51. According to the classical description of angular distributions of particles emitted from compound nuclei with a given average angular momentum[53], it is likely that the anisotropy is nearly proportional to ε (cf. paragraph 4.4.).

The complex statistical-model approach to fission neutron emission based on the main mechanism can be stated by the following relation:

$$\varphi(\varepsilon, \vartheta : A, Z, TKE)$$
$$= \sum_i \sum_I \int dE^x \cdot P_i(E^x, I : A, Z, TKE) \cdot \varphi_i(\varepsilon, \vartheta : E^x, I, A, Z) \qquad (3)$$

i.e. the emission probability is calculated for a fixed fragment configuration defined by A, Z, and TKE. The sum over i (emission step index) means consideration of cascade emission.
The transformation of the CMS distribution into the laboratory system LS is carried out by the use of the formula

$$N(E,\Theta)\, dE d\Omega = \sqrt{\frac{E}{\varepsilon}} \cdot \varphi(\varepsilon,\vartheta)\, dE d\Omega , \qquad (4)$$

where

$$\varepsilon = E + E_f - 2 \cdot \sqrt{E \cdot E_f} \cdot \cos\Theta , \qquad (5)$$

$$E_f = \frac{E_k}{A} = TKE \cdot \left(\frac{1}{A} - \frac{1}{A_{FN}}\right) \qquad (6)$$

(E,Θ are the LS energy and angle respectively; A_{FN} is the mass number of the fissioning nucleus).

The weighted concentration taking into account the fragment occurance probability $P(A,Z,TKE)$ yields LS emission probabilities for eligible fragment parameter bins. Specifically the total distributions $N(E,\Theta)$ and $N(E)$ can be derived.

4.2. Recent theoretical treatments

The whole scheme of Equ. (3) has not yet been realised in praxis. Most of the hitherto published treatments rely on average fragment parameters, i.e. the diversity of fragment configurations is often neglected. The influence of several approximations is discussed in paragraph 4.3.

The Madland-Nix-Model (MNM)[59] is based on a simplified distribution P(T) in nuclear temperature of the residual fragments which is triangular in shape extending from 0 to the maximum temperature T_m. In this way, $P_0(E^x)$ and the cascade emission are considered roughly. It is assumed that P(T) is unique for the both considered fragment groups. σ_c and the CMS-LS transformation are considered in regard of average fragment group parameters. A model similar to the MNM was proposed recently[60]. Here, P(T) is modified to consider it more realistically.

The A dependence of T_m, E_f, σ_c, and the weight of the partial spectra is taken into account in the generalised Madland-Nix model (GMNM)[61], i.e. the complexity of fission fragment configurations is considered in more detail. Both the MNM and the GMNM are, however, rather rough models because of the assumption of an idealised temperature distribution and the use of a simplified Weisskopf ansatz based on the constant-temperature discription of nuclear level density.

The concept of the complex cascade evaporation model (CEM)[51,62] corresponds to the scheme described in paragraph 4.1 but the explicit consideration of P(Z,I). Here, the Weisskopf formula is used to calculate $\mathcal{P}(\mathcal{E}:E^x,A)$ on the base of a semiempirical description of the level density $\rho(U,I=0)$ including shell and pairing correction. σ_c is calculated by the use of the optical model. Further, the initial distribution in excitation energy (cf. paragraph 2) $P_0(E^x:A,TKE)$ is assumed to be Gaussian for fixed A and TKE. The CMS anisotropy is considered roughly according to

$$\mathcal{P}(\mathcal{E},\vartheta : A,TKE) = \mathcal{P}(\mathcal{E} : A,TKE) \cdot \frac{1 + \beta(\mathcal{E}) \cdot \cos^2\vartheta}{1 + \frac{1}{3}\beta(\mathcal{E})} . \qquad (7)$$

$\beta(\mathcal{E})$ denotes the CMS anisotropy parameter.

Applying the Hauser-Feshbach theory for fission neutron spectrum calculations one is able to account for the competition of neutron and γ-ray emission as well as the initial distribution in fragment spin. The first study was presented by Browne and Dietrich[63]. Similar calculations have been done by the Leningrad group (HFC)[64] without consideration of CMS anisotropy and the spectrum dependence on Z and TKE.
Both the CEM and the HFC involve a more realistic consideration of $P_0(E^x)$ as well as improved semiempirical descriptions of the level density.
A review of earlier models of fission neutron emission was presented in Ref. 50.

4.3. Sensitivity of calculations in regard of approximations and input data variations

The study of sensitivity effects is a necessary precondition for the evaluation of the calculation accuracy as well as for the interpretation of systematic deviations between measured and calculated spectra. A first analysis in the framework of the CEM has been published in Ref. 50 for ^{252}Cf(sf) yielding the following conclusions:

i) The calculated average number of emitted neutrons is strongly changed by variations of $\overline{E^x}$ and the average neutron separation energy.

ii) The shape of the calculated spectrum is mostly sensitive to variations of $\overline{E^x}$, the width of $P(E^x)$, and the level density parameter.

iii) The calculated spectrum of the low-excited fragments with A close to 132 exhibits large uncertainties, specifically at energies higher than 3 MeV.

iv) The description of σ_c in the framework of the optical model reduces the average emission energy by about 5 % with reference to the calculation with constant σ_c.

v) If neglecting the TKE dependence of the spectra for fixed A, i.e. CMS-LS transformation based on the average kinetik energy ($\bar{E}_k$ approximation), the calculated spectrum is strongly enhanced at high energy.

vi) The consideration of the CMS anisotropy yields an enhanced spectrum at low and high energy and a lower emission probability at intermediate energy (Fig. 4).

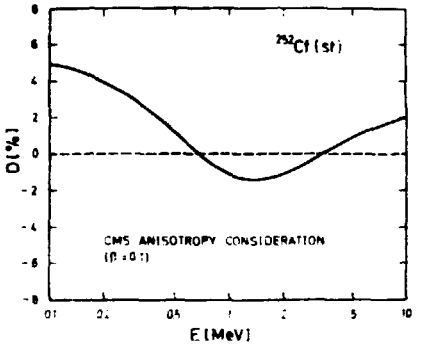

Fig. 4
Percentage departures of the $^{252}Cf(sf)$ neutron spectrum calculated in the framework of the CEM considering the CMS anisotropy ($B = 0.1$) from the $B = 0$ calculation.
The assumption that $B \approx 0.1 \cdot \epsilon$ (cf. paragraph 4.2.) yields a similar result but a larger deviation at high energy.

Figs. 5 - 9 represent the influence of the most important input data on the shape of calculated angular distributions (CEM study for the most probable mass split).
These results indicate that the accuracy of $N(E,\theta)$ calculations is limited due to the uncertainties of input parameters. Therefore, the study of secondary emission mechanisms is restricted on principal.

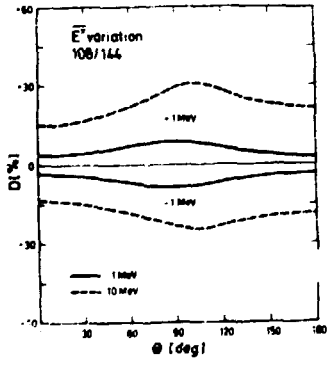

Fig. 5
Percentage departures of LS angular distributions calculated for plus/minus 1 MeV variations of $\bar{E}^X$ from the corresponding reference spectrum for the LS energies 1 and 10 MeV

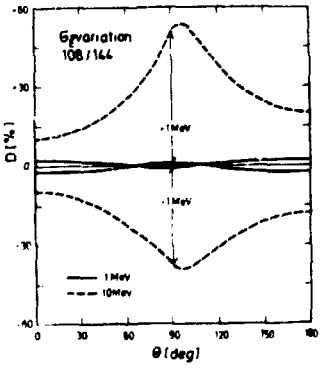

Fig. 6
The same as Fig. 5 for ± 1 MeV variations of the width of $P_0(E^X)$

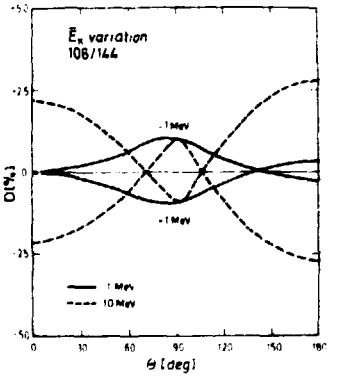

Fig. 7
The same as Fig. 5 for ± 1 MeV variations of the average fragment kinetic energy

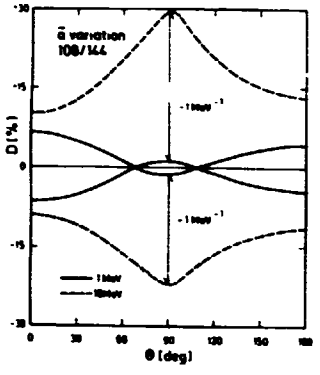

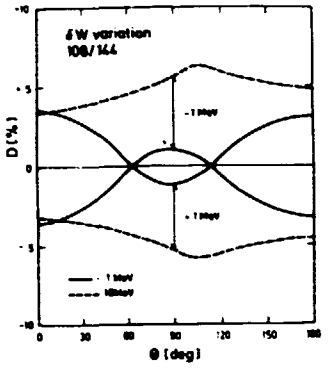

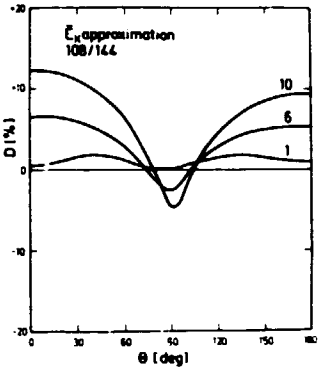

Fig. 8
The same as Fig. 5 for ± 1 MeV^{-1} variations of the level density parameter

ig. 9
The same as Fig. 5 for ± 1 MeV variations of the shell correction energy (level density description)

Fig. 10
The same as Fig. 5 concerning the $\bar{E}_k$ approximation, i.e. neglection of the TKE dependence in Eqs. 1-4, for selected LS energies (parameter in MeV)

If using the $\bar{E}_k$ approximation, calculated angular distributions are more anisotropic (at high energy especially). Pronounced influences are obtained considering the CMS anisotropy as discussed below in more detail.

4.4. The neglection of CMS anisotropy as a reason of fictive scission neutrons?

It was shown in paragraph 4.1. that the fragment angular momentum directed perpendicular to the fission axis[54] causes a CMS anisotropy of neutron emission. We studied its influence on LS angular distributions assuming $\beta = 0.1$, i.e. constant anisotropy, (version 1) and $\beta = 0.1 \cdot \mathcal{E}$ (version 2) according to Ref. 53. Figs. 11 and 12 represent the results for the version - 1 calculation. Angular distributions are enhanced in polar and equatorial direction and reduced at intermediate angles if considering CMS anisotropy. Similar results have been deduced for version 2 (which is probably more realistic) but the higher anisotropy at high energy and less pronounced polar "nose".

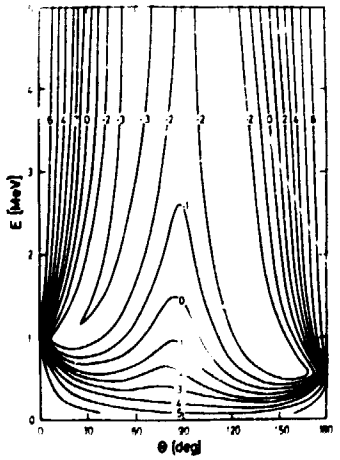

Fig. 11
Percentage departures of $N(E,\Theta)$ calculated with a constant CMS anisotropy ($\beta = 0.1$) with reference to the $\beta = 0$ calculation (spontaneous fission of ^{252}Cf). The plot represents the lines of equal deviations (parameter in %)

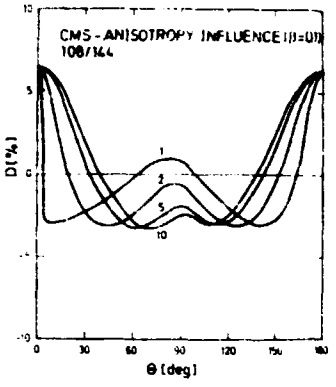

Fig. 12
The same as Fig. 11, but for selected LS energies (parameter in MeV).

The most important conclusion of this investigation is the following: If neglecting the CMS anisotropy in the calculation of fission neutron angular distributions to be compared with experimental data, one deduces a special emission component which could be interpreted as scission neutrons. These "scission neutrons" are fictive obviously. Similar systematic errors appear, if one neglects the diversity of fragment configurations (cf. paragraph 4.1.). These approximations yield deviations of calculated $N(E,\Theta)$ distributions. All previous studies of scission neutron emissions[8-20] had been based on rather rough descriptions of $N(E,\Theta)$. Specifically the CMS anisotropy was not considered in any work. Therefore, the conclusions drawn in paragraph 3 are confirmed.

4.5. Kinematic dips of multi-differential emission probabilities?

The CMS-LS transformation formula (Eq. 4) exhibits a singular point at $\mathcal{E} = 0$. If approximating the CMS spectrum by

$$\varphi(\mathcal{E}) \sim \mathcal{E}^{k_1} \cdot \exp(-k_2 \cdot \mathcal{E}), \qquad (8)$$

one has to distinguish three cases:

i) $k_1 < \frac{1}{2}$: pole

ii) $k_1 = \frac{1}{2}$, i.e. $\varphi(\mathcal{E})$ is a Maxwellian distribution : no structure

iii) $k_1 > \frac{1}{2}$: zero (kinematic dip)

$\mathcal{E}$ becomes zero for $E = E_f$ and $\Theta = 0$ (Eq. 3). The consequence of case (iii) is a polar "dip" of $N(E,\Theta)$ at $E = E_f$. Calculations in the framework of both the CEM and the GMNM indicate that $k_1 \geq 0.6$ if fitting CMS spectra for light as well as heavy fragments to Eq. (8) at low energy.
Experimental data[65,62] have confirmed the existence of dips, i.e. case (iii), for the light fragment group.

The analysis of experimental and theoretical emission distributions has to be carried out carefully. Specifically mechanism studies require further detailed investigations in the concerned E,Θ-region.

5. Special emission mechanisms

5.1. Neutron emission due to ^{5}He decay

It is expected that neutrons from the decay of ^{5}He nuclei are predominantly directed close to 90 deg (equatorial plane). Consequently, such neutrons might influence the angular distribution of ordinary fission neutrons in this angular range. The double-differential emission probability of ^{5}He neutrons $N_H(E,\Theta)$ from ^{252}Cf(sf) was estimated considering the following:

i) isotropic decay of ^{5}He nuclei (about $3\cdot10^{-4}$ per fission) in the CMS with a $8\cdot10^{-22}$s half life[38],

ii) time-dependent distribution of ^{5}He kinetic energy according to Ref. 38 (Coulomb problem),

iii) angular distribution of ^{5}He emission with reference to the fission axis (assumed to be the same as in ^{4}He-accompanied fission).

The model parameters as far as not known from Ref. 38 were fixed by the intercomparison of the calculated and the measured ^{5}He neutron energy spectrum considering the angular resolution of the experimental arrangement employed. The CMS distribution was transformed into the LS for the considered time bins, i.e. certain average ^{5}He kinetic energy, taking into account the decay probability.
Further, the total (i.e. time-integrated) LS distribution deduced with reference to ^{5}He direction was folded with the angular distribution of ^{5}He nuclei (Legendre polynom formalism) yielding $N_H(E,\Theta)$. The obtained probability distribution normalized to the yield of ^{5}He nuclei per fission are represented in Fig. 13 for selected neutron energies.

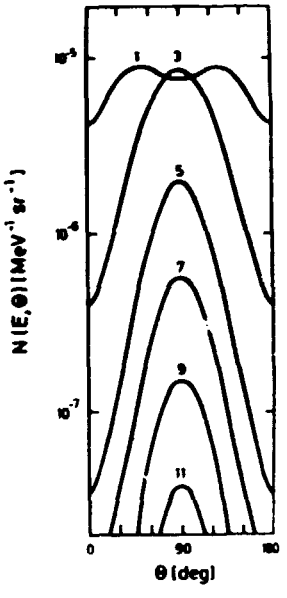

Fig. 13
Calculated angular distributions of ^{5}He neutrons represented for selected emission energies (parameter in MeV)

Comparing these results with the total distribution of fission neutrons we conclude that the 90 deg emission probability of ^{5}He neutrons is lower than 1 % of the equatorial spectrum of prompt fission neutrons (~ 0.1 % at 3 MeV, ~ 0.5 % at 10 MeV). Hence, ^{5}He neutron emission is an appearence of minor importance.

5.2. Neutron evaporation during fragment acceleration

Based on dynamical calculations of post-scission processes[42] we introduced the time-dependence of fragment excitation energy $E^x(t)$ and kinetic energy $E_k(t)$ into the cascade evaporation model[51] to estimate the influence of neutrons emitted during fragment acceleration on the total double-differential emission probability ($N(E,\Theta)$). The considered emission mechanism was assumed to be significant in different fission reactions[40,20,41], but earlier studies involved arbitrary approximations like the reduction of the problem to a single intermediate emission time. Nevertheless, the used post-scission data (cf. Fig. 14) for dynamically changing fragments with one-body dissipation[42] exhibit large uncertainties.

The calculation of the CMS emission distribution $P_0(\varepsilon)$ of the first cascade step was carried out as a function of t, i.e.

$$P_0(\varepsilon : E_k(t),t)dt = W(t)\int dE^x \cdot P_0(E^x : t) \cdot P(\varepsilon : E^x)\, dt, \qquad (9)$$

where $P_0(E^x:t)$ - distribution in E^x assumed to be Gaussian. The emission probability per time unit $W(t)$ was deduced according to statistical assumptions[40].

The obtained $N(E,\Theta)$ data (Fig. 15) show a time-dependent 0° / 90° - anisotropy (Fig. 16), which can be approximated by sinh $(\beta \cdot \sqrt{E \cdot E_k(t) / A} / \bar{\varepsilon}(t))$. Hence, the relative

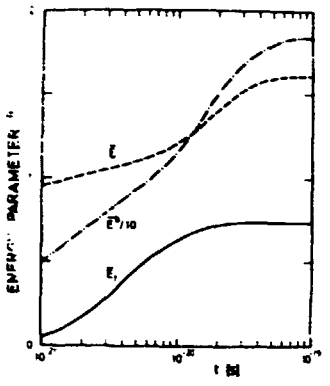

Fig. 14
Fragment kinetic energy per nucleon E_f, the average excitation energy $\overline{E^*}$ and the average CMS emission energy $\overline{\varepsilon}$ as a function of time t after scission for symmetric fission of ^{252}Cf.

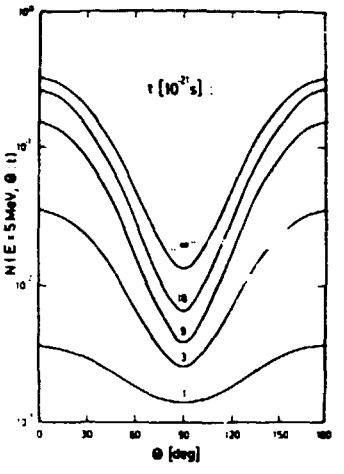

Fig. 15
The angular distribution of fission neutrons for a fixed emission energy (2 MeV) in dependence of t for ^{252}Cf(sf) (symmetric).

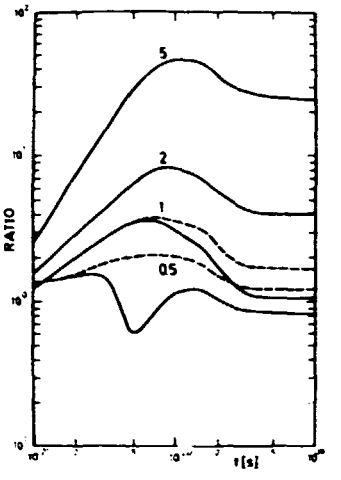

Fig. 16
0° / 90° - anisotropy (continuous lines) of ^{252}Cf(sf) neutron emission versus t for fixed emission energies (parameter in MeV). The structure at low energy appears due to kinematics (cf. paragraph 4.5.). The dashed lines represent the ratio of the N(Θ) maximum and N(90°).

behaviour of $E_k(t)$ and $\overline{E^*}(t)$ as well as W(t) determine N(E,Θ:t). The used input data[42] give rise to an unexpected anisotropy maximum close to 10^{-20}s (Fig. 16) for a symmetric mass split in ^{252}Cf(sf).
A remarkable enhancement of neutron emission in equatorial direction can only be deduced for unreasonable short life times (high nuclear temperatures ≥ 2 MeV), i.e. simulation of non-equilibrium emission.

6. The ^{252}Cf(sf) neutron energy spectrum

The Cf neutron spectrum is one of the nuclear standards[26]. It has been measured with rather high accuracy in the 1 keV - 30 MeV energy region[66]. Recent experimental data as well as theoretical spectra obtained in the framework of new models (cf. paragraph 4.2.) are represented in Fig. 17 for comparison.
All statistical-model versions considered yield similar results in the energy range from 0.5 to 10 MeV. The MMM underestimates experimental data at both spectrum ends.
The results of the GMMM, HFC, and CEM (β = 0.) calculations are in very good agreement, but they tend to underestimate the low-energy data (-10 % deviation). Considering the CMS anisotropy the spectrum is changed as represented in Fig. 4, i.e. the low-energy part of the spectrum is in better agreement with experimental data. Fig. 17 illustrates that the total energy spectrum can be described by a statistical-model approach (the CEM including CMS anisotropy specifically) in the energy range below 20 MeV. No further conclusions concerning the emission mechanism of fission neutrons can be drawn for this energy range. The high energy region (> 15 MeV) was made accessible experimentally due

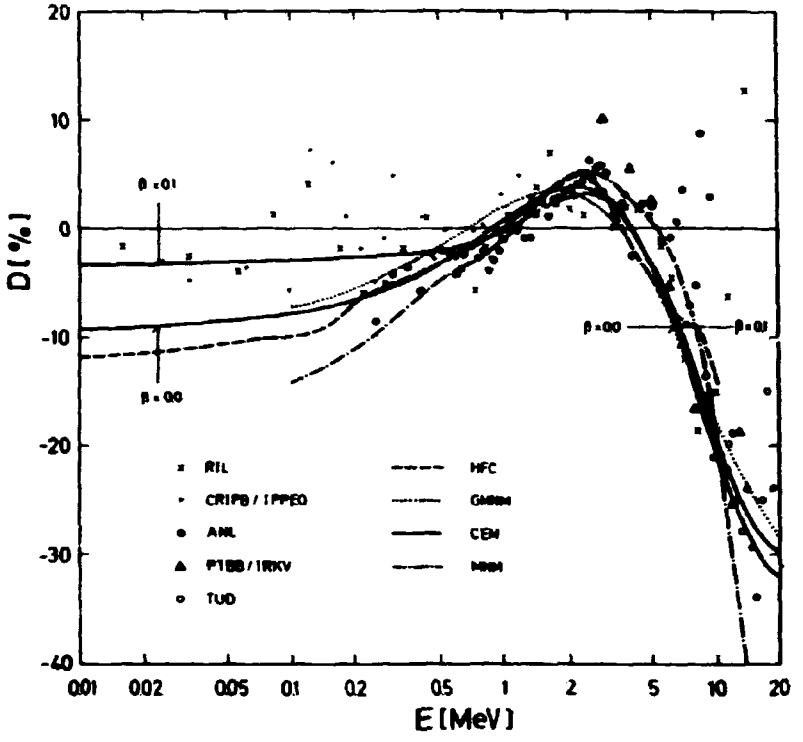

Fig. 17
Percentage deviations D of recent experimental data (RIL - Ref. 67, CRIPB/IPPEO - Ref. 68, ANL - Ref. 69, PTBB/IRKV - Ref. 70, TUD - Ref. 71) on the Cf neutron spectrum from a Maxwellian distribution with a "temperature" T = 1.42 MeV. The curves represent energy distributions calculated in the framework of HFC, GMNM, CEM, and MNM. The CEM spectrum is shown for two CMS anisotropy parameter β (Eq. (5)).
Fig. taken from Ref. 66.

to the use of a high-sensitive neutron spectrometer in conjunction with the effective electronic suppression of γ-rays and cosmic background (μ).[71] The found excess of neutrons above 20 MeV could be interpreted as non-equilibrium emission (paragraph 2).

7. The anisotropy of ^{252}Cf(sf) neutron emission

Obviously, the measurement of anisotropy of fission neutron emission (ratio of spectra measured in polar and equatorial direction) should give more clues to the study of emission mechanisms. Several authors tried to show the existence of scission neutrons by the investigation of anisotropy. An excess of neutrons measured in equatorial direction with reference to rough evaporation calculations was considered as central component or scission neutron component, i.e. a part of fission neutrons emitted from the scissioning nucleus with an angular distribution close to an isotropic one.
Earlier measurements [8,14] had shown a rather hard equatorial spectrum of Cf fission neutrons. The anisotropy was found to be about one order of magnitude lower than calculated values at 10 MeV emission energy. Recent experimental data[20,72,73] do not confirm

these results. Fig. 18 represents a comparison of our data[72] obtained by the use of the high-sensitive method mentioned in paragraph 6. with the equatorial spectrum measured by Bowman et al.[8] as well as the CEM calculation.

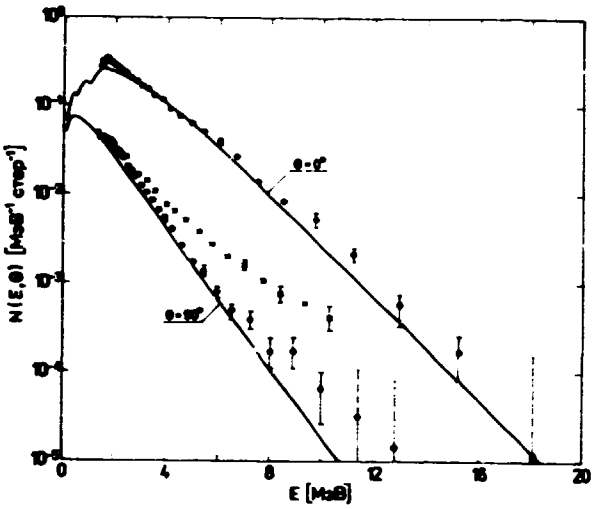

Fig. 18
Polar and equatorial spectrum of Cf fission neutrons (• - Ref. 72, x - Ref. 8). The continuous lines represents the result of the CEM calculation showing the kinematic dips at low energy (cf. paragraph 4.5.). The 0°-spectrum was measured without distinction of light and heavy fragments.

The anisotropy ratio defined by

$$R(E) = \frac{N(E,0^{o}) + N(E,180^{o})}{2 \cdot N(E,90^{o})} \qquad (10)$$

is shown in Fig. 19 (experimental and calculated (CEM, GMNM) data).

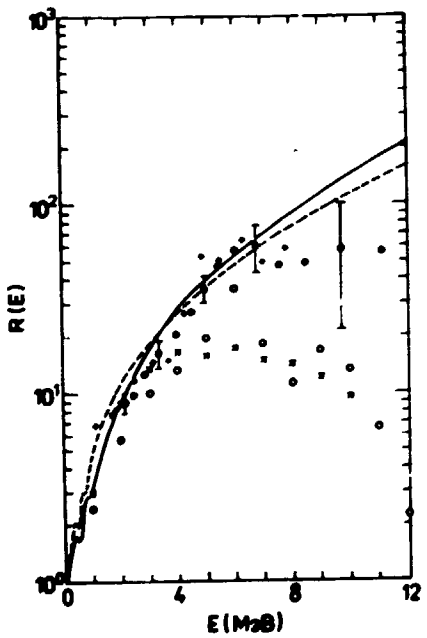

Fig. 19
The anisotropy ratio (Eq. 10) of Cf neutron emission versus emission energy (x - Ref. 8, o - Ref. 14, + - Ref. 20, • - Ref. 72). The full and the dashed curve represent calculated results (CEM and GMNM respectively).

Recently measured anisotropy data[20,72] are in rather good agreement with the evaporation calculation. The measurements of Bowman et al.[8] as well as of Bishop et al.[14] had been carried out without n/γ-discrimination for background suppression. Therefore, systematic errors, specifically in the case of the low-yield equatorial spectrum at high energy, cannot be excluded. It is emphasized that the 90°-spectrum of Bowman agrees well with the CEM calculation at energy below 1.6 MeV.

Finally, we conclude that the study of anisotropy has <u>not</u> yet given an unambiguous argument of the existence of scission neutrons.

Based on our experimental and theoretical results (concerning the experimental as well as the theoretical uncertainties) we found an upper yield of scission neutrons close to 5 %.

8. New experimental methods for the measurement of multiple-differential emission probabilities of fission neutrons

A detailed study of the mechanism of fission neutron emission requires precise measurements of multiple-differential emission probabilities and an appropriate, i.e. complex, analysis in the framework of the statistical model to describe the main evaporation component. Hence, $N(E,\Theta;P_f)$ (P_f-fragment parameter set) or at least $N(E,\Theta)$ (total distribution in E and Θ) should be investigated.
The first comprehensive study was presented by Bowman et al.[8]. Concerning this work, inadequate aspects (possible experimental errors - paragraph 7., rough theoretical approximation - paragraph 3.) have been discussed.
Note that the measurement or $N(E,\Theta;P_f)$ for strongly confined fragment configuration regions is rather difficult. Resolution effects and rather high statistical uncertainties could be the reason of errors of analysed data.
In any case of such measurements, the determination of fragment direction as well as specified fragment parameters (at least the distinction between light and heavy fragment group) has to be arranged. An alternative to the fragment detection at a fixed direction and the employment of one neutron detector[8] or a multi-detector system[74,75] for neutron spectrum measurement is the application of a direction-sensitive method of fragment detection and the use of only one neutron detector. In this case, several systematic experimental errors are avoided.
Recently, two different arrangements for direction-sensitive fission fragment detection and their use in $N(E,\Theta)$ measurements have been described[72,73] :

i) application of a gridded twin chamber (ionisation type) and the use of one neutron detector perpendicular to the electrode plane[73],

ii) application of a set-up consisting of two parallel-plate avalanche counters (one position-sensitive) and use of two neutron detectors.[72]

Both methods which include neutron time-of-flight spectroscopy have special advantages:

method (i): high fragment detection efficiency, determination of A_L/A_H and TKE, but limited angular resolution at polar direction,

method (ii): steady angular resolution, but hitherto distinction between light and heavy fragment group only, i.e. $N(E,\Theta)$ measurement (extension to a twin set-up enabling the measurement of A_L/A_H and TKE is possible).

For details and first results, we refer to the contributions presented at this conference. The measurements based on both methods are in progress.

9. Summary

We tried to review the present knowledge about prompt fission neutron emission emphasizing possible mechanisms. Further, the requirements to be met in the analysis of experimental data in conjunction with theoretical calculations have been discussed. We have questioned the truth of earlier results concerning scission neutron emission based on a study of neutron emission probabilities in the framework of a complex statistical-model approach. Here, we emphasized the influence of several approximations made in earlier works. It was shown that neutron emission due to the decay of ^{5}He nuclei is a minor effect which doesn't contribute to the total distribution $N(E,\Theta)$ significantly. Further, it is indicated that neutron evaporation during fragment acceleration yields not a considerable enhancement of the energy spectrum at equatorial direction. The results are, however, very sensitive about post-scission data ($E^*(t)$ and $E_k(t)$) and the fragment life time concerning neutron emission.
Energy spectra $N(E)$ of prompt fission neutrons can be described adequately on the base of a complex statistical-model approach assuming evaporation from fully accelerated

fragments in the full energy range ≤ 20 MeV. It is, however, indicated that a very hard emission component appears in the E > 20 MeV range, whose nature is not clear.
Measured ^{252}Cf(sf) neutron emission anisotropies agree with statistical-model calculations within the experimental and theoretical uncertainties. A significant hard emission component at equatorial direction doesn't exist very probably.
New measurements of multiple-differential emission probabilities and corresponding statistical-model calculations are in progress. It is expected that these studies yield new informations about the mechanism of prompt fission neutron emission.

References

1) N. Bohr, J.A. Wheeler, Phys. Rev. 56 (1939) 426
2) N. Feather, U.S. Atomic Energy Commission, Document BR 335 A (1942), unpublished, cf. Ref. 4
3) B.E. Watt, Phys. Rev. 87 (1952) 1037
4) J. Terrell, Phys. Rev. 113 (1959) 527
5) R.R. Wilson, Phys. Rev. 72 (1947) 189
6) J.S. Fraser, Phys. Rev. 88 (1952) 536
7) V.N. Nefedov, J.E.T.F. 38 (1960) 1657
8) H.R. Bowman, S.G. Thomson, J.C.D. Milton, W.J. Swiatecki, Phys. Rev. 126 (1962) 2120
9) S.S. Kapoor, R. Ramanna, P.N. Ramo Rao, Phys. Rev. 131 (1963) 283
10) K. Skarsvag, K. Bergheim, Nucl. Phys. 45 (1963) 72
11) C.P. Sargent, W. Bertozzi, P.T. Thomas, J.L. Matthews, Phys. Rev. B 137 (1965) 89
12) J.C.D. Milton, J.S. Fraser, Physics and Chemistry of Fission, Proc. IAEA Symp., Salzburg, 1965, Vol. 2 (1965) 39
13) M.V. Blinov, N.M. Kasarinov, I.G. Krisyuk, Yad. Fiz. 12 (1970) 41 and Yad Fiz. 16 (1972) 1155
14) C.J. Bishop, I. Halpern, R.W. Shaw, R. Vandenbosch, Nucl. Phys. A 198 (1972) 161
15) Z. Fraenkel, I. Mayk, J.P. Unik, A.J. Gorski, W.D. Loveland, Phys. Rev. C 12 (1975) 1809
16) S. Nair, D.B. Gayther, J. Phys. G 3 (1977) 949
17) S. Nair, D.B. Gayther, B.H. Patrick, E.M. Bowey, J. Phys. G. 3 (1977) 965
18) V.M. Piksaikin, P.P. Dyatchenko, L.S. Kuzaeva, Yad. Fiz. 25 (1977) 723
19) J.S. Samyatnin, D.K. Ryasanov, B.G. Basova, A.D. Rabinovich, V.A. Koristilev, Yad. Fiz. 29 (1979) 595
20) P. Riehs, Acta Phys. Austr. 53 (1981) 271
21) V.S. Stavinski, J.E.T.P. 36 (1959) 629
22) R.W. Fuller, Phys. Rev. 126 (1962) 684
23) Y. Boneh, Z. Fraenkel, Phys. Rev. C 10 (1974) 893
24) V.A. Rubtchenya, preprint RI-28, Leningrad (1974)
25) P. Mädler, Z. Phys. A 321 (1985) 343
26) Proc. IAEA Cons. Meet. on the U-235 Fast-Neutron Fission Cross-Section and the Cf-252 Fission Neutron Spectrum, Smolenice, 1983, INDC(NDS)-146 L (1983)
27) R. Vandenbosch, Nucl. Phys. 46 (1963) 129
28) P. Fong, Statistical Theory of Nuclear Fission, Gordon and Beach, 1969
29) J.R. Nix, W.J. Swiatecki, Nucl. Phys. 71 (1965) 1
30) J.J. Griffin, Physics and Chemistry of Fission, Proc. IAEA Symp., Vienna, 1969, p. 3
31) W. Nörenberg, Physics and Chemistry of Fission, Proc. IAEA Symp., Vienna (1969) 51 and Phys. Lett. 31 B (1970) 621 and Phys. Rev. C 5 (1972) 2020
32) B.D. Wilkins, E.P. Steinberg, R.R. Chasman, Phys. Rev. C 14 (1976) 1832
33) U. Facchini, G. Sassi, J. Phys. G 3 (1977) 269
34) S.E. Koonin, J.R. Nix, Phys. Rev. C 13 (1976) 209
35) T. Ledergerber, Z. Faltiel, Z. Fraenkel, H.C. Pauli, Nucl. Phys. A 275 (1977) 280
36) G. Schütte, L. Wilets, Nucl. Phys. A 252 (1975) 21

37) J.W. Negele, S.E. Koonin, P. Möller, J.R. Nix, A.J. Sierk, Phys. Rev. C 17 (1978)1098

38) E. Cheifetz, B. Eylon, E. Fraenkel, A. Gavron, Phys. Rev. Lett. 29 (1972) 805

39) V.P. Eismont, At. En. 19 (1965) 113

40) G.A. Pik-Pichak, Yad. Fiz. 10 (1969) 321

41) D.J. Hinde et al., Phys. Rev. Lett. 52 (1984) 986

42) B.C. Samanta, D. Sperber, M. Zielinska-Pfabe, S.K. Samaddar, Phys. Lett 108 B (1982) 83

43) J.J. Griffin, Phys. Rev. Lett. 17 (1966) 478

44) H. Märten, Thesis, 1981, Technische Universität Dresden

45) H. Märten, D. Seeliger, B. Stobinski, Proc. Europhysics Topical Conf. on Neutron Induced Reactions, June 21-25, 1982, Smolenice, Physics and Applications Vol. 10 (1982) 287

46) B.G. Geilikman, O.V. Zimina, Yad. Fiz. 23 (1976) 1175

47) M. Kildir, N.K. Aras, Phys. Rev. C 25 (1982) 365

48) C. Signarbieux, R. Babinet, H. Nifenecker, J. Poitou, Proc. IAEA Symp. on Physics and Chemistry of Fission, Aug. 13 - 17, 1973, Rochester, IAEA (Vienna, 1974) Vol. II, p. 179

49) H. Nifenecker, C. Signarbieux, R. Babinet, J. Poitou, loc. cit. (48), p. 117

50) H. Märten, D. Neumann, D. Seeliger, loc. cit. (26), p. 199

51) H. Märten, D. Seeliger, J. Phys. G 10 (1984) 349

52) N. Feather, loc. cit. (31a), p. 83

53) T. Ericson, V. Strutinski, Nucl. Phys. 8 (1958) L 84 (Errata Nucl. Phys. 9 (1959)689)

54) J.B. Wilhelmy, E. Cheifetz, R.C. Jared, S.G. Thomson, H.R. Bowman, J.O. Rasmussen, Phys. Rev. C 5 (1972) 2041

55) A. Gavron, Phys. Rev. C 13 (1976) 2561

56) J.M. Blatt, V.F. Weisskopf, Theoretical Nuclear Physics (New York, 1952)

57) W. Hauser, W. Feshbach, Phys. Rev. 87 (1952) 366

58) E. Nardi, L.G. Moretto, S.G. Thomson, Phys. Lett. 43 B (1973) 259

59) D.G. Madland, J.R. Nix, Nucl. Sci. Eng. 81 (1982) 213

60) A.F. Graschin, M.V. Lepeschkin, At. En. 58 (1985) 59

61) H. Märten, D. Seeliger, INDC(GDR)-30/L (1984) and Nucl. Sci. Eng.

62) H. Märten, D. Seeliger, Proc. Int. Conf. on Nuclear Data for Basic and Applied Science, Santa Fe, USA, May 13 - 17, 1985

63) J.C. Browne, F.S. Dietrich, Phys. Rev. C 10 (1974) 2545

64) B.F. Gerasimenko, V.A. Rubtchenya, Neutron Physics (Proc. All-Union Conf., Kiev, 1983), Moscow (1984) Vol. I, p. 349

65) O.I. Batenkov, A.B. Blinov, M.V. Blinov, S.N. Smirnov, loc. cit. (64), p. 334

66) H. Märten, D. Seeliger, Proc. IAEA Advisory Group Meeting on Nuclear Standard Reference Data, Geel, Belgium, Nov. 12 - 16, 1984, IAEA-TECDOC-335 (1985) 255

67) M.V. Blinov, G.S. Boykov, V.A. Vitenko, Proc. Int. Conf. on Nucl. Data for Science and Technology, Sept. 6 - 10, 1982, Antwerp, ed. by K.H. Böckhoff, D. Reichel Publ. Comp. Eindhoven (1983) 479

68) A. Lajtai, P.P. Dyachenko, L.S. Kutzaeva, V.N. Kononov, P.A. Androsenko, loc. cit. (26), p. 177

69) W.P. Poenitz, T. Tamura, loc. cit. (67), p. 465 and loc. cit. (26), p. 175

70) R. Böttger, H. Klein, A. Chalupka, B. Strohmaier, loc. cit. (67), p. 484

71) H. Märten, D. Seeliger, B. Stobinski, loc. cit. (67), p. 488 and H. Märten, D. Richter, D. Seeliger, INDC(GDR)-28/L (1984)

72) H. Märten, W. Neubert, D. Richter, D. Seeliger, loc. cit. (62)

73) C. Butz-Jørgensen, H.-H. Knitter, loc. cit. (62)

74) Yu. A. Vasilev, Yu.A. Sidorov et al. INDC(CCP)-177/L (1982) 49

75) E.A. Seregina, P.P. Dyachenko, Yad. Const. 1 (1985) 58.

SIMULTANEOUS INVESTIGATION OF FISSION FRAGMENTS AND NEUTRONS IN ^{252}Cf(S,F)

C. Budtz-Jørgensen and H.-H. Knitter

Commission of the European Communities

JRC - Central Bureau for Nuclear Measurements, Geel, Belgium

Abstract

The gridded twin ion chamber developed at CBNM is used to measure the kinetic energy-, mass- and angular distributions of the fission fragments of ^{252}Cf in an advantageous 4π-geometry. Together with a neutron time-of-flight detector this experimental arrangement permits to measure the correlation between neutron emission, fragment angle, mass and energy in the spontaneous fission of ^{252}Cf. With the present experimental set-up a mass resolution for fission fragments of 0.5 a.m.u., an angular resolution of $\Delta\cos\theta$ = 0.05 and a timing resolution of 0.7 ns FWHM were observed. Preliminary evaluations of the raw experimental data are presented for the fission fragment mass distribution, the average total kinetic energy and their variance as function of mass, the angular distribution between fragments and neutrons, the number of neutrons emitted per fragment as function of fragment mass, the average neutron emission energies as function of mass, and the prompt fission neutron spectrum averaged over all fragments.

I. INTRODUCTION

Nuclear fission has been a longstanding theme of scientific investigation and here the spontaneous fission of ^{252}Cf gives a relatively easy opportunity to study the correlations between neutron emission and fission fragment parameters. The measurement of such correlations can contribute to a better understanding of the fission process. On ^{252}Cf much more effort than on other nuclei was devoted to the measurement and interpretation of the prompt fission neutron spectrum, because this spectrum is used also as a neutron spectrum shape standard. Several attempts 1,2) have recently been made to give a theoretical description of the prompt fission neutron spectrum of ^{252}Cf. These models are based on the assumption that the mechanism of neutron emission is the evaporation from the fully accelerated fragments. However, the comprehensive measurements of Bowman et al. 3) of the prompt neutron anisotropy have led to the conclusion that a fraction (~10-20 %) of the total number of fission neutrons is emitted isotropically in the laboratory frame of reference. In spite of many further investigations the knowledge of the so-called scission neutron emission is poor and partially contradictory. Therefore it is of much interest for the basic understanding of the neutron emission process, not only to measure precisely the integral prompt fission neutron spectrum, but to obtain also in multiple-dimensional measurements the correlations between the neutron emission and the different fission fragment parameters which can help to clarify the nature of this scission neutrons.

II EXPERIMENTAL METHOD

At present a multiple parameter measurement of the ^{252}Cf prompt neutron spectrum, $N(E_n, \theta_n, A, TKE)$ is being performed at CBNM. The experimental set-up is shown in fig. 1.Fission fragment detection is made using the gridded ion chamber 4,5) developed at our lab with which fission fragment angle, kinetic energy, and mass can be determined simultaneously. The fission fragment kinetic energies (E_L,E_H) are determined using the anode pulses from the twin chamber. The two energy informations are used to derive the fragment masses. The excellent energy and mass resolution of this detector is illustrated in fig. 2 which shows a part of the measured ^{252}Cf light fragment mass distribution.

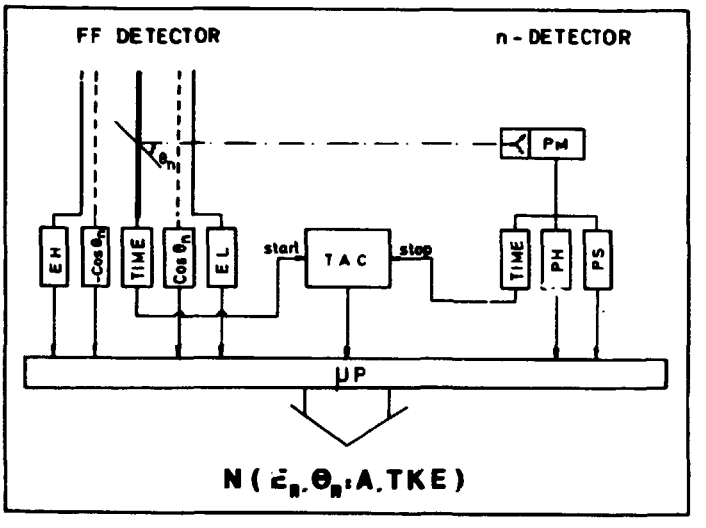

Fig. 1 : Experimental set-up

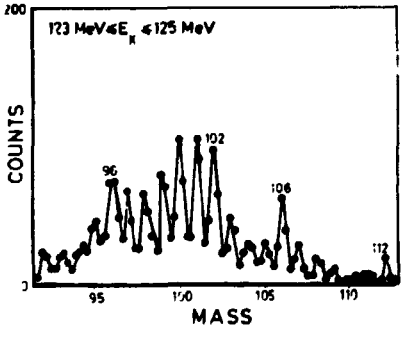

Fig. 2 : Mass distributions of cold fragments

neutron detector, is shown in fig. 3 together with the average total kinetic energy and their variance as function of fragment mass. Good agreement with published distributions is observed for the mass yields. The yield enhancement in far-out asymmetric fission ($A_H \geq 176$), which was recently seen by Barreau 6) is confirmed in our measurement as well as the fluctuations of the TKE(A), σ(TKE) for fragments in this region. The fragment angle information is determined as cosine of the angle θ between the normal of the electrodes and the path of the fission fragments. The cosθ resolution is ~ 0.05. For timing the pulses from the common cathode are used giving a

The fragment kinetic energies have been selected so high (cold fragmentation) that neutron emission is improbable and corrections to the mass determination are avoided. A mass resolution of 0.5 a.m.u. corresponding to a kinetic energy resolution < 0.6 MeV is observed. A ^{252}Cf (SF) mass-yield measurement based on $4 \cdot 10^7$ fission events recorded with the above set-up, however without demanding coincidences with the

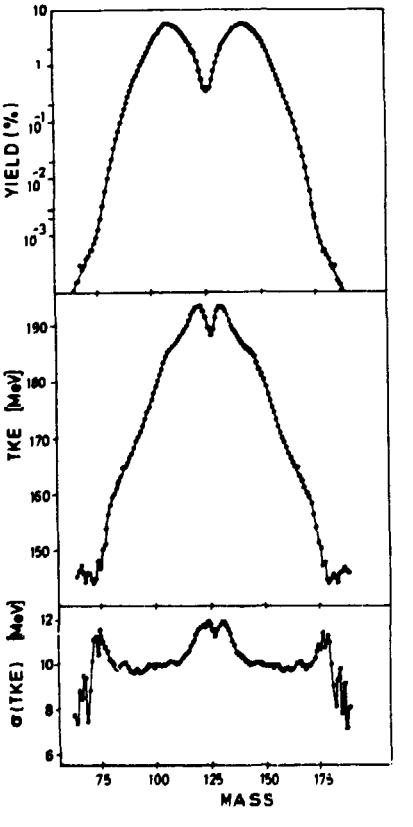

Fig. 3 : Yield, average total kinetic energy, and the variance are plotted versus the fragment mass

resolution < 0.7 ns FWHM together with the neutron detector. The neutron detector, a 4"x1" NE 213 scintillator, is located on the axis of the ionization chamber. The distance between the ^{252}Cf-source and the neutron detector was 0.51 m. Both, the pulse height and the pulse shape for n/γ discrimination are recorded. Neutron energies are determined using conventional time-of-flight technique. All 7 parameters are digitized, each allocated 8192 channels, and stored sequentially on tape for off-line analysis. At present a ^{252}Cf source prepared by vacuum evaporation onto a 120 $\mu g \cdot cm^{-2}$ thick Ni-foil is mounted in the chamber. The source activity is $\sim 3 \cdot 10^2$ $fiss \cdot s^{-1}$, yielding a fragment-neutron coincidence rate of 1 s^{-1} for the present geometry of the experiment.

III FIRST RESULTS AND DISCUSSION

So far $1.5 \cdot 10^6$ coincidences have been recorded on which the present analysis is based. The results should be regarded as preliminary since corrections such as the recoil correction for the determination of masses and kinetic energies of the fragments have not been applied. The results are uncorrected for mass resolution. The experimental data contain the needed information for a determination of these corrections but a more complex analysis code has to be written. However, the effect on the result presented here is expected to be minor.
Fig. 4 displays the neutron TOF spectrum integrated over all fragments but with a threshold for the recoil protons of 0.7 MeV.

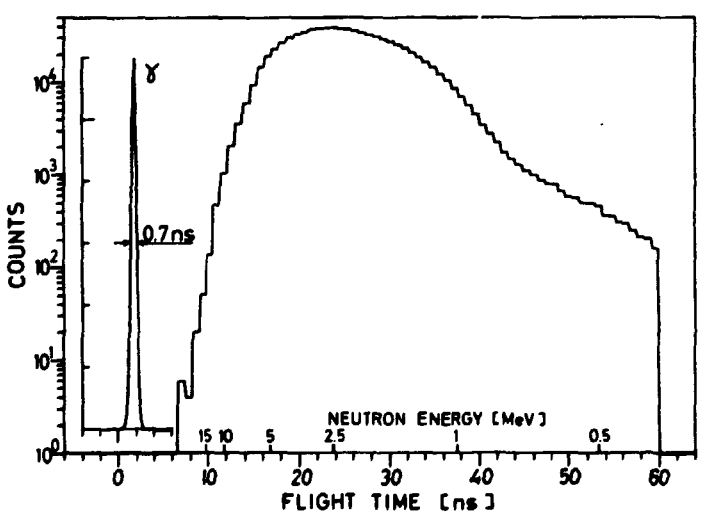

Fig. 4 : Neutron time-of-flight spectrum integrated over all fragments

The advantage of having a weak source is seen here since the influence of accidental coincidences ($\sim 1 \cdot 10^{-3} \cdot ns^{-1} \cdot h^{-1}$) can be completely neglected. It is especially gratifying that no background events were detected to the left of the gamma peak, a consequence of the near 100 % efficiency of the ionization chamber. This means that the analysis can be extended to very high neutron energies, where scission neutrons might play a role 2).

The mass integrated prompt fission neutron spectrum of $^{252}Cf(S,F)$ was evaluated in some more detail. For the present preliminary evaluation the neutron detection efficiency, which is needed to obtain the spectrum shape, was calculated using the Monte Carlo-code from the thourough detector efficiency investigation of Dietze and Klein 7). This code calculates the absolute neutron detection efficiency for a given pulse height threshold. These calculations will in the future be backed up also by detector efficiency measurements. The spontaneous fission process is not only accompagnied by neutrons but also by γ-rays which might be detected by the neutron

detector. Most of the γ-emission is made at the instant of fission and up to a few ns later. In this time range fall also the high energetic neutrons which are emitted with a very low intensity. Therefore the very high energy region of the neutron spectrum is most sensitive to false events induced by γ-rays. The pulse shape circuit emplcyed in the present set-up was not able to give a clean discrimination between γ- and neutron events for pulse heights corresponding to a proton recoil energy smaller than 2 MeV. Therefore several neutron time-of-flight spectra with different pulse height thresholds in the neutron detector were selected from the same raw experimental data. Absolute detector efficiency curves were calculated for the same pulse height thresholds. This way one obtains for each of the selected detector thresholds a neutron spectrum. These spectra are automatically normalized with respect to each other by the absolute detector efficiency calculations. Therefore, in overlaping energy ranges and where the measurements are not disturbed by γ-events, the spectra must coincide with each other. This was observed and a single neutron energy spectrum was composed containing at low neutron energies the data from a spectrum with a low threshold of 0.5 MeV and at higher neutron energies data from a spectrum with a threshold of 2 MeV. The data above 14 MeV were obtained using a detector threshold of 7.2 MeV where the pulse shape discrimination could eliminate γ-ray events completely. This spectrum divided by $\sqrt{E}$ is plotted in fig. 5 logarithmically versus the incident neutron energy. The ful line in fig. 5 represents the result of a least squares fit through the experimental data with a Maxwellian energy distribution. The temperature parameter obtained by the fit is T=1,41 MeV. An error for this value was not yet evaluated, also since the experimental determination of the detector efficiency is not yet made. This preliminary neutron energy spectrum shows no major deviations from the Maxwell distribution in the neutron energy range from 0.8 MeV to 20 MeV. The deviations from the Maxwell distribution are in

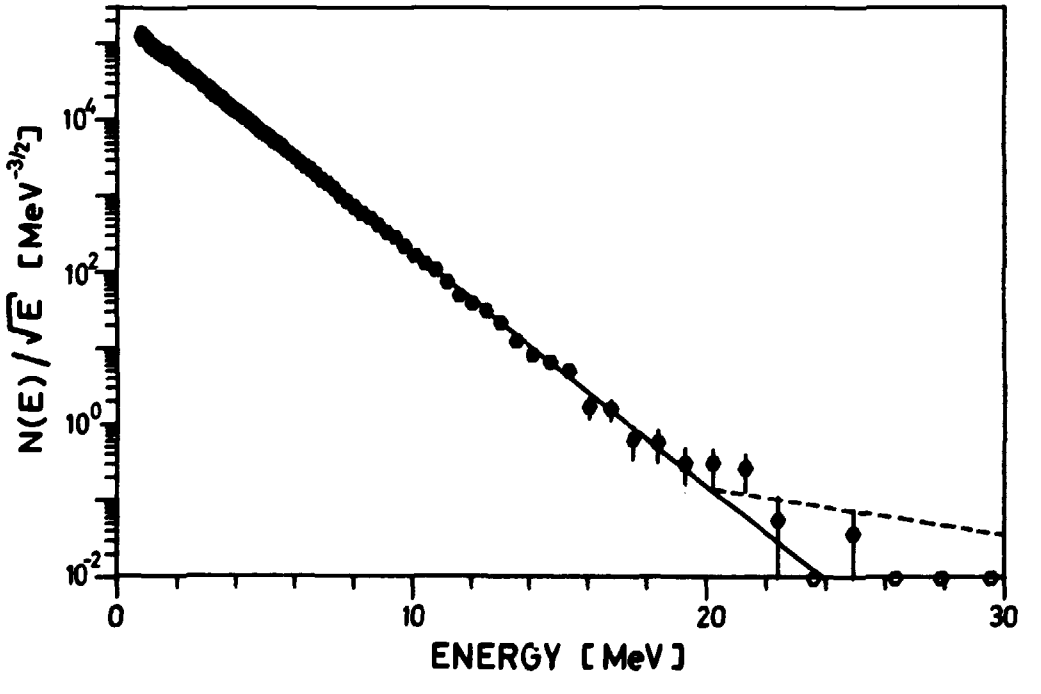

Fig. 5 : Preliminary neutron energy spectrum divided by $\sqrt{E}$ versus the neutron energy.

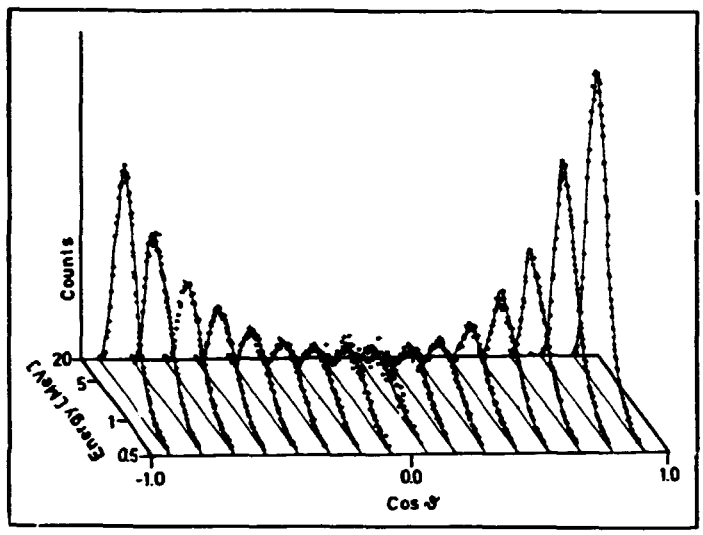

Fig. 6 : Bi-parametric plot of number of fission events versus neutron energy and cos ϑ·ϑis the angle between the light fragment and neutron emission direction

general less than 5% in the above mentioned range. The dashed line corresponds to the experimental spectrum measurements of Märten et al. 8,9), who found a large excess of neutrons above 20 MeV. With the presently evaluated data we can not confirm nor contradict the measured excess of neutrons. From a total of about 2·10⁶ events the statistics obtained in the high energy region above 20 MeV is not sufficient. The two data points at the highest neutron energy with values $>10^{-2}$ contain only one event each. Points plotted at the 10^{-2}-line contain zero events.

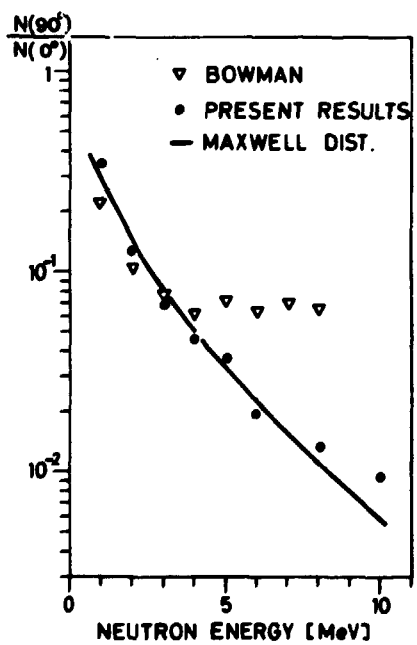

Fig. 7 : The neutron-fragment i. ·nsity ratio is plotted versus the neutron energy.

The measured fragment-neutron angular distributions integrated over all fragments versus the neutron energy are shown in a bi-parametric representation in fig. 6. The neutron emission angular distributions as function of neutron energy for each mass split are also available. The present data agree fairly well with the results of Bowman et al. 3) below 4 MeV. However, at higher neutron energies our data are much more anisotropic with intensity ratios N(90°)/N(0°) more than one order of magnitude smaller than those of Bowman above 8 MeV. The comparison between the present angular anisotropy measurements as function of fission neutron energy and those of Bowman et al. 3) is made in fig. 7. The full line in fig. 7 represents calculations of the angular anisotropy as function of the neutron energy with the assumption that all neutrons are emitted from the fully accelerated fragments. The according equations and the needed numerical values were taken from Terrell 10). The energy dependence of the present N(90°)/N(0°) intensity ratio is conformable to the assumption that all neutrons are emitted from the fully accelerated fragments and the existence of a hard (T≈2.0-2.5 MeV)

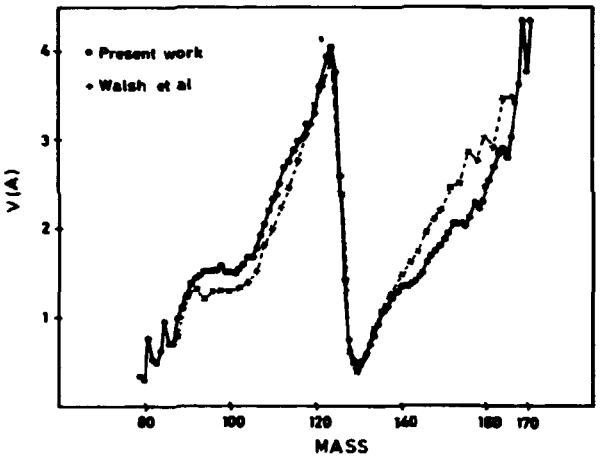

Fig. 8 : Preliminary neutron emission multiplicity versus fragment mass.

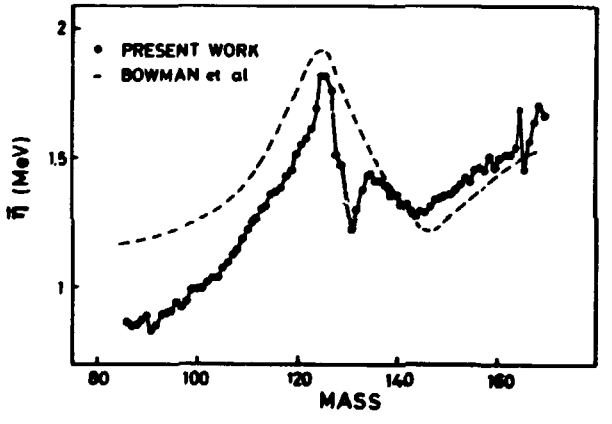

Fig. 9 : Preliminary centre of mass average fission neutron energy versus fragment mass.

scission neutron component which Märten 2) concluded from the Bowman angular distributions must be refuted. A more thorough analysis of our angular distributions is needed in order to decide whether perhaps a soft component is present. Fig. 8 shows the measured neutron emission multiplicity $\nu(A)$ from the individual fragments compared to those of Walsh 11). The minor differences in these two data sets might be due to the neglect of recoil effects in the present analysis. However, our data seem not to confirm the fine structures in $\nu(A)$ seen by Walsh 11).

Since the measurement of Bowman in 1962 very little experimental information has been gained on the average neutron emission energies $\eta(A)$ in the center-of-mass frame. Fig. 9 displays the measured dependence of the average η on A as compared to the results of Bowman. Some striking differences may be observed. The present data show a pronounced dip at $A \approx 130$, also seen in $\nu(A)$, followed by a broad hump extending to $A \approx 145$. This behaviour is also reproduced in theoretical calculations 2,12) of $\eta(A)$.

IV CONCLUSIONS

Although most of the results of the ongoing multi-parameter neutron-fragment correlation experiment are preliminary, some conclusion might already be drawn now :

- The more pronounced angular anisotropies measured in the present experiment compared to those of Bowman et al. at higher neutron energies lead to at least a much smaller portion of scission neutrons if their existence has not even to be refuted.

- With the presently calculated neutron detector efficiency no major deviation from a Maxwellian distribution between 0.8 MeV $\leq$ En $\leq$ 20 MeV is observed.

- The yield enhancement for far-out asymmetric fission is confirmed.

- Pronounced structure as function of mass was observed for the average c.m. fission neutron energy, in relative agreement with theoretical calculations.

At present the experiment is being improved by the use of a ten times stronger source. However a pulse pile-up rejection must be introduced, in order to maintain the good mass resolution of 0.5 a.m.u..

Acknowledgements : The authors are indepted to Dr. R. Wiltshire from AERE Harwell U.K. for the preparation of the thin ^{252}Cf-sources. Also the large help in the execution and evaluation of the present work given by Messrs. H. Bax and R. Vogt is gratefully acknowledged.

REFERENCES

1. D.C. Madland and J.R. Nix, Nucl. Sci. Eng. 81, 213 (1982)
2. H. Märten, D. Neumann and D. Seeliger, Proc. IAEA Consultants' Meeting on the ^{235}U Fast Neutron Fission Cross-Section and the ^{252}Cf Fission Neutron Spectrum, Smolenice, March 1983, INDC(NDS) - 146, p. 195 (1983)
3. H.R. Bowman, S.G. Thompson, J.C.D. Milton, W.J. Swiatecki, Phys. Rev. 126, 2120 (1962).
4. H.-H. Knitter and C. Budtz-Jørgensen, Proc. of the Int. Conf. on Nuclear Cross Sections for Technology, Knoxville, U.S.A., Oct. 1979, NBS Spec. Publ. 594, p. 947 (1980).
5. C. Budtz-Jørgensen and H.-H. Knitter, Nucl. Sci. Eng. 86, 10 (1984).
6. G. Barreau, W. Sicre, F. Caïtucoli, M. Asghar, T.P. Doan, B. Leroux, G. Martinez and T. Benfoughal, Nucl. Phys. A432, 411 (1985).
7. G. Dietze and H. Klein, Bericht ND-22, Physikalisch Technische Bundesanstalt, Braunschweig, Germany, (1982).
8. H. Märten, D. Seeliger and B. Strobinski Proc. Int. Con. on Nuclear Data for Science and Technology, Antwerp, Sept. 1982, D. Reidel Publishing Company, NL, page 488.
9. H. Märten and D. Seeliger
   Proc. IAEA Advisory Group Meeting on Nuclear Standard Reference DATA, Geel, Nov. 1984, IAEA-TECDOC-335, page 255, Vienna (1985).
10. J. Terrell, Phys. Rev. 127, 880 (1962).
11. R.L. Walsh and J.W. Boldeman, Nucl. Phys. A276, 189 (1977)
12 E. Nardi, L.G. Moretto and S.G. Thompson
   Phys. Lett. 43B, 259(1973)

EXPERIMENTAL STUDY OF CORRELATIONS OF ENERGY AND ANGULAR DISTRIBUTIONS OF CF-252 SPONTANEOUS FISSION NEUTRONS

O.I. Batenkov, A.B. Blinov, M.V. Blinov, S.N. Smirnov

V.G. Khlopin Radium Institute, Leningrad, USSR

Abstract

The measurements of differential energy distributions of Cf-252 fission prompt neutrons have been carried out for different emission angles.

In the present work precision measurements of differential energy spectra were carried out for different masses and total kinetic energies of the fragments at different emission angles of neutrons. Special attention was payed to the neutron spectra at small angles (less than 6°). Using these data, for the first time by the direct method it was possible to determine the velocities of the fragments during the neutron emission. The analysis of the same spectra enabled to obtain information on the behaviour of the cross-section of the reverse process (the capture of neutrons by the excited nucleus) for the region of low energies of neutrons. The comparison of the data for small and big angles enabled to specify the limits of applicability of the evaporation model.

The obtained data are very useful for correct formation of the Cf-252 integral spectrum -international standard, as it is possible only on the base of complete understanding of the mechanism of the neutron emission process.

For each fission event in the measurements were determined: neutron energy (E), masses of the fragments (M1, M2) total kinetic energy of the fragments (E_k), the emission angle of neutrons relative to the direction of fragments motion (φ) in l.s.. Fragments were detected by two semiconductor surface-barrier silicon detectors (SCD). The energy of neutrons was determined by the time-of-flight method. A stilbene crystal with a photomultiplier (FEU-30) was used as a neutron detector. The measurements were done for the angles of 2,6,15,30,45,60,75,90^{o}, and were doubled on three flight bases: 37.5, 75.0, 150.0 cm. During the measurements the accumulation of the data was carried out in form the matrix of fragment-fragment coincidences in the coordinates $N_f(M,E_k,I)$, where I - the number of the detector, in form the matrix of fragment-fragment-neutron coincidences in the coordinates $N_n(T,M,E_k,I)$ and the matrix of velocities $V_f(M,E_k,I)$. For each event was done: the compensation of the time-amplitude dependence the fragment energies correction associated with the account of the neutron recoil effect, leading to a systematic shift of the coordinates of the N_n matrix relative to the coordinates of the N_f matrix.

Results

The most precise information on the neutron spectrum in the c.m.s. is obtained from the measurements at small angles in relation to the direction of the motion of the fragments. The advantage of those measurements is evident. First, here the contribution of the neutrons from the opposite fragment is minimum and is possible to account for it correctly, secondly, due to the additional velocity of the fragment the low-energy part of the neutron spectrum is shifted to the region of energies of the order 1 MeV and the relative yield of such neutrons increase sharply. Besides, there is a special point in the neutron spectrum at small angles. That point, where the neutron s velocity (V_n) is equal to the velocity of the fragment (V_f), corresponds to the zero energy of the neutron in the c.m.s.. From the correlation $N(E_l)= N(E_c)\sqrt{E_l}/\sqrt{E_c}$, connecting the spectra in the l.s. $N(E_l)$ and in the center of mass system of the fragment $N(E_c)$ it is seen that at $E_c \to 0$ there is an uncertainty of the kind 0/0, which can be differently disclosed in dependece on the spectrum shape $N(E_c)$ near the $E_c = 0$. If the spectrum in the c.m.s. behaves as E_c^{α}, then in dependence on the value of the parameter α in the laboratory spectrum a dip ($\alpha > 0,5$), a peak ($\alpha < 0,5$) or a smooth dependence ($\alpha = 0.5$) can be observed. Different theoretical calcu-

lations /1-3/ give a full set of these possibilities.

In this work we have found a dip in the spectrum of light fragments, the position of which coincides with the average velocity of the fragment and the value is rigidly connected with the emission angle of neutrons. At 15° the dip is not observed. In Fig. 1 are shown experimental spectra at the angles 2°, 15°, and 30°, summed up by all the masses and kinetic energies of the light fragments. A distribution symmetry is seen relative to V_f = 1.37 cm/ns. The dips are also observed in the neutron spectra for groups of light

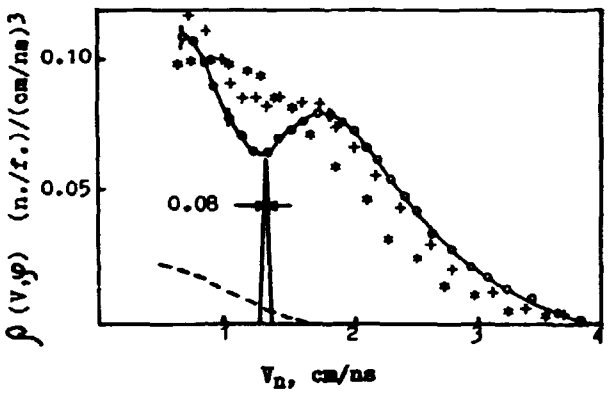

Fig. 1:
Spectrum of neutrons emitted by a light fragment at the angles:
o - 2°, + - 15°, * - 30° in the l.s.
---- - neutrons, emitted by the additional fragment.

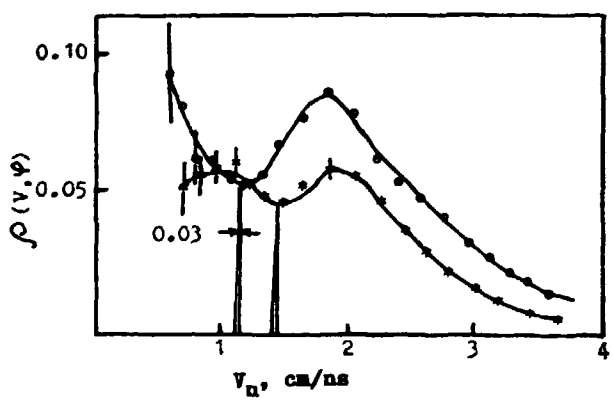

Fig. 2:
Spectrum of neutrons emitted at the angle 5°
- M = 98 ± 4 amu, E_k = 175 ± 4 MeV, V_f= 1.44 cm/ns
o - M = 117 ± 4 amu, E_k = 175 ± 4 MeV, V_f= 1.22 cm/ns.

fragments selected by their masses and kinetic energies (fig. 2). The positions of the dips within the limits of measurement error coincide with the average velocities of the fragments for these groups, which confirms the hypothesis of neutron emission from fully accelerated fragments. In the spectra of heavy fragments the dip is not observed. This seems to be associated with the different shape of the neutron spectrum in the low energy region (c.m.s.) for different masses of the fragments ($\alpha > 0.5$ for light and $\alpha < 0.5$ for heavy fragments). Such a difference can be explained by the different cross-section course of the neutron capture by an excited nucleus for different masses of the fragments. The cross-section course of the neutron capture by an excited nucleus in the low energy region for light and heavy fragments was obtained from the measured spectra. The comparison with the results of calculations of the cross-section σ_c for unexcited nuclei by the optical model /4/ with application of different potentials shows that the general course of σ_c from E_n for an excited nucleus is preserved in principle, though there are some differences.

In the work a comparison was made of the spectra of neutrons emitted from the fragments at the angles 0° and 90° in the l.s.. The spectra measured at the angle 90° and the one calculated for the angle 90° from the data of the angle 0° in assumption of neutron emission from a fully accelerated fragments agree by the integral within the limits of statistical error (2-3%). An analogous comparison of the spectra at 90° was carried out also for separate groups of fragments (fig. 3). Within the error limits (3-10 %) the experi-

mental and the calculated neutron yield coincide. We mark that on the initial stage of t the given work the discrepancy of the measured and the calculated spectra composed 7 % by the integral for 90° /11/. The difference of the results of the work from the previous one can be explained by the following: the improvement of spectrometer's characteristics, a thorough determination of the neutron detector s efficiency on the base of recent experimental data /5-8/ on the Cf-252 integral spectrum, the breaking of the whole range of fragment into 108 groups, for which the velocity of the fragment, was determined immediately in the course of the experiment, the development of the method enabling to account for the influence of the neutron recoiling effect for each angle in each separately registered event, the introduction of anisotropy in the c.m.s., associated with the angular momentum of the fragment in the form $1 + B P_2 (\cos\theta)$, where $B = 0.04$.

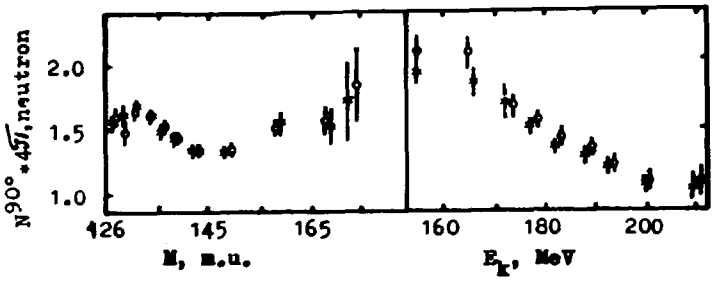

Fig. 3: Neutron yield at the angle 90° in dependence on the fragment's mass for the sum of E_k and on the total kinetic energy for sum of masses.
ψ - obtained from the data for the angle 0°(calcul.)
o - obtained from the data for the angle 90° (exp.)

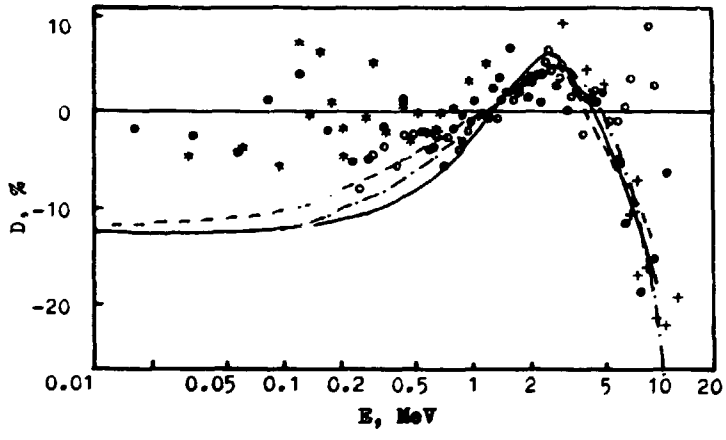

Fig. 4: Deviation of the integral spectra from Maxwell distribution (T = 1.42 MeV)
data of ref. * - /6/, o - /7/, + - /8/, • - /5/, — - data of this work, calculation of ref. -·- /9/, - - - /10/.

In the present work there was also a comparison of the integral spectrum (fig. 4), obtained from the data at small angles and measured by the direct method in the ref. /5-8/. In connection with the fact that the spectrum of Cf-252 fission neutrons is an international standard, the shape of this spectrum must be determined with a high precision. The highest precision in the determination of the spectrum is reached for the energy range 1-5 MeV. It seems interesting to determine the integral spectrum from our data for 0° in assumption that the neutron emission takes place only within the limits of the model of evaporation from fully accelerated fragments. In this case the correlation of the energy intervals for different angles of neutron emission due to the kinematic effect leads to the

appearing possibility for the determination of the shape of the integral spectrum in the region of low and high energies, basing on a comparatively well known shape of the spectrum in the energy range 1-5 MeV. Besides, by means of an iteration procedure a description was carried out of the total sum of our experimental differential data in the energy range 0.2-10 MeV (in l.s.). The spectrum obtained in this way is shown in fig. 4. The theoretical calculation spectra obtained on the base of statistical models in ref. /9-10/ are close by their shape to this distribution, which shows a reasonable degree of simplification in calculations.

It is worth mentioning that in the energy range 1-10 MeV our integral spectrum (from 0°) goes close enough to a number of direct measurements experimental data /5-8/. In the low energy region (less than 1 MeV) our integral spectrum is some what lower than the data of direct measurements /5-6/. The difference in the low energy region can be associated with the influence of the anisotropy effect in the c.m.s., caused by the angular momentum of the fragments, and also with the presence of nonevaporating neutrons. The variation of the anisotropy coefficient, when using experimental spectra at 0° (l.s.) as the basis data, does not enable to reach an agreement of integral spectra in the whole energy region. The introduction of neutrons of nonevaporating character (2 % of the total amount) enables to explain the discrepancy of the spectra.

References

/ 1/ R.J. Le Couter, Proc. Phys. Soc., v. A 65, p. 718 (1952)

/ 2/ G.M. Ahmedov, V.S. Stavinski, Report (FEI-970, Obninsk, 1979)

/ 3/ V.F. Weisskopf, Phys. Rev., v. 52, p. 95 (1973)

/ 4/ D.J. Madland, J.R. Nix, Nucl. Sci. Eng., v. 81, p. 213, (1982)

/ 5/ M.V. Blinov, et al., Proc. Int. Conf. on Nucl. Data for Sci. and Techn. editer by K.M. Bockhoff, (D. Reichel Publ. Comp. Eindhoven), Antverpen, 1983

/ 6/ A. Lajtai, et al., IAEA Cons. Meet. on the U-235 fast neutron fission cross-section, and the Cf-252 fission neutron spectrum, (proc. (NDS)-146/L, 1983

/ 7/ W.P. Poenitz, T. Tamura, loc. cit. (5), p. 465 and loc. cit. (6), p. 175

/ 8/ R. Böttger, et al., loc. cit. (11), p. 484

/ 9/ D.J. Madland, R.J. Labauve, Report, (LA-UR-84-129, 1984)

/10/ B.F. Gerasimenko, V.A. Rubtchenya, Nejtronnaya Fizika (Kiev, 1984), part 1, p. 349

/11/ O.I. Batenkov, M.V. Blinov, V.A. Vitenko, Physics and chemistry of fission, (Vienna, 1980), p. 267

STUDY OF THE RELATIONSHIPS BETWEEN THE CHARACTERISTICS OF MASS, ENERGY, AND NEUTRON MULTIPLICITY DISTRIBUTIONS AT THE ^{252}CF SPONTANEOUS FISSION

I.D. Alkhazov, V.D. Dmitriev, A.V. Kuznetsov, S.S. Kovalenko, K.A. Petrzhak, B.F. Petrov, L.Z. Malkin, V.I. Shpakov
V.G. Khlopin Radium Institute, Leningrad, USSR

The main purpose of this work was to study relationships between the characteristics of energy and mass distributions of the ^{252}Cf spontaneous fission fragments and those of prompt neutron multiplicity distributions.

The experiment was performed using an experimental set-up consisting of a large liquid gadolinium loaded scintillation neutron counter, a chamber with two surface-barrier silicon fission fragments detectors and a data aquisition system based on the two processor computer system. The information on both fragment pulse-height and the number of neutrons was received by the terminal computer and after preliminary processing was transmitted to the main computer, where it was written down in a form of three dimensional array A1-A2-N (where A1 and A2 were fragment pulse heights, N - was number of neutrons). Further processing of the data was performed by means of the main computer after the experiment had been completed. The experimental data array was transformed thereat from the A1-A2 coordinates into coordinates of total kinetic energy-mass (E_k, M) using the procedure proposed by Schmitt /1/. Then the momenta of neutron multiplicity distributions were calculated for each particular value of E_k, M and besides an unfolding of initial multiplicity distributions was performed to obtain fragment masses distributions for every separate number of neutrons. The schematic drawings of the main contours of these distributions are presented in Fig. 1. It can be seen, that the distributions are shifted in position along the energy axis as the neutron number rises and do not move relative to the mass axis. The widths of both distributions increase.

The characteristics of both neutron and energy-mass distributions quoted in some works before (for instance /2, 3/ agree with our results and we will not therefore fix attention on its descriptions and discussions. Complexity of the multidimensional information representation forces us to be restricted by a consideration of some separate correlations obtained mainly for the first time.

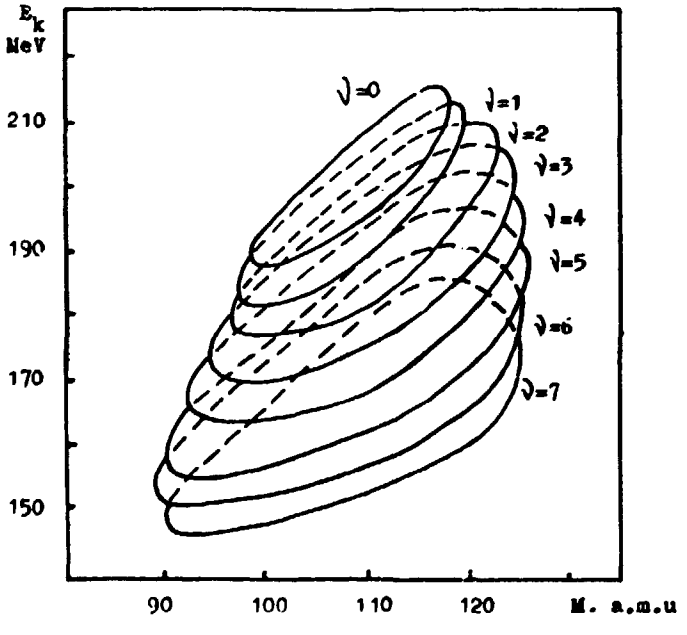

Fig. 1:
Main countors of the fragment mass-energy distributions for separate fixed numbers of neutrons.

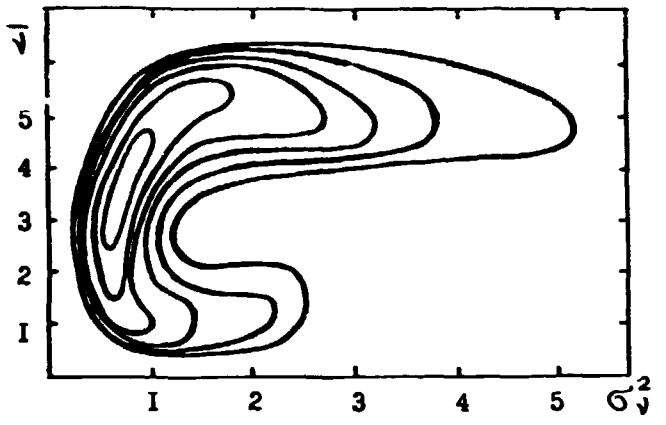

Fig. 2:
Distribution of experimental events in coordinates of (total number of events about $2 \cdot 10^6$).

Fig. 2 shows schematically the twodimensional distribution of all the array in coordinates of $\bar{\nu}$ - σ_ν^2. The essential part of this distribution corresponds to a conventional form of multiplicity distribution with a weakly varying parameter of form. At the same time two regions can be seen with practicaly constant $\bar{\nu}$ -value and significant variation of dispensions σ_ν^2. These are regions with high value of $\bar{\nu}$ ($\bar{\nu} \sim 5$) and low value of($\nu \sim 1$). Presence of these two separate branches can suggest, on our opinion, existense of two different processes in the fission mechanism. One of the possible assumptions is: the lower branch corresponds to the ternary fission. The upper branch corresponds apparently to the region of low fragment kinetic energies, where, as it can be seen in Fig. 3a, an increase of dispersion takes place with E_k decrease for the mass range of 85-105.

The following peculiarity in the relations presented in this figure can be mentioned: in the region of rather high E_k $\bar{\nu}$ rises as E_k falls down which corresponds to increase both of fragment deformation at scission point and accordingly of fragment excitation energy. For low E_k $\bar{\nu}$ does not vary with E_k for fragment masses near the symmetric ones and even decreases with E_k decrease for more asymmetric modes.

Another peculiarity can be noted in the dependences of $\bar{\nu}$ on fragment mass given in Fig.3b. The $\bar{\nu}$ -value averaged over all E_k weakly depends on fragment mass. At the same time for separate energy intervals this dependence became significant and its character changes as E_k varies. Small variations of σ_ν^2 can be seen at large variations of $\bar{\nu}$ in the region of high values of E_k. Fig. 4 presents both fragment total kinetic energy and its dispersion as a function of fragment mass for some fixed numbers of neutrons. It can be seen that as the dependences of E_k for different ν are similar to that averaged over all values of ν the character of the $\sigma^2_{E_k}$ dependences varies with the ν and is different in separate intervals of fragment masses. In the interval of the most probable masses the $\sigma^2_{E_k}$ value for fixed neutron numbers is much less than the averaged one and increases with ν , while in the mass interval $120 < M < 126$ this dependence reverses. Such behaviour of the $\sigma^2_{E_k}$ can be more obviously illustrated by Fig. 5 in which the dependences of $\sigma^2_{E_k}$ on ν is plotted for various grades of fission asymmetry.

Fig. 6 presents dependences of both mean mass value $\langle M \rangle$ and dispersions of mass distributions σ^2_M on total kinetic energy E_k for different numbers of neutrons. The dependence of $\langle M \rangle$ averaged over all ν values has a minimum at the E_k of about 150 MeV whose position is correlated with the position of the maximum observed in the dependence of σ^2_M on E_k. Similar correlation can be seen in the dependences of partial values of $\langle M \rangle$ and σ^2_M on E_k as well. It can be noted that position of such minima dependences for partial values of $\langle M \rangle$ are shifted into lower kinetic energies as $\bar{\nu}$ increases.

Complex character of the dependences of $\langle M \rangle$ and σ^2_M is confirmed by Fig. 7 and 8 in which these dependences on ν are presented in various energy intervals. It can be seen from Fig. 7 that the $\langle M \rangle$ value averaged over all E_k practically does not depend on ν , while

for separate E_k this dependence becomes significant and its character is different at different E_k. Comparison of dependences of $\langle M \rangle$ and σ^2_M on $\bar{\nu}$ as well as those on E_k allows to say about anticorrelation between them.

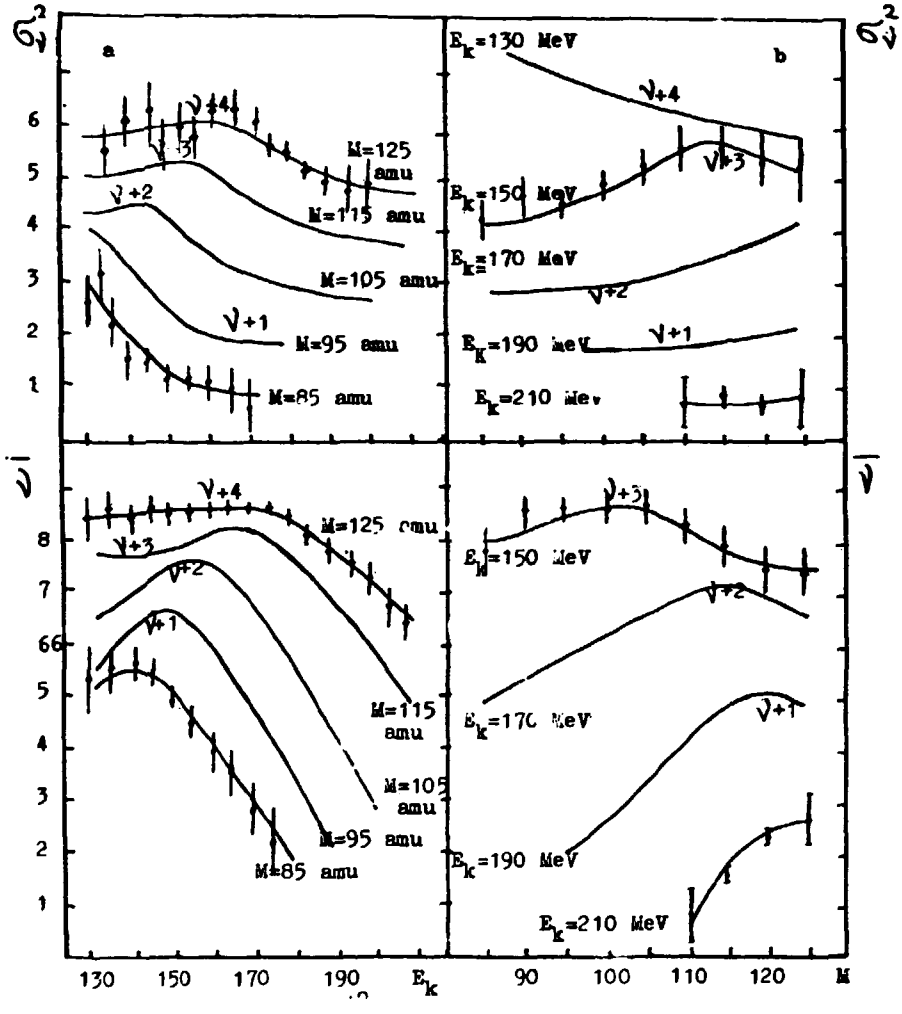

Fig. 3:
Variation of $\bar{\nu}$ and $\sigma^2_{E_k}$ as a function of the fragment total kinetic energy E_k (a) and of the fragment mass M (b).
(to avoid overlaping the curves marked ν + i are shifted along the y -axis by a value of i).

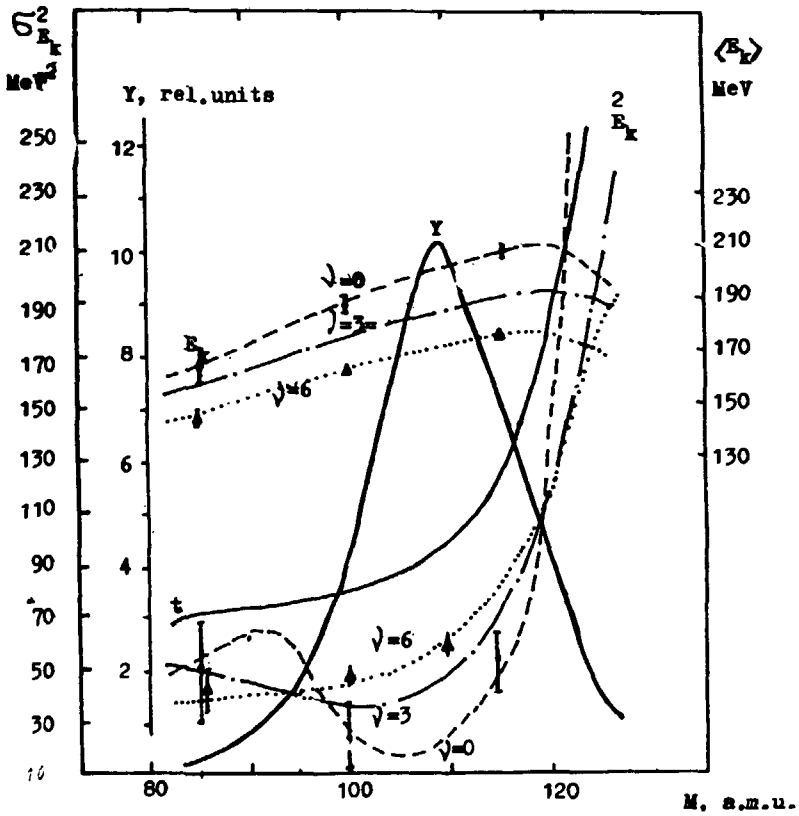

Fig. 4:

Dependencies of the fragment total kinetic energy E_k and its dispersion $\sigma^2_{E_k}$ on the fragment mass M for various numbers of neutrons

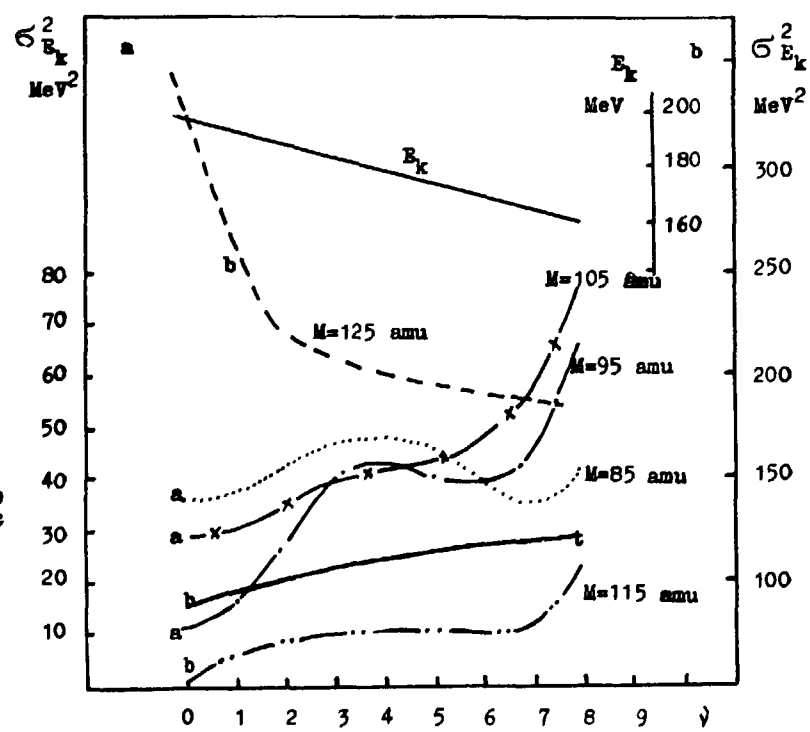

Fig. 5:

Variation of the kinetic energy dispersion $\sigma^2_{E_k}$ as a function of the number of neutrons ν for various fragment masses.
Solid lines shows both the dispersion and the kinetic energy averaged over the mass distribution.

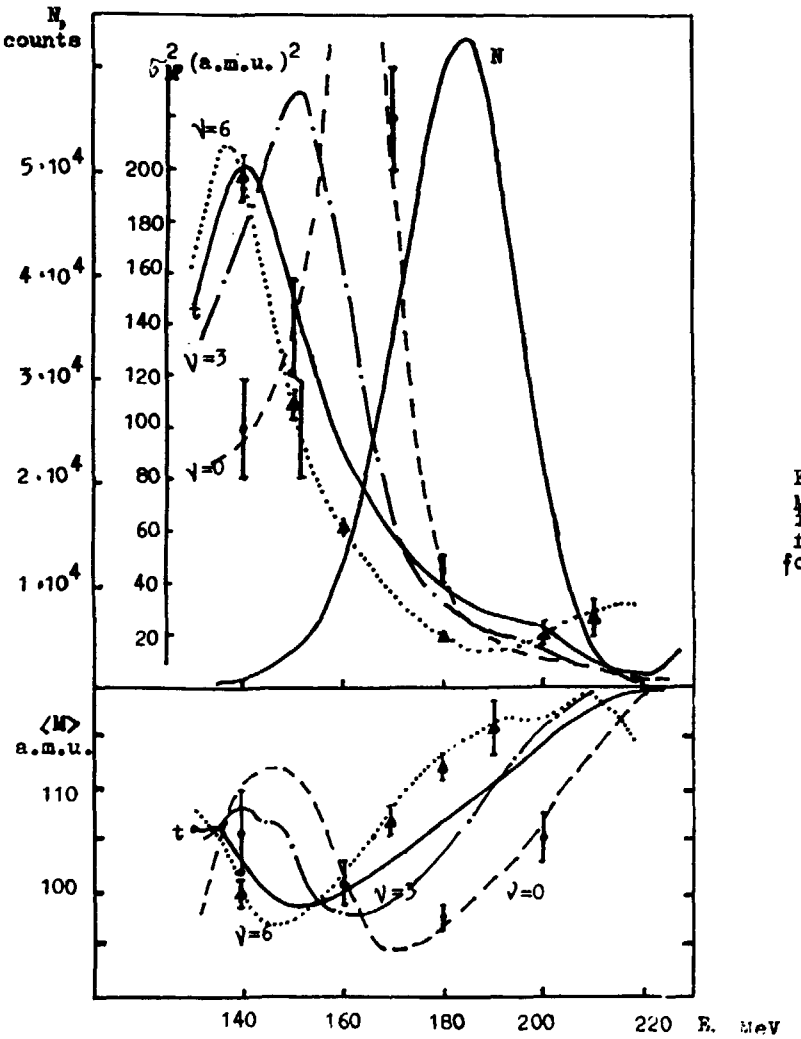

Fig. 6:
Mean fragment mass ⟨M⟩ and its dispersion σ_M^2 as a function of kinetic energy E_k for various number of neutrons

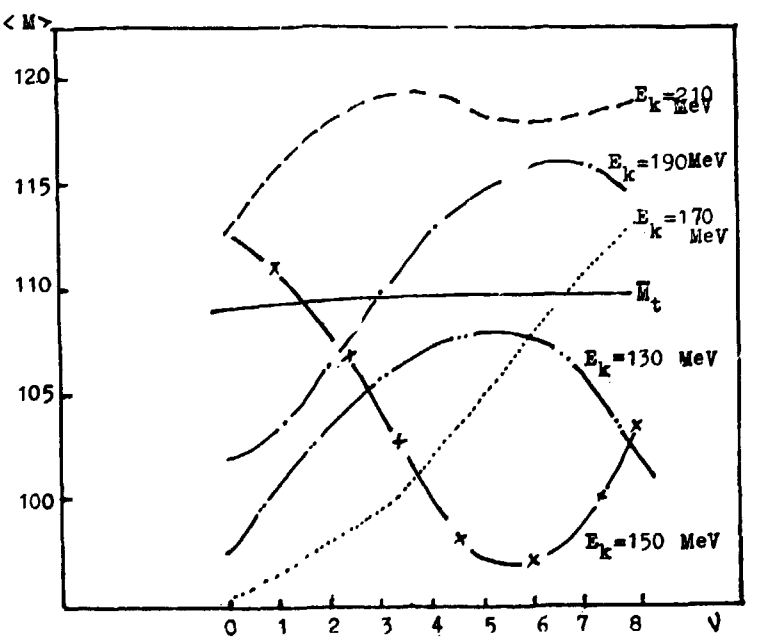

Fig. 7:
Dependence of the mean fragment mass ⟨M⟩ on the number of neutrons ν for various values of kinetic energy E_k

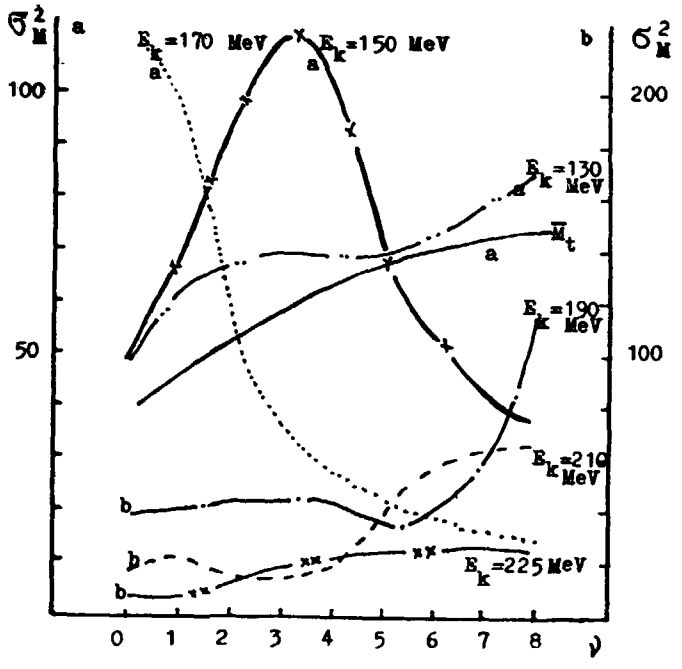

Fig. 8:
Dependence of the dispersions of mass distributions σ_M^2 on the number of neutrons ν for various values of kinetic energy E_k

No comments on relations described are proposed in this paper as the interpretation of observed peculiarities requires both careful analysis and additional information. The latter will be obtained after processing and analysis of the 2π-experiment data is completed.

References

/ 1/ H.W. Schmitt, et al., Proc. of the Internat. Symp. on the Physics and Chem. of Fission, Salzburg, 1965, Vienna, 1965, p. 531

/ 2/ H. Nifenecker, C. Signarbieux, R. Babinet, Y. Poitou, Report LBL-1950, Berkeley, USA, 1973

/ 3/ B.G. Basova, D.K. Riazanov, A.D. Rabinivich, V.A. Korostylev, Atomnaya Energiya, 46, 240, (1979)

LOW MASS FRAGMENTS FROM ^{252}Cf SPONTANEOUS FISSION

H.-G. Ortlepp, R. Kotte, F. Stary
CINR Rossendorf, GDR

Abstract: An experimental arrangement for the investigation of light charged particles from ternary fission or for searching for superasymmetric binary fission products is presented. Using a time-of-flight/energy spectrometer low mass fission products were looked for in the ^{252}Cf spontaneous fission. For the expected most probable superasymmetric fission fragment ^{48}Ca an upper limit for the superasymmetric decay branch relative to alpha emission was deduced ~~$(T_{1/2}(\alpha)/T_{1/2}(^{48}Ca) \leq 10^{-8})$~~. Measured distributions of light products with masses around A = 13, A = 18 and A = 31 and with yields of $Y = 10^{-5}$, $Y = 1.5 \cdot 10^{-5}$ and $Y = 3 \cdot 10^{-6}$ respectively, were ascribed to ternary fission.

1. Introduction

Starting with the discovery of ^{14}C emission from ^{223}Ra by Rose and Jones /1/ in 1984 both theoretical and experimental physicists were attracted by this new kind of radioactivity intermediate between alpha decay and spontaneous fission. Gales et al. /2/ and Alexandrov et al. /3/ confirmed the experimental results. Already in 1980 Sandulescu et al. /4/ predicted in the region of heavy nuclei with $Z \geq 88$, "a new type of decay which can be interpreted as highly mass-asymmetric fission or as emission of a heavy cluster". It was shown that the influence of shell effects for some particular two-body fragmentations gives rise to a barrier penetrability which is comparable to the penetrability for alpha decay. The first predictions for branching ratios relative to alpha emission delivered values which underestimated the heavy cluster emission mode (with the 1980 variant one obtains a partial lifetime of $T_{1/2}(^{14}C) = 10^{17.7}$ s instead of 10^{15} s found in the later experiment /1/). More refined calculations of Poenaru et al. /5,6,14,18,19/ and Shi & Swiatecki /9,10/ were not only in excellent agreement with the experimental findings but predicted a broad range of cluster emitting nuclei deserving attention for further experiments. Recently, a number of such superasymmetric fission modes was observed: Price et al. /12/ found the ^{14}C radioactivity of ^{222}Ra and ^{224}Ra with branching ratios relative to the alpha decay of $B = (3.7 \pm 0.6) \times 10^{-10}$ and $B = (4.3 \pm 1.2) \times 10^{-11}$, respectively. The spontaneous ^{24}Ne emission modes were discovered by Barwick et al. /11/ for ^{232}U ($B = (2.0 \pm .5) \times 10^{-12}$), by Sandulescu et al. /7/ for ^{231}Pa ($B = 6 \times 10^{-12}$) and by Tretyakova et al. /8/ for ^{233}U ($B = (7.5 \pm 2.5) \times 10^{-13}$). All these heavy cluster emissions lead to the doubly magic ^{208}Pb or to isotopes in it's immediate neighbourhood as was expected by the theoretical estimations. The experimentally determined branching ratios offer now the possibility to test and improve the barrier penetrability calculations.

Rose and Jones /1/ identified the ^{223}Ra decay products with a solid state counter telescope. They kept the alpha-rate below 4000/s to avoid unacceptable multiple alpha-pile up. Extending the measurement over 189 days they collected eleven events of ^{14}C. By using a 7.5 times more intensive source in connection with the superconducting magnetic spectrometer SOLENO Gales et al. /2/ obtained the same number of ^{14}C events within five days. The second confirmation by Alexandrov et al. /3/ was undertaken with the technique as used by R. & J. but with a more intensive source. After 30 days seven events of ^{14}C were collected. The ^{14}C radioactivities of ^{222,224}Ra were found with polycarbonate track-recording films /12/. The ^{24}Ne decays of ^{231}Pa /7/, ^{232}U /11/ and ^{233}U /8/ were discovered with the help of polyethyleneterephthalate track detectors. Plastic track detectors proved to be ideally suited for selecting afew highly ionizing particles on a huge background of less ionizing particles.

2. Measurements with a time-of-flight spectrometer

The aim of our experiment was to search for rare decay modes with pure electronic instrumentation. We investigated the spontaneous fission fragment distribution of a 3 μCi ^{252}Cf source by measuring the time-of-flight (TOF) and energy (E) of the emitted particles (fig. 1). The heavy products release secondary electrons in a 27 $\mu g \cdot cm^{-2}$ Formvar foil covered with

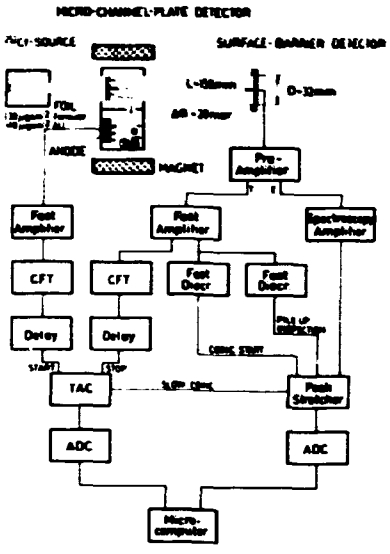

Fig. 1: Experimental set-up

10 μg·cm^{-2} Al which are accelerated and bent on a Chevron set-up of microchannel plates (MCP) delivering the start signals for the time-to-amplitude-converter (TAC) via a constant fraction trigger (CFT). The stop signals as well as the E-information were taken from an 800 mm^2 surface barrier detector (SSD) 15 cm apart from the start detector. For the 6.12 MeV ^{252}Cf alpha-particles the energy resolution amounted to $\Delta E/E$ = 2 %. The resolving time of Δt = 670 ps (FWHM) dominated the mass resolution of $\Delta m/m \sim 15$ % for alpha particles which should be somewhat better for heavier particles. Multiple alpha-pile up and alpha-fission fragment-pile up were suppressed by the pile up inspector of a special pulse stretcher which also provided the slow coincidence with the TAC. The signals were digitized by two ADCs and stored into a 64 x 64 channels matrix of a microcomputer. The data were analysed off-line. The solid angle $\Delta\Omega$= 20 msr and the efficiency $\varepsilon_\alpha < 50$ % of the MCP-detector resulted in an alpha particle counting rate of $\dot{N}_{\alpha,c} \sim 120\ s^{-1}$ In a first run 1.2 x 10^6 fission fragments (ff) were collected, but a fairly big number (50) of α-ff-pile up events was recognized due to the finite resolving time (100 ns) of the pile up inspector. The single counting rates of the SSD were $\dot{N}_\alpha \sim 270\ s^{-1}$ and $\dot{N}_{ff} \sim 10\ s^{-1}$, respectively. In a second run 3 x 10^6 fission events were measured with a raised threshold of the start-CFT in order to avoid 99 % of alpha particle triggering, which resulted in a two orders of magnitude reduction of α-ff-pile up. The TOF-calibration was performed with calibrated delay cables and with the help of the known velocity of the 1.54 MeV/amu ^{252}Cf alpha particles. The energy calibration was based on the alpha particle and light fragment energy peaks as well as the TOF-E correlation of the light fragments.

From recent predictions of Poenaru et al. /18/ the most favoured superasymmetric fission products of ^{252}Cf should be ^{46}Ar or ^{48}Ca with branching ratios of B $\sim$ 2.5 x 10^{-14} relative to alpha decay and kinetic energies of $E_k \sim 100$ MeV, i.e. E/A $\sim$2.2 MeV. No event has been found in this area of the TOF-E-plot.

The low energy tails of the fission fragment peaks with correct TOF we ascribe to backscattering of fission fragments in the SSD. All other events within the region $E > E_\alpha$, $v \gtrsim v_\alpha$ are to be ascribed to one of the following effects:

i) Events with flight times within the non-linear TAC characteristics are out of range of reasonable physical velocities.

ii) Events with $E > E_\alpha$ and flight times TOF = TOF(α) $\pm$ Δt, i.e. E/A = 1.35...1.85 MeV, were attributed to α-ff-pile up.

iii) Light fragments with A $\leq$ 20 and high velocities (E/A $>$ 2 MeV) which are not allowed for binary fission due to the Q-value systematics were attributed to the known ternary fission process:

Raisbeck et al. /15/ measured light charged particles (LCP) up to carbon from ^{252}Cf ternary fission. Energy ranges of E_α = 7...41 MeV and E_t = 5...24 MeV and abundances per fission of 3.2 x 10^{-3} and 2 x 10^{-4} for alpha particles and tritons, respectively, were determined. These high energetic LCP are present in our TOF-E-plots, especially in the first run (fig. 2a). However, from our experiment no yield value may be deduced because of the unknown efficiency of the start detector for the lightest particles.

Raisbeck et al. found also an abundance of 1.4 x 10^{-6} carbon ions per fission in the energy range E_c = 33...75 MeV. It is highly probable that this abundance will further increase if one extends the energy range to lower energies which they couldn't measure due to the necessity to shield their particle telescope from natural alpha particles by a 7.6 mg cm^{-2} Al foil. For the same reason they couldn't detect events with Z $>$ 6. Natowitz et al. /16/ observed long-range products of ^{252}Cf by track detection in mica and lexan. Integrated yields of

$Y \geqslant 1.8 \times 10^{-5}$ events per binary fission and energies of E = 1.5...4 MeV/amu were obtained for fragments of B, C, N and O. Integrated yields of $Y \geqslant 3 \times 10^{-6}$ per fission and energies of E = 1.5...2.5 MeV/amu were indicated for fragments of oxygen or even heavier nuclei ($8 \leqslant Z \leqslant 12$). Fig. 2 shows also distributions of heavier fragments with A = 13 ± 2; A = 18 ± 3; and A = 31 ± 5 which energy ranges extend down to E/A ~ 0.9 MeV. These fragments might be attributed to the ternary fission process due to their energy and velocity ranges. From our experimental results yields per binary fission of $Y_{13} = 10^{-5}$, $Y_{18} = 1.5 \times 10^{-5}$, and $Y_{31} = 3 \times 10^{-6}$ were deduced for the emission of low energy fragments with masses A ~ 13, A ~ 18 and A ~ 31, respectively, in the velocity range corresponding to 0.9 MeV $\leqslant$ E/A $\lesssim$ 3 MeV.

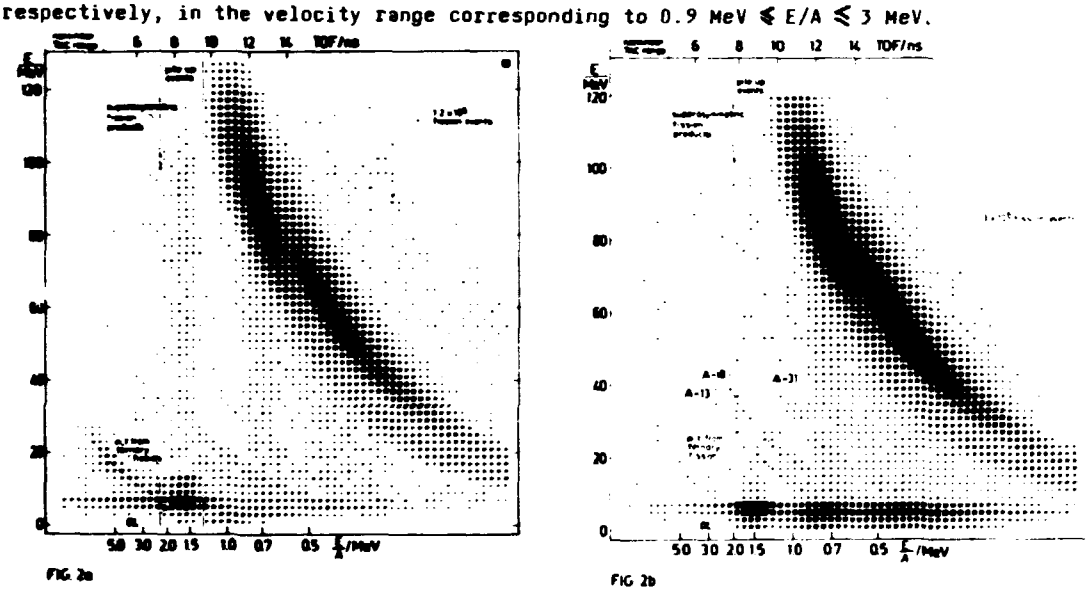

FIG. 2a FIG 2b

Fig. 2: TOF-E-plots for ^{252}Cf fission products
a) low start trigger level; b) high start trigger level

3. Conclusions

We tried to identify rare ^{252}Cf-fission events by a time-of-flight-spectrometer. Due to the low ^{252}Cf source acitivity (3 μCi) only 3×10^6 fission events could be collected within a run of 64 hours allowing to determine an upper limit $B_{max} = 10^{-8}$ for the branching ratio of spontaneously emitted superasymmetric fission product as ^{46}Ar or ^{43}Ca. In order to detect this rare decay mode of ^{252}Cf which was predicted by Poenaru et al. /18/ with branching ratios of $B \sim 10^{-14}...10^{-13}$ the counting rate must be increased by four orders of magnitude and the measuring time by one or two orders of magnitude. Simultaneously, the radiation damage of the solid state detector will increase considerably. The radiation damage by 'normal' binary fission products could be prevented by an Al absorber foil of thickness $\Delta x \sim 4$ mg·cm^{-2} which allows the superasymmetric fragments to be detected. However, the ^{252}Cf alpha particles would not be absorbed, too. The alpha counting rate would exceed the lethal dose ($\sim 10^{11}$ cm^{-2}) of the SSD by two orders of magnitude. Consequently, the search for superasymmetric fragment emission from the ^{252}Cf binary fission is hopeless with our electronic equipment. ^{252}Cf highly mass-asymmetric binary fission products in our opinion could be detected by plastic track detectors which are not only insensitive to $\sim 10^{14}$ cm^{-2} alpha particles but also to $\sim 10^6$ cm^{-2} high energetic light nuclei from ternary fission, e.g. 50 MeV ^{12}C. 'Normal' binary fission products might be stopped in an absorber foil.

However, ^{252}Cf ternary fission with abundances per binary fission from 3×10^{-3} to 10^{-6} for alphas and carbon ions, respectively, may be an object of investigation with our TOF-E-technique.

4. References

/1/ Rose, H.J. and G.A. Jones, Nature 307 (1984) 245

/2/ Gales, S., E. Hourani, M. Hussanois, J.P. Schapira, L. Stab, and M. Vergues, Phys. Rev. Lett. 53 (1984) 759

/3/ Alexandrov, D.V., A.F. Beljazkij, J.A. Gluchov, E.J. Nikolskij, B.G. Novazkij, A.A. Ogloblin, and O.N. Stepanov, Letters to the Sov. Journ. Exp. Theor. Phys. 40 (1984) 152

/4/ Sandulescu, A., D.N. Poenaru, and W. Greiner, Sov. Journ. Part. Nucl. 11 (1980) 528 (E.Ch.A.Ja. 11 (1980) 1334)

/5/ Poenaru, D.N. and M. Ivascu, J. Phys. (Paris) 44 (1983) 791

/6/ Poenaru, D.N., M. Ivascu, A. Sandulescu, and W. Greiner, J. Phys. G10 (1984) L183

/7/ Sandulescu, A., Y.S. Zamyatnin, I.A. Lebedev, B.F. Myasoedov, S.P. Tretyakova, D. Hasegan, JINR (Dubna) Rapid Communications No. 5-85

/8/ Tretyakova, S.P., A. Sandulescu, Y.S. Zamyatnin, Y.S. Korotkin, and V.L. Micheev, JINR (Dubna) Rapid Comm. No. 7-85

/9/ Shi Yi-Jin and W.J. Swiatecki, Nucl. Phys. A438 (1985) 450

/10/ Shi Yi-Jin and W.J. Swiatecki, Phys. Rev. Lett. 54 (1985) 300

/11/ Barwick, S.W., P.B. Price, and J.D. Stevenson, Phys. Rev. C31 (1985) 1984

/12/ Price, P.B., J.D. Stevenson, S.W. Barwick, and H.L. Ravn, Phys. Rev. Lett. 54 (1985) 297

/13/ CERN-Courier 24 (1984) 380

/14/ Poenaru, D.N., M. Ivascu, A. Sandulescu, and W. Greiner, JINR (Dubna) Comm. E4-84-446, E4-84-811

/15/ Raisbeck, G.M. and T.D. Thomas, Phys. Rev. 172 (1968) 1272

/16/ Natowitz et al., Phys, Rev. 169 (1968) 993

/17/ Kondurov, I.A., A.M. Nikitin, D.M. Selivestov, and B.P. Konstantinov, IAEA INDC(CCR)-162)GJ

/18/ Poenaru, D.N., M. Ivascu, ICEFI (Bucuresti) - NP-39-1984, NP-41-1985

/19/ Poenaru, D.N., W. Greiner, K. Depta, M. Ivascu, D. Mazilu, and A. Sandulescu, JINR (Dubna) Communications E7-85-431

EXPERIMENTAL ARRANGEMENT FOR THE MEASUREMENT OF CORRELATIONS BETWEEN FISSION PRODUCTS AND NEUTRONS

W.D. Fromm[a)], H. Märten[b)], W. Neubert[a)], D. Richter[b)], and D. Seeliger[b)]

[a)] Zentralinstitut für Kernforschung Rossendorf, DDR - 8051 Dresden, PF 19, GDR

[b)] Technische Universität Dresden, Sektion Physik, DDR - 8027 Dresden, Mommsenstrasse 13, GDR

Abstract

The energy (E) and angle (Θ) dependent emission probability N(E,Θ) of fission neutrons is measured by the use of two parallel-plate avalanche counters (PPAC, one position-sensitive) for fragment detection (time of flight, direction) as well as two neutron detectors (D1, D2) for neutron detection (time of flight, detector response). The paper includes a description of the experimental set-up, the multiparameter data acquisition and processing, and the analysis procedures. The arrangement permits the measurement of neutron angular distributions (in dependence of E) (i) for the whole angular range, (ii) with an angular resolution close to 3 deg, and (iii) with a rather high angle point density (up to 120 points in π).
Due to the determination of the emission angle Θ by the measurement of fragment direction, i. e. fixed neutron detector position, systematic errors are avoided widely.

1. Introduction

A detailed study of the mechanism of fission neutron emission is only possible on the base of a precise measurement of $N(E,\Theta;P_f)$ (P_f-fragment parameter set) or at least $N(E,\Theta)$ as recommended by an IAEA Consultants' Meeting.[1]
Such investigations are important because of open fundamental questions (scission neutrons) as well as for practical purposes (development of models for the calculation of fission neutron spectra).[2] Concerning asymmetric fission reactions, Θ is defined as the angle between neutron and light fragment direction commonly. In any case of N(E,Θ) measurements, the determination of the fragment direction and the distinction between the light and the heavy fragment group have to be arranged. On principle, the following methods of the N(E,Θ) measurement can be applied:

i) Detection of the fragments at a fixed direction; use of one neutron detector and consecutive measurement of the neutron energy spectra for selected angles.[3]

ii) As item i), but use of several neutron detectors (multidetectorsystem) to measure N(E,Θ) at the selected angle points simultaneously (Ref. 4, but without distinction of light and heavy fragments).

iii) Use of only one neutron detector and application of a direction-sensitive method of fragment detection.

The method according to item (iii) implies the simultaneous measurement of the whole N(E,Θ) distribution applying only one neutron detector. Systematic errors concerning the other methods are avoided obviously. Two papers concerning a type-(iii) experiment have been published recently.[5,6] These arrangements rely on the use of a gridded ion twin chamber[5] and a double-PPAC set-up (one position-sensitive) - to be described in this paper in more detail - respectively.

2. Experimental arrangement

The set-up of the fragment-neutron correlation experiment is illustrated in Fig. 1 schematically. A single PPAC located beside the fission sample S (5 mm normal distance) provides the timing (STOP) signal T-PPAC for the fragment time-of-flight (TOF) and the

neutron TOF measurement (cf. Fig. 2).

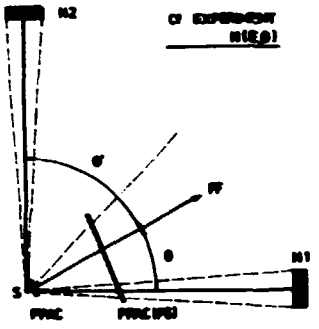

Figure 1
Schematic representation of the experimental arrangement

The position-sensitive parallel-plate avalanche counter PPAC(PS)[7] consists of an anode with an area (35 x 180) mm^2 and the complementary electrode subdived into 36 segments of 4.5 mm width. The time difference between T-PPAC and the anode signal T-A is a measure of the fragment TOF.
The PPAC(PS) segment signals are coupled into a delay line inductively (220 ns maximum delay) yielding the time signal T-DL. Measuring the time difference between T-A and T-DL one obtains the position signal which bears the information on fission-fragment (FF) direction. Two variants of the PPAC arrangement are used. The first one (variant I) covers a θ range of π/4 as illustrated in Fig. 1. In this case, the two neutron detectors N1 and N2 consist of a NE213 scintillator (5" in diameter, 1,5" thickness) and a fast photomultiplier XP 2040. The neutron flight path is chosen to be 1.6 m to measure N(E,θ) for neutron energies between 1 and 10 MeV. The normal distance between both PPAC amounts to 170 mm.
Variant II+) is used to measure N(E,θ) at low neutron energies (0.1 - 2 MeV). In this case, the PPAC set-up covers a θ range of $\frac{\pi}{2}$. Hence, the normal distance between both PPAC is lower (70 mm). Two NE 912 scintillators (35 mm in diameter, 5 mm thickness) viewed by 56 AVP photomultipliers are located at a distance of 350 mm from the source. A chamber filled with low-pressure heptane ($\sim 10^3$Pa) encases the PPAC arrangement. The timing signals T-A, T-DL, and T-PPAC are obtained by fast discrimination of the amplified PPAC pulses. They act as input signals of the time-to-amplitude converters (TAC) as illustrated in Fig. 2.

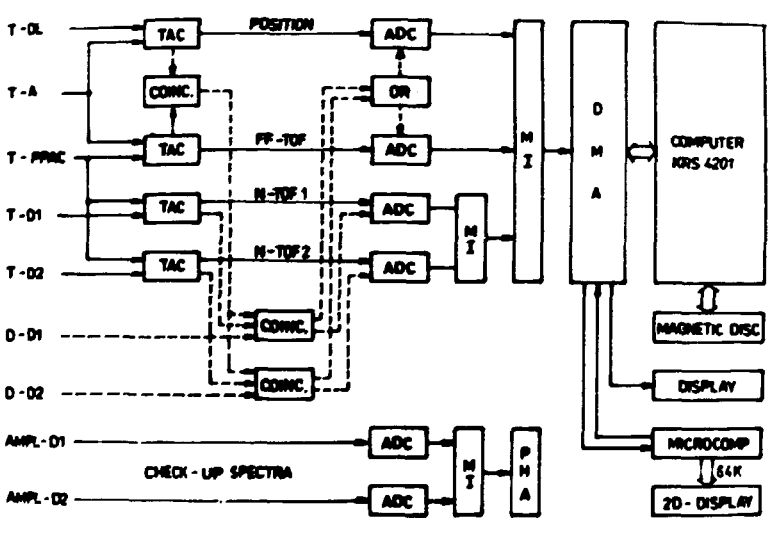

Figure 2
Scheme of signal processing and data acquisition.
Dashed lines represent logical signals.

+) Present co-operation with the Central Research Institute for Physics, Budapest (cf. Ref. 8)

If employing NE 213 scintillators for neutron detection, n/γ-discrimination is used to suppress the background. In this case, D-D1 and D-D2 (Fig.2) are the neutron identifying signals including amplitude discrimination. The application of Li-glass scintillators (NE 912) enables amplitude discrimination only (timing single-channel analysing).
The logical signals are combined as shown in Fig. 2, i.e. the position-ADC (analogue-to-digital converter) as well as the FF - TOF - ADC are only triggered if a neutron was detected by detector D1 or detector D2 (logical OR) in correlation with a fission event (coincidence units COINC). Both neutron TOF words are combined to one digital word by an interface MI (standard interface SI 1.2). One bit bears the information on the detector number.

3. Data acquisition and analysis

Fig. 2 represents the most important components of the data acquisition system. The three-parameter data (position, FF - TOF, neutron-TOF) are red by the computer KRS 4201 via a second MI and a DMA unit (direct memory access) into a buffer (double-buffer system working alternatively). Event blocks corresponding to the buffer capacity are stored on magnetic disc. A display shows the deduced single spectra. Further, a two-dimensional spectrum whose co-ordinates (data word numbers) have to be defined can be generated by a microprocessor-controlled system with a coulor 2D-display (made in C.I.N.R. Rossendorf) simultaneously. This "2D-device" is coupled to the KRS computer via DMA. It can also be used autonomously for the acquisition of two-dimensional spectra. The amplitude spectra of both neutron detectors (AMPL-N1 and AMPL-N2, cf. Fig. 2) are also recorded by an analyser (PHA) for a continuous check-up of stability. The computer codes for the on-line data acquisition and the off-line data sorting have been written in assembler language to guarantee a very high processing speed.
All further analysis operations are performed at the KRS by the use of FORTRAN codes. The dividing line between heavy and light fragment group to be set in the FF-TOF spectrum (cf. Fig. 3) is a function of FF-direction (position amplitude) due to the position-dependend FF flight path (cf. Fig. 1). Therefore, a corresponding channel limit table has to be determined using either the 2D-device (channel-marking mode) or a special computer code. The sorting code generates the two-dimensional (neutron TOF, position)-spectra for both fragments groups on the base of this table.
The position spectra of all selected neutron energy intervals (cf. Fig. 4) are unfolded by the use of a rather simple Gaussian-fit algorithm. The peak area for a given FF direction (angle Θ) and a selected E interval divided by the PPAC(PS) segment efficiency (to be measured) is proportional to $N(E,\Theta)$.

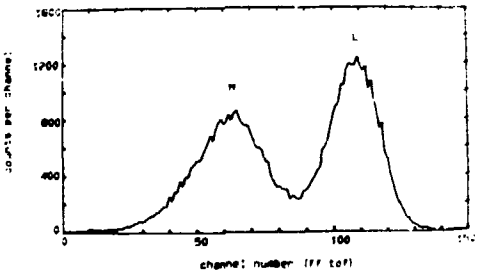

Figure 3

Typical FF-TOF-spectrum for a selected position. The arrow indicates the dividing point to distinguish between both fragment groups (minimum point)

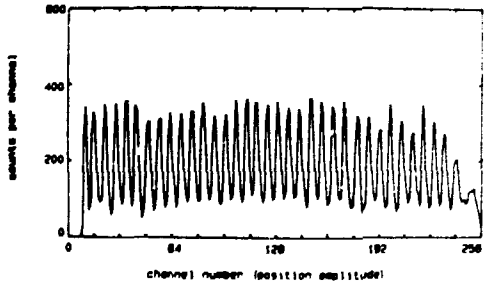

Figure 4

Typical position spectrum exhibiting 36 peaks which correspond to the PPAC(PS) segments

4. Results, Discussion

At present, the experimental arrangement described above is employed to measure the emission probability N(E,Θ) of neutrons from spontaneous fission of ^{252}Cf. This reaction represents a "standard" subject for the study of fission neutron emission. The Figures 3 and 4 show typical single spectra (FF-TOF, position). The position spectra can be unfolded satisfactorily (resolved peaks).
Using the FF-TOF spectrum for the distinction of both fragment groups a small part (2.5 %) of the fragments is not correctly classified for physical (FF-TOF is a function of fragment kinetic energy per nucleon) as well as experimental reasons (time resolution). We estimated this effect concerning the uncertainty of the N(E,Θ) data for the two variants described in chapter 2 and found it to be of minor importance.

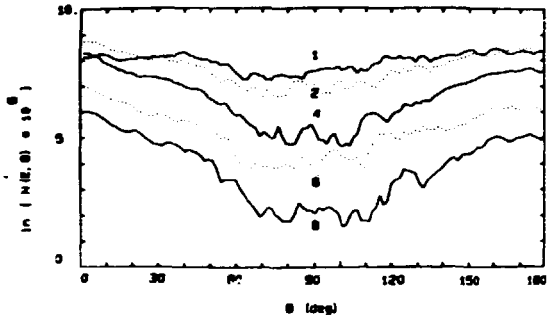

Figure 5
Measured angular distributions of neutrons shown for selected E (parameter in MeV)

Non-concentrated N(E,Θ) data measured by the use of the variant-I arrangement are shown in Fig. 5 (preliminary results of the first run, 3.1 deg angular resolution). The angular distributions represented for selected neutron energies consist of 120 angular points covering the whole angular range. A reasonable data concentration is intended to be realized in the final analysis of all experiments.
Note that the two variants of experimental arrangements are adapted to the expected attributes of N(E,Θ) in both energy ranges. This concerns the PPAC set-up specifically. The higher average FF flight path of variant I enables a better distinction between the fragment groups. This is necessary due to the high emission anisotropies at high E. First experimental results concerning variant-I measurements have been discussed in Ref. 6. The data exhibit much higher anisotropies for neutron energies above 4 MeV than previous ones[3,9].
Further measurements and comprehensive comparisons between experiment and theory[6] are in progress to make a contribution to the clarification of the picture of fission neutron emission.

References

1 Proc. IAEA Cons. Meet. on the U-235 Fast-Neutron Fission Cross-Section, and the Cf-252 Fission Neutron Spectrum, 1983, Smolenice (CSSR), INDC(NDS)-146/L (1983)

2 H. Märten and D. Seeliger, Proc. IAEA AGM on Nuclear Standard Reference Data, Nov. 1984, Geel (Belgium), IAEA-TECDOC-335 (1985) 255

3 H.R. Bowman et al., Phys. Rev. 126(1962)2120

4 E.A. Seregina and P.P. Dyachenko, Yad. Const. Vol. 1(1985)58

5 C. Budtz-Jørgensen and H.H. Knitter, Proc. Int. Conf. on Nucl. Data for Basic and Appl. Sci., May 1985, Santa Fe (USA), in press

6 H. Märten et al., ibid

7 W. Neubert et al., Nucl. Instr. Meth. 204(1983)453

8 A. Lajtai et al., loc. cit. (2), p. 123

9 C.J. Bishop et al., Nucl. Phys. A 198(1972)161

MULTIPARAMETER MEASUREMENTS ON CHARGED PARTICLE ASSOCIATED FISSION OF ^{236}U

J.P. Theobald

Institut für Kernphysik der Technischen Hochschule, D-6100 Darmstadt

Abstract

This is a report on two different multiparameter measurements on charged particle accompanied thermal neutron induced fission of ^{235}U:

- a measurement of relative charged particle yields and their kinetic energy distributions with the fission product separator "LOHENGRIN"

and

- a measurement of a complete set of kinematic parameters for fission fragments and associated alpha particles with the double torus ionization chamber "DIOGENES".

Both instruments are operated at the high flux reactor of the ILL in Grenoble.

1. INTRODUCTION

Light charged particles are emitted in some permillage of the essentially binary fragmentations of spontaneously or induced fissioning nuclei. In about ninety percent of these cases the charged particle is a long range alpha particle (LRA), so called because of its high kinetic energy of about 16 MeV. Particles, which have been identified as fission associates are indicated in the chart of nuclides in figure 1. There is some indication for the emission of ^{20}O 1) and ^{21}Ne 2). The search for the double magic ^{10}He was till now not successfull. This isotope can be considered as particle unstable 3)2)4).

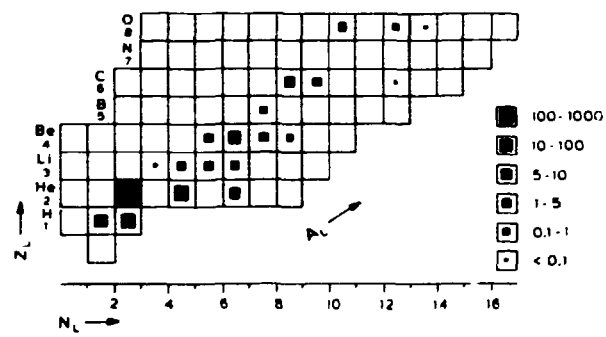

Fig. 1

Yields of observed light charged particles associating fission

Emission nearly perpendicular to the fission direction 5) is called "equatorial" that one into the fission direction "polar" 6). The latter one has been observed for alpha particles, protons, and tritons 7). Equatorial emission is followed by Coulomb focussing in the two center field of the main fission fragments. Therefore it is generally accepted that at least this type of emission occurs in space and time close to the scission point 8). The origin of the polar particles is still debated and there exist several hypotheses for their emission mechanism 9).

I shall report on results of two experiments, which were performed by a collaboration between the Technische Hochschule Darmstadt and the Centre d'Études Nucléaires de Bordeaux-Gradignan

a) Measurement of the relative light charged particles yields

Collaborators:

G. Barreau, T.P. Doan, P. Koczon, B. Leroux, M. Mutterer, C. Preuss, A. Sicre and K. Weingärtner

b) Measurement of a complete set of kinematic parameters of LRA-fission

Collaborators:

J. Pannicke, M. Mutterer, P. Heeg, F. Kraske, K. Weingärtner, G. Barreau, B. Leroux and F. Gönnenwein

The experiments were performed at the high flux reactor of the "Institut Max von Laue - Paul Langevin"(ILL) at Grenoble.

2. THE YIELD MEASUREMENT

Mass- and energy distributions of light charged particles have been measured with the fission product separator "LOHENGRIN" 10). It is an electromagnetic mass spectrometer which focusses fission products with a fixed ratio of mass number A to ionic charge q onto parabolas. Particles with different kinetic energies are displayed at different positions on these parabolas. Mass and energy resolutions $A/\Delta A$ and $E/\Delta E$ are about 10^3. "LOHENGRIN" is shown in figure 2.

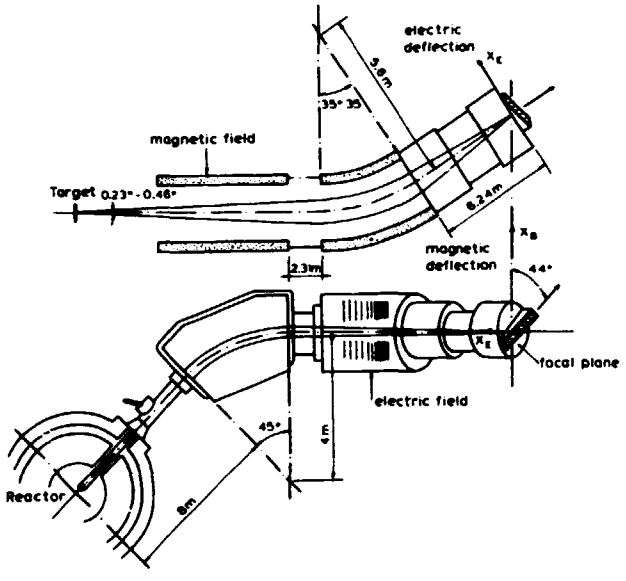

Fig. 2
The fission product separator "LOHENGRIN"

In the focal plane the light charged particles are detected in a $\Delta E/E$ telescope of surface barrier detectors for E and a ΔE proportional counter for nuclear charge identification. The telescope has a sensitive length of 52 cm and is presented in figure 3.

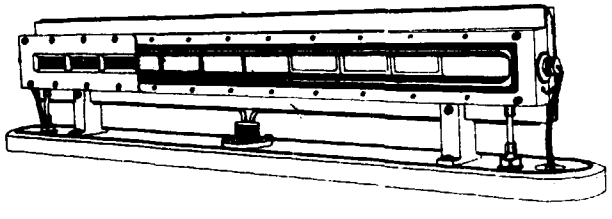

Fig. 3
The $\Delta E/E$ detector telescope in the focal plane of "LOHENGRIN"

Typical $\Delta E/E$ spectra as the one shown in Figure 4 for the case of $A/q = 3$ at $E/q = 5.6$ MeV allows a determination of the relative light particle yields, if all ionic charge states and complete energy distributions have been measured. This is not always possible due to the high voltage limitation on the electric deflector of the spectrometer, which is around 700 kV. Incomplete energy distributions have been extrapolated with Gaussians, lacking q-states by a method described in ref. 11)

(figure 5). Some of the results are listed in table 1 together with previous data by A.A. Vorobyov et al. 1).

In the third column theoretical yield values are presented calculated with a statistical model formula given by G.V. Val'ski 12).

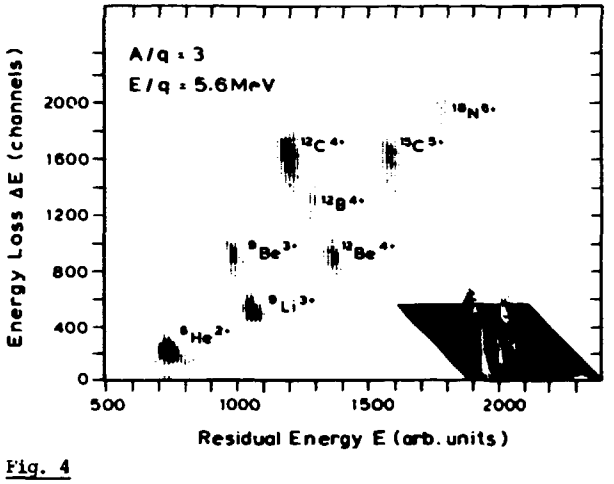

Fig. 4

Typical ΔE/E spectrum

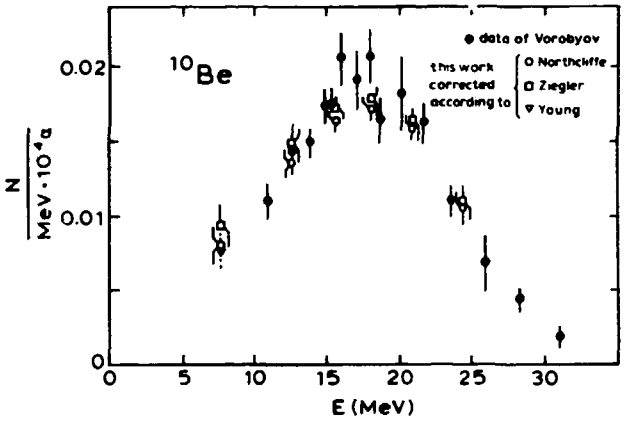

Fig. 5

Energy spectrum of ^{10}Be

ISOTOPE	YIELD/10^4 PARTICLES			MOST PROBABLE ENERGY (MeV)		FWHM OF ENERGY-DISTRIBUTION	
	[illegible]	VOROBYOV ET AL.	VAL'SKI	[illegible]	VOROBYOV	[illegible]	VOROBYOV
[illegible]		50 ± 2	130		8.05 ± 0.15		7.1 ± 0.2
		720 ± 30	1900		8.2 ± 0.2		6.5 ± 0.2
[illegible]		10^6	9200		15.9 ± 0.1		9.8 ± 0.1
	169 ± 2	191 ± 8	420	10.73 ± 0.03	11.3 ± 0.2	9.5 ± 0.1	10.8 ± 0.4
		8.2 ± 0.6	7.9		9.3 ± 0.3		8.9 ± 0.6
[illegible]		0.05 ± 0.02	0.01				
		4.1 ± 0.3	4.9		15.1 ± 0.3		13.3 ± 0.6
		1.8 ± 0.3	2.5		13.8 ± 0.4		11 ± 1
	2.2 ± 0.1	3.0 ± 0.4	3.2	12.9 ± 0.2	11.3 ± 0.4	9.8 ± 0.5	11 ± 2
[illegible]	1.7 ± 0.8	2.9 ± 0.3	1.6	12.5 ± 0.7	17.5 ± 0.4	9 ± 3	12.9 ± 0.9
	32.00± 0.07	32 ± 2	7.6	17.2 ± 0.1	17.7 ± 0.4	17.8 ± 0.3	16.1 ± 0.6
		2.0 ± 0.3	2.5		15.9 ± 0.8		15 ± 2
	0.7 ± 0.1	1.5 ± 0.3	0.7	14.9 ± 0.9	12 ± 2	11 ± 2	16 ± 3
	0.22± 0.02		0.4	18.8 ± 0.8		13 ± 2	
		5.4 ± 0.6	4.5		21.8 ± 0.7		19 ± 2
	1.3 ± 0.1		5.1	21.5 ± 0.4		12.8 ± 0.8	
	0.06± 0.02		0.6	19 ± 1		14 ± 2	
	2.7 ± 0.06		0.9	19 ± 1		11 ± 1	
		0.5 ± 0.2					
	< 0.1						
	(13 ± 2)			19 ± 1		16 ± 1	

Table 1

2.1 Conclusions

From the data of table 1 and the calculations with Val'ski's formula the following conclusion can be drawn:

i) Light particles with even Z are more frequent than odd Z nuclei (figure 1)

ii) A similar odd-even effect for the neutron numbers is less pronounced

iii) The mean kinetic energy of particles with $Z \geq 5$ does not vary considerably

iv) Emission of particles as heavy as Neon have been observed

v) Yields of protons are covered by neutron-proton recoil products.
Reliable yields of ^{12}C and ^{16}O are also not available, as collisions of fission fragments with natural nuclei prohibit accurate yield measurements.

vi) ^{10}He is most probably particle unstable.

vii) Heavier charged particles $Z > 2$ are created also in low excited states.

3. THE KINEMATIC PARAMETER MEASUREMENT

The measurement of a complete set of kinematic parameters for charged particle associated fission have to be restricted to the case of alpha particle emission, because of the rareness of the other species. Even in this case highly efficient detector systems are necessary.

We have constructed the double torus ionization chamber "DIOGENES" 13) shown in figure 6. It consists of two concentric gridded chambers with a toroidal shape surrounding an evacuated target cylinder. Position sensitive proportional counters are inserted into the window frames between the two chambers. The inner chamber measures fragment, the outer one and the proportional counters alpha particle parameters.

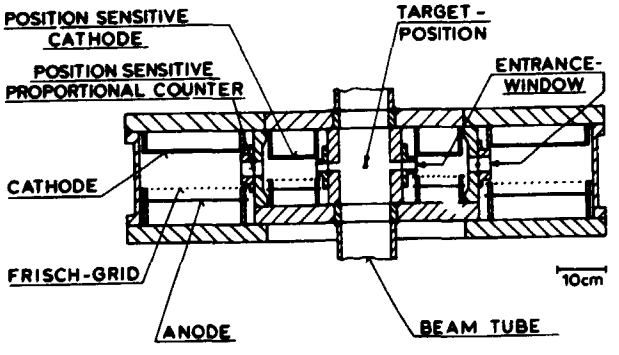

Fig. 6
Double torus ionization chamber "DIOGENES"

The following quantities have been recorded during the experiment in list mode

i) the kinetic energy of the main fragments,

ii) their specific energy loss,

iii) two angles to define their flight path direction,

iv) the light charged particle kinetic energy,

v) their specific energy loss,

vi) their flight path direction.

From these quantities energy and angular distributions for alpha particles from mass, energy separated main fragments can be deduced.

Figure 7 displays the integral particle yield as function of their energy and emission angle relative to the main light fragment direction as well as a projection of the yield onto the angle axis.

About $1.5 \cdot 10^5$ multiple coincidences have been recorded. Equatorial and polar particles are clearly separated. Therefore it is possible to plot in figure 8 fragment mass and energy distributions for alpha emission into the direction of the light and heavy main fragments (polar emission) and perpendicular to the fission axis (equatorial emission). From these plots the most probable masses

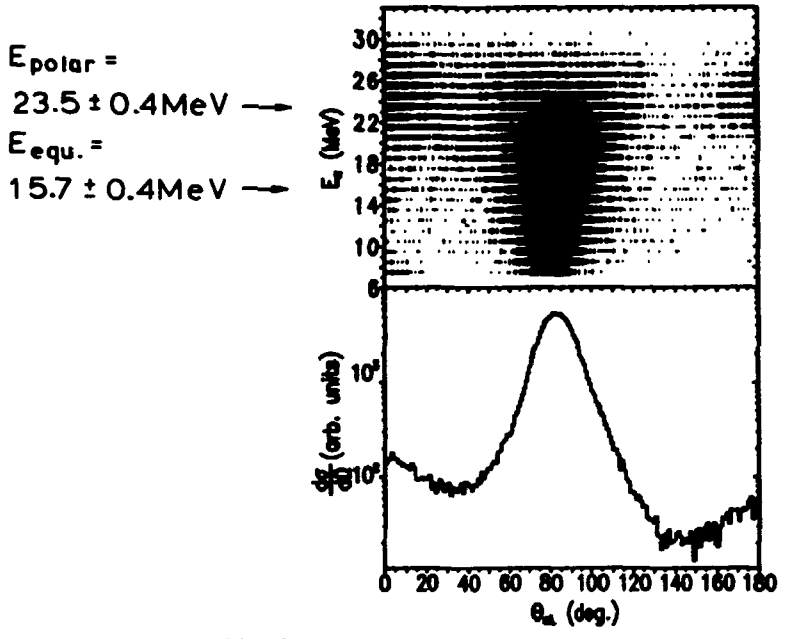

Fig. 7

Alpha particle yield as function of emission angle and kinetic energy and projection of the yield onto the angle axis.

and energies as well as the widths of the mass and energy distributions for light and heavy main fragments for the three cases can be derived and listed in table 2.

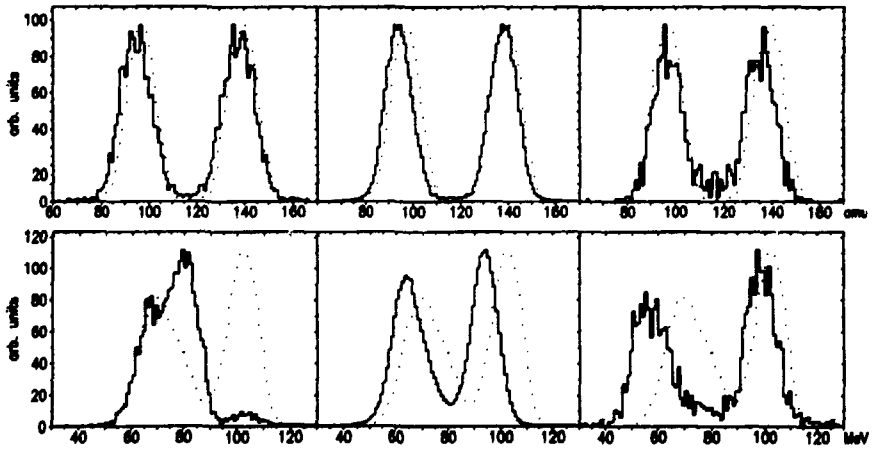

Fig. 8

Fragment mass (above) and energy (below) distributions for polar emission into the directions of the light (first column) and the heavy (last column) fragments and for equatorial emission (middle). Dotted lines represent binary fission.

	binary	θ=0°	θ=90°	θ=180°
$\langle M_L \rangle$	96.8	94.7	94.0	96.9
σ_{ML}	5.8	6.6	5.6	6.2
$\langle M_H \rangle$	139.2	137.3	138.0	135.1
σ_{MH}	5.8	6.6	5.6	6.2
$\langle E_L \rangle$	102.0	80.7	93.5	98.6
σ_{EL}	5.5	4.9	5.2	5.9
$\langle E_H \rangle$	71.4	67.5	65.0	57.8
σ_{EH}	7.7	5.8	6.5	7.0

Table 2

From our data a series of parameter correlations are available. As examples the most probable emission angles and most probable particle energies together with the width of angular and energy distributions as functions of the fragments mass ratios are displayed in figures 9 and 10.

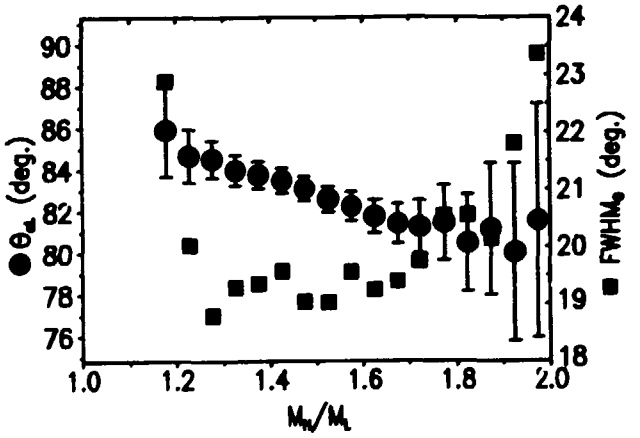

Fig. 9

Most probable emission angles and widths of the angular distributions of LRA as function of main fragments mass ratio.

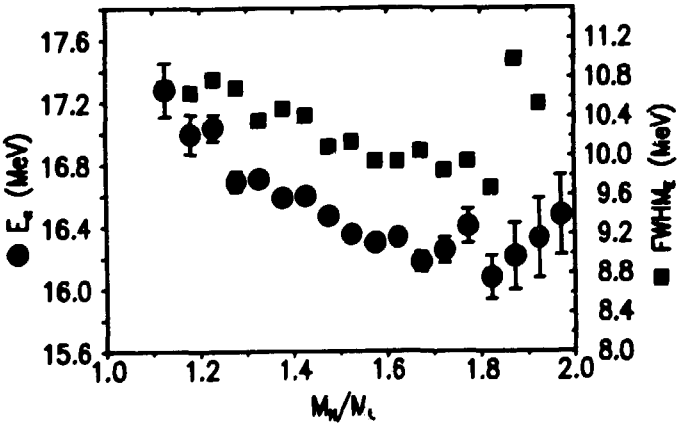

Fig. 10

Most probable kinetic energy and widths of energy distributions of LRA as function of main fragments mass ratio.

3.1 Discussion

Since the discovery of LRA fission in 1947 it has been the hope of physicists that the alpha particle carries information about the scission configuration in the fission process, i.e.

i) fragment deformation,

ii) neck elongation,

iii) interfragment distance,

iv) prescission kinetic fragment energies,

v) fragment excitation.

An interesting and encouraging paper on this subject has been published recently by H.M.A. Radi et al. 14). We have tried an inverse trajectory calculation in a two center Coulomb plus nuclear potential. From the alpha particles final kinetic energies and emission angles and the main fragments total kinetic energies the corresponding initial quan ies have been determined. Essential byproducts of these calculations are interfragment distances and fragment deformations at the instant of alpha emission. Finally spatial distributions of the starting points of the nascent particles are obtained and displayed in figures 11 and 12 for equatorial and polar emission respectively. The interfragment dis-

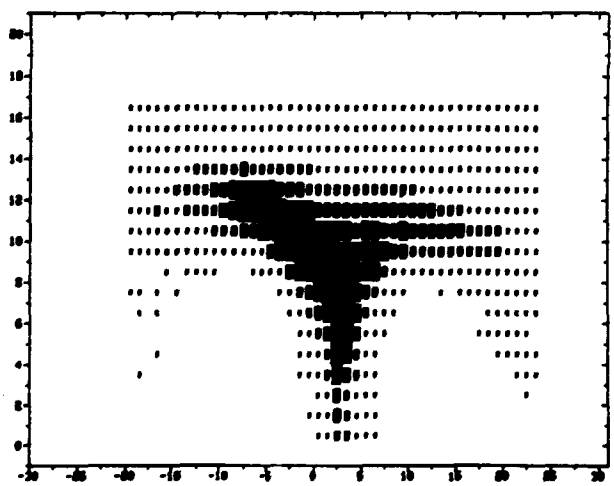

Fig. 11

Origins of equatorial alpha particles.
x-axis: distance from the center of mass
y-axis: distance from the fission axis

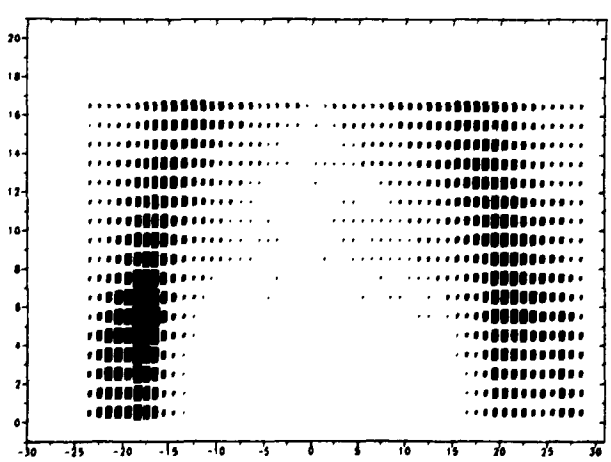

Fig. 12

Origin of polar alpha particles

tance distribution is shown in figure 13. It agrees quite well with the theoretical results of H.F.A. Radi et al. 14). Only for the fragment mass ratio of 1.4 and spherical fragments the inverse trajectory calculations have been completed. More general calculations are under way.

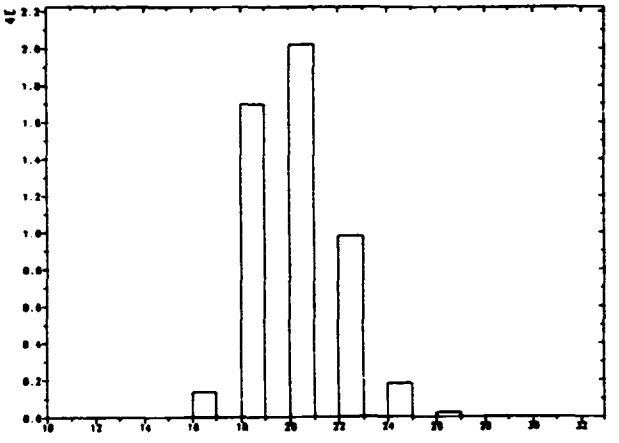

Fig. 13
Interfragment distance distribution (in fm) from trajectory calculations

3.2 Conclusions

At the present state of evaluation of our data the following conclusions are allowed:

A) on equatorial emission:

i) Equatorial alpha particles are not necessarily emitted from the neck between the nascent fragments. They can as well be emitted from the fragment bodies close to the neck, where the fragment-fragment interaction reduces the potential barrier.

ii) For the reproduction of the experimental data by inverse trajectory calculations a broad initial alpha particle kinetic energy up to about 8 MeV is imperative. Sharp initial energies do not reproduce the data.

iii) The light fragment is the main contributor to LRA fission. This underlines the fact that the heavy fragment mass peak is stabilized by the 82 spherical and the 88 deformed neutron shells. LRA fission of ^{236}U has similar fragment mass distributions as ^{232}Th binary fission.

iv) The kinetic energy of the alpha particles increases with decreasing fragment mass asymmetry, while the width of the kinetic energy distribution stays about constant.

v) The most probable angle of alpha emission Θ_α approaches 90° + the fragment's recoil angle when the fragment mass asymmetry decreases. This effect is enhanced close to symmetric fragmentation. The width of the angular distribution of the alpha particles is nearly constant as function of fragment mass ratio down to about 1.2 in spite of the increasing kinetic energy. Close to symmetric fragmentation the width increases by about 50 %. The reason for this behaviour may be the relatively high shell stabilized deformation of symmetric fragments 15) and the absence of a light fragment dominant as particle emitter.

B) on polar emission

i) Polar alpha emission is a process which can experimentally be separated from equatorial emission, i.e. the alpha yields show distinct peaks in the directions of the fission fragments. The reason for polar emission may be the enhanced barrier transparency of the poles caused by the relatively high surface curvature.

ii) Polar alpha particles into the direction of the light and heavy fragments are emitted from the corresponding fragments. This observation excludes the possibility that polar particles are scattered from the neck region.

iii) The ratio of polar to equatorial alpha particle yields are
for the emission into the direction of the light fragment ($\Theta_\alpha \leq 25^o$) 0.0240
for the emission into the direction of the heavy fragment ($\Theta_\alpha \geq 155^o$) 0.0080

iv) A part of the recoil energy on the alpha emitting fragment is transferred to the fragment partner.

C) in general

i) Inverted trajectory calculations offer a sensitive tool to derive scission point configurations from measured kinematic LRA parameter. At present, we are, however, not yet able to discuss in greater detail the quality of this information.

ii) For the understanding of LRA fission, for which multiparameter measurements have provided complete kinematic parameter sets it is essential to develop a quantum theory of alpha decay from fast changing nuclear potentials on the basis of a time dependent Schrädinger equation with a time dependent potential for alpha particles in a fissioning nuclear system. It is to be expected that equatiorial alpha emission results frm slowly variable wave functions in the region of fast neck rupture 16).

4. References

1) A.A. Vorobyov, D.M. Seleverstov, V.T. Grachov, I.A. Kondurov, A.M. Nikitin, N.N. Smirnov and Yu. K. Zalite,
Phys. Lett. 40B (1972) 102.

2) T.P. Doan, G. Barreau, A. Sicre, F. Caitucoli, B. Leroux, J.P. Theobald, M. Mutterer and P. Koczon,
International Conference on Nuclear Data for Basic and Applied Science, Santa Fe, New Mexico (1985), proceedihgs, paper J A 73

3) D.V. Aleksandrov, Yu.A. Glukhov, A.S. Demyanova, V.I. Dukhanov, I.B. Mazurov B.G. Novatskii, A. Aogloblin, S.B. Sakuta and D.N. Stepanov,
Sov. Jour. of Nucl. Phys. 36 (1982) 783

4) M. Uno and M. Yamada, private communication (1985)

5) T. San-Tsiang, Ho Zah-Wei, R. Chastel and L. Vigneron,
Phys. Rev. 71 (1947) 382
and
C. Guet, C. Signarbieux, P. Perrin, H. Nifenecker, M. Asghar, F. Caitucoli and B. Leroux,
Nucl. Phys. A314 (1979) 1

6) E. Piasecki, M. Dakowski, T. Krogulski, J. Tys and J. Chwaszczewska,
Phys. Lett. 33B (1970) 568

7) V.M. Adamov, L.V. Drapchinsky, S.S. Kovalenko, K.A. Petrzhak, L.A. Pleskachevsky and I.I. Tyutyugin,
Phys. Lett 48B (1973) 311

8) N. Cârjan, A. Sandulesku and V.V. Pashkevich,
Phys. Rev. C11 (1975) 782

9) A.J. Kordyasz, E. Piasecki, L. Nowicki, P. Koczon, J. Sobolewski, M. Kisielinski and W. Czarnacki,
Nucl. Phys. A439 (1985) 28

10) E. Moll, H. Schrader, G. Siegert, M. Asghar, J.P. Bocquet, G. Bailleul, J.P. Gautheron, J. Greif, G.I. Crawford, C. Chauvin, H. Ewald, H. Wollnick, P. Armbruster, G. Fiebig, H. Lawin and K. Sistemich,
Nucl. Instr. and Methods 123 (1975) 615

11) J.B. Marion and F.C. Young
Nuclear Reaction Analysis (1968) 34
North Holland Publ.
L. Northcliffe
Ann. Rev. Nucl. Sci. 13 (1963) 67
J.F. Ziegler
Stopping Power and Ranges in All Elements V (1977) 4, Pergamon Press

12) G.V. Val'skii
Sov. Jour. of Nucl. Phys. 24 (1976) 140

13) P. Heeg, K.F. Hoffmann, M. Mutterer, J.P. Theobald, K. Weingärtner, J. Pannicke, F. Gönnenwein, G. Barreau and B. Leroux,
Nucl. Phys. A409 (1983) 379

14) H.M.A. Radi, J.O. Rasmussen, R. Donangelo, L.F. Canto and L.F. Oliveira,
Phys. Rev. C26 (1982) 2049

15) B.D. Wilkins, E.P. Steinberg and R.R. Chasman,
Phys. Rev. C14 (1976) 1832

16) *T. Fließbach, (1985) private communication*

TRITON AND ALPHA EMISSION IN THE TERNARY FISSION OF THE ACTINIDES

C. WAGEMANS[1,2], P. D'HONDT[2], P. SCHILLEBEECKX[1,2], R. BRISSOT[3]

[1] Nuclear Physics Laboratory, B-9000 Gent, Belgium

[2] SCK/CEN, B-2400 Mol, Belgium

[3] Institut Laue-Langevin, F-38042 Grenoble, France

Abstract : The energy characteristics and the emission probabilities of the tritons and the α-particles emitted in the thermal neutron induced ternary fission of ^{233}U, ^{235}U, ^{239}Pu, ^{241}Pu and ^{241}Am have been studied using surface barrier ΔE-E telescope detectors. Within the experimental uncertainties, E_α and E_t appear to be constant, but the widths of these distributions and the α and t emission probabilities seem to be correlated with Z^2/A and with the constant for radioactive α-decay λ of the fissioning system.

1. INTRODUCTION

Although the thermal neutron induced ternary fission of the fissile isotopes has been studied since almost fourty years, significant progress has been realized mainly after 1970 with the advent of high resolution detectors, powerfull data acquisition systems and intense and clean thermal neutron beams. Taking profit of these new possibilities, a study of the thermal neutron induced ternary fission of ^{235}U has been performed by D'hondt et al.[1], with as most striking result the observation of a non-gaussian low-energy tail of the α-particle energy distribution, in contrast to the gaussian shape of the p,d,t and ^6He energy distributions. This non-gaussian α-particle energy distribution was confirmed by Caïtucoli et al.[2] (down to 2 MeV α-energy). By combining both measurements, a deviation of +6% with respect to a gaussian distribution has been determined (fig. 1).

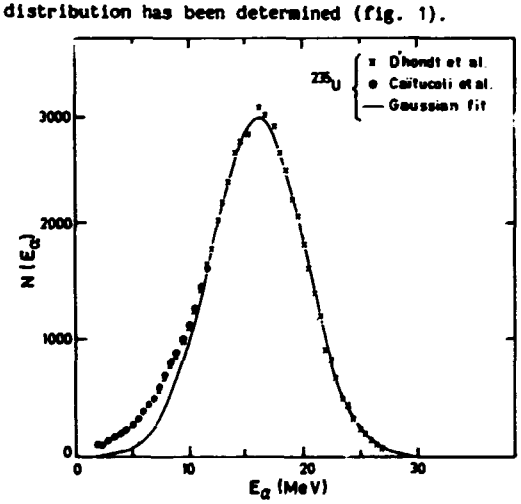

Fig.1 Demonstration of the non-gaussian tailing in the $^{235}U(n_{th},f)$ ternary α energy distribution

In the present experiments, the characteristics of the ternary α and triton emission in the thermal neutron induced fission of ^{233}U, ^{235}U, ^{239}Pu, ^{241}Pu and ^{241}Am are studied under identical experimental conditions, with high statistical accuracy, duely considering the low-energy part of the spectra and using highly enriched target material. So the relative errors are fairly small, allowing a good comparison of these characteristics as a function of Z and A of the fissioning nucleus.

2. MEASUREMENTS AND RESULTS

The measurements were performed at the 87 m curved neutron guide at the High Flux Reactor of the Institute Laue-Langevin (Grenoble). The flux at the sample position was 6 x 10^8 neutrons/cm^2.sec and the ratio of slow neutrons to epithermal and fast neutrons was about 10^6.

So the background due to fast neutron induced reactions was extremely small. The same can be said for the background due to photon induced reactions, since the direct γ-ray flux from the reactor was reduced by a factor of 10^6.

The ternary particles were detected by means of a surface barrier ΔE-E telescope detector. Several fully depleted ΔE-detectors have been used with thicknesses around 30 μm, an active area of 300 mm^2 and an energy resolution of about 40 keV for 5.5 MeV α's. The E-detector had a thickness of 700 μm, an active area of 450 mm^2 and an energy resolution of 25 keV. After amplification, the detector signals were coded and coincident ΔE-E data pairs were stored in a 512 x 512 channels matrix of a HP1000A700 computer with on-line data reduction.

Three different types of experiments have been performed, starting with the ternary α energy distribution for ^{233}U and ^{239}Pu down to about 8 MeV α-energy. In all previous work, these reactions were studied with an absorber in between target and detector, resulting in an additional energy loss and a spectral distortion. This was not done in the present experiments. Moreover, the high intensity of the neutron beam permitted to use fissile layers of 5 μg/cm^2, resulting in a negligible energy loss of the ternary α-particles in the target. These measurements clearly demonstrated that the ^{233}U and $^{239}Pu(n_{th},f)$ ternary α-particles have an energy distribution like that of $^{235}U(n_{th},f)$, i.e. deviating by about 6% from a gaussian shape.

In the second group of experiments we determined the triton-to-ternary α ratio (t/LRA) for ^{233}U, ^{235}U, ^{239}Pu and $^{241}Pu(n_{th},f)$. For $^{241}Am(n_{th},f)$, preliminary results have been obtained. During these experiments, the ΔE-E detector was shielded with 30 μm of Al, which was thick enough to stop the binary fission fragments and the α-particles emitted during the radioactive decay of the nuclei studied. In fig. 2 the energy distributions of the α-particles(a) and the tritons(b)

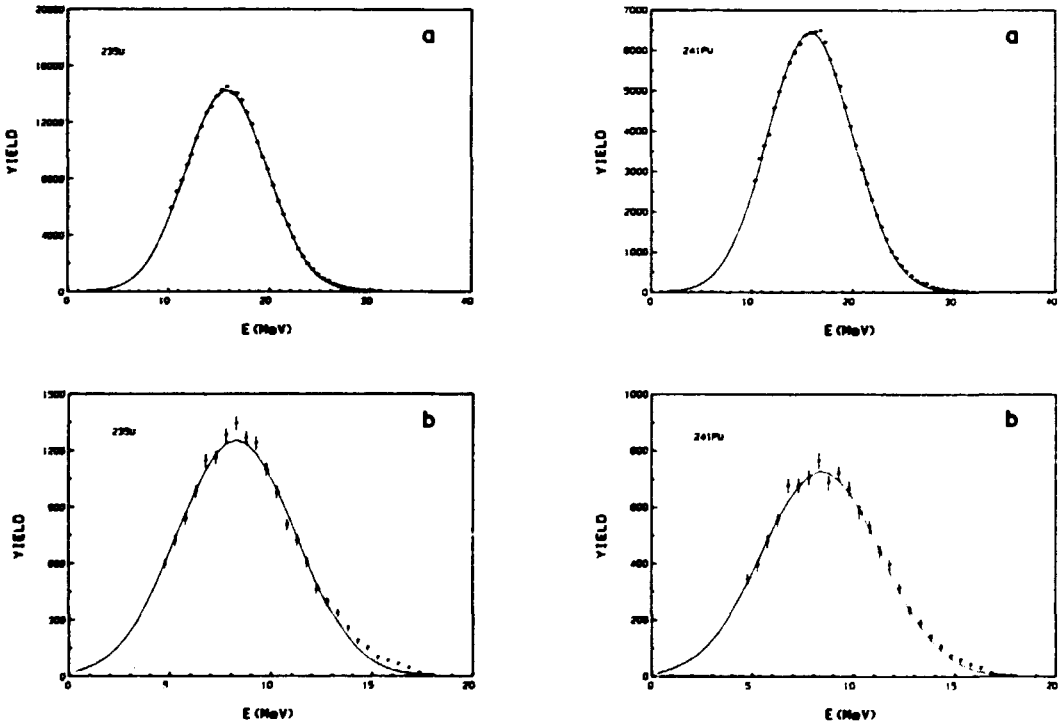

Fig. 2 Energy distributions of the ternary α-particles(a) and tritons(b) emitted in the thermal neutron induced ternary fission of ^{235}U and ^{241}Pu.

emitted in the thermal neutron induced ternary fission of ^{235}U and ^{241}Pu are shown. The full line represents a least squares gaussian fit to the data points (in the LRA case, only points above 12.5 MeV have been considered in the fit). Numerical values for the parameters of these distributions are given in table 1. In this table, also the t/LRA ratios obtained from these measurements are given, including a correction of +6% to the gaussian extrapolated LRA-yield.

Reaction	$\bar{E}_\alpha$(MeV)	FWHM(MeV)	$\bar{E}_t$(MeV)	FWHM(MeV)	t/LRA(%)	LRA/B(x10³)	t/B(x10⁴)
$^{233}U+n_{th}$	15.8±0.1	9.7±0.1	8.3±0.1	7.1±0.2	5.27±0.14	2.17±0.07	1.14±0.05
$^{235}U+n_{th}$	15.8±0.1	9.5±0.1	8.3±0.1	6.8±0.2	6.35±0.14	1.70±0.03	1.08±0.04
$^{239}Pu+n_{th}$	15.9±0.1	10.0±0.1	8.5±0.1	7.2±0.2	6.41±0.19	2.22±0.07	1.42±0.07
$^{241}Pu+n_{th}$	15.9±0.1	9.8±0.1	8.4±0.1	6.9±0.2	7.61±0.19	1.86±0.05	1.41±0.06

Table 1 Summary of the triton and LRA energy characteristics and emission probabilities

These t/LRA ratios can be converted into absolute triton emission rates once the LRA yield is determined in an absolute way. This has been done very accurately for ^{235}U by D'hondt et al.[1], who obtained a value of 589±9 for the B/LRA ratio (i.e. the number of binary fissions needed for the emission of one LRA particle). In this value the non-gaussian low-energy LRA component is included. In a third group of experiments we determined the B/LRA values for the thermal neutron induced ternary fission of ^{233}U, ^{239}Pu and ^{241}Pu relative to that of ^{235}U. For $^{241}Am(n_{th},f)$, preliminary results have been obtained. In table 1, the absolute triton and LRA emission probabilities obtained in this way are summarized.

3. DISCUSSION

The results summarized in table 1 generally agree with the corresponding data reported in the literature, when available. A detailed comparison is beyond the scope of this paper. However, all the data are compatible with a constant $\bar{E}_\alpha$- and $\bar{E}_t$- value, which is not the case for the FWHM and the yields.

In fig. 3 the FWHM-values and the absolute triton and LRA emission probabilities obtained during these measurements are plotted as a function of Z^2/A and of -log λ (λ being the radioactive α-decay constant) of the fissioning system. This figure is completed with results on the ternary α-emission for $^{237}Np(n_{th},f)$ previously obtained[3] under the same experimental conditions. The general trend for LRA/B, t/B and the FWHM of the triton and LRA energy distributions is an increase with increasing Z^2/A and a decrease with increasing -log λ. In the following alinéas we will try to interpret these correlations.

A correlation between T/B-values and Z^2/A was already observed by Nobles [4] in 1962. The quantity Z^2/A appears in the liquid drop model as the ratio of the electrostatic to the surface energy of the drop. So Z^2/A is a measure of the fissility of the fissioning system considered. Hence it has been widely used to be correlated with all sort of fission observables. Halpern[5] on the other hand correlated the LRA/B-values with a parameter 4Z-A. Both methods have in common that the proton number Z of the fissioning system is the dominant factor.

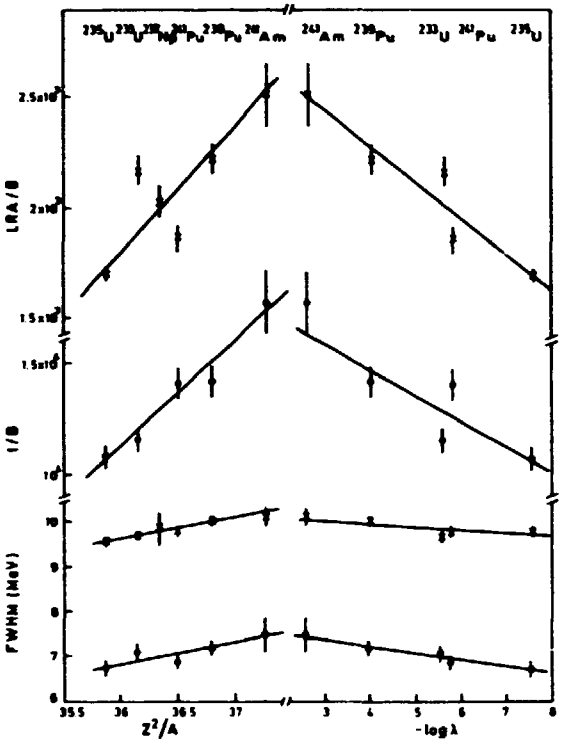

Fig. 3 Absolute ternary α and triton yields and FWHM of the α(x) resp. triton(•) energy distribution as a function of Z^2/A and of -log λ (λ being the ground-state radioactive α-decay constant) of the fissioning system. Here λ is given in year^{-1}.

The observed <u>increase of the light particle yield with increasing Z^2/A</u> can be understood as follows : Both the neutron yield and the mass yield data show that α-particle emission occurs at the expense of the excitation energy of those fragments having the largest deformation energy at scission. So the light particle yield increases with increasing deformation at scission. Since liquid drop model calculations show an increase in the deformation energy at scission with increasing Z^2/A, the observed increase of LRA/B and t/B with Z^2/A is expected. In a very recent paper, Wild et al.[6] found some evidence for a correlation between the ternary particles emission probability and the deformation energy for several spontaneously fissioning isotopes. Since the internal heating in the case of spontaneous fission is expected to be very small, they approximated the deformation potential energy at scission by Q - <TKE>. Such an approximation is however not valid for thermal neutron induced fission, since the fission mode appears to be strongly damped below the barrier.

For the observed <u>increase of the width of the LRA energy distribution with Z^2/A</u> we propose the following explanation : From trajectory calculations we know that the broadening of the LRA energy distribution is due to the coulomb field that amplifies small differences occurring in the initial LRA kinetic energy spectrum. These initial differences result from fluctuations of the scission shapes (stretching modes) which become more important with increasing deformation energy. Since the deformation energy increases with increasing Z^2/A, the observed correlation of the width of the LRA energy distribution with Z^2/A is not surprising.

Since the yield of the light particles as well as the width of their energy distributions seem to vary with Z^2/A, we want to understand why the <u>average energies $\bar{E}_\alpha$ and $\bar{E}_t$ are constant</u> within the experimental uncertainties. From the trajectory calculations we learn that the initial energies of the LRA-particles can be roughly approximated by a Boltzmann distribution with a temperature around 1.5 MeV. So the determining factors for the final LRA-energies are the angle of emission of the particles and the focusing coulomb field between both fission fragments. Guet et al.[7] for $^{235}U(n_{th},f)$ and Tsuji et al.[8] and Fluss et al.[9] for ^{252}Cf(s.f.)

determined the angular distribution of the LRA-particles with respect to the light fission fragment. For both reactions a strongly peaked distribution has been observed with a FWHM of 18.5°, the most probable angle being 81.3° for ^{235}U and 84.3° for ^{252}Cf. Apart from this peak shift of 3°, also $\bar{E}_\alpha$ as a function of the angle of emission is very similar in both cases. So the focusing coulomb field as well as the conus in which the LRA-particles are emitted appear to be rather stable when going from $^{235}U(n_{th},f)$ to $^{252}Cf(s.f.)$. This stability is probably a consequence of the well-known stability of the heavy fragment peak in the fission fragments mass-distribution, which is mainly due to the spherical Z=50, N=82 and to the deformed N=88 shells. Indeed, since $\bar{m}_H$ remains almost constant, this will also be the case for $\bar{Z}_H$, which has a strong impact on the coulomb field.The constancy of $\bar{Z}_H$ for some of the fissioning systems considered is also illustrated in a very recent paper by Gönnenwein[10]

Finally, we want to discuss the apparent correlation between the ternary fission characteristics and log λ. The idea to interpret ternary fission as an α (or t, d, p, ...) decay of the fissioning system during the last phase of the scission process has been forwarded by Cârjan[11]. In such a picture, the ternary α-emission probability is expected to be correlated with the coulomb barrier penetrability P and with the reduced α-emission width δ^2 (i.e. the probability of having an α-particle inside the nucleus). Since $\lambda=\delta^2P/h$ (h being Planck's constant), a correlation between λ and the ternary α-emission probability is likely to occur in the framework of Cârjan's model, although the λ-values used in fig. 3 are for ground-state transitions and the (n_{th},f) reactions considered are leading to a fissioning system in an excited state.

However, the parameters Z^2/A and λ are not fully uncorrelated. From a least-squares adjustment in the region $84 \leq Z \leq 98$, Viola and Seaborg[12] determined a semi-empirical relation between λ and Z : $\log 0.693 - \log \lambda = (2.11\ Z - 48.99)\ Q_\alpha^{-1/2} - (0.39\ Z + 16.95)$, λ being in sec^{-1} and Q_α being in MeV. So clearly Z is a common parameter in Z^2/A as well as in $-\log\lambda$. This makes the interpretation of the results not easier.
The apparent correlation between the ternary fission characteristics and log λ could be interpreted as giving evidence to Cârjan's model, in which the α-penetrability plays a prominent role. The Z-dependency of λ and the correlation of the ternary fission characteristics with Z^2/A on the other hand certainly do not contradict earlier models like e.g. the three point charge model, in which Z is a very important parameter.

REFERENCES

(1) P. D'hondt et al., Nucl. Phys. A 303(1978) 275 and A 346(1980) 461
(2) F. Caïtucoli et al., Z. Phys. A 298(1980) 219
(3) C. Wagemans et al., Nucl. Phys. A 369(1981) 1
(4) R. Nobles, Phys. Rev. 126(1962) 1508
(5) I. Halpern, Ann. Rev. of Nucl. Sc. 21(1971) 245
(6) J. Wild et al., Phys. Rev. C 32(1985) 488
(7) C. Guet et al., Nucl. Phys. A 314(1979) 1
(8) K. Tsuji et al., Proc. Symp. on Phys. and Chem. of Fission, Rochester (1973) p. 405
(9) M. Fluss et al., Phys. Rev. C 7(1973) 353
(10) F. Gönnenwein, Proc. Int. Conf. on Nucl. Data for Basic and Applied Science, Santa Fe(1985)
(11) N. Cârjan, J. de Phys. 37(1976) 1279
(12) V. Viola and G. Seaborg, J. Inorg. Nucl. Chem. 28(1966) 741

RESONANCE PARAMETERS OF PU-239 IN THE RESOLVED AND UNRESOLVED RESONANCE REGION

N. Janeva, Institute for Nuclear Research and Nuclear Energy,
Boul. Lenin 72, Sofia 1784, Bulgaria

ABSTRACT

The new approach to the multilevel analysis of Pu-239 neutron cross sections in the resolved and unresolved resonance region is presented. The resonance parameters and their average values in the unresolved resonance energy have been obtained.

This presentation summarizes the results obtained in cooperation between the group of Dr. Vankov from the Institute of Physics and Power Engineering, Obninsk, USSR, and our group in Sofia. The results were briefly presented at the Santa Fe Nuclear Data Conference[1] for the resolved resonance region and in some papers[2,3] for unresolved resonance region.

In the resolved resonance region the new approach to the multilevel analysis, based on the S-matrix unitarity property, is developed. The collision matrix elements for given total momentum J are

$$S^{J}_{nc}(E) = e^{i(\varphi_n+\varphi_c)}\left[\delta_{nc} + \sum_{k(J)} \frac{\Gamma^{1/2}_{kn}\Gamma^{1/2}_{ck}}{\mathcal{E}_k - E}\right] \tag{1}$$

where width amplitude $\Gamma^{1/2}_{ck}$ and level energy $\mathcal{E}_k = \mu_k + i\nu_k$ are complex values. Summing of $k(J)$ comprises the same level system.

The total cross section is a sum of Breit-Wigner terms

$$\sigma^{J}(E) = |1 - \mathrm{Re}\, S^{J}_{nn}| = \sigma_p + \frac{G_k\nu_k - H_k(\mu_k - E)}{(\mu_k - E)^2 - \nu_k^2}, \tag{2}$$

where $\sqrt{E}\,(G_k + iH_k) = 2g(J)\,\Gamma_{kn}\exp(-2i\varphi_n)$, $\sigma_p^{J} = 4\pi k^{-2} g(J)\sin^2\varphi_n$ is the potential cross section (φ_n - phase not depending on J).

The observed cross section in the resolved resonance region is a sum of two level systems with J = 1 and 0 $\sigma(E) = \sigma^1(E) + \sigma^0(E)$. Broadening with Gaussian kernel of total cross section (2) leads to the expression:

$$\sigma(E) = \sigma_p + \pi k^{-2}\sqrt{E}\sum_k \left[\frac{G_k}{\nu_k}\Psi\left(\frac{\mu_k - E}{\nu_k}, \frac{\nu_k}{\Delta}\right) - \frac{H_k}{\nu_k}\chi\left(\frac{\mu_k - E}{\nu_k}, \frac{\nu_k}{\Delta}\right)\right] \tag{3}$$

where $\Delta^2 = \Delta_R^2 + \Delta_T^2$, Δ_R - dispersion of the resolution function, Δ_T - Doppler broadening, Ψ and χ are Voigt profiles.

Using the unitarity properties in the frame of the S-matrix formalism, we obtain

$$\sum |S_{nc}|^2 = 1 = \sum\left(\delta_{nc} + i\sum_k \frac{\tilde{\Gamma}^{1/2}_{kn}\tilde{\Gamma}^{1/2}_{kc}}{\tilde{\mathcal{E}}_k - E}\right) \times \left(\delta_{nc} + i\sum_k \frac{\tilde{\Gamma}^{*1/2}_{kn}\tilde{\Gamma}^{*1/2}_{kc}}{\tilde{\mathcal{E}}^*_k - E}\right) \tag{4}$$

From (4) we have the following general relation between the resonance parameters:

$$\tilde{\Gamma}_{kn} = i \sum_{k'c} \frac{\left(\tilde{\Gamma}_{kn} \tilde{\Gamma}_{kc} \tilde{\Gamma}^{*}_{k'n} \tilde{\Gamma}^{*}_{k'c}\right)^{1/2}}{\tilde{\varepsilon}^{*}_{k} - \tilde{\varepsilon}_{k}} \tag{5}$$

From the unitarity properties of the S-matrix also follows:

$$1 - |S_{nn}|^2 = \sum_{c \neq n} |S_{nc}|^2 \tag{6}$$

The relation (2) for the total cross section leads to

$$\begin{aligned} 2\left(1 - \mathrm{Re}\, S_{nn}\right) &= 4 \sin^2 \varphi + \sum_{k} \frac{G_k \nu_k + (\mu_k - E) H_k}{(\mu_k - E)^2 + \nu_k} = \\ &= 4 \sin^2 \varphi + \mathrm{Im} \sum_{k} \frac{G_k + i H_k}{\mu_k - E - i \nu_k} \end{aligned} \tag{7}$$

Comparing (5) and (7), we obtain

$$\tilde{\Gamma}_{kn} = \frac{1}{2} e^{2i\varphi} \left(G_k + i H_k\right) \tag{8}$$

This is an unambiguous relation between the Adler-Adler parameters for the total cross section and $\tilde{\Gamma}_{kn}$ (when the phase is known).

The reaction cross section is given by the expression

$$\sigma_c = |S_{nc}|^2 = \sum_{k} \frac{G^c_k \nu_k + (\mu_k - E) H^c_k}{(\mu_k - E)^2 + \nu_k^2} \tag{9}$$

where G^c_k and H^c_k are Adler-Adler parameters for the reaction C.

This gives us the relation

$$G^c_k + i H^c_k = 2i \sum_{k'} \frac{\tilde{\Gamma}^{1/2}_{kn} \tilde{\Gamma}^{1/2}_{kc} \tilde{\Gamma}^{*1/2}_{k'c} \tilde{\Gamma}^{*1/2}_{k'n}}{\tilde{\varepsilon}^{*}_{k'} - \tilde{\varepsilon}_{k}} \tag{10}$$

or with the same meaning

$$2 \tilde{\Gamma}_{kn} = \sum_{c} \left(G^c_k + i H^c_k\right) \tag{11}$$

From (8) and (11), we obtain

$$\sum_{c \neq n} \left(G^c_k + i H^c_k\right) = e^{2i\varphi} \left(G_k + i H_k\right) - \sum_{k'} \frac{\left(G_k + i H_k\right)\left(G_{k'} - i H_{k'}\right)}{\tilde{\varepsilon}^{*}_{k'} - \tilde{\varepsilon}_{k}} \tag{12}$$

Analogously, the parameters of the absorption cross section σ_a are determined:

$$G^a_k + i H^a_k = e^{2i\varphi} \left(G_k + i H_k\right) - \sum_{k'} \frac{\left(G_k + i H_k\right)\left(G_{k'} - i H_{k'}\right)}{\tilde{\varepsilon}^{*}_{k'} - \tilde{\varepsilon}_{k}} \tag{13}$$

The absorption cross section σ_a is a sum of fission σ_f and capture σ_γ cross sections. We have the corresponding set of capture parameters:

$$G^\gamma_k + i H^\gamma_k = G^a_k + i H^a_k - \left(G^f_k + i H^f_k\right) \tag{14}$$

We elaborated the practical scheme for constructing the ^{239}Pu neutron cross sections for absorption, capture and elastic scattering, using the resonance parameters of total and fission cross sections only. We performed the multilevel analysis of the ^{239}Pu total cross section in the energy region up to 500 eV using the experimental data from /4/ with the complementary information about the level spin and the parameters from one-level analysis/5/. Our set of parameters G_k, H_k, ν_k, μ_k with σ_p = 11.3 reproduce the detailed resonance

structure of the total cross section in this region (see Fig. 1).

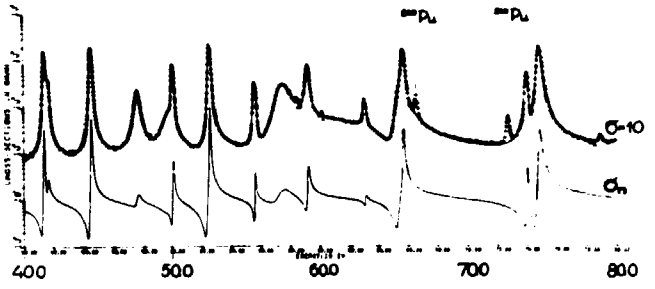

Figure 1. Total cross section of ^{239}Pu: Δ - experimental points and multilevel parametrization (-) and calculated multilevel elastic scattering cross section.

The elastic scattering cross section has the same form

$$\sigma_n^{\gamma}(E) = \pi k^{-2} g(\gamma) |1 - S_{nn}^{\gamma}|^2 =$$

$$= \sigma_p + \pi k^{-2} \sqrt{E} \sum_k \frac{G_k^n \nu_k - (\mu_k - E) H_k^n}{(\mu_k - E)^2 + \nu_k^2} \qquad (15)$$

where G_k^n and H_k^n can be obtained as a difference

$$G_k^n = G_k - G_k^a \qquad H_k^n = H_k - H_k^a \qquad (16)$$

We performed the multilevel analysis of ^{239}Pu fission cross section using the experimental data from /6/. Our set of resonance parameters for a fission cross section is adjusted with parameters of a total cross section in resonance region. On Figures 1 and 2 the ^{239}Pu neutron cross sections are shown constructed by the use of the total and fission cross sections parameters. This result has been compared with the experimental data from /7/ after broadening over the resolution and Doppler functions. The good agreement can be seen on Figures 1 and 2.

We compared our set of resonance parameters with the new results from the multilevel analysis of ^{239}Pu neutron cross sections in the frame of the Rich-Moore R-matrix scheme /8/. The authors of this work transformed their parameters into the Adler-Adler ones in the energy region 0 - 45 eV. Generally, these parameters are in good agreement with our results. The parameters μ and ν agree very well, which is to be expected. In the set of G^T and G^F parameters, the discrepancy is less than 20% with the exception of 3 levels in the end of the interval. There is a significant disagreement between results of two works about the parameters H^T and H^F.

Practically, the realisation of our scheme is connected with a number of

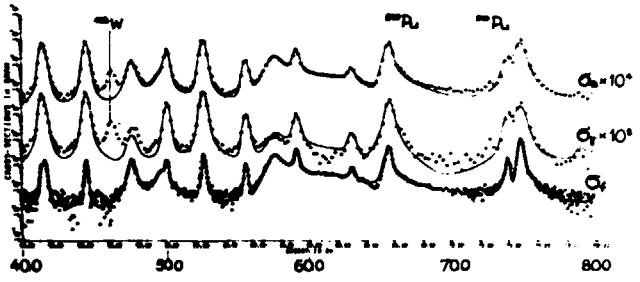

Figure 2. Neutron absorption (σ_a), radiative capture (σ_γ) and fission (σ_f) cross sections: △ experimental points, (-) multilevel parametrization.

difficulties due to insufficient accuracy of experimental data, incorrect identification of total momentum of levels and determination of the full set of total and fission cross sections resonance parameters. Nevertheless, unitarity gives additional possibilities for resolving the common problem in multilevel analysis which is the unique choice of the resonance parameters set

In the unresolved resonance region we used the stochastical simulation of neutron cross sections (ladder method) on the basis of the multilevel formalism. We adopt the approximation of reduced R-matrix /9/, whose elements for the state with given total momentum are:

$$R_{cc'} = \frac{\gamma_{\lambda c}\,\gamma_{\lambda c'}}{E_\lambda - E - i\Gamma_\gamma/2} \tag{17}$$

here $\gamma_{\lambda c}$ is the reduced width amplitude in the reaction channel c, E_λ - level energy, $\bar{\Gamma}_\gamma$ - mean radiative width.

It is convenient to use the K-matrix related to collision S-matrix by

$$S = e^{-i\varphi}\left[(1+iK)(1-iK)^{-1}\right]e^{-i\varphi} \tag{18}$$

Including the values $\beta_{\lambda c} = \gamma_{\lambda c}/\bar{\gamma}_c$ (normally distributed) and $(E_\lambda - E_{\lambda-1})/\bar{D}$ (following Wigner distribution law), the K-matrix elements are expressed as:

$$K_{cc'} = \frac{\sqrt{\Gamma_c\Gamma_{c'}}}{\bar{D}}\sum_\lambda \frac{\beta_{\lambda c}\beta_{\lambda c'}}{\frac{E_\lambda - E}{\bar{D}} - i\frac{\Gamma_\gamma}{2\bar{D}}} \tag{19}$$

Then the neutron cross sections are

$$\sigma_t = 2\pi\lambda\!\!\!^{-2}\sum_J g(J)\sum_{l=l'j'}\left(1 - R\,S^{J\pi}_{nlj,\,nl'j'}\right), \tag{20}$$

$$\sigma_f = \pi \lambda\!\!\!^{-2} \sum_{J} g(J) \sum_{\ell_j \ell'_j} | S^{Jn}_{n\ell_j, n\ell'_j} |^2,$$
$$\sigma_e = \pi \lambda\!\!\!^{-2} \sum_{J} g(J) \sum_{\ell_j \ell'_j} | 1 - S_{n\ell_j, n\ell'_j} |^2. \tag{20}$$

Inelastic scattering at E < 20 KeV is neglected. The radiative capture cross section due to the S-matrix unitarity properties is determined as a difference between the total cross section and the sum of fission and elastic scattering cross sections. In the energy range under consideration the contributions of S and p neutrons are accounted for. The parameters Γ_n and φ_ℓ , which depend on are expressed as usual:

$$\varphi_0 = k R_0,$$
$$\varphi_1 = k R_1 - \mathrm{arc\,tg}\,(k R_1), \tag{21}$$
$$\Gamma_n (\ell = 0) = \Gamma^0_{n0} \sqrt{E}\, V_0,$$
$$\Gamma_n (\ell = 1) = \Gamma^0_{n1} \sqrt{E}\, V_1.$$

V_0 , V_1 are the penetrative coefficients for S and p neutrons, R_0 , R_1 are the potential scattering radii for S and p neutrons, assumed to be equal.

In our approach some problems of the ladder method are overcome using a new idea. For the Doppler broadening calculation we use the following procedure. We employ the statistical sampling in the form of multiple "emission" of neutrons at the energy points of a uniform lethargy mesh with spacing Δu . This permits us to avoid the point-to-point quadrature. A "run" will mean a set of random sampling statistics in the total interval ΔU , where a random picture (realization) of neutron cross sections with many resonances for the states is defined by a set of random number: level energies and widths for a given system. Actually, a 10-level approximation turns to be sufficient. In our case the K-matrix is of rank three - the number of channels: one neutron channel and two fission channels. The resulting cross section is obtained by summing the corresponding cross section over all states of different angular momentum and parity. Information about a given realization is stored in the computers memory.

The probability table method is applied for calculation of mean cross sections functionals. The distribution function of total cross section $\rho(\sigma_t)$ and correlation function $\sigma_x(\sigma_t)$ are stored too. If these functions are available, it is easy to calculate any functional $F(\sigma_t, \sigma_x)$

$$\langle F \rangle = \int F(\sigma_t, \sigma_x)\, \rho(\sigma_t)\, d\sigma_t \tag{22}$$

The estimates of calculated functional dispersions were determined in the following way:

$$D_F = \langle F^2 \rangle - \langle F \rangle^2 \tag{23}$$

The average resonance parameters values X ,which are the parameters of a neutron cross section model, are evaluated on the basis of experimental data Y for average cross sections and transmission functions using statistical procedure (Bayes approach). The a posteriori estimate of the parameters is giving by expressions:

$$\hat{X} = X^{apr} + D(X^{apr}) K^T [K D(X^{apr}) K^T + D(\hat{Y})]^{-1} (Y - K X^{apr}),$$
$$\hat{D}(\hat{X}) = D(X^{apr}) - D(X^{apr}) K^T [K D(X^{apr}) K^T + D(\hat{Y})]^{-1} K D X^{apr}, \qquad (24)$$

here D is covariance matrix, K - matrix of sensitivity coefficients.

The Monte-Karlo calculation of the functionals has been performed simultaneously with that of the sensitivity coefficient at the same random samplings of resonance. The optimization expression needs sensitivity coefficients of functionals to parameters:

$$K_{ij} = \frac{\delta F_i}{\delta P_j} \Big/ \frac{F_i}{P_j} . \qquad (25)$$

Having the estimates of $\hat{X}$, $D(\hat{X})$ the improved estimates of any set of functionals (C) can be obtained:

$$\hat{C} = \hat{C}(X^{apr}) + (\hat{X} - X^{apr}),$$
$$D(\hat{C}) = K^T D(\hat{X}) K, \qquad (26)$$
$$(K_c)_{lm} = \frac{\delta C_l}{\delta P_m} \Big/ \frac{C_l}{P_m} .$$

We used the Monte-Carlo modelling of neutron cross sections of ^{239}Pu, Bayessian optimization procedure and our experimental data[10] for transmission and self-identification in fission and obtained the average values of the resonance parameters of this nucleus in the energy interval 2 eV - 20 keV. On Fig. 3 the fit to the experimental data for transmission and self-identification is shown.

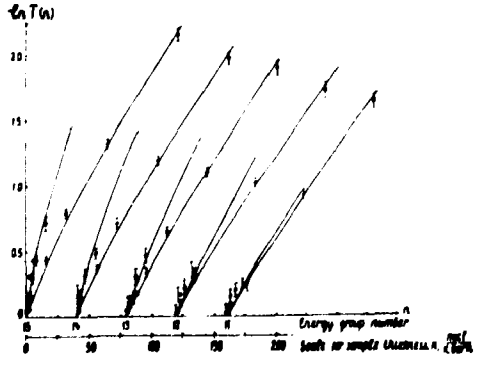

Figure 3. Transmission $T(n)$ and self-identification $T_f(n)$ for ^{239}Pu, ϕ - $T(n)$ experiment, $\bar{\phi}$ - $T_f(n)$ experiment.

The mean values of ^{239}Pu resonance parameters are given on Table 1. The energy dependence of parameters R and Γ_f are presented in Table 2.

Table 1

A posteriori estimation of the averaged resonance parameters of ^{239}Pu not depending of the energy

J^π	D(eV)	$\bar{\Gamma}_\gamma$(meV)	$S_n \cdot 10^4$	$\bar{\Gamma}_f$(eV)	f_1	f_2	ν_n	ν_f
0^+	9,34	39,5	0,982	1,83	0,8	0,2	1	2
1^+	3,17	39,5	0,982	var	1	0	1	1
0^-	9,34	39,5	2,17	0,01	1	0	1	1
1^-	3,17	39,5	2,17	1,021	0,5	0,5	2	2
2^-	1,96	39,5	2,17	0,614	0,5	0,5	1	2

Table 2

A posteriori estimation of the averaged resonance parameters of ^{239}Pu depending on the energy

No. gr. (ABBN)	R (fm)	Γ_f (meV, $J^\pi = 1^+$)
11	9.1	35,0
12	9.1	23.3
13	9.1	26.2
14	9.2	30.4
15	9.5	51.0

REFERENCES

1. V.V. Kolesov, A.A. Lukyanov et al., Santa Fe Nucl.Data Conf.(USA, May 1985).
2. Bakalov T. et al., JINR P3-83-51, Dubna, 1983.
3. Van'kov A.A. et al., Sov. Nuclear Constants, 4(53), p.40, 1983.
4. H. Darrien et al., Proc.IAEA, Paris 1966, v.2, p.195.
5. G.V. Antsipov et al., Nucl.Const. for Pu, Minsk 1982.
6. J. Blons, NSE, v. 51, 1973, p.130.
7. R. Gwin et al., NSE, v.59, 1976, p.79.
8. G. de Saussure et al., Santa Fe, Nucl. Data Conf.(USA, May 1985).
9. A. Lukyanov, The Structure of Neutron Cross Sections (Atomizdat,Moscow,1978).
10. Bakalov T. et al., NBS Special Publication 594, Proc. of Int.Conf.Knoxvill (USA, 1979).

MEASUREMENT OF THE MEAN-SQUARE CHARGE RADII OF NEUTRON RESONANCE STATES IN URANIUM NUCLEI

A. Meister, S. Mittag, L.B. Pikelner, W. Pilz, D. Seeliger, K. Seidel
Technische Universität Dresden, Dresden, GDR
Joint Institute for Nuclear Research, Dubna, USSR

Abstract:
The measurement of chemically induced shifts of neutron resonances provides information about the mean-square charge radii of nuclei at excitation energies around the neutron binding energies. Shifts were determined in neutron transmission spectra measured with time-of-flight technique at the Dubna pulsed reactor for several chemical uranium compounds , and analysed for ten low-energy resonances of ^{234}U, ^{235}U and ^{238}U.

1. Introduction

Neutron resonances of a nuclide inserted in different chemical compounds are slightly shifted as a result of the electric hyperfine interaction energy between the nucleus and the surrounding electrons. For two samples,I and II, the positions of a considered resonance differ approximately by

$$\Delta E_0 = \frac{\pi^2}{6\varepsilon_0} \cdot Z \cdot \Delta\varrho_e(0) \cdot \Delta\langle r^2\rangle \quad , \tag{1}$$

with $\Delta\varrho_e(0) = \varrho_{eI}(0) - \varrho_{eII}(0)$ being the difference of the electron densities in the nuclear region, Z is the proton number of the nucleus, and $\Delta\langle r^2\rangle$ is the change of its mean-square charge radius due to neutron capture.

This neutron resonance shift is an analogon of the well-known Mössbauer isomer-shift. Measurements of isomer shifts have been provided information about the mean-square radii of many excited nuclear states having energies $\angle$ 200 keV. In the case of chemically induced neutron resonance shifts the states investigated have excitation energies little above the neutron binding energies. There are no other experimental data on the $\langle r^2\rangle$ of so relatively high excited compound-nucleus states. Their structure determines at actinide nuclei such important properties as the fission widths.

Chemically induced shifts are very small compared to the widths of the resonances. A crude estimate shows under favourable conditions and with $\Delta\langle r^2\rangle / \langle r^2\rangle = 0.01$ for the shifts $\Delta E_0 \approx 10\,\mu eV$ at mass numbers $A \approx 150$ and $\Delta E_0 \approx 100\,\mu eV$ at $A \approx 200$, whereas the widths of low-energy resonances are of the order of 0,1 eV. Nevertheless the shifts can be measured in transmission experiments using the time-of-flight method at an intense neutron source.An additional difficulty arises from different Doppler broadenings of the resonances observed in samples of different crystalline structures. Any influence of shape differences on shifts of the resonances must be carefully eliminated.
Hitherto measurements of chemically shifts of neutron resonances were accomplished for the 5.2 eV resonance of ^{234}U, the 6.7 eV resonance of ^{238}U and eight resonances of ^{235}U /1,2/.

2. Experiment

Transmission spectra were measured with a time-of-flight spectrometer at the Dubna fast pulsed reactor IBR-30 operated in booster mode with the electron linac LUE-40 /3/. With a flight path of about 60 m and a time resolution of 4 μs; the energy resolution lay between 2 and 80 meV in the energy region of interest from 1 to 12 eV. The samples of metallic U, UO_2, U_3O_8 and UO_3 used for investigations of ^{235}U and ^{234}U resonances, were

enriched in ^{235}U to about 90 %.
Searching for differences, two or three samples were measured quasi-simultaneously by dividing the time of about 400 h necessary for sufficient statistical accuracy into short-time runs of about five minutes with automatic sample alternation. A minicomputer-operated spectrometer allowed also to inspect after each short-time run the obtained spectrum and data from a neutron-beam monitor, a timer, and a reactor-pulse counter. Only those spectra were accumulated for which the experimental conditions were identical to within a few percent as compared with the preceding runs.
A tantalum foil of about 0.1 mm thickness was permanently placed in the neutron beam, in addition to the uranium samples. The Ta-resonances observed in the transmission spectra of the different uranium compounds, were analysed in the same way as the U-resonances, so that possible shifts and other differences between the measured spectra, with the exception of those attributed to the uranium samples, were revealed.
The spectrometer arrangement is shown in Fig. 1; one of the spectra obtained is presented in Fig. 2.

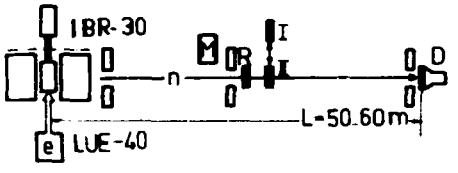

Fig. 1
Experimental arrangement.
I and II, Uranium samples; R, reference sample;
D, ^{6}Li-glass scintillation detector;
M, BF_3-counter as monitor.

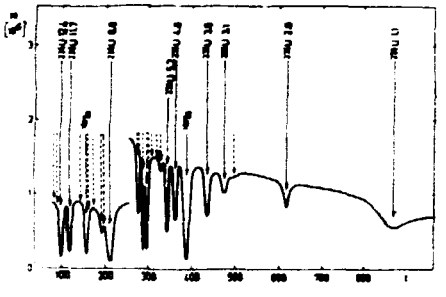

Fig. 2
Time-of-flight spectrum obtained with an uranium sample enriched in ^{235}U to about 90 %. The widths of the time channels t are 2 μs for t < 256 and 4 μs for t ≥ 256.

3. Analysis of the spectra

Two methods were used to extract the chemical shifts from the spectra obtained in the measurements.

The first method applied to all uranium resonances analysed in the presented work, is based on the comparison of the resonance positions in the transmission spectra N_I and N_{II} of the two samples I and II, respectively, by a least-square fit:

$$N'_{II}(t) = A\left[N_{II}(t + \Delta t_{exp}) + N_B\right], \tag{2}$$

minimizing

$$\chi^2 = \sum_{t=t_1}^{t_2} \frac{\left[N_I(t) - N'_{II}(t)\right]^2}{N_I(t) + N_{II}(t)} \tag{3}$$

for a given channel range $(t_1 \ldots t_2)$ with variation of the resonance position difference Δt_{exp} and of the parameters A and N_B taking into account small differences in the transmitted neutron beam and background intensities, respectively.

To eliminate contributions in Δt_{exp} arising from different resonance shapes caused first of all by different Doppler broadenings, a corresponding pair of transmission spectra, $C_I(t)$ and $C_{II}(t)$, was calculated, having the same shape differences as $N_I(t)$ and $N_{II}(t)$ but no chemical resonance shifts. Then, the fit (2) and (3) carried out with the spectra C_I and C_{II}, yields a shift value Δt_{1v} which results together with Δt_{exp} in the desired chemical shift

$$\Delta E_0 = -2.77 \cdot 10^{-2} \cdot E^{3/2} (\Delta t_{exp} - \Delta t_{1v})/L , \qquad (4)$$

with the resonance energy E_0 and ΔE_0 in eV, the flight path L in m, and the Δt in μs.

The calculations of C_I and C_{II} include different Doppler broadenings in both samples /1,2/, spectrum shape of the open beam (without uranium sample), background spectrum, sample thickness, detector dead-time, resolution function of the spectrometer, and finite time-channel widths.

The Δt_{1v} were of the same order of magnitude as the Δt_{exp}. In the second method, where the chemically induced shifts were extracted as center-of-resonance-shifts ΔE_σ of the cross sections deduced from the transmission spectra, the influence of different Doppler broadenings on ΔE_σ is very much smaller. But this method can be applied only at well seperated resonances and demands a more careful determination of the open-beam and the Background spectra. The center-of-resonance shift is used as

$$\Delta E_\sigma = \int_{E_1}^{E_2} E_n \cdot \sigma_{RI}(E_n) \cdot dE_n - \int_{E_1}^{E_2} E_n \cdot \sigma_{RII}(E_n) \cdot dE_n \Big/ \int_{E_1}^{E_2} \sigma_{RI}(E_n) \cdot dE_n , \qquad (5)$$

where the $\sigma_R(E_n)$ are the resonance parts of the cross sections for which at the limits of integration holds

$$\sigma_R(E_1) \approx \sigma_R(E_2) \approx 0. \qquad (6)$$

Because the mean kinetic energies of the uranium atoms (mass number A) in the different crystal lattices can be different by $\Delta\langle\varepsilon_k\rangle$, a shift ΔE_k /4,5/ should be taken into account;

$$\Delta E_k = -\Delta\langle\varepsilon_k\rangle / (3 \cdot A), \qquad (7)$$

with which the chemically induced shift follows as

$$\Delta E_0 = \Delta E_\sigma - \Delta E_k. \qquad (8)$$

But, with the $\Delta\langle\varepsilon\rangle = 3/2\Delta\langle\varepsilon_k\rangle$ from Refs./1,2/, ΔE_k is for uranium samples at equal temperatures (T = 293 K) smaller than 5 μeV in all cases and may be neglected.

4. Determination of electron density differences

To determine the nuclear mean-square radius change $\Delta\langle r^2\rangle$ from the chemical shifts ΔE_0, the electron density differences $\Delta\varrho_e(0)$ must be known.
This problem was solved in the framework of a generalized free-ion model with occupation numbers P_{nl} of the nl valence electrons not restricted to integer values.
This model was used to connect experimental chemical X-ray shifts ΔE_x with the desired electron density differences $\Delta\varrho_e(0)$;

$$\Delta E_x = \sum_{nl} \delta P_{nl} \cdot \delta E_x^{nl} \tag{9}$$

$$\Delta \varrho_e(0) = \sum_{nl} \delta P_{nl} \cdot \delta \varrho_e^{nl}(0), \tag{10}$$

with δP_{nl} as effective occupation number differences for chemical compounds of different oxidation numbers, and $\delta \varrho_e^{nl}$ denotes the changes of the electron densities in the nuclear region caused by completely removing one nl valence electron. These values were calculated in the framework of relativistic Hartree-Fock-Slater-calculations.
The results for $\Delta \varrho_e(0)$ are listet in Table 1.

Table 1

Electron density differences

samples I	samples II	$\Delta \varrho_e(0)$ $[10^{26}\ cm^{-3}]$
U	UO_2	2.8 ± 2.5
UO_3	U_3O_8	3.1 ± 1.2
U_3O_8	U	3.5 ± 2.2
U_3O_8	UO_2	6.3 ± 1.6
UO_3	U	6.6 ± 3.0
UO_3	UO_2	9.4 ± 2.0
UO_3	$UF_4 \cdot H_2O$	8.7 ± 2.0
$UO_2(NO_3)_2 \cdot 6H_2O$	U	6.8 ± 3.0
$UF_4 \cdot H_2O$	UO_2	0.8 ± 0.3
$UO_2(NO_3)_2 \cdot 6H_2O$	UO_3	0.2 ± 1.0

These results are in agreement with $\Delta \varrho_e(0)$ data from Mössbauer isomer-shift measurements with the neighbouring element Neptunium /1/.

5. Results

With the experimental ΔE_0 and the $\Delta \varrho_e(0)$ data, the mean-square charge radius changes $\Delta\langle r^2\rangle$ were determined according to equ. (1) by least-square fits with straight lines through the origin.
They are given in Table 2
For discussions of the changes of the mean-square charge radii with excitation energy, the $\Delta\langle r^2\rangle$ must be reduced by the differences of the mean-square charge radii between the ground-states of target and compound nuclei. They were deduced from optical isotope shifts /6/ and amount to + 0.05 ± 0.02 fm^2 when adding a neutron to ^{234}U or ^{238}U and + 0.10 ± 0.03 fm^2 in the case of the ^{235}U target nucleus. These reduced values $\Delta\langle r^2\rangle_n$ are also presented in Table 2.
The average of the eight data for ^{236}U compound-nucleus states is

$$\overline{\Delta\langle r^2\rangle_n} = -0.18 \pm 0.10\ fm^2.$$

A comparison of this result with a theoretical prediction and a discussion of a dependence of the $\Delta\langle r^2\rangle_n$ on the fission widths of the resonance states is given in an other contribution to this Symposium /7/.

Table 2

Mean-square charge radius changes

Target nuclide	Resonance E_0 [eV]	Γ_f [meV] /8/	$\Delta\langle r^2\rangle$ [fm^2]	$\Delta\langle r^2\rangle_n$ [fm^2]
^{234}U	5.16	0.02 /9/	-0.41 ± 0.25	-0.46 ± 0.25
^{235}U	1.14	107	+0.01 ± 0.22	-0.09 ± 0.22
^{235}U	2.03	11	-0.13 ± 0.21	-0.23 ± 0.21
^{235}U	3.15	103	+0.20 ± 0.48	+0.10 ± 0.48
^{235}U	3.61	53	+0.02 ± 0.25	-0.08 ± 0.25
^{235}U	4.85	4	-0.52 ± 0.25	-0.62 ± 0.25
^{235}U	3.77	98	+0.09 ± 0.26	-0.01 ± 0.26
^{235}U	11.67	6	-0.24 ± 0.29	-0.34 ± 0.29
^{235}U	12.39	23	+0.25 ± 0.31	+0.15 ± 0.31
^{238}U	6.67	10^{-5} /10/	-1.7 ± 0.5	-1.75 ± 0.5

References

/1/ A. Meister, D. Pabst, L.B. Pikelner, K. Seidel, Nucl.Phys. A 362 (1981) 18.

/2/ S. Mittag, D. Pabst, L.B. Pikelner, W. Pilz, R. Tschammer, A. Meister, D. Seeliger, K. Seidel, Nucl. Phys. A 435 (1985) 97.

/3/ V.V. Golikov, Zh. A. Kozlov, L.K. Kulkin, L.B. Pikelner, V.T. Rudenko, B.I. Sharapov, JINR-report 3-5736 (1971).

/4/ K. Seidel, D. Seeliger, V.K. Ignatovich, A. Meister, S. Mittag, W. Pilz, Yad. Fiz. 42 (1985) 1041.

/5/ V.K. Ignatovich, A. Meister, S. Mittag, W. Pilz, D. Seeliger, K. Seidel, Proceedings of this Symposium, p. 47

/6/ K. Heilig, A. Steudel, At. Nucl. Data. Tables 14 (1974) 613.

/7/ A. Meister, S. Mittag, L.B. Pikelner, W. Pilz, D. Seeliger, K. Seidel, Proceedings of this Symposium, p. 70

/8/ M.S. Moore, J.D. Moses, G.A. Keyworth, J.W.T. Dabbs, N.W. Hill, Phys. Rev. C 18 (1978) 1328.

/9/ G.D. James, J.W.T. Dabbs, J.A. Harvey, N.W. Hill, R. Schindler, Phys. Rev. C 15 (1977) 2033.

/10/ F.C. Difilippo, R.B. Perez, G. de Saussure, D.K. Olsen, R.W. Ingle, Phys. Rev. 21 (1980) 1400.

MEAN-SQUARE RADII OF THE ^{236}U NUCLEUS IN EXCITED STATES WITH DIFFERENT FISSION WIDTHS

A. Meister, S. Mittag, L.B. Pikelner, W. Pilz, D. Seeliger, K. Seidel

Technische Universität Dresden, Dresden, GDR
Joint Institute for Nuclear Research, Dubna, USSR

Abstract

Experimentally determined mean-square charge radii of ^{236}U compound-nucleus states excited by neutron resonance absorption in ^{235}U, show on average a weak diminution as compared with the ground state data. A correlation of the $\langle r^2 \rangle$ with the fission widths of the states seems to appear. An attempt is made to discuss this correlation in the frame of the double-humped barrier model successfully used to describe subthreshold fission. The $\langle r^2 \rangle$ data are used to estimate the fraction of class II configurations in the excited compound-nucleus states with different fission widths.

1. Introduction

Measurements of chemically induced shifts of neutron resonances provide data on the mean-square charge radii ($\langle r^2 \rangle$) of nuclear states having excitation energies of about the neutron binding energy /1/. Shifts between uranium compounds determined with the intense neutron beam of the Dubna pulsed reactor, were up to some 10^{-4} eV only, that is very small compared for example to the widths of the resonances typically being about 10^{-1} eV. Hitherto, such measurements were accomplished for the 6.7 eV resonance of ^{238}U /2/, the 5.2 eV resonance of ^{234}U /3/ and 8 low-energy resonances of ^{235}U /3/. The data obtained on ^{235}U are especially of interest because resonances were simultaneously measured having very different fission widths (Γ_f), so that inspite of the small values compared to the experimental uncertainties, an attempt can be made to discuss a correlation of the $\langle r^2 \rangle$ with the Γ_f of the excited states. This is done in chapter 3 in the frame of the double-humped barrier model, whereas the average of all $\langle r^2 \rangle$ is compared in chapter 2 with a statistical model calculation.

2. Experimental results and comparison with statistical model calculation

The changes of $\langle r^2 \rangle$ by resonance neutron capture in ^{235}U were deduced from chemically induced resonance shifts in Ref. /3/. Taking into account the difference of $\langle r^2 \rangle$ between the ground states of ^{236}U and ^{235}U /4/, the differences of $\langle r^2 \rangle$ between excited compound nucleus states of ^{236}U and its ground state ($\Delta\langle r^2 \rangle_n$) are obtained. The $\Delta\langle r^2 \rangle_n$ of all investigated resonances (E_0 = 1.2 eV, 2.0 eV, 3.1 eV, 3.6 eV, 4.8 eV, 8.8 eV, 11.7 eV and 12.4 eV) are presented in Fig. 1. The error bars include uncertainties arising from both

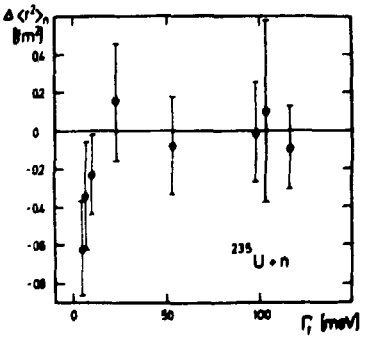

Fig. 1
Differences $\Delta\langle r^2 \rangle_n$ of the mean-square charge radii between ^{236}U compound-nucleus states and the ^{236}U ground-state in dependence on their fission widths Γ_f.

the statistical errors of the measured spectra and systematical uncertainties in the data reduction procedure.
The experimental results show that the $\langle r^2\rangle_n$ of the excited compound-nucleus states are different from the ground-state value, $\langle r^2\rangle_{no} = 33.8\ fm^2$ /4/, only by 2 % or less. The average of all data is $\Delta\langle r^2\rangle_n = -0.18 \pm 0.10\ fm^2$. A diminution of $\langle r^2\rangle_n$ with the excitation energy can not be understood in the frame of an ideal Fermi-gas. Bunatian /5/ used a statistical model with interaction in the particle-hole channel and with pair-correlation. At temperatures corresponding to the neutron binding energy, he found $\Delta\langle r^2\rangle_n \approx -0{,}1\ fm^2$, in good agreement with the experimental result. The negative sign is attributed in this work to a release of the pair-correlation.

Fig. 1 also suggests a possible correlation between $\Delta\langle r^2\rangle_n$ and Γ_f. The average of the $\Delta\langle r^2\rangle_n$ for the states with larger fission widths, $\Gamma_f > \frac{1}{2}\cdot\Gamma_\gamma$ (The radiation widths are $\Gamma_\gamma \approx 35$ meV), is $\overline{\Delta\langle r^2\rangle_{nf>}} = -0.02 \pm 0.12\ fm^2$, whereas those for the states with smaller fission widths, $\Gamma_f < \frac{1}{2}\cdot\Gamma_\gamma$, is $\overline{\Delta\langle r^2\rangle_{nf<}} = -0.38 \pm 0.14\ fm^2$. The quoted uncertainties include a systematical contribution of about 0.06 fm^2 in both cases, so that the dependence of the averages on Γ_f is significant with about the halves of the given error intervals.

3. Mean-square radii and fission widths

The experimental data on $\Delta\langle r^2\rangle_n$ suggest that in compound-nucleus states with larger fission widths, configurations or components contribute which enlarge $\Delta\langle r^2\rangle_n$. Subthreshold fission processes are understood in the frame of the double-humped barrier model with wave functions partitioned into two classes of configurations, class I and class II, attributed to the first and second well, respectively /6,7/,

$$\Psi_n = \alpha_{In}\cdot\Psi_I + \alpha_{IIn}\cdot\Psi_{II}\ . \qquad (1)$$

An illustration to the ^{236}U barriers is given in Fig. 2.

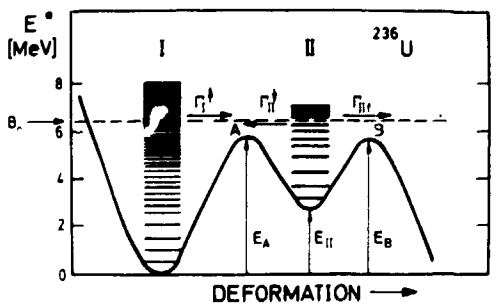

Fig. 2
Deformation potential of the ^{236}U nucleus. The excitation energy corresponding to the neutron binding energy is indicated by a dashed line.

At subbarrier fission, configurations I and II are well separated by wall A, whereas for states lying highly above the barriers, a strong mixing of both classes is expected, resulting in fluctuations of both $\langle r^2\rangle_n$ and Γ_f, independently from each other.
In the present case, states about 1 MeV above the barriers are excited. The correlation of the $\Delta\langle r^2\rangle_n$ with Γ_f should be an indication that at this energy the mixing is not very strong. This is in agreement with investigations of the fission cross section of $^{235}U+n$ in the unresolved resonance region where Moore et al. /8/ interprete a pronounced intermediate structure in the same way that has been used to describe structure in sub-threshold fission.

Following this picture, the admixture $\alpha_{IIn} \cdot \Psi_{II}$ would be dominating for the fission probability whereas Ψ_I describes the typical behaviour of capture resonances. Then, a simple relation between mean-square radii of class I and class II configurations, $\langle r^2 \rangle_I$ and $\langle r^2 \rangle_{II}$, and measured values of $\Delta \langle r^2 \rangle_n$ for resonances i and j, respectively, may be deduced /9/:

$$\Delta \langle r^2 \rangle_{ni} - \Delta \langle r^2 \rangle_{nj} \approx (\alpha_{IIi}^2 - \alpha_{IIj}^2) \cdot (\langle r^2 \rangle_{II} - \langle r^2 \rangle_I) \qquad (2)$$

Terms as $\langle \Psi_I / r^2 / \Psi_{II} \rangle$ are neglected in this rough estimate. The difference $(\langle r^2 \rangle_{II} - \langle r^2 \rangle_I)$ may be evaluated with (5.1 ± 0.2) fm^2 as found for ^{240}Am /10/. Using $\Delta \langle r^2 \rangle_n$ of the 4.8 eV resonance which has a fission width of only 4 meV, as reference (j), the admixture coefficient differences shown in Fig. 3, are obtained.

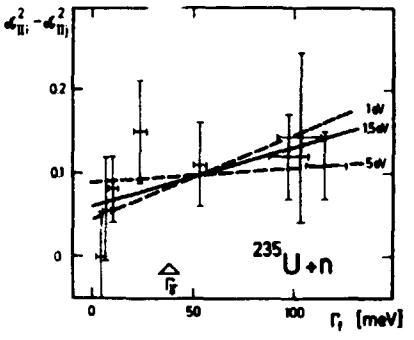

Fig. 3
Differences of coefficients for the admixture of class II configurations in ^{236}U compound-nucleus states in dependence on their fission widths (⊢⊣) and equ. (3) with the indicated Γ_{IIf} (---).

α_{II}^2 is an expression for the probability to find the excited nucleus at deformations corresponding to the second well. Let us estimate it with the transition rates between the wells. From a study of the time developement of a two-well system starting in the first well /6/, one can find the relation

$$\alpha_{II}^2 \approx \frac{\Gamma_f}{(\Gamma_I + \Gamma_{II} - 2\Gamma_t) \cdot \Gamma_{IIf}/\Gamma_{II}} \cdot \left[1 + \frac{\Gamma_t}{\Gamma_I + \Gamma_{II} - \Gamma_t} \cdot \left(\exp\left(1 - \frac{\Gamma_I + \Gamma_{II}}{\Gamma_t}\right) - 1 \right) \right]. \qquad (3)$$

Γ_I and Γ_{II} are the total widths of class I and class II states; Γ_{IIf} is the class II state fission width; Γ_t is the total width of the neutron resonance.
With $\Gamma_{II} \gg \Gamma_t$, Γ_I, the leading term in eq. (3) gives the transparent estimate $\alpha_{II}^2 \approx \Gamma_f / \Gamma_{II_f}$.

If the spacing of the s-wave class II states D_{II} would be larger than Γ_{II}, one could assume that all compound-nucleus states investigated here (Their differences in E^* are smaller than 12 eV.), couple with the same class II state or only with the same small group of class II states. Assuming equal Γ_{IIf} and Γ_{II} for this compound-nucleus states, their individual fission widths Γ_f would arise from the coupling strengths between class I and class II configurations in these states,

$$\Gamma_f \approx \Gamma_I' \cdot \frac{\Gamma_{IIf}}{\Gamma_{II}'} \quad . \qquad (4)$$

A comparison of the data obtained on $\Delta \alpha_{II}^2$, with expression (3) by means of the least-square method yields values for Γ_{IIf} of 1 to 5 eV (Fig. 3). With respect to Γ_{II}, the fit is insensitive.

On the other hand, an estimate of average widths of class II states can be obtained with expressions like the Bohr - Wheeler formula /6/:

$$\overline{\Gamma_{IIf}} \approx \frac{D_{II}}{2\pi} \cdot N_B \qquad (5)$$

and

$$\overline{\Gamma_{II}^{\downarrow}} \approx \frac{D_{II}}{2\pi} \cdot N_A \qquad (6)$$

where N_A and N_B are the effective numbers of transition states at barrier A and B, respectively.
D_{II} is found to be 210 ± 70 eV /8/. The analysis of fluctuations of Γ_f together with data on the barrier highs ($E_A \approx E_B$) provide an estimate for $N_A \approx N_B \approx 2...3$, and finally $\overline{\Gamma_{IIf}} \approx 1/2 \cdot \overline{\Gamma_{II}} \approx 50...120$ eV.
The Γ_{IIf} and $\Gamma_{II}^{\downarrow}$ of the individual class II states should fluctuate around the averages with a Porter-Thomas distribution.

Summarizing this discussion, it may be said that the double-humped fission barrier model with excited state configurations, classified into class I and class II components, as done to describe structures in subthreshold fission cross sections, yields an increase of $\langle r^2 \rangle_n$ with increasing Γ_f as observed in the presented experimental data. But, using barrier paramenters obtained in other experiments, in the statistical average this increase should be smaller by one or even two orders of magnitude. In principle, large statistical fluctuations are possible for a Porter-Thomas distribution.
On the other hand, it can not be excluded that the observed correlation of the $\langle r^2 \rangle_n$ with the Γ_f are in connection with any other phenomenon not discussed in the frame of the model.

References

/1/ A. Meister, S. Mittag, L.B. Pikelner, W. Pilz, D. Seeliger and K. Seidel, contribution to this symposium, Proc. p. 65

/2/ A. Meister, D. Pabst, L.B. Pikelner and K. Seidel, Nucl. Phys. A 362 (1981) 18.

/3/ S. Mittag, D. Pabst, L.B. Pikelner, W. Pilz, R. Tschammer, A. Meister, D. Seeliger and K. Seidel, Nucl. Phys. A 435 (1985) 97.

/4/ K. Heilig and A. Steudel, At.Nucl.Data Tables 14 (1974) 613.

/5/ G.G. Bunatian, Yad. Fiz. 35 (1982) 16.

/6/ S. Bjornholm and V.M. Strutinsky, Nucl.Phys. A 136 (1969) 1.

/7/ S. Bjornholm and J.E. Lynn, Rev.Mod.Phys. 52 (1980) 725.

/8/ M.S. Moore, L. Calebretta, F. Corvia and H. Weigmann, Phys.Rev. C 30 (1984) 214.

/9/ S. Mittag, D. Pabst, L.B. Pikelner, W. Pilz, R. Tschammer, A. Meister, D. Seeliger and K. Seidel, 15th Mazurian Summer School on Nuclear Physics, Mikolajki (Poland), 1983, Proc. p. 12.

/10/ C.E. Bemis. J.R. Beene, J.P. Young and S.D. Kramer, Phys. Rev. Lett. 43 (1979) 1854.

TEMPERATURE SHIFT OF NEUTRON RESONANCES

V.K. Ignatovich, A. Meister, S. Mittag, W. Pilz, D. Seeliger, K. Seidel
Technische Universität Dresden, Dresden, GDR
Joint Institute for Nuclear Research, Dubna, USSR

Abstract:
Temperature induced shifts of neutron resonances has been experimentally observed studying low-energy resonances of Rh-103, Ag-109, Dy-161 and Dy-163 with a time-of-flight spectrometer at the Dubna pulsed reactor. The shifts observed for the first time, are regarded as an analogue to the second-order Doppler effect in Mössbauer γ-ray spectroscopy.

1. Introduction

The interaction cross-sections of slow neutrons with atomic nuclei have resonances shaped by both the properties of the nuclei (neutron width, fission width, capture width etc.) and the thermal motion of the target atoms relative to the incident neutrons. Therefore, high-resolution spectroscopy of neutron resonances gives also insight into interactions of the atoms with their surrounding. The most striking effect of the thermal motion is the Doppler broadening of the resonances described already in 1937 by Bethe and Placzek /1/ for gaseous motion and in 1939 by Lamb /2/ for neutron capture in crystals. In 1960, a so-called Doppler effect of second order has been observed in experiments with γ-rays /3,4/. It was shown by Mössbauer spectroscopy that the γ-peak is shifted if the temperatures of absorber (T_a) and emitter (T_e) are different:

$$\Delta E_\gamma = -\frac{E_\gamma}{Mc^2}\cdot\Delta\langle\varepsilon_k\rangle, \qquad (1)$$

where $\Delta\langle\varepsilon_k\rangle = \langle\varepsilon_k\rangle_a - \langle\varepsilon_k\rangle_e$ is the difference of the mean kinetic energies of the absorber and of the emitter atoms which is at high temperatures $\approx 3/2\cdot k_B\cdot(T_a - T_e)$; M is the atomic mass and k_B is the Boltzmann constant.
If eq. (1) is formally transformed to the absorption of neutrons, a corresponding neutron resonance should be temperature-dependent shifted by /5/

$$\Delta E_n = -\frac{1}{A}\cdot\Delta\langle\varepsilon_k\rangle, \qquad (2)$$

where A is the mass number of the absorbing atoms related to the neutron mass number. However, in contrast to Mössbauer-γ-peaks, neutron resonances have widths $\Gamma \gg \Delta E_n$ and are Doppler broadened; that means, a recoilless component is not separately observed. In this case, the resonance position may be defined as

$$\bar{E}_n = \int_{E_1}^{E_2} \sigma_R(E_n)\cdot E_n\cdot dE_n \Big/ \int_{E_1}^{E_2} \sigma_R(E_n)\cdot dE_n, \qquad (3)$$

where σ_R is the resonance part of the cross section and E_1, E_2 are choosen so that $\sigma_R(E_1) \approx \sigma_R(E_2) \approx 0$.
Then, the temperature shift follows as

$$\Delta\bar{E}_T = \bar{E}_n(T_2) - \bar{E}_n(T_1). \qquad (4)$$

Theoretical considerations /6/ have resulted in

$$\Delta \bar{E}_T = + \frac{1}{3A} \cdot \Delta\langle \varepsilon_k \rangle \quad \text{for free gas atoms} \tag{5}$$

and $$\Delta \bar{E}_T = - \frac{1}{3A} \cdot \Delta\langle \delta_k \rangle \quad \text{for absorption in crystals,} \tag{6}$$

if $\Gamma \gg \Gamma_n$ and $\Gamma \gg \hbar\nu$ where Γ_n is the neutron width and $\hbar\nu$ is the energy of the crystal phonons. A possible anisotropy indicated by the theoretical approach, is neglected. The difference between eqs. (5) and (6) in sign appears if the momentum conservation in the absorption process is applied to the system neutron + atom or, in the other case, to the system neutron + crystal. This temperature shift of neutron resonances is searched in the presented experiment.

2. Experiment

Neutron transmission spectra were measured with metallic samples of Rh, Ag, and Dy at several temperatures in the region of low-energy resonances using a time-of-flight spectrometer at the Dubna pulsed reactor IBR-30 operated in booster mode with the linac LUE-40. The experimental arrangement is shown in Fig. 1. The samples at different temperatures have been alternately put in the beam in each case for 10 min. Every 12 h, the temperatures of the samples were interchanged. At the end of a period of the order of one week, all spectra measured at T_1 and T_2, respectively, were added. Examples of obtained spectra are shown in Figs. 2 and 3.

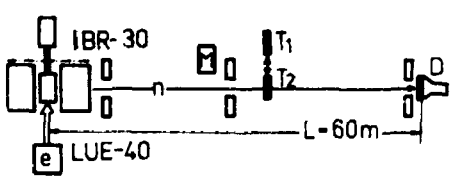

Fig. 1
Experimental arrangement. T_1 and T_2, samples at temperatures T_1 and T_2, respectively; D, ^{6}Li-glass scintillation detector; M, neutron monitor.

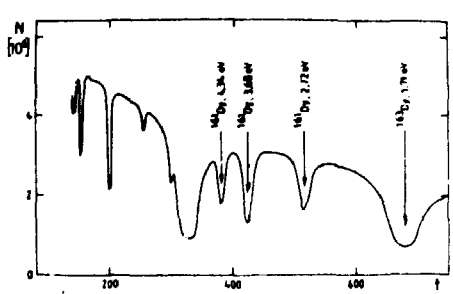

Fig. 2
Time-of-flight spectrum of the Dy sample at 303 K. The width of the time channels is 4 μs.

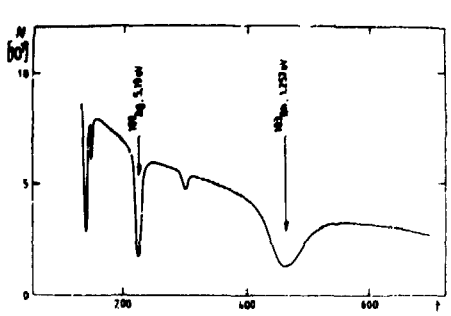

Fig. 3
Time-of-flight spectrum of the sample with Rh and Ag at 294 K. The width of the time channels is 8 μs.

In supplementary runs, the spectrum of the neutron beam without samples was measured. The background was determined with thick resonance probes.
The temperature shifts were extracted from the experimental data by two independent methods:

a) From the transmission spectra, $\Delta\sigma_R(E_n) = \sigma_R(T_2,E_n) - \sigma_R(T_1,E_n)$ was calculated with which the shift is

$$\Delta \bar{E}_T = \int_{E_1}^{E_2} \Delta\sigma_R(E_n) \cdot E_n \cdot dE_n \Big/ \int_{E_1}^{E_2} \sigma_R(T_1,E_n) \cdot dE_n \,, \qquad (7)$$

$$\int_{E_1}^{E_2} \sigma_R(T_1,E_n) \cdot dE_n = \int_{E_1}^{E_2} \sigma_R(T_2,E_n) \cdot dE_n \,.$$

b) The time-of-flight spectra $N(T_1,t)$ and $N(T_2,t)$ were compared with the aid of least-square fits as at the analysis of chemically induced shifts /7/. Then, the obtained difference curves were interpreted as differences of the Doppler broadenings using the theoretical approach of Jackson and Lynn /8/ with the Einstein model for the phonon spectra, and with a shift parameter in one of the both resonance cross sections.

3. Results

The obtained resonance shifts are compiled in Fig. 4. The expected theoretical behaviour (eq.(6)) is also inserted. If $\alpha_T = \Delta \bar{E}_T \cdot A/\Delta\langle\varepsilon_a\rangle$ is calculated corresponding to eq. (6), the average of the data obtained with method a) is $\bar{\alpha}_T^a = -0.49 \pm 0.13$ and with method b) $\bar{\alpha}_T^b = -0.43 \pm 0.09$, respectively.

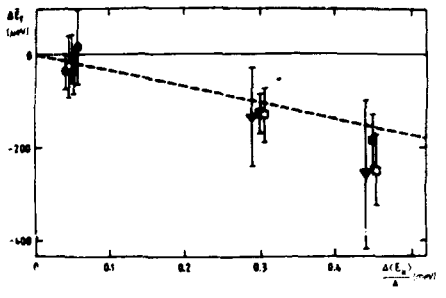

Fig. 4
Experimental shift values and theoretical prediction (eq.(6),---)). ■ , Rh-103, E_0=1.257 eV, T_1=294±2 K, T_2 = 667 ± 10 K and T_1 = 294 ± 2 K, T_2 = 538 ± 10 K; ▼ , Ag-109, E_0 = 5,19 eV, T_1 = 294 ± 2 K, T_2 = 667 ± 10 K and T_1 = 294 ± 2 K, T_2 = 532 ± 10 K; ● Dy-163, E_0=1.713 eV, Dy-161, E_0 = 2.72 eV, 3.68 eV, 4.34 eV, T_1 = 303 ± 1 K, T_2 = 370 ± 3 K; open signs, values extracted by method a); full signs, values extracted by method b)

In Fig. 5, the α_T of all resonances analysed are plotted versus the neutron resonance energies. It can be seen that any other systematic correlations of the shifts with the recoil energies, the resonances parameters or the phonon energies, which could imitate the searched temperature shift, were not observed.

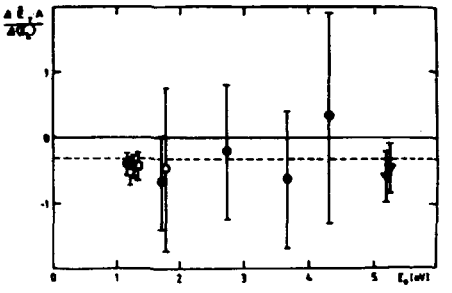

Fig. 5
Temperature shifts normalized to $\langle \varepsilon_k \rangle / A$ plottet versus the resonance energies.

References

/1/ H. Bethe and G. Placzek, Phys. Rev. 51 (1937) 462.
/2/ W.E. Lamb, Phys. Rev. 55 (1939) 150.
/3/ R. Pound and G.A. Rebka, Phys. Rev. Lett. 4 (1969) 274.
/4/ B.D. Josephson, Phys. Rev. Lett. 4 (1969) 341.
/5/ V.K. Ignatovich et al., Report JINR P4-7296 (1973).
/6/ K. Seidel et al., Yad. Fiz. 42 (1985) 1041.
/7/ A. Meister et al., Proceedings of this Symposium p.65
/8/ H.E. Jackson and J.E. Lynn, Phys. Rev. 127 (1962) 461.

СЕЧЕНИЕ ДЕЛЕНИЯ ^{243}Am В ОБЛАСТИ ПОРОГА (n,n'f) .

А.А.Говердовский, Б.Д.Кузьминов, В.Ф.Митрофанов, А.И.Сергачёв
Физико-энергетический институт, Обнинск, СССР

Аннотация
Приводятся результаты измерений сечения деления америция-243 нейтронами с энергией 5-II МэВ. Наблюдаемые нерегулярности в энергетической зависимости связываются в рамках статистической модели с проявлением конкуренции делительного и нейтронного каналов распада составного ядра.

Работа была выполнена на перезарядном генераторе ЭГП-IOM Физико-энергетического института. Источником нейтронов служила реакция D(d,n) ^{3}He в газовой дейтериевой мишени. В качестве детектора осколков деления использовалась быстрая двойная ионизационная камера деления, наполненная смесью ксенона и метана до давления I,5 10^{5} Па. Эффективность регистрации актов деления ядер урана-235 и америция-243 составила соответственно 99% и 95,5%. Электронный тракт регистрации работал в режиме импульсной синхронизации, что позволило выделить в время-пролётных спектрах (пролётная база L ~ 0,7 м) значительную фоновую компоненту. В работе использовались мишени из окислов урана и америция. Изотопическая чистота мишени из ^{235}U - 99,992 %. В мишени из америция-243 содержались примеси ядер ^{241}Am (2,7 %) и изотопов кюрия (10^{-3} %). С образцами указанного состава измеряли энергетическую зависимость отношений сечений деления ^{243}Am и ^{235}U . Абсолютизация этой зависимости осуществлялась методом "элементных примесей", для чего в мишень из ^{243}Am вносилась добавка ядер ^{235}U (35 %) ; после этого сборка америций-уран облучалась поочерёдно в потоках быстрых и замедленных нейтронов. Более подробно методика измерений отношений сечений деления быстрыми нейтронами описана нами в /I/ .

Результаты измерений сечений деления ^{243}Am (сечение деления урана-235- стандартные данные /2/) представлены на рис.I. Данные работы /3/ показаны светлыми кружками. Результаты /4/ нормированы на значение сечений деления ^{243}Am в области первого плато σ_f = I,56 барн. На эту же величину нормированы и данные настоящей работы , хотя абсолютизация энергетической зависимости в области E_n ~ 7,3 - 8,5 МэВ приводит к значению σ_f = I,6I ± 0,03 барн . Выбранная на

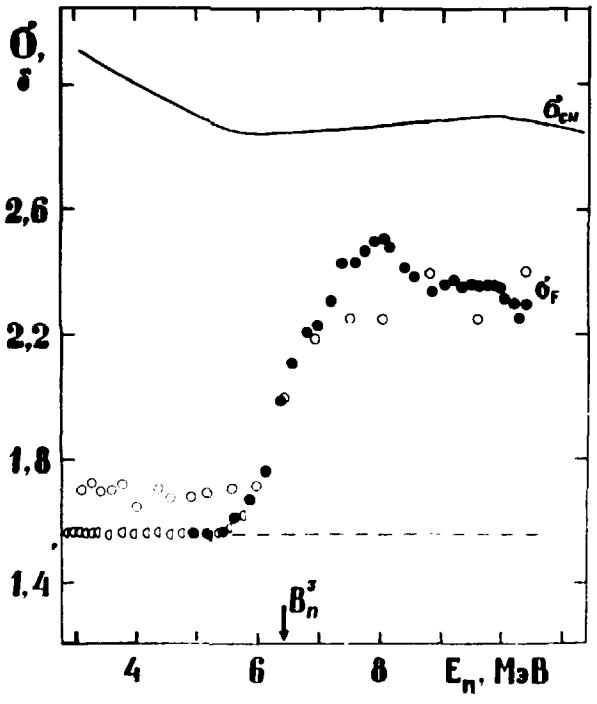

Рис. I. Сечение деления ^{243}Ам нейтронами: ● - настоящая работа; ○ - /3/ ; ◐ - /4/; - - - - - экстраполяция первого делительного шанса .

рис.I нормировка соответствует среднему значению σ_f по совокупности данных работ /3,4,5/ и наших. Сечение образования составного ядра σ_c вычислено согласно /6,7/ . Как видно из рис.I, энергетическая зависимость сечения деления ^{243}Ам в области порога (n,n'f) обнаруживает значительные нерегулярности. В области $E_n \sim 6{,}4$ МэВ (порог канала ^{243}Ам(n ,2n) ^{242}Ам) кривая σ_f меняет наклон, что соответствует включению в конкуренцию каналов распада составного ядра эмиссии второго нейтрона. По мере роста нейтронной ширины Γ_n рост вероятности деления замедляется и при $E_n \sim 8$ МэВ наблюдается резкое падение сечения на 10 - 15 %. Далее следует непродолжительное "плато" и снова падение σ_f.

Слабая энергетическая зависимость $\sigma_{сн}$, а также довольно простая экстраполяция первого делительного шанса в область $E_n \sim 6$ МэВ (рис.I) позволяют достаточно надёжно определить среднюю вероятность деления ядра ^{243}Ам, исходя из соотношения:

$$\sigma_f = \sigma_f^I + (\sigma_{сн} - \sigma_f^I) \int_0^\infty \frac{\varepsilon}{T^2} e^{-\frac{\varepsilon}{T}} \frac{\Gamma_f}{\Gamma_f + \Sigma\Gamma_c} d\varepsilon \quad , \qquad (1)$$

где ε - энергия эмиссионного нейтрона, $\Sigma\Gamma_c$ - суммарная ширина всех каналов распада составного (^{243}Ам) ядра неделительной природы. Основной вклад в $\Sigma\Gamma_c$ при $E_n \sim 6{,}5 \div 7$ МэВ вносит радиационная ширина, а для более высоких энергий - Γ_n .

Температуру эмиссионного спектра T можно определить по наилучшему согласию низкоэнергетических участков $\langle P_f \rangle$ из настоящей работы и $\langle P_f^* \rangle$ – значениям P_f работы /8/, усреднённым с плотностью вероятности $\rho(\varepsilon) = \frac{\varepsilon}{T^2} e^{-\varepsilon/T}$. Такое сравнение приводит к величине T= 0,5I ± 0,I МэВ.

Параметр барьера деления составного ядра ^{243}Am – B_f определялся в процессе описания экспоненциальной части кривой средней вероятности деления (E_n ≤6,5 МэВ):

$$\langle P_f \rangle = \int_0^\infty \frac{\varepsilon}{T^2} e^{-\frac{\varepsilon}{T}} \frac{T_f}{T_f + \Sigma T_c} d\varepsilon \quad , \qquad (2)$$

где T_c – проницаемость соответствующих каналов распада. Для проницаемости барьера деления T_f использовали выражение:

$$T_f(E^*) = (1 + EXP(\frac{2\pi}{\hbar\omega}(B_f - E^*)))^{-1} \quad , \qquad (3).$$

Параметр $\hbar\omega$ слабо влияет на вычисляемые значения $\langle P_f \rangle$, поэтому его значение принималось в соответствии с систематикой /9/ равным 0,8 МэВ. Результаты расчётов по (2) – (3) представлены на рис.2а. Варьировался лишь один

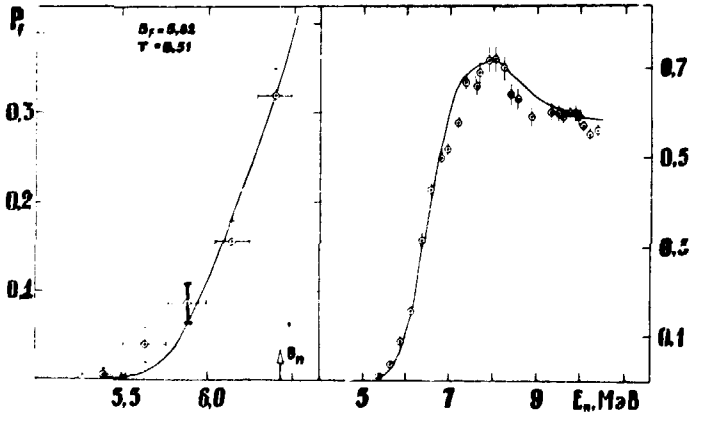

Рис.2. Результаты расчёта средней по спектру возбуждения делящегося ядра вероятности деления $\langle P_f \rangle$: —— расчёт, ⊕ – экспериментальные значения.

параметр – B_f; его наилучшая величина составила 5,82 ± 0,20 МэВ

Высокоэнергетическая часть $\langle P_f \rangle$(E_n >6,9 МэВ) рассчитывалась с указанными выше параметрами T и B_f по формуле (I). Нейтронная и делительная ширины определялись аналогично /7/. Плотность состояний при равновесной и седловой деформациях ядра ^{243}Am рассчитывалась в модели Ферми-Газа с феноменологичес-

ким учётом парных корреляций . При низких энергиях возбуждения $E_n < 3,2$ МэВ использовались соотношения модели постоянной температуры /10/ . Результаты вычислений представлены на рис.2б и свидетельствуют о том , что в рамках описанного выше упрощённого подхода можно сделать однозначный вывод о природе наблюдаемого в сечении деления ^{243}Am максимума в области порога (n,n'f) заключающейся в конкуренции двух основных каналов распада составного ядра : деления и испускания нейтронов. Учёт в расчётах сечения деления таких явлений, как потеря аксиальной симметрии ядром на внутреннем барьере, влияние коллективных степеней свободы на плотность состояний ядра и др., даст основание для более детального сравнения экспериментальных и расчётных результатов .

ЛИТЕРАТУРА

1. Говердовский А.А. и др. - Атомная Энергия , 58 (1985) 137 .
2. ENDF/B-V, 3rd ed., BNL, 1979, U-235 (MAT 1395) .
3. Behrens J.W. et.al. - Nucl.Sci.Engng., 77 (1981) 444 .
4. Fursov B.I. et.al. - In: Proc.Int. Conf. on Nuclear Data for Basic & Appl. Physics, Santa-Fe, USA, may 1985 .
5. Knitter H.-H., Budtz-Jørgensen C. - ibid.
6. Lagrange Ch. - INDC(FR)56/L-NEANDC(E)228"L", 1982 .
7. Бычков В. и др. - Препринт ФЭИ-1052, Обнинск, 1982 .
8. Gavron A.,Britt H.C. - Phys. Rev., C13 , (1976) 2374 .
9. Bjørnholm S., Lynn J.E. - Rev. Mod. Phys., 52 , (1980) 725 .
10. Gilbert A. & Cameron A.G.W. - Can.J.Phys., 43 , (1965) 1446 .

ЭКСПЕРИМЕНТАЛЬНОЕ ИЗУЧЕНИЕ ПОДБАРЬЕРНОЙ СТРУКТУРЫ СЕЧЕНИЯ ФОТОДЕЛЕНИЯ ^{232}Th.

А.С. Солдатов, З.А.Александрова, Г.Н.Смиренкин, М.З.Тараско
Физико-энергетический институт, Обнинск, СССР

Аннотация

Сообщаются результаты детальных исследований выхода и сечений фотоделения ^{232}Th на пучке тормозного излучения микротрона. Измерения проведены для интервалов энергии 5,0 - 5,3 МэВ и 5,5 - 5,8 МэВ , где в более ранних экспериментах обнаруживались широкие подбарьерные резонансы. Результаты нового эксперимента свидетельствуют об их тонкой структуре с характерным расстоянием между резонансами ~0,1МэВ.

Последние годы большое внимание к себе привлекает исследование процесса деления лёгких актинидов в связи с проблемой так называемой "ториевой аномалии", которая заключается в трудности описания резонансной структуры сечений ядер в районе Th с помощью модели двугорбого барьера / I,2 /. Расчеты потенциальной энергии деформации для этих ядер предсказывают значительную разницу между высотами внутреннего и внешнего горбов E_f^A и E_f^B ($E_f^B > E_f^A$), из чего можно ожидать,что резонансной структуры в области энергии возбуждения $E > E_f^A$ не будет. В эксперименте она, напротив, отчетливо проявляется в широкой окрестности наблюдаемого порога, определяемого высотой более высокого горба - в данном случае E_f^B . Выход из противоречия связывают с результатами более детальных расчетов, которые свидетельствуют о расщеплении горба B и образовании третьей ямы.

Концепция трехгорбого барьера получила широкое распространение при интерпретации околопороговых эффектов в вероятности деления легких актинидов. Однако, многие из возникающих в ней вопросов остаются открытыми. Среди них вопрос о глубине третьей ямы, о наблюдении и идентификации резонансных состояний в разных ямах барьера и другие. Естественный путь к получению такой информации - это исследование подбарьерной области энергий, но оно сталкивается с большими трудностями. При уменьшении энергии возбуждения составного ядра E на I МэВ ниже порога делимость падает на 5-6 порядков , и лишь очень ограниченный круг методических средств может обеспечить достаточную чувствительность в таком диапазоне.

В данной работе при изучении реакции $^{232}Th(\gamma, f)$ мы основывались на подходе ,

объединяющем достоинства мощного пучка тормозного излучения микротрона и трековых детекторов осколков, который в предыдущих наших работах /3,4/ был с успехом использован для изучения глубокоподбарьерного фотоделения ядер. Недостаток его заключается в том, что спектр тормозного излучения $N(E, E_{max})$ является сплошным, монотонно убывающим с увеличением E на интервале (0,E_{max}) (E_{max}- энергия ускоренных электронов), что очень затрудняет получение информации об интересующем сечении деления $\sigma_f(E)$ из наблюдаемого выхода

$$Y(E_{max}) \sim \int_0^{E_{max}} \sigma_f(E) N(E, E_{max}) dE \qquad (I)$$

В предыдущих наших работах измерения выхода производились с шагом ΔE_{max}=0,I-0,25МэВ, что существенно больше энергетического разрешения электронного пучка микротрона ~ 20 кэВ. В данной работе мы попытались использовать энергетическое разрешение полностью, и с этой целью изменяли энергию электронов с шагом 25 кэВ.

Подробные измерения выхода $Y(E_{max})$ проводились нами в двух интервалах E_{max}= 5,5 - 5,8 МэВ и 5,0 - 5,3 МэВ, где ранее наблюдались нерегулярности ступенчатого типа, которые при восстановлении сечения из (I) становились резонансами / 4,5 /. Нерегулярности в этой области энергии наблюдались и в измерениях непосредственно сечения фотоделения ^{232}Th на монохроматических гамма-квантах /6,7/. В последней работе исследования проводились методом "Меченных фотонов" с разрешением I2-I4 кэВ и широкий резонанс при E = 5,5 - 5,8 МэВ распался на группу резонансов со средним расстоянием между ними ~ 0,I МэВ. Поэтому мы вправе были рассчитывать на наблюдение подобной структуры и при измерении энергетической зависимости выходов $Y(E_{max})$.

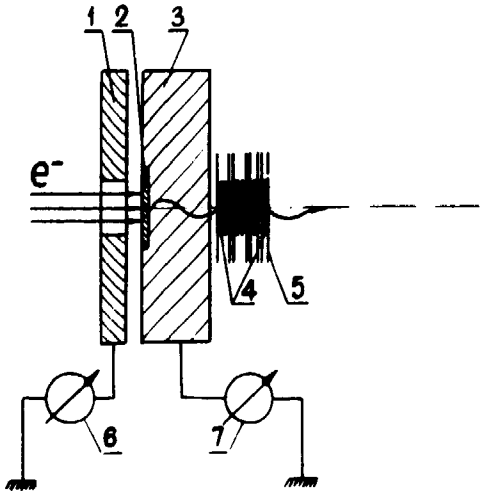

Рис.I. Схема опыта.
I-диафрагма; 2-тормозная мишень из вольфрама; 3-алюминиевый поглотитель электронов; 4-ториевые и урановые фольги; 5-слюдяные детекторы; 6-индикатор тока; 7-интегратор тока.

Эксперимент был выполнен на выведенном пучке микротрона Физико-энергетического института. Схема облучения показана на рис. I. Пучок электронов попадал на тормозную, охлаждаемую водой мишень из вольфрама толщиной I мм, за которой помещался алюминиевый поглотитель электронов толщиной I2 мм. Сразу после поглотителя помещались 4 сборки из металлических фольг делящегося вещества толщиной 0,I мм и детекторов из телевизионной слюды. В первых двух сборках использовалось по одной фольге ^{232}Th и ^{238}U, которые располагались вплотную друг к другу. В остальных- только ториевые фольги с двух сторон обложенные детекторами. Такая композиция позволяла в некоторой степени скомпенсировать более быстрое уменьшение выхода фотоделений ^{232}Th с уменьшением энергии. Делящиеся фольги и детекторы разделялись алюминиевыми перегородками толщиной 0,3 мм с отверстием диаметром I0 мм. Протяженность всех 4 сборок по оси пучка составляла 2,5 мм, расстояние от вольфрамовой мишени до первой сборки - I4 мм.

Таким образом, эксперимент позволял измерять две характеристики: выход $Y(E_{max})$ в числах делений на микрокулон для бесконечно толстой по отношению к пробегу осколков металлической фольги и описанных выше условий опыта (в таких единицах выход $Y(E_{max})$ представлен на рис. 2) и более благоприятную для ряда целей величину- отношение выходов реакции (γ, f) на ^{232}Th и ^{238}U

$$R(E_{max}) = Y_{Th}(E_{max}) / Y_U(E_{max}) \quad (2)$$

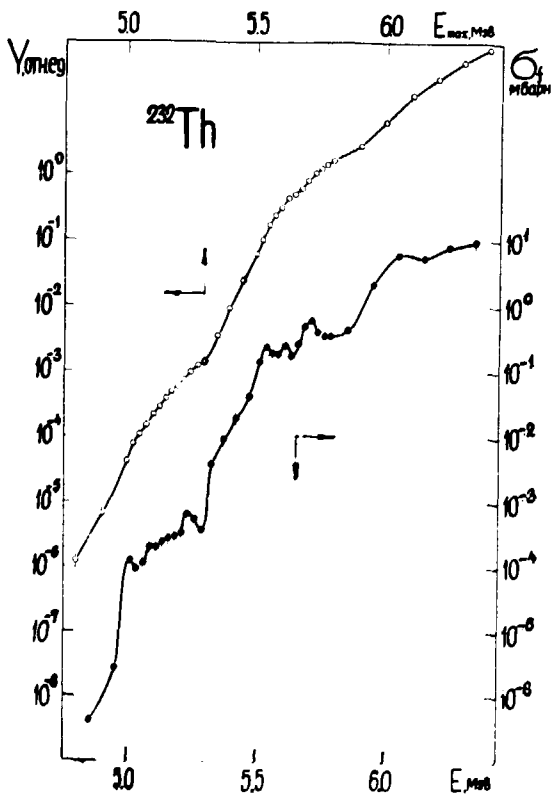

Рис. 2. Выход реакции $^{232}Th(\gamma, f)$ от граничной энергии тормозного спектра в числах делений на один детектор и интеграл тока I микрокулон (вверху). Сечение фотоделения ^{232}Th.

В рассматриваемом нами здесь диапазоне E_{max} = 4,8 - 6,4 МэВ выход $Y(E_{max})$ изменяется на 8 порядков. В таком масштабе никакие важные для нас детали энергетической зависимости $Y(E_{max})$ увидеть невозможно. Отношение $R(E_{max})$ в этом случае изменяется в гораздо меньших пределах на 3 порядка, но тоже достаточно больших, чтобы представить соответствующую кривую в удобном линейном масштабе. Все это хорошо видно на приведенных ниже рисунках, где показаны: на рис.2 -выход $Y_{Th}(E_{max})$ и восстановленное из него сечение $\sigma_f(E)$ в широкой области E_{max}, E = 4,8 - 6,4 МэВ и на рис.3 - отношение выходов $R(E_{max})$ и сечение фотоделения ^{232}Th на участках E, E_{max}= 5 - 5,3 МэВ и 5,5 - 5,8 МэВ.
На вставке к рис.3 (внизу) представлен участок $\sigma_f(E)$ для ^{232}Th, изученный в работе /7/ в области E = 5,4 - 5,8 МэВ. Вертикальными пунктирными линиями указаны положения нерегулярностей в $R(E_{max})$ и резонансов в $\sigma_f(E)$.

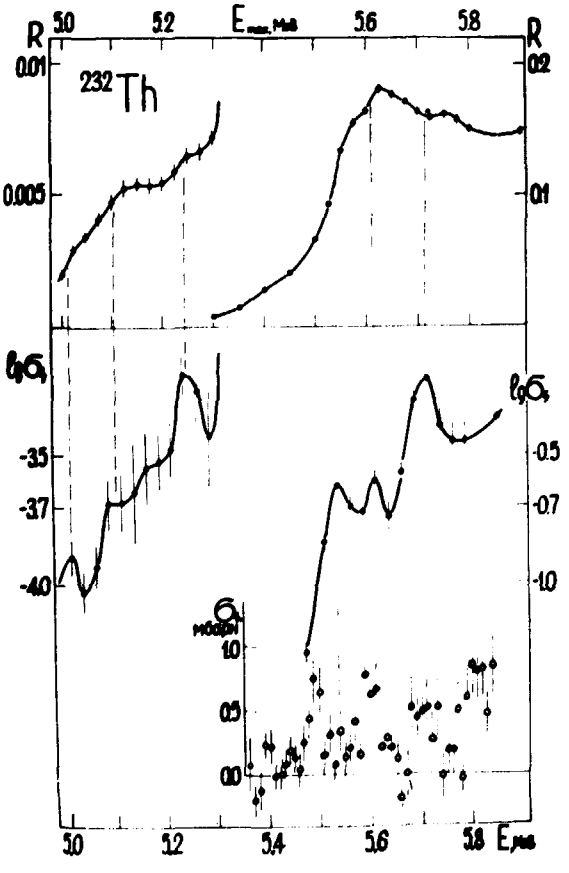

Рис.3. Сопоставление нерегулярностей в отношениях выходов реакции (γ, f) на ^{232}Th и ^{238}U и в сечении фотоделения ^{232}Th, полученных в настоящей работе (темные точки) и в работе /7/ (светлые точки) для интервалов энергии, исследовавшихся подробно. Вертикальные пунктирные линии - положения нерегулярностей.

В связи с отчетливой корреляцией особенностей представленных на рис.3 характеристик - "ступенек" в отношении $R(E_{max})$ и резонансов $\sigma_f(E)$ - необходимо отметить следующее. Во-первых, наличие знаменателя в (2), по-видимому, не мешает качественному анализу структуры $Y_{Th}(E_{max})$, поскольку $Y_U(E_{max})$ является более плавной, но, разумеется не идеальной гладкой кривой / 4,6,8,9/. Во-вторых, наличие корреляции свидетельствует о качестве восстановления $\sigma_f(E)$ из интегрального уравнения (I), которое осуществлялось итерационным методом минимизации направленного расхождения Тараско /I0/. Как и каждой некорректно поставленной задаче этому методу присуща проблема регуляризации решения. Для выбора "Наилучшего" числа итераций производился анализ близких тестовых вариантов. Погрешности $\sigma_f(E)$ на рис.2 и 3 оценивались из дисперсии многократных решений (I) для значений $Y(E_{max})$, варьировавшихся по нормальному закону с экспериментальными дисперсиями.

Отметим удовлетворительное согласие с результатами работы /7/, в которой были впервые обнаружены резонансы тонкой структуры в сечении фотоделения ^{232}Th. На энергии 5,8 МэВ обрываются наши подробные измерения $Y(E_{max})$ и, вероятно, этим можно объяснить пропуск последнего резонанса в интервале 5,5 - 5,8 МэВ. Структурный характер, согласно нашим данным, имеет сечение фотоделения и на интервале 5,0-5,3 МэВ, хотя статистические погрешности в этом случае примерно в 3 раза больше.

Таким образом, обе исследованные нами "ступеньки" в подбарьерном сечении $\sigma_f(E)$ для ^{232}Th обнаруживают сходную резонансную структуру. Для интервала E= 5,5-5,8МэВ можно достаточно надежно оценить среднее расстояние между резонансами "микроструктуры" $\mathcal{D} \approx 80 - 100$ кэВ. В этой области энергий согласно /5/ сильно преобладает дипольная компонента, то есть соответствующие делительные состояния имеют характеристику J^{π}, $K = I^-, 0$. Следуя работе /II/, где рассмотрен вопрос о статистическом описании уровней в первой и второй ямах барьера, из приведенного значения $\mathcal{D}$ легко оценить энергию возбуждения ≈ 2 МэВ и положение дна ямы 3,5 - 3,8 МэВ. Если обсуждаемые уровни принадлежат второй яме, то необходимо допустить, что высота внутреннего горба E_f^A для J^{π}, $K = I^-, 0$ больше 5,8 МэВ. Это существенно превышает теоретические предсказания для нижайшего состояния 0^+ $E_f^A \approx 4$ МэВ /2/. С другой стороны, данную выше оценку трудно согласовать с имеющимися представлениями о небольшой глубине третьей ямы /2/. Иначе говоря, интерпретация результатов сталкивается с трудностями.

ЛИТЕРАТУРА

1. S.Bjornholm, V.M.Strutinsky, Nucl.Phys.,v.A136 , p.1 ,1969.
2. P.Möller,J.R.Nix. Phys. and Chem. of Fission, IAEA, Vienna, 1974,p.103.
3. В.Е.Жучко, Ю.Б.Остапенко, Г.Н.Смиренкин, А.С.Солдатов,Ю.М.Ципенюк. Ядерная физика. т.28, с.1185 , 1978.
4. В.Е.Жучко,Ю.Б.Остапенко, Г.Н.Смиренкин, А.С.Солдатов, Ю.М.Ципенюк. Ядерная физика, т. 28, с.1170 , 1978.
5. В.Е.Жучко, С.П.Капица, Ю.Б.Остапенко,Г.Н.Смиренкин,А.С.Солдатов, Ю.М.Ципенюк. Письма в ЖЭТФ , т.26, с.718 , 1977.
6. A.M. Khan, J.W.Knowles.Nucl. .Phys.,v.A179,p.333,1972.
7. J.W.Knowles,W.E.Mills,R.N.King, B.O.Pich, S.Yen, R.Sobie,L.Watt, T.E.Drake. Phys.Lett.,v.116B, p.315,1982.
8. P.A.Dickey, P.Axel, Phys.Lett.,v.35, p.501,1975.
9. L.J.Lindgren,A.Alm , A.Sandell. Nucl.Phys.,v.A298,p.43,1978.
10. М.З.Тарасчо. Метод минимума направленного расхождения в задачах поиска распределений.Препринт ФЭИ-1446,1983.
    V.E.Zhuchko,Yu.B.Ostapenko,A.S.Soldatov, Yu.M.Tsipenyuk. Nucl.Instl.Meth.,v.136,p.373,1976.
11. В.М.Купрянов,Г.Н.Смиренкин. Ядерная физика, т.35,с.598,1982.

ВЫХОД И СЕЧЕНИЕ ФОТОДЕЛЕНИЯ ^{231}Pa

А.С.Солдатов, В.Е.Рудников, З.А.Александрова, Г.Н.Смиренкин
Физико-энергетический институт, Обнинск, СССР

Аннотация

Сообщаются результаты впервые измеренных выходов и восстановленных из них сечений деления в реакции $^{231}Pa(\gamma, f)$ для области энергий γ- квантов 4,8 - 7,0 МэВ.

Деление легких актинидов (Th, Pa) обнаружило ряд свойств, неукладывающихся в рамки классической модели двугорбого барьера [I] . Учёт в теоретических расчётах зеркально-асимметричной деформации привел к предсказанию на месте горба В третьей ямы. На его основе сложились представления трехгорбой модели барьера, с помощью которой удалось объяснить, пока , правда в основном качественно, "аномалии" процесса деления ядер в районе Th .

В исследованиях легких актинидов внимание приковано к околопороговой области энергий возбуждения, в которой наиболее информативны нейтронные эксперименты с высоким энергетическим разрешением [2] . Эти эксперименты снизу ограничены энергией связи нейтрона. Таких ограничений нет в прямых реакциях и фотоделении.

Вероятность деления ядра ^{231}Pa была изучена только в реакции $^{230}Th(^3He, df)$ в области околопороговых энергий возбуждения , 5,5 - 7,5 МэВ [3] . Отсутствие данных в глубокоподбарьерной области энергий мы попытались восполнить исследованиями реакции (γ, f) с помощью тормозного излучения микротрона. Измеренные интегрального выхода фотоделения $Y(E_{max})$ позволяет путём решения уравнения

$$Y(E_{max}) = \int_0^{E_{max}} \sigma_f(E)\, N(E, E_{max})\, dE \qquad (I)$$

найти энергетическую зависимость физически более интересной величины - сечения фотоделения $\sigma_f(E)$ ($N(E, E_{max})$- спектр тормозного излучения). В прошлом такие эксперименты были осуществлены для широкого круга ядер при $E_{max} \leq 7$ МэВ с шагом $\Delta E_{max} = 0,I$ МэВ [4] , а в другом докладе на настоящем симпозиуме [5] , сообщаются результаты последних измерений для реакции $^{232}Th(\gamma, f)$ с шагом $\Delta E_{max} = 0,025$ МэВ , близким к энергетическому разрешению ускорителя в микротроне

электронов. В данной работе сообщаются результаты впервые проведенных измерений выхода $Y(E_{max})$ и восстановленного из него сечения $\sigma_f(E)$ для реакции $^{231}Pa(\gamma, f)$ в диапазоне энергий 4,8 – 7,0 МэВ.

Эксперимент был поставлен на импульсном микротроне физико-энергетического института. Тормозной мишенью служил вольфрамовый диск толщиной I мм с I2-миллиметровым алюминиевым поглотителем электронов. На расстоянии 30 мм от вольфрамовой мишени вплотную друг к другу располагались слои ^{231}Pa и ^{238}U толщиной 0,33 и 0,74 мг/см^2, соответственно, диафрагмированные алюминиевой непрозрачной для осколков деления фольгой с окном диаметром I0мм. Детектирование осколков производилось слюдяными детекторами, которые помещались в жестко скрепленные с делящимися слоями кассеты. Стенки кассет с отверстием диаметром I2 мм для пролёта осколков находились на расстоянии 3,5 мм от делящихся слоёв. Во время облучения производилось интегрирование тока электронов, попадающих на тормозную мишень. Более подробно детали эксперимента описаны в работах [4], в которых проводились аналогичные измерения.

Были выполнены две серии измерений. В первой облучения проводились в широкой области граничных энергий тормозного спектра E_{max} от 4,8 до 7,0 МэВ с шагом 0,I МэВ. Внимание к себе привлекла подбарьерная нерегулярность в энергетической зависимости выхода реакции $^{231}Pa(\gamma, f)$ $Y(E_{max})$ при E_{max} = 5 МэВ, ещё более отчетливо проявившаяся в энергетической зависимости отношения выходов для ^{231}Pa и ^{238}U $R(E_{max}) = Y_{Pa}(E_{max}) / Y_U(E_{max})$. Энергетический диапазон E_{max} = 4,8 – 5,I МэВ решено было исследовать более подробно – с шагом 0.05 МэВ и с лучшей статистической точностью.

Во второй серии вдвое было уменьшено расстояние от делящихся слоев до тормозной мишени. Боксы с детекторами также были приближены к делящимся слоям так, что расстояние между ними стало I,5 мм. Вместе с увеличением экспозиций это позволило почти на порядок увеличить число регистрируемых актов деления.

На рис. I представлена энергетическая зависимость выхода для ^{231}Pa по сумме обеих серий измерения: кривой I – во всем диапазоне E_{max}, кривой II – на более подробно изученном низкоэнергетическом участке. Внизу показаны отношения выходов ^{231}Pa и ^{238}U – $R(E_{max})$. Максимум $R(E_{max})$ отчетливо проявился в обеих сериях измерения. Отметим, что отношения выходов $R(E_{max})$ нечувствительны к погрешностям, связанным с встроенной пучка и определением экспозиции, но несут в себе некото-

рую неоднозначность в идентификации нерегулярностей. Из анализа выходов для различных ядер и их отношений мы пришли к заключению, что на интервале энергий 4,9–5,2 МэВ $Y(E_{max})$ для ядра ^{238}U ведет себя плавно, и максимум $R(E_{max})$ на рис. I всецело связан с исследуемым ядром ^{231}Pa.

Для восстановления сечения фотоделения $\sigma_f(E)$ из выхода $Y(E_{max})$ (I) применялся итерационный метод минимизации направленного расхождения [6]. Предметом дискуссии в этом методе решения некорректно поставленных задач является выбор числа итераций и определение погрешности из дисперсии многократных решений с левой частью (I), варьируемой по нормальному закону с экспериментальной дисперсией. По этой причине мы уделили выше много внимания демонстрации статистической значимости особенности при $E_{max} \approx 5$ МэВ в непосредственно наблюдаемой информации о $Y(E_{max})$ и $R(E_{max})$. В сечении $\sigma_f(E)$, показанном на рис.2, ей соответствует резонанс.

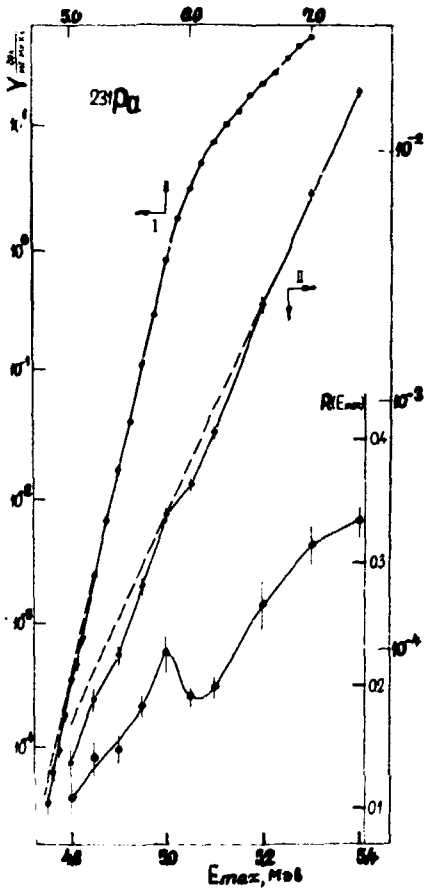

Рис. I. Зависимость выхода Y реакции $^{231}Pa(\gamma, f)$ (кривые I и II) и отношения выходов R для реакций $^{231}Pa(\gamma, f)$ и $^{238}U(\gamma, f)$ от граничной энергии тормозного спектра E_{max}. Экспериментальные точки: ● – $Y(E_{max})$, ○ – $R(E_{max})$

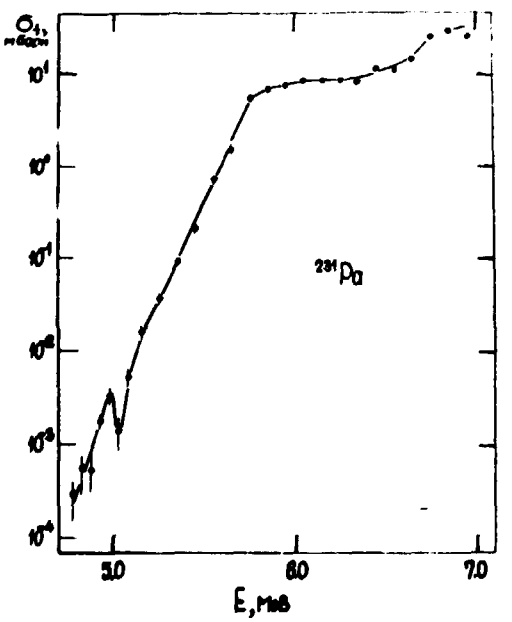

Рис. 2. Зависимость сечения фотоделения σ_f ядра ^{231}Pa от энергии γ-квантов.

Сечение фотоделения ^{231}Pa, если его пересчитать в делимость

$$P_f(E) = \frac{\sigma_f(E)}{\sigma_c(E)}, \qquad (2)$$

где $\sigma_c(E)$ - сечение фотопоглощения, в области E = 5,5 - 7,0 МэВ удовлетворительно согласуется с делимостью, непосредственно измеренной в реакции ^{230}Th (^3He, df) [3]. Обнаруженный нами резонанс существенен для уточнения параметров барьера деления ядра ^{231}Pa. С этой целью желательно продолжить измерения при E < 4,8 МэВ, однако для их осуществления необходима мишень с большим количеством делящегося вещества.

Авторы благодарны Б.Ф.Масеодону и Л.А.Ивановой за предоставление ^{231}Pa и группе эксплуатации микротрона за содействие измерениям.

ЛИТЕРАТУРА

1. S.Bjornholm, V.M.Strutinsky. Nucl.Phys.,v.A 136, p.1, 1969.
P.Möller, J.R.Nix.Phys. and Chem. of Fission, IAEA,Vienna, 1974,p.103.
2. A.Michaudon. Rep. CEA - N - 2232 ,INDC (FR-51/L-NEANDC (E)-224, 1981.
3. B.B.Back , O.Hansen, H.C.Britt, J.D.Garratt. B.Leroux.Phys.and Chem.of Fission, IAEA,1974, v.1, p.3
4. В.Е.Жучко ,Ю.Б.Остапенко, Г.Н.Смиренкин,А.С.Солдатов, Ю.М.Ципенюк. Ядерная физика , т.28, стр.1170,1185,1978
5. А.С.Солдатов,З.А.Александрова.Г.Н.Смиренкин, М.З.Тараско "Экспериментальное изучение подбарьерных резонансов сечения фотоделения ^{232}Th " доклад на настоящем симпозиуме.
6. М.З.Тараско. Метод минимизации направленного расхождения в задачах поиска распределений. 1983, препринт ФЭИ - 1446 .

V.E.Zhuchko, Yu.Ostapenko, A.S.Soldatov,Yu.Tsipenyuk.Nucl. Instr.Meth., v.136,p.373, 1976.

PHOTON INDUCED FISSION OF ^{232}Th WITH 12 AND 20 MeV BREMSSTRAHLUNG.

(M.Piessens, E.Jacobs, D.De Frenne, A.De Clercq, M.Verboven, G.De Smet)
Nuclear Physics Laboratory, Proeftuinstraat 86, B-9000 Gent, Belgium

ABSTRACT

Gamma ray spectrometry of fission product catcherfoils and energy correlation measurements were performed for the photon induced fission of ^{232}Th with 12 and 20 MeV bremsstrahlung. The postneutron mass distributions show a third peak for symmetric fission. In the light and heavy mass wings strong fine structures are observed, probably due to odd-even effects. As usually observed, the total preneutron fragment kinetic energy decreases with increasing excitation energy of the compound nucleus in the vicinity of mass 130. For symmetric fission however, the fragment kinetic energies show an increase. Compared to 12 MeV bremsstrahlung induced fission, the number of emitted neutrons increases for fission induced with 20 MeV bremsstrahlung. This can completely be attributed to the heavy fragment.

I. INTRODUCTION

This work presents the first results concerning a study of the compound nucleus excitation energy dependence of some important fission characteristics in the photon induced fission of ^{232}Th. The overall mass and kinetic energy distributions, the total kinetic energy and the number of emitted neutrons as a function of the fragment mass are discussed for 12 and 20 MeV bremsstrahlung induced fission.

II. EXPERIMENTAL

The postneutron mass distribution was determined by gamma ray spectrometry of fission product catcherfoils. For 12 MeV bremsstrahlung irradiations varying in time between 15 M and 4 D were carried out on 10 thorium targets of 175 mg/cm^2 separated by Al-catcherfoils. Successive gamma-ray spectra were taken using a 50 cm^3 Ortec Ge(Li) detector with a resolution of 1.8 keV FWHM at 1333 keV. It was shown that for a target with thickness exceeding the range of fission fragments in the target material, a correction to the observed mass yields proportional to the inversed range of fragments of the considered mass in the target has to be introduced, to take into account the difference in range for different fragments1). This correction of the observed yields was determined experimentally by comparing the photopeak areas of the catcherfoil spectra obtained with the 175 mg/cm^2 targets with those obtained with 0.5 mg/cm^2 thick targets in the same geometry. Because of the low yields with the 0.5 mg/cm^2 targets these measurements were performed with 20 MeV bremsstrahlung. This experiment supplied at the same time the postneutron mass distribution for 20 MeV bremsstrahlung.

In the calculation of the mass distributions special attention was payed to the determination of the yields in the valley region. Therefore chemical separations of Ru and Sb were carried out. This allowed an accurate determination of the yields of mass 105, 106 (only for 20 MeV bremsstrahlung induced fission) and 125 relative to the yields of mass 103 and 127 resp.. The latter are well defined from the catcherfoil method.

Energy correlation measurements for the photofission of ^{232}Th with 12 and 20 MeV bremsstrahlung were performed using two surface barrier detectors with an active area of 600 mm^2. These measurements were calibrated using the Schmitt calibration method and constants for ^{235}U(n_{th},f)2). The thorium target consisted of a 100 µg/cm^2 ThF_4 layer evaporated on a 32 µg/cm^2 polyimide backing with 20 µg/cm^2 Au. The energy loss of the fission fragments in the target was experimentally determined by measuring the energy loss of ^{252}Cf(sf) fragments in it. From the energy correlation measurements the provisional mass and postneutron kinetic energy distributions and their correlations can be deduced.

Combining the results of the energy correlation measurements and the postneutron mass distribution the average number of emitted neutrons as a function of the preneutron mass was determined following the iterative method described in ref. 3). Simultaneously the preneutron mass and kinetic energy distributions and their correlations could be deduced.

III. RESULTS AND DISCUSSION

The postneutron mass distributions for fission induced with 12 and 20 MeV bremsstrahlung are shown in fig.1. The distributions are normalized to a total yield of 200%. The error bars contain the uncertainties of the peak area, the absolute gamma ray intensities and the relative efficiency of the detector.
The presence of a distinct third peak in the symmetric mass region is clear. This peak is less pronounced for 20 MeV bremsstrahlung induced fission. In the neutron induced fission of ^{232}Th Glendenin et al.4) found also a similar peak in the symmetric mass region which also seemes to wash out with increasing excitation energy, while the valley yield increases. The decrease of the third hump in the symmetric fission region with increasing excitation energy suggests that this peak is caused by shell effects in the fragments and not by the symmetric fission component expected from an enhanced liquid drop behaviour at higher excitation energy of the compound nucleus. Calculations in the framework of the static scission point model of Wilkins 5) based on deformed shells in the fragments predict indeed that thorium is situated in the transition region where the sym-

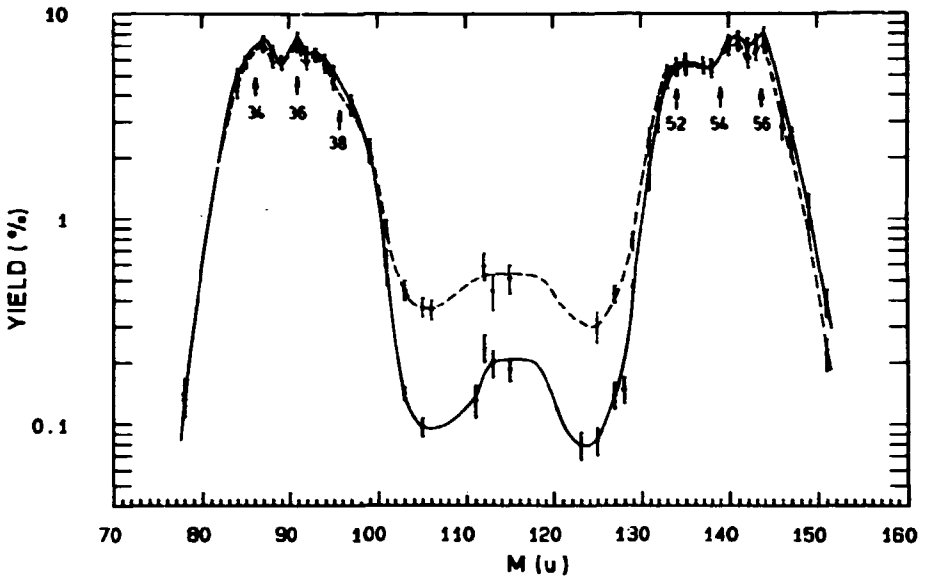

Fig.1. Comparison of the postneutron mass distribution for 12 MeV (—•—) and 20 MeV(-•-) bremsstrahlung induced fission. The arrows indicate the positions of the fragment masses corresponding with the even Z-values.

metric peak disappears for heavier nuclei.

Some characteristics of the postneutron mass distributions are summarized in table I.

Table I : Parameters of the postneutron mass distributions

E_e(MeV)	$\langle M_L \rangle$(u)	$\langle M_H \rangle$(u)	$\langle \nu \rangle$	A/S	$\langle E_{exc} \rangle$(MeV)
12	90.55±0.09	139.40±0.09	2.05±0.13	35±5	8.8
20	91.31±0.09	138.15±0.09	2.54±0.13	11±1.5	12.4

The $\langle \nu \rangle$ values are calculated from the conservation of mass. The parameter A/S indicates the ratio of the asymmetric to symmetric fission yield. The average excitacion energy $\langle E_{exc} \rangle$ of the compound nucleus, excited with bremsstrahlung with endpoint energy E_e, was calculated from the fission cross section of ^{232}Th 6) combined with the Schiff bremsstrahlung spectrum 7). The $\langle M_L \rangle$ and $\langle M_H \rangle$ values are in good agreement with the systematics of Unik 8) which predict values of resp. 90.5 and 139.2. The shift of $\langle M_L \rangle$ and $\langle M_H \rangle$ for E_e = 20 MeV is partly due to the enhancement of the symmetric fission component and partly to the increase of the number of emitted neutrons. The arrows in fig.1 indicate the positions of the calculated fragment masses associated with the even charges 34, 36, 38, 52, 54 and 56. In this calculation we used the expression for the most probable fragment charge $Z_p = Z_{UCD} \pm 0.3$ (+ for the light fragments and - for the heavy ones) with Z_{UCD} the fragment charge assuming the same N/Z ratio as the compound nucleus. The additional term 0.3 is an average value deduced from photofission studies of ^{235}U and ^{238}U 9).

In the necessary conversion of preneutron masses to postneutron masses the deduced neutron emission curve was used. (see further).

The enhanced yields in the vicinity of the light masses 86 and 91 and the complementary heavy masses 139 and 144 can indeed be explained by proton pairing effects. A further study of charge distributions could confirm this conclusion. It is well known that strong odd-even effects are present in the fission of thorium 10). In the mass 134 region a shoulder in the mass distribution is observed, but a pronounced enhanced yield of mass 134 as seen by Glendenin 4) is not present. In the complementary light mass region we see an enhancement of mass 95 but much less pronounced as in the corresponding heavy mass region. This difference between light and heavy mass region can be attributed to the relative high neutron emission for the light masses.

All these fine structures in the mass distributions are also present for E_e = 20 MeV but there is a slight decrease. The fact that the fine structures are not decreasing more strongly can probably be attributed to the considerable amount of second chance fission (about 30%).

Some characteristics of the overall pre- and postneutron kinetic energy distributions and the preneutron mass distributions are summarized in table VI.

Table II : Parameters of kinetic energy and preneutron mass distributions

E_e (MeV)	$\langle E_k \rangle$ (MeV)	$\langle E_k^* \rangle$ (MeV)	$\langle M_L^* \rangle$ (u)	$\langle M_H^* \rangle$ (u)
12	160.10±0.45	161.69±0.45	91.83±0.17	140.19±0.17
20	159.43±0.16	161.10±0.16	92.64±0.10	139.37±0.10

The values of $\langle E_k^* \rangle$, $\langle M_L^* \rangle$ and $\langle M_H^* \rangle$ are in agreement with the systematics of Unik et al 8) predicting values of resp. 163.9, 92.2 and 139.8.

The preneutron kinetic energy as a function of the preneutron fragment mass is presented in fig.2 for 12 and 20 MeV bremsstrahlung induced fission.

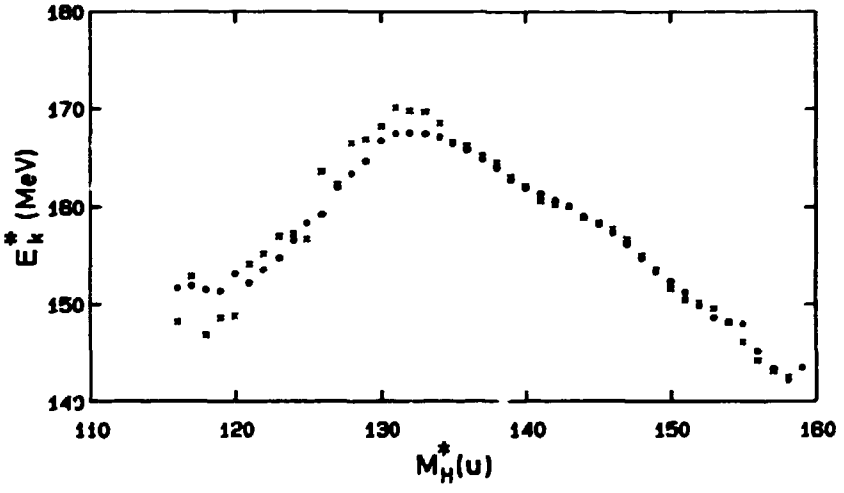

Fig.2. The total preneutron kinetic energy as a function of the heavy preneutron mass for 12 MeV (x) and 20 MeV (o) induced fission.

Striking in this comparison is the complete identical behaviour of the kinetic energy for M_H^* above 135. In the vicinity of heavy mass 130 we see a decrease of the fragment kinetic energy for E_e = 20 MeV compared to 12 MeV. This is the usual behaviour caused by the diminishing influence of the strong spherical N = 82 neutron shell correction when the excitation energy is increased. In the symmetric fission region an increase of the kinetic energy for E_e = 20 MeV compared to 12 MeV is observed. This behaviour indicates that the scission configuration associated with the deformed fragment shells in the symmetric fission region, which is responsible for the existence of the third symmetric hump in the mass distributions, has a larger deformation compared to the liquid drop model configuration.

In fig.3 the number of emitted neutrons as a function of the fragment mass is shown. These curves show the usual saw-tooth behaviour and an increase with increasing excitation energy of the compound nucleus of the number of neutrons emitted by the heavy fragments.

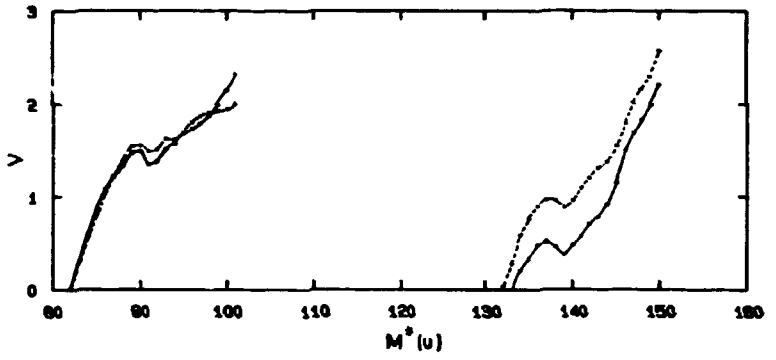

Fig.3. The number of emitted neutrons as a function of the preneutron mass for 12 MeV (—•—) and 20 MeV (-••-) bremsstrahlung induced fission.

ACKNOWLEDGMENTS

This research was supported by the Interuniversity Institute for Nuclear Sciences - National Fund for Scientific Research. The authors wish to thank Prof.A.J.Deruytter for his interest in this work. Mrs.L.Schepens is acknowledged for the careful chemical separations. Thanks are expressed to the Linac team of our laboratory for the operation of the accelerator.

REFERENCES

1) H.Thierens, D.De Frenne, E.Jacobs, P.D'hondt and A.J.Deruytter, Nucl. Instr. & Meth., 134 (1976) 299
2) H.W.Schmitt, W.M.Gibson, J.H.Neiler,F.J.Walter and T.D.Thomas, in Proceedings of the first Symposium on the Physics and Chemistry of Fission, Salzburg, 1965 (IAEA, Vienna, 1965) Vol.I, p.511
3) E.Jacobs, H.Thierens, A.De Clercq, D.De Frenne, P.D'hondt and A.J.Deruytter, Phys.Rev. C14 (1976) 1874
4) L.E.Glendenin, J.E.Gindler, I.Ahmad, D.J.Henderson and J.W.Meadows, Phys.Rev. C22 (1980) 152
5) B.D.Wilkins, E.P.Steinberg and R.R.Chasman, Phys.Rev. C14 (1976) 1832
6) J.T.Caldwell, E.J.Dowdy, B.L.Berman, R.A.Alvarez and P.Meyer, Phys.Rev. C21 (1980) 1215
7) L.I.Schiff, Phys.Rev. 83 (1951) 252
8) J.P.Unik, J.E.Gindler, L.E.Glendenin, K.J.Flynn, A.Gorski and R.K.Sjoblom in Proceedings of the Third International Symposium on the Physics and Chemistry of Fission, Rochester, 1973 (IAEA, Vienna, 1974) Vol.II, p.19
9) D.De Frenne, H.Thierens, B.Proot, E.Jacobs, P.De Gelder, A.De Clercq and W.Westmeier, Phys. Rev. C26 (1982) 1356
10) G.Mariolopoulos,C.H.Hamelin, J.Blachot, J.P.Bocquet, R.Brissot, J.Carçon, H.Nifenecker,C.H.Ristori, Nucl. Phys. A361 (1981) 213

EMISSION OF ^{3}H AND ^{4}HE PARTICLES IN THE PHOTOFISSION OF ACTINIDES.

(M.Verboven,E.Jacobs,P.D'hondt, A.De Clercq,D.De Frenne,M.Piessens and G.De Smet).

Nuclear Physics Laboratory,Proeftuinstraat 86, B-9000 Gent,Belgium

ABSTRACT

The emission of light charged particles (LCP) in the photofission of ^{233}U, ^{235}U, ^{237}Np and ^{242}Pu with 12, 15 and 20 MeV bremsstrahlung was studied. For the identification of the LCP ΔE-E detectortelescopes were used. We have determined the triton and α particle emission probabilities and the characteristics of the kinetic energy distribution of the α particles. Our measurements show that the excitation energy transferred to the compound nucleus essentially doesn't change the emission probability of the LCP. Our results are compared to sf and thermal neutron induced fission results. They are consistent with the idea that the LCP emission probability is correlated to the deformation energy of the system at scission.

1. INTRODUCTION

Although the thermal neutron induced ternary fission of fissile isotopes has been studied since fourty years, information on light charged particle accompanied fission induced by γ-rays is very scarce 1) and 2).

We report here on the first extensive study of the ternary photofission of actinides. For the nuclei ^{233}U, ^{235}U, ^{238}U, ^{237}Np and ^{242}Pu we measured the relative emission probabilities (LRA/B ratio) and the energy distribution characteristics (<E> and FWHM) of the ternary α particles and the triton to α emission probability (t/LRA) as a function of the excitation energy of the compound nucleus.

2. EXPERIMENTAL SET UP AND DATA HANDLING

Ternary photofission experiments were performed with bremsstrahlung,produced by 12,15 and 20MeV electrons in a 0.1 mm thick gold foil. The photon beam was cleared of electrons with a magnet and collimated to a diameter of 1.5 cm at the target location. The target is placed perpendicular to the incident photon beam.

The detector system consisted of 8 telescopes. An identification of the light charged particles was necessary to separate them from the high proton background, which was produced predominantly by (γ,p) reactions in the target and in the target backing. The identification of the light particles is based on the difference in energy loss in the ΔE detector for the different light particles with the same initial energy. The detector telescopes consisted of two Au-Si surface barrier detectors, a totally depleted ΔE detector of ± 30 μm thickness, followed by an E detector depleted to a depth of 500 μm, each with an active area of 150 mm^2. The telescopes were shielded with a 20 μm Al foil to stop the fission fragments and the natural α particles, originating from the target and also to reduce the background due to secondary electrons, produced in the target by the bremsstrahlung.The telescopes are placed circularly around the photon beam axis at an angle of 45 degrees and at a distance of 71 mm of the target.

The fission fragments were counted simultaneously in a separate detector with an active area of 600 mm^2, placed on the opposite side of the target at a distance of 92 mm. The geometry factor between this detector and the telescope set-up was determined for each experiment by counting in both detector systems the number of fission events. A correction for coincidence losses in the telescopes was obtained by measuring the natural α-particle countrate from a ^{235}U target in the E- and the ΔE-detector separately.

The amplified pulses from the detectors were coded and stored event by event on a PDP11/10 system via a CAMAC-interface. The γ pile-up during the pulse of the linac (γ-flash) was measured continuously and an on-line subtraction of an average of it was performed. The detectors were calibrated using well known natural α lines from an ^{235}U target and from a ^{228}Th source. The stability was continuously checked with a precision pulser. The two-dimensional ΔE-E data are handled off-line with our VAX-11/780 system. A typical ΔE-E energy spectrum is shown in fig.1. The ternary α particles are clearly separated from the high background in the low-energy part of the spectrum. The measured coincident ΔE and E values are combined via the relation $T/a = (E + \Delta E)^{1.73} - E^{1.73}$ (with T the thickness of the ΔE detector) to obtain an identification spectrum 3). Fig.2 gives an example of such an identification spectrum.

3. RESULTS AND DISCUSSION

A typical energy spectrum of the LRA-particles is shown in fig.3. The parameters of the energy distribution are obtained by fitting a Gaussian through the data points above 12.5 MeV. As a consequence of this procedure the non-Gaussian low-energy tail of the energy distribution is not taken into account (see e.g.4)).

In table I we summarize our results. The parameters of the energy distribution and the emission probabilities of the LRA-particles relative to the binary fission probability (LRA/B) are given together with the triton to α emission probability ratios (t/LRA). The quoted errors are only statistical ones. The energy of the electrons producing the bremsstrahlung is indicated by E_e. As a consequence of the high proton background for measurements with 20 MeV bremsstrahlung, it's impossible to distinguish the tritons.

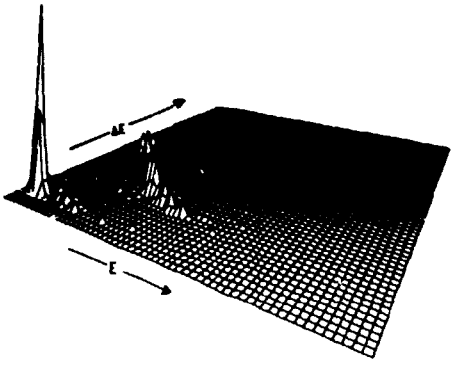

Fig. 1 Threedimensional representation of the ΔE-E spectrum ($^{235}U(\gamma,f)$ - 12 MeV bremsstrahlung)

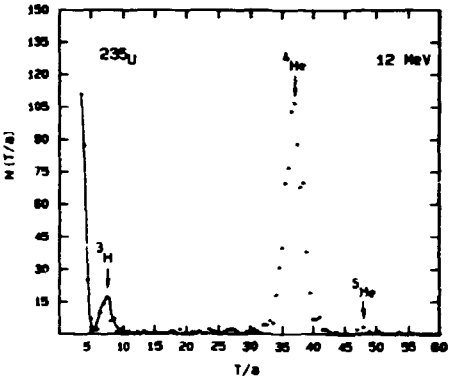

Fig. 2 Identification spectrum of the LCP ($^{23}U(\gamma,f)$ 12 MeV bremsstrahlung)

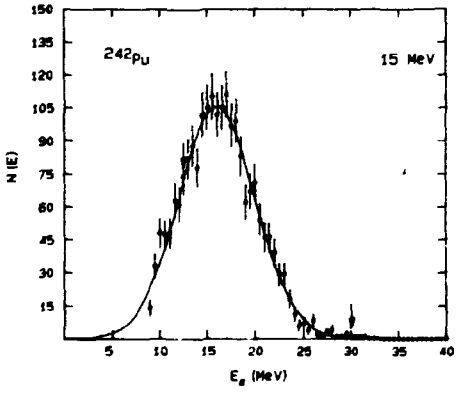

Fig. 3 The LRA energy distribution and the Gaussian fit from 12.5 MeV ($^{242}Pu(\gamma,f)$ - 15 MeV bremsstrahlung)

Consistent with the general trend observed in ternary fission, the average LRA energy,<E>,seems to be practically constant over the whole range of nuclei and excitation energies (the average value for our measurements is 15.8 ± 0.1 MeV).Although the considerable amount of dispersion in the full width at half maximum values, these FWHM values show a tendency of a systematic increase in going to a higher excited nucleus. The average value for the FWHM raises from 9.54 ± 0.2 MeV for fission induced by 15MeV bremsstrahlung to 10.1 ± 0.2 MeV for fission induced by 20 MeV bremsstrahlung. A partial explanation for this observation can be the following. The measurements of Mehta et al. 5) for $^{252}Cf(sf)$ show that the FWHM of the energy distribution as a function of fragment mass is rather constant, except for symmetric fission where it increases. We can assume the same behaviour for induced fission. It's well known that for higher excitation energies of the compound

Table 1 : Summary of our photofission results

Target	E_e(MeV)	<E>(MeV)	FWHM(MeV)	LRA/B*10^{-3}	t/LRA(%)
^{233}U	12	15.7±0.2	9.5±0.3	1.93±0.12	6.4±1.0
^{233}U	15	15.5±0.2	9.3±0.3	1.97±0.06	-
^{233}U	20	15.6±0.1	10.2±0.2	2.13±0.07	-
^{235}U	12	15.7±0.2	9.0±0.2	1.57±0.08	6.5±1.1
^{235}U	15	15.9±0.2	9.6±0.2	1.67±0.06	6.3±0.7
^{235}U	20	16.0±0.2	9.7±0.2	1.72±0.04	-
^{238}U	15	15.6±0.2	9.7±0.3	1.28±0.06	7.8±1.2
^{239}U	20	15.9±0.1	9.9±0.2	1.46±0.07	-
^{237}Np	15	15.9±0.1	9.6±0.1	1.64±0.13	8.3±0.9
^{237}Np	20	15.8±0.1	10.5±0.2	1.79±0.07	-
^{242}Pu	15	15.9±0.1	9.5±0.2	1.88±0.06	-
^{242}Pu	20	15.9±0.1	10.2±0.2	1.86±0.07	-

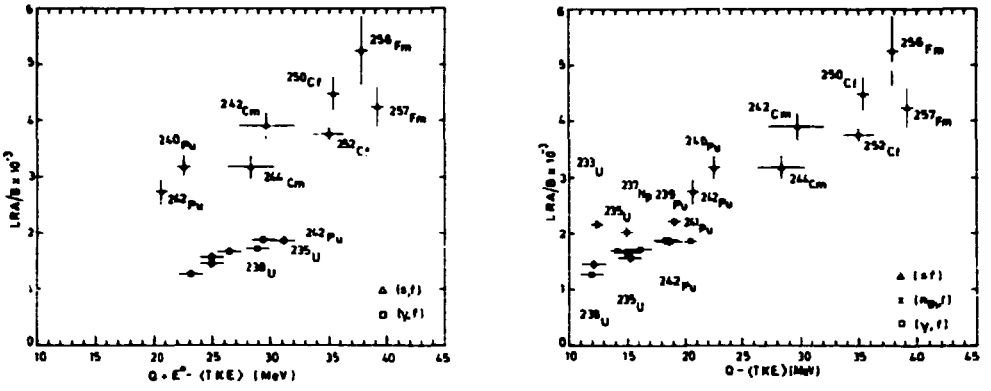

Fig. 4 Emission probabilities of LCP (sf) and LRA (γ,f and n_{th},f) versus Q+E*-<TKE> (fig. 4a) or versus Q-<TKE> (fig. 4b). E* is the average excitation energy of the compound nucleus induced by the photons or the neutrons.

nucleus, the symmetric fission yield increases. For $^{235}U(\gamma,f)$ the peak to valley ratio decreases from 24 to 14 in going from 15 MeV bremsstrahlung to 20 MeV bremsstrahlung 6). However this increase in symmetric fission yield cannot account for the whole increase of the FWHM.

The triton to LRA emission probabilities (t/LRA) seem to be constant.Although ^{237}Np is an odd-Z nucleus and the existence of an unpaired proton in the compound nucleus could perhaps enhance the yield of H-particles, our measurements indicate that there is no significant increase in the triton yield for ^{237}Np.

As generally observed our results show an increased LRA yield with increasing Z^2/A 7). This is interpreted as a confirmation of the idea that the LRA-yield is correlated with the amount of deformation at scission 8). A better way to control this hypothesis is probably to plot the LRA-yield as a function of Q-<TKE> 9). The difference between the calculated reaction Q-value and the measured average total kinetic energy of the fragments gives the deformation energy plus the internal heating. As for spontaneous fission the internal heating is probably low, the difference Q-<TKE> represents an estimate of the deformation energy at scission (see 9)). The Q-values for our photofission experiments were obtained by averaging the ground-state atomic masses, using the tables of Moller and Nix 10) over the experimental massdistributions. These were however only available for ^{235}U, ^{238}U and ^{242}Pu 6), 11) and 12). The most probable fragment atomic numbers were taken from our earlier work(^{235}U and ^{238}U, 13) or calculated for ^{242}Pu via the method presented by Nethaway 14). For photofission the calculated difference Q-<TKE> should include the average excitation energy of the compound nucleus. When we plot our results together with those for spontaneously fissioning nuclei, given in a very recent survey by Wild et al. 9) a significant different trend between induced and spontaneous fission is obvious (fig.4a). However, if we do not include the extra excitation energy contributed by the photons, the LRA yield, as well for s.f. as for induced fission, can be represented by a single straight line (fig.4b). If we assume that most of the extra excitation energy remains as internal excitation and only a small fraction of it is converted into deformation energy and if the amount of deformation at the moment of scission determines the emission probability of light particles, an increase of the excitation energy of the compound nucleus should have only a small influence on the LRA emission probability, as we have observed (see table 1). It justifies also that in comparing our photofission results with results on s.f. (see fig.4b) we don't have to include the excitation energy of the compound nucleus. Together with our photofission values we plotted some results from thermal neutron induced ternary fission, confirming the trend of nearly excitation energy independence of the α emission probability.

We think we can conclude that also our results on the emission of light charged particles during photon induced fission support the idea that the emission probability of these light charged particles is correlated with the deformation energy available at the moment of scission.

4. ACKNOWLEDGMENTS

This research was supported by the Interuniversity Institute for Nuclear Sciences- National Fund for

Scientific Research. M. Verboven likes to thank the IWONL (Instituut voor Wetenschappelijk Onderzoek in Landbouw en Nijverheid) for the financial support which helped to start this research. The authors wish to thank Prof. Dr. A.J. Deruytter for his interest in this work and the operating personnel of the linear accelerator at the Nuclear Physics Laboratory.

REFERENCES

1) E.W.Titterton and F.K.Goward, Phys.Rev. C2 (1970) 1.56
2) P.D'hondt, E.Jacobs, A.De Clercq, D.De Frenne, H.Thierens, P.De Gelder and A.J.Deruytter, Phys.Rev. C21 (1980) 963
3) F.S.Goulding, D.A.Landis, J.Cerny and R.H.Pehl, Nucl. Instr. & Meth. 31 (1964) 1
4) P.D'hondt, C.Wagemans, A.De Clercq, G.Barreau, A.J.Deruytter, Nucl.Phys. A346 (1980) 461
5) G.Mehta, J.Poitou, M.Ribrag, C.Signarbieux, Phys.Rev. C7 (1973) 373
6) E.Jacobs, A.De Clercq, H.Thierens, D.De Frenne, P.D'hondt, P.De Gelder and A.J.Deruytter, Phys.Rev. C24 (1981) 1795
7) R.A.Nobles, Phys.Rev. 126 (1962) 1508
8) R.Vandenbosch and J.R.Huizenga, Nuclear Fission, Academic Press (1973)
9) F.Wild, P.A.Baisden, R.J.Dougan, E.K.Hulet, R.W.Lougheed and J.H.Landrum, Phys.Rev. C32 (1985) 488
10) P.Moller and J.R.Nix, At. Data and Nucl. Data Tables 26 (1981) 165
11) E.Jacobs, A.De Clercq, H.Thierens, D.De Frenne, P.D'hondt, P.De Gelder and A.J.Deruytter, Phys.Rev. C20 (1979) 2249
12) H.Thierens, E.Jacobs, P.D'hondt, A.De Clercq, M.Piessens and D.De Frenne, Phys.Rev. C29 (1984) 498
13) D.De Frenne, H.Thierens, B.Proot, E.Jacobs, P.De Gelder and A.De Clercq, Phys.Rev. C26 (1982) 1356
14) R.Nethaway, University of California Radiation Laboratory Report UCRL-51538 (1974)

ODD HARMONICS IN THE ANGULAR DISTRIBUTION OF FISSION FRAGMENTS

V.V. Flambaum

Institute of Nuclear Physics

630090 Novosibirsk, USSR

A b s t r a c t

Asymmetry in the angular distribution of light and heavy fragments may become a source of information about a direct nuclear fission (induced by photons, neutrons and charged particles) and about the statistical properties of compound states. Investigation of the asymmetry can prove to be useful for further study of the properties of the fission channels and in a search for new parity violating effects.

1. The odd harmonics in the angular distribution of fission fragments have been observed in fission of the nuclei by polarized neutrons (see, e.g. Refs. /1-4/ and the theoretical review /5/). Studies of the asymmetry in the direction of flight of a light (or heavy) fragment corresponding to the parity-violating correlation $\vec{\sigma}\,\vec{p}_f$ and parity-conserving correlation $\vec{\sigma}\,\vec{p}_n \times \vec{p}_f$, have been carried out ($\vec{\sigma}$, $\vec{p}_n$ are the spin and momentum of a neutron, $\vec{p}_f$ is momentum of a light fragment). In these experiments the energy of the intermediate nuclear state was fixed with the accuracy $\Delta \ll \mathcal{D}$ where $\mathcal{D}$ is the distance between the compound resonances with a fixed angular momentum J and parity. In the case of $\Delta \gg \mathcal{D}$, the contribution of compound resonances to the odd harmonics of the angular distribution turns out to be strongly suppressed (Ref. /5/) (for details see the text below). One can use this circumstance to separate the contribution of direct fission occuring without the intermediate compound-nucleus stage (or at least to impose the limits on the amplitudes of direct processes).

2. For an example, let us consider the photofission of a spinless nucleus (of ^{238}U, ^{232}Th, ^{240}Pu, etc.) at energy of γ-quanta 5-10 MeV. Here the capture of E1 or E2 photons dominates. The angular distribution of the fragments is formed at the stage of a cold strongly-deformed nucleus where nearly all the excitation energy is given off to overcome the potential fission barrier. The cold fission stage is connected with the concept of fission channels suggested by A. Bohr.

The reasons for the appearance of fission channels is easy to understand if the fission amplitude is represented as an integral over trajectories in 3A-dimensional space (A is the number of nucleons). Among the whole of the trajectories, a substantial contribution to the amplitude can be given only by those for which the classical potential energy $\mathcal{U}(r_1, \ldots r_A)$ is not too high in comparison with the total energy E (the contribution from the others is small according to the quasi-classical estimate). If the average nuclear deformation is taken as a collective variable, then at a certain value of the former, which corresponds to a fission barier, the condition $\mathcal{U} \lesssim E$ uniquely determines the nucleon density distribution. (In reality antisymmetrization of nucleon coordinates probably leads to condition $\mathcal{U}_{eff} \lesssim E$, $\mathcal{U}_{eff} > \mathcal{U}$, where $\mathcal{U}_{eff}$ includes minimal kinetic energy of nucleons connected with Pauli principle). Thus, all the trajectories giving a noticeable contribution to the fission amplitude, have common interval in the potential-barrier region (with a precision up to the rearrangement of the identical particles and insignificant displacements without the variation in mean density). Exception is only the angular variables characterizing the nuclear orientation in a space. The potential energy is independent of these variables, while the kinetic ro-

tation energy and the Coriolis force are small (adiabatic approximation). In this case, the amplitude of the probability of the fact that the nuclear axis $\vec{n}$ has a fixed direction in space (angular wave function) depends only on the angular quantum numbers: the nuclear moment (J), its projection onto the z-axis (M) as well as on the projection of $\vec{J}$ onto the axis of the nucleus ($K = \vec{J}\vec{n}$), i.e. is described by the Wigner D-function $\mathcal{D}^{J}_{MK}(\vec{n})$.

In fission initiated by γ-quanta with $E_\gamma \lesssim 5$ MeV, only the channel with K = 0, corresponding to the lowest intrinsic nuclear energy at the external fission barrier, is open. Upon E1- and E2-photon capture, the angular momentum J equals 1 and 2, respectively; the angular momentum projection $M = \lambda$ and $\lambda = \pm 1$, the photon helicity. The angular wave function of a cold pear-shaped nucleus is of the form, for this case,

$$\Psi(\vec{n}) = A_{E1}(E)\, Y_{1\lambda}(\vec{n}) + A_{E2}(E)\, Y_{2\lambda}(\vec{n}) \tag{1}$$

where A_{E1} and A_{E2} are the amplitudes of transition to the cold stage. We have taken into account that at K = 0 the D-function is expressed via $Y_{\ell m}$. Behind the barrier the motion trajectories diverge. However, if the nucleus breaks fast (in comparison with its rotation), the angular wave function has no time to change and the angular distribution of the fragments is proportional to $|\Psi|^2$:

$$W(\vec{n}) \sim |A_{E1}|^2 |Y_{1\lambda}|^2 + |A_{E2}|^2 |Y_{2\lambda}|^2 + (A^*_{E1} A_{E2} + A^*_{E2} A_{E1}) Y^*_{1\lambda} Y_{2\lambda} \tag{2}$$

Note that for the existence of fission channels there is no need for that the cold nuclear state be a quasi-stationary state (resonance). It is only necessary that a sufficiently-large-action ($\Delta S > 1$) part of the trajectory correspond to the cold nucleus in order to exclude 'incorrect' trajectories.

If allowance is made for the channels with K = 1 and K = 2, which are significant at $E_\gamma > 5$ MeV, the expression for the angular distribution of the fragments in the centre-of-mass system takes the form

$$\begin{aligned}
W(\vec{n}) &= P + Q \cdot \cos\theta \\
P &= a + b \sin^2\theta + c \sin^2 2\theta \\
Q &= d + e \sin^2\theta \\
a &= \tfrac{3}{4}|A_{11}|^2 + \tfrac{5}{4}|A_{21}|^2 \\
b &= \tfrac{3}{4}|A_{10}|^2 - \tfrac{3}{8}|A_{11}|^2 - \tfrac{5}{8}|A_{21}|^2 + \tfrac{5}{8}|A_{22}|^2 \\
c &= \tfrac{15}{16}|A_{20}|^2 - \tfrac{5}{8}|A_{21}|^2 + \tfrac{5}{32}|A_{22}|^2 \\
d &= -\tfrac{\sqrt{15}}{2}\,\mathrm{Re}\,(A^*_{21} A_{11}) \\
e &= \mathrm{Re}\,\left(\tfrac{3\sqrt{5}}{2} A^*_{20} A_{10} + \tfrac{\sqrt{15}}{2} A^*_{21} A_{11}\right)
\end{aligned} \tag{3}$$

Here A_{JK} is the EJ-amplitude of photon-induced fission via the channel K. It can be normalized in such a way that $\int W \sin\theta\, d\theta = \sum_{JK} |A_{JK}|^2 = 1$. The channels with different K do not interfere because these correspond to different intrinsic nuclear states. The angular distribution (3) without the interference term $Q \cdot \cos\theta$ is given, for example, in Ref. /6/ ($|A_{JK}|^2 = P(JK)$ in the notations of Ref. /6/). The angle θ is

here count off the direction of photon motion, i.e. the point is concerned with the angular correlation $\vec{q}\ \vec{p}_f$ ($\vec{q}$ is the momentum of a photon and $\vec{p}_f$ is the momentum of a light fragment). The odd harmonics in the angular distribution of fragments appear also due to an interference of E1 and M1 amplitudes, and in electrofission the latter are complemented by the E1 and E0 interference.

For monochromatic photons, the magnitude of asymmetry

$$a \approx \frac{Q}{P} \sim \frac{\mathrm{Re}\,(A^*_{E1}\ A_{E2})}{|A_{E1}|^2 + |A_{E2}|^2} \tag{4}$$

is not small because at $E_\gamma \sim 5$ MeV $A_{E1} \sim A_{E2}$. The matter is that the first fission barrier for $J^\pi = 2^+$ (π is the parity of a state) lies lower than for 1^-; this compensates for the smallness of the E2-amplitude (see, e.g., Refs /6,7/). At higher energies, A_{E2} is in average smaller than A_{E1}, however, the smallness of the E2-amplitude is possible to compensate using the resonance energy dependence of the fission amplitudes:

$$A\,(E) = A_n + \sum_\alpha \frac{M_\alpha\ f_\alpha}{E - E_\alpha + i\,\Gamma_\alpha/2} \tag{5}$$

Here A_n is the non-resonance amplitude of direct fission, M_α is the capture amplitude, f_α is the fission amplitude, and E_α and Γ_α are the energy and width of the compound resonance, respectively.

3. The angular distribution (3) is independent of the photon helicity λ . However, the dependence on λ arises if we take into account a weak nucleon-nucleon interaction H_w which does not conserve the parity. The parity-violating amplitude can be written as follows:

$$\tilde{A} = \tilde{A}_n + \sum_b \frac{M_b\ \tilde{f}_b}{E - E_b + i\,\Gamma_b/2} + \sum_c \frac{\tilde{M}_c\ f_c}{E - E_c + i\,\Gamma_c/2} + \sum_{b,c} \frac{M_b \langle c\,/\,H_w\,/\,b\rangle\ f_c}{(E - E_b + i\,\Gamma_b/2)\,(E - E_c + i\,\Gamma_c/2)} \tag{6}$$

Here $\tilde{A}_n$ is a non-resonant amplitude, $\tilde{M}_c$ is an amplitude of particle capture with parity violation, and $\tilde{f}_c$ is an amplitude of fission with parity-violation. Its appearance is connected with the mixing of opposite-parity levels in the second potential well, or directly with the mixing of the rotational states of a cold nucleus (Ref. /8/). The latter term corresponds to taking into account the mixing of opposite-parity compound states ($|b\rangle$ and $|c\rangle$). According to the $\sqrt{N}$-classification (Ref. /9/), it is the term which is the largest and causes the observed parity-violating effects considered in Refs. /10,11,5/. Note that, for example, in E1-capture the $\tilde{A}_{E1}$ results in the nucleus prior to the scission in the rotational state 1^+, while A_{E1} does in the 1^-.

Amont the parity-nonconserving effects there is the dependence of the photofission cross section on the helicity of γ -quanta:

$$P_\gamma = \frac{\sigma_+ - \sigma_-}{\sigma_+ + \sigma_-} = \frac{\sum_{K=0,1} 2\,\mathrm{Re}(\tilde{A}^*_{E1} A_{M1} + \tilde{A}^*_{M1} A_{E1})_{\lambda=1,K}}{\sum_{K=0,1,2} (|A_{E1}|^2 + |A_{M1}|^2 + |A_{E2}|^2)_{\lambda=1,K}} \qquad (7)$$

The summation is carried out over the fission channels; σ_+ and σ_- are the cross sections, respectively, for the right-hand- and left-hand-polarized photons. The maxima of P_γ lie in the vicinity of the energies of the 1^+ -resonances into which the M1-capture of the photon does (in these resonances an enhancement of the M_{E1}/M_{M1} type is possible). The magnitude of P_γ similar to the parity-nonconserving effect in the (n, f) reaction is about 10^{-4}-10^{-3}.

The correlation $\lambda \vec{q}\,\vec{p}_f$ in the angular distribution of the fragments is also one of the parity-nonconserving effects. For example, interference of the basic and admixture E1-amplitudes leads to the following addition to the angular distribution of the fragments (3):

$$W_{pv} = \lambda \frac{3}{2} \mathrm{Re}(\tilde{A}_{11} A^*_{11}) \cos\theta \qquad (8)$$

Remind that $\lambda = \pm 1$ is the helicity of a photon. In this case, the relative magnitude of the effect W_{pv}/W is also about 10^{-4}-10^{-3} and its maxima lie in the vicinity of 1^+ resonances. An increase of the effect also occurs at the energies when the penetrability of the barrier for a nucleus with quantum numbers 1^+ is enhanced owing to the resonances in the second well (the possibility of such an enhancement for the (n, f) reaction was mentioned in Ref. /12/).

The correlations P_γ and $\lambda(\vec{q}\,\vec{p}_f)$ arise of course in the other photoprocesses: (γ, n), (γ, p), (γ, α), etc. A substantial kinematic enhancement of the second correlation ($\sim f_s/f_p$) can arise here if the basic amplitude corresponds to the emission of a slow particle in the s -wave, while an admixture amplitude corresponds to the emission of that particle in the p-wave. The difference in the cross sections P_γ might be sought for also in the total cross section of photon capture, measuring the number of γ-quanta passed through a sample. However, the situation is complicated by an electron-photon interaction giving rise to the absorption of γ-quanta.

4. Both the parity-conserving and the parity-nonconserving asymmetries in the angular distributions of light and heavy fragments is connected with an interference of the fission amplitudes from the opposite-parity compound states. In fission initiated by monochromatic particles, this does not lead to a significant suppression of the effect. The situation becomes different in nuclear fission induced by nonmonochromatic particles. In this case, the interference term is suppressed at the energy spread $\Delta \gg \mathcal{D}$. Let us assume that the energy distribution is described by a function normalized over unity ($\int P(E)\,dE = 1$):

$$P(E) = \frac{1}{2\pi} \frac{\Delta}{(E-E_0)^2 + \Delta^2/4} \qquad (9)$$

Integration over the energy gives

$$\int A_k(E)\, A_\ell^*(E) P(E) dE = A_{nk} A_{n\ell}^* + \sum_{\alpha,\beta} M_\alpha f_\alpha M_\beta^* f_\beta^* \times$$

$$\times \frac{E_0 - E_\alpha + i(\Delta + \frac{\Gamma_\alpha}{2} + \frac{\Gamma_\beta}{2})}{\left[E_0 - E_\alpha + i(\Delta + \Gamma_\alpha)/2\right]\left[E_0 - E_\beta - i(\Delta + \Gamma_\beta)/2\right]\left[E_\beta - E_\alpha + i(\Gamma_\beta + \Gamma_\alpha)/2\right]} + \tag{10}$$

$$+ A_{n\ell}^* \sum_\alpha \frac{f_\alpha M_\alpha}{E_0 - E_\alpha + i(\Gamma_\alpha + \Delta)/2} + A_{nk} \sum_\beta \frac{f_\beta^* M_\beta^*}{E_0 - E_\beta - i(\Gamma_\beta + \Delta)/2} .$$

We suggest that on the scale Δ the non-resonance amplitudes vary slightly. The index α corresponds to the amplitude A_k, β - A_ℓ. We make an assumption that $\Delta \gg \mathcal{D} > \Gamma$. In this case, the interval of the averaging involves a lot of resonances ($N \sim \Delta/\mathcal{D}$). The fission amplitudes via different compound resonances will be assumed to be independent, and the sums appeared will be averaged as the sums of random numbers. The magnitude of the squared resonance amplitude is

$$|A^{(r)}|^2 \sim \frac{M^2 f^2}{\Gamma \mathcal{D}} , \quad M \equiv \sqrt{\overline{|M_\alpha|^2}} , \quad f \equiv \sqrt{\overline{|f_\alpha|^2}} \tag{11}$$

The main contribution to this estimate comes from the diagonal terms ($\alpha = \beta$).

The estimate of an interference of different amplitudes is mainly contributed by the compound resonances $|\alpha\rangle$ and $|\beta\rangle$ with as close energies as possible ($|E_\alpha - E_\beta| \sim \Gamma$). The number of such terms in the double sum in eq. (10) is not large ($N_\Gamma \sim \frac{\Gamma}{\mathcal{D}} \cdot N \sim \frac{\Gamma}{\mathcal{D}} \frac{\Delta}{\mathcal{D}}$). Basing on the fact that the sum of N_Γ incoherent terms grows as $\sqrt{N_\Gamma}$, we find a mean square estimate of the resonance contribution to interference:

$$\sqrt{\overline{|A_k^{(r)} A_\ell^{(r)*}|^2}} \sim \frac{M_k f_k M_l f_l}{\mathcal{D}\sqrt{\Delta\Gamma}} \tag{12}$$

The contribution from the terms with $|E_\alpha - E_\beta| \sim \mathcal{D}$ turns out to be less by a factor of $\sqrt{\mathcal{D}/\Gamma}$, and from those with $|E_\alpha - E_\beta| \sim \Delta$ the contribution is less by a factor of $\sqrt{\Delta/\Gamma}$.

With the typical photofission values: $\Delta \sim 100$ keV, $\mathcal{D} \sim 1$ eV and $\Gamma/\mathcal{D} \sim 0{,}1$, we obtain that when averaging over the energy there arises the following factor of suppression of the contribution of the compound resonances to asymmetry:

$$\sqrt{\frac{\Gamma}{\Delta}} \sim 10^{-3} \tag{13}$$

Thus, the contribution of direct fission to asymmetry proves to be $\sqrt{\Delta/\Gamma}$ times larger than to the fission cross section.

An interference of the direct and resonance amplitudes whose contribution is

$$\sim \left(|A_{nk}| M_l f_l + |A_{n\ell}| f_k M_k\right) / \sqrt{\Delta\mathcal{D}} \tag{14}$$

can prove to be significant as well.

The magnitudes of parity-violating effects may be estimated in a similar way. In an interference of the amplitudes A and $\tilde{A}$ (see eqs. (5) and (6)), a triple sum over the indices α, b and c arises. After integration over energy, the main contribution to this sum comes from N^2 terms whose indices corresponding to the levels with equal quantum numbers coincide ($b = \alpha$ for $A^*_{E1}\tilde{A}_{E1}$, and $c = \alpha$ for $\tilde{A}_{M1}A^*_{E1}$ and $\tilde{A}_{E1}A^*_{M1}$). In the thus separated double sum, $N_\Gamma \sim \frac{\Gamma}{D}N$ terms dominate for which the energy difference of the opposite-parity levels is $|E_b - E_c| \sim \Gamma$. As a result, we find that the resonance contribution to the averaged parity-violating effects is the following:

$$P_\gamma^{(\tau)} \sim \frac{M_{M1}}{M_{E1}} \frac{|\langle b|H_W|c\rangle}{\sqrt{\Delta\Gamma}} \sim 10^{-5} - 10^{-6}$$

$$\frac{W_{PV}^{(\tau)}}{W} \sim \sqrt{\frac{\Gamma_f(1^+)}{\Gamma_f(1^-)}} \frac{|\langle b|H_W|c\rangle|}{\sqrt{\Delta\Gamma}} \sim 10^{-5} - 10^{-6}. \qquad (15)$$

It is worth emphasizing that the obtained mean square estimate for the coefficient of mixing of the nearest opposit-parity levels in the compound nucleus,

$$|\alpha| \sim \frac{|\langle b|H_W|c\rangle|}{\sqrt{D\Gamma}} \qquad (16)$$

exceeds the naive estimate $|\langle b|H_W|c\rangle|/D$ and diverges at $\Gamma \to 0$. The reason ist that the main contribution to the estimate (16) is given by the opposite-parity levels with $|E_b - E_c| \sim \Gamma$. This circumstance may prove to be important, for instance, when estimating the contribution from the γ-cascades for the parity-violating effects in the (n, γ) reaction in the integral spectrum of γ-quants.

The appearance of a proportional to $1/\sqrt{\Delta}$ factor of suppression of the P-even and P-odd asymmetry may be interpreted in terms of the time picture of fission (Ref. /5/). At a fixed energy when $\Delta \ll D, \Gamma$, adequate is the description of the fission process by means of the wave function $\Psi(E)\, e^{-iEt}$. Such a wave function includes the parts corresponding to both the initial compound nucleus and the cold stage. The time separation of the process into subsequent stages has no sence in this case, because, according to the uncertainty relation $\delta t \cdot \Delta \sim \hbar$, the uncertainty in time at $\Delta < \Gamma$ proves to be considerably larger than the lifetime of the nucleus. However, if $\Delta \gg D, \Gamma$, the time picture of the subsequent stages of fission has sence; though, in going to the cold stage, the mixing of the opposite-parity levels of the compound nucleus is "forgotten" (both the mixing induced by weak interaction and the mixing due to capture from the opposite-parity waves of a neutron (l = 0 and l = 1) or a photon (E1 and E2)). The randomness of the signs of the fission amplitudes from different compound states, because of which the suppression factor $\sqrt{D/\Delta}$ arises, is directly connected with the complexity of the nucleon motion in the compound nucleus in terms of the time picture. In view of this, a study of the statistical properties of interference effects is one of methods of analysing the compound nucleus as an example of the quantum stochastic system.

Conclusion

The study of asymmetry in the angular distribution of light and heavy fragments in nuclear fission induced by polarized neutrons has already enabled the following conclusions to be drawn:

1. Before its scission into fragments, the nucleus is pearshaped and the angular distributions are formed prior to the scission. This conclusion is consistent with the photofission data (see, e.g., review /7/).

2. The fission channels with different parity or angular momentum interfere in the angular distribution of fragments. This means that they are related to a rotational band constructed on the same intrinsic state of the cold pear-shaped nucleus (if the intrinsic states of the nucleus in the opposite-parity channels substantially differ from each other, interference effects would disappear upon summation over an enormous amount of final states of the excited fragments due to the difference in the fission amplitudes).

3. Asymmetry arises because of the mixing of the wave functions of opposite-parity compound states. This is the reason for which the characteristic scale of its energy dependence is determined by the energy levels and by the widths of the compound resonances (see Refs. /5,13,14/).

4. The initial 'hot' stage is not forgotten in the fission process if the energy spread Δ does not exceed the distance between the compound resonances with equal quantum numbers. The mixing of the opposite-parity states, which have appeared at the initial stage, is transferred, without losses, at the cold stage.

5. The existence of a dynamical enhancement of small interactions (for instance, of a weak one) in the compound nucleus is confirmed. Enhancement arises due to a dense spectrum and stochastic internal structure of the compound states (Refs. /15-17, 11/). These properties permit one to construct the $\sqrt{N}$- classification of amplitudes, universal for complex nuclei (Ref. /9/) ($N \sim \Gamma_{sp\,z}/\mathcal{D} \sim 10^4$-$10^6$ is the parameter characterizing complexity of the system and $\Gamma_{sp\,z}$ is the spread width of one-quasi-particle states, i.e. the scale of the residual strong interaction mixing the simple states of the nucleus).

An analysis of the odd harmonics in photofission induced by monochromatic γ-quanta (produced, for example, by means of the (n ,γ) or (n, f) reactions) would enable one to testify the correctness of the conclusions drawn for this process too. It is worth emphasizing also that photofission experiments are usually performed not on the nuclei which have been used in neutron experiments.

Fission by the monochromatic beams of particles offers the possibility of studying the statistical properties of the process (for example, the asymmetry dispersion decreases as $\sqrt{\Gamma/\Delta}$, and is zero in its average value). It is probable that the amplitudes of direct fission, without the compound-nucleus stage, can manifest themselves here. In photofission, this process can arise owing to direct decay of some giant resonance to the fission mode (for example, of an isoscalar quadrupole giant resonance). There exists another possibility. With the particle captured, the nucleus can get not to the first but immediately to the second minimum of the potential deformation energy. The levels in the second well are placed considerably more rare than in the first. Therefore, the situation when $\mathcal{D}_1 \ll \Delta \lesssim \mathcal{D}_2$ ($\mathcal{D}_1$ and $\mathcal{D}_2$ are the mean distances between the levels in the first and second wells, respectively) is real. It is natural that an interference between such amplitudes does not disappear when averaging with scale Δ .

Similarly, a study of the p-odd asymmetry in fission induced by monochromatic particles enables one to investigate the mixing of opposite-parity states in the second potential well as well as the direct mixing of rotational states of the strongly deformed nucleus by a weak interaction. The expected magnitude of the parity-violating effects is $\lesssim 10^{-5}$ for this case.

Reference

1. Danilyan G.V. et al. ZhETF Pisma (JETP Lett.) 1977, 26, 197.
2. Andreev V.N. et al. ZhETF Pisma 1978, 27, 68.
3. Vesna V.A. et al. ZhETF Pisma 1980, 31, 704.
4. Petukhov A.K. et al. ZhETF Pisma 1980, 32, 324.
5. Sushkov O.P., Flambaum V.V. Usp. Fiz. Nauk, 1982, 136, 3 (Sov. Phys. Usp. 1982, 25, 1)
6. Bohr, A., Mottelson B.R. Nuclear structure, v. 2 (Mir, Moscow, 1977) p. 118.
7. Smirenkin G.N., Tsypenjyk Yu.M. In "Physics and Chemistry of Fission" (Vienna, IAEA, 1980) v. 1, p. 31.
8. Sushkov O.P., Flambaum V.V. Yad. Fiz. (Sov. Nucl. Phys.)1980, 31, 55.
9. Flambaum V.V., Sushkov O.P. Nucl. Phys. 1984, A412, 13.
10. Flambaum V.V., Sushkov O.P. Phys. Lett. 1980, B94, 277.
11. Sushkov O.P., Flambaum V.V. Yad. Fiz. 1981, 33, 59.
12. Budnik A.P., Rabotnov N.S. Phys. Lett. 1973, B46, 155.
13. Valsky G.V. et al. Preprint LINP 796, 1982.
14. Sushkov O.P., Flambaum V.V. Preprint INP 83-31, 1983.
15. Haas R., Leipuner L.B., Adair R.K. Phys. Rev., 1959, 116, 121.
16. Blin-Stoyle R.J. Phys. Rev. 1960, 120, 181.
17. Shapiro I.S. Usp. Fis. Nauk 1968, 95, 647.

ИССЛЕДОВАНИЯ ПО ФИЗИКЕ ДЕЛЕНИЯ НА МЕЗОННОЙ ФАБРИКЕ ИЯИ АН СССР

Ю.Я. Ставинский

Институт ядерных исследований АН СССР

Аннотация

Рассматриваются основные направления исследований деления ядер, возможные на основе пучков протонов, нейтронов, π- и μ-мезонов Московской мезонной фабрики, сооружаемой в ИЯИ АН СССР.

Со времени открытия деления тяжелых ядер прошло почти полвека (О.Ган, Ф.Штрассман, Л.Мейтнер, 1939 г.) - срок достаточно большой, чтобы практически исчерпалась любая область исследований. Тем не менее, физика деления, испытав за свою историю несколько подъемов и спадов, до сих пор остается предметом интенсивных исследований (см.напр. /I/), не говоря уже о прикладном значении процесса как источника ядерной энергии, существенным образом повлияевшем на развитие ядерных исследований вообще.

Можно, в известной степени условно, разграничить исследования процесса деления несколькими основными областями.

I. Область низких энергий возбуждения.

2. Деление адронами средних энергий.

3. Деление μ - мезонами.

4. Деление как средство изучения ядерных процессов и свойств ядер.

5. Сечения деления и спектры вторичных нейтронов для атомной энергетики.

Создаваемая в ИЯИ АН СССР мезонная фабрика позволит развить новое поколение исследований процесса деления ядер практически во всех упомянутых областях при интенсивностях протонов, нейтронов, π- и μ- мезонов в десятки и сотни раз превосходящих достигнутые ныне.

Мезонная фабрика ИЯИ АН СССР /2/ включает линейный ускоритель протонов на энергию 600 МэВ /3/ и экспериментальный комплекс (рис.I) с разводкой пучков /4/, системой формирования временной структуры тока на основе накопителя протонов, с комплексом интенсивных источников нейтронов /5/ (рис.2).

Ожидаемые интенсивности протонов, нейтронов, π- и μ - мезонов таковы:

протоны с энергией 600 МэВ, ток в пучке средний, прот/с

временная структура:	I00 мкс, I00 гц		3.10^{15}
	0,2 нс, 200 Мгц		3.10^{15}
	0,2 нс, 200 Кгц		3.10^{13}
	0,3 мкс, I00 гц	Накопитель	3.10^{15}
	непрерывно	Накопитель	10^{15}

протоны поляризованные, прот/с

	I00 мкс, I00 гц		10^{12} - 10^{13}

Соответствующую временную структуру будут иметь и потоки вторичных частиц из мишеней в протонных пучках (кроме медленных нейтронов)

Нейтроны:	холодные	($\bar{T} \sim 30$ K),	плотн. потока средняя нейтр/см^{2}с	10^{13}
	тепловые	($\bar{T} \sim 300$ K)	плотн. потока средняя,	3.10^{13}
			импульсная (100 гц, θ~35 мкс)	$2\text{-}5.10^{15}$
	резонансные	(1< E < 100 эВ),	ток в 2π, средний, нейтр/с (100 гц, 0,2 мкс)	$3,5.10^{14}$
		(1<E<100КэВ)		$4,0.10^{14}$
	быстрые	(до 600 МэВ),	поток в 4π средний, нейтр/с	6.10^{16}
π - мезоны		(100-350 МэВ),	ток в пучке средний (импульсный)	1/с $\pi^+ \sim 10^{11}$ (10^{13}) $\pi^- \sim 10^{10}$ (10^{12})
μ - мезоны		(0 - 50 МэВ, μ SR)		$\mu^+ \sim 10^9$ (10^{11}) $\mu^- \sim 2.10^8$ (2.10^{10})
		(до 100 МэВ, очищ.)		$\mu^+ \sim 10^9$ (10^{11}) $\mu^- \sim 2.10^8$ (2.10^{10})

I. Область низких энергий возбуждения

При низких энергиях возбуждения в делении отчетливо проявляются квантовые эффекты - (каналы деления - квантовые состояния в седловой точке /6/), оболочечные эффекты в распределении осколков по массам /7/, в высоте и форме барьера деления /8/, /9/. Здесь большую информацию дают эксперименты с нейтронами низких энергий и γ -лучами. Интенсивные импульсные потоки нейтронов от мишеней нейтронного комплекса /5/, рис.2, позволят существенно повысить светосилу нейтронных экспериментов по физике деления, проводимых техникой по времени пролета. Здесь можно указать ряд возможных направлений исследований.

Изучение угловых распределений разлета осколков и полных сечений деления ориентированных ядер при энергиях нейтронов от тепловых до 100 - 200 КэВ дает информацию о механизме процесса (каналовая структура, двугорбый барьер), о взаимодействии нейтронов с ядрами (силовые функции и проницаемости) (/10/, /11/). Варьирование за счет ориентации кинематики реакции позволяет по разному комбинировать квантовые характеристики составных ядер и детализировать сведения о влиянии этих характеристик как на сечения взаимодействия нейтронов с ядрами, так и на процесс деления. Высокие интенсивности нейтронов (на 3-4 порядка выше чем в работе /10/) позволят проводить светосильные эксперименты в отдельных резонансах известной природы и в области усредненных сечений.

Детальные исследования распределений осколков по энергиям, массам и зарядам при делении в отдельных резонансах и в области усредненных сечений позволит изучить влияние оболочечных эффектов на процесс деления.

Значительный интерес представляют исследования глубоко подбарьерного деления. Высокая интенсивность нейтронов позволит проводить детальные эксперименты по изучению групп резонансов в глубоко подбарьерном делении U234, U236, Pu 240, связываемых со вторым минимумом потенциальной энергии деформации (двугорбый барьер деления). Появится возможность идентификации резонансов в группах, измерений анизотропии разлета осколков при делении в отдельных резонансах, возможность разрешить резонансы высоколежащих групп. Все эти подходы пока

ограничены доступной интенсивностью нейтронов.

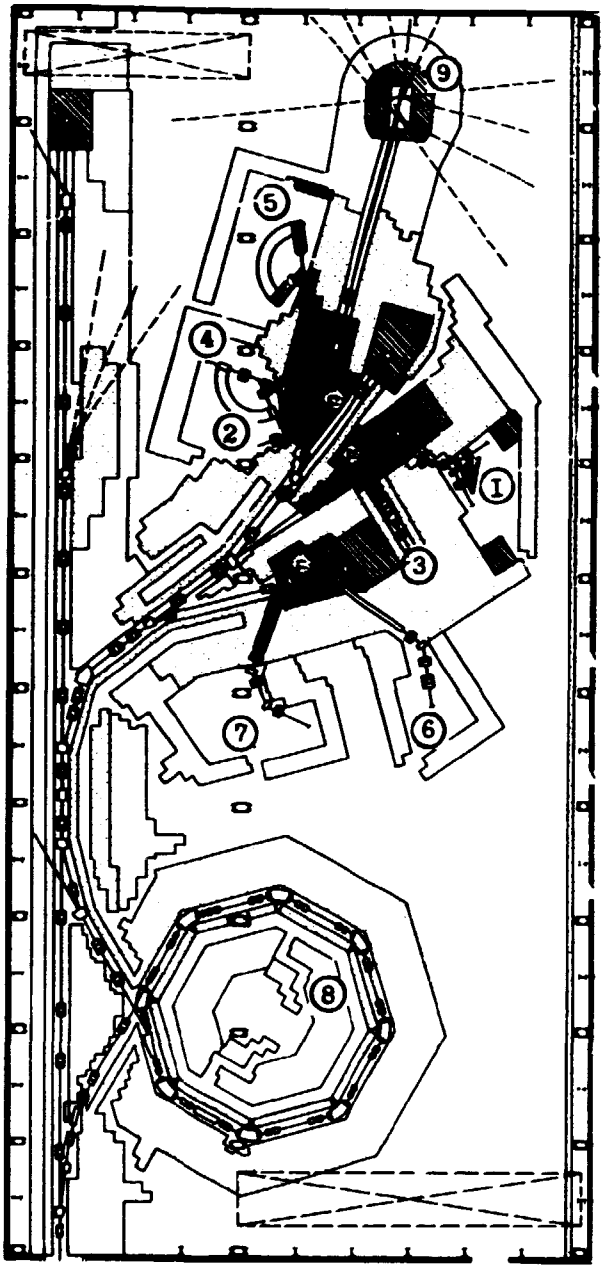

Рис.I. Экспериментальный комплекс Московской мезонной фабрики.
I-канал пионов высоких энергий; 2-канал пионов низких энергий; 3-медико-биологический канал; 4-светосильный спектрометр; 5-спектрометр высокого разрешения; 6-канал "чистых" мюонов; 7-[illegible]-канал; 8-накопитель протонов; 9-комплекс интенсивных источников нейтронов.

2. Деление протонами средних энергий

Изучение деления ядер протонами средних энергий (до ~ 600 МэВ) позволит получить информацию как о процессе деления при высоких возбуждениях (барьеры деления, механизм деления ядер с A < I50), так и о глубоко неупругих процессах в ядрах /I2/. Так как деление испытывают, в основном, "термализованные" ядра, изучение осколков деления, их энергетических, массовых и зарядовых распределений позволит подойти к пониманию процесса диссипации начальной энергии, приводящего к образованию высоковозбужденного ядра. Значительный интерес может представить изучение затухания оболочечных эффектов в ядрах путем наблюдения, например, изменения массовых распределений осколков при изменении энергии протонов в диапазоне 20-I60 МэВ /I2/. В пучке протонов мезонной фабрики могут проводиться как исследования делимости ядер (сечения деления), имеющие и прикладной характер, так и детальное изучение осколков деления - многопараметровые исследования кинематики разлета, массовых и энергетических характеристик осколков в зависимости от A, Z и энергии протонов /I2/. Методически такие исследования могут быть реализованы с помощью двухплечевого время-пролетного спектрометра, аналогичного описанному в /I4/, дополненного

время-пролетным спектрометром нейтронов (/12/).

3. Деление π^-- и μ-мезонами

Самостоятельный интерес имеет изучение процесса деления с помощью пучков π и μ-мезонов. Наряду с исследованиями глубоко неупругих процессов при поглощении π^--мезонов ядрами /15/, большой интерес представляют процессы деления из состояния мезоатома, например - изучение мезорентгеновского излучения до и после "перехвата" μ^--мезонов осколками деления, изучение безрадиационных переходов и т.п. Интенсивность пучка μ-мезонов, и, особенно, "чистых" μ-мезонов позволит проводить эксперименты в настоящее время ограниченные светосилой /16/, /17/.

4. Деление как средство изучения ядерных процессов и свойств ядра

Процесс деления может быть использован как индикатор образования составного ядра, что позволяет выделять соответствующие ядерные процессы. В частности, измерение полных сечений деления ориентированных и неориентированных ядер и, сравнение их с результатами расчетов по оптической модели открывает путь к прямым наблюдениям деформации ядер. Подобные эксперименты могут проводиться в пучках квазимоноэнергетических нейтронов с энергией в диапазоне 150-600 МэВ (см., например /18/).

Регистрация осколков деления в потоках поляризованных медленных нейтронов - один из путей проверки гипотезы универсальности слабого взаимодействия по эффектам нарушения пространственной четности в нуклон-ядерных взаимодействиях. Обнаруженные в свое время группой Данилина /19/ P-нечетные эффекты при делении ядер поляризованными тепловыми нейтронами (ассиметрия вылета легкого и тяжелого осколков относительно спина поглощенного нейтрона) были первым экспериментальным указанием на это явление. Величина P-нечетных эффектов $\sim 10^{-4}$ и более, т.е. имеет место значительное усиление в сравнении с одночастичной оценкой (10^{-6}-10^{-7}). Механизм усиления может быть связан со смешиванием компаунд-состояний разной четности и одного спина, с резонансным усилением в окрестности p-резонансов. Высокая светосила время-пролетного нейтронного спектрометра мезонной фабрики позволит развить исследования P-нечетных эффектов в делении с поляризованными нейтронами в области энергий до $\sim$ 100 эв при надежной идентификации уровней, и что весьма существенно, в слабых p-резонансах.

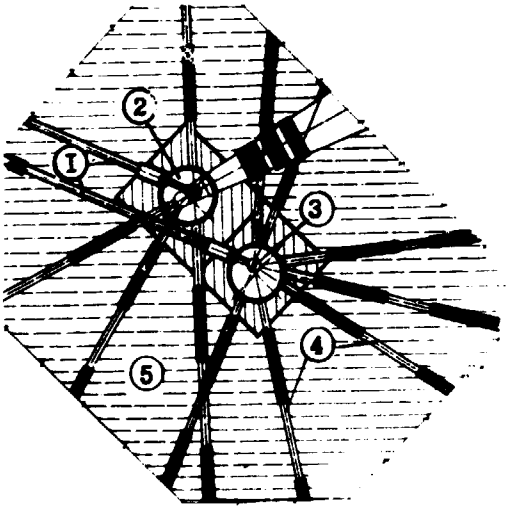

Рис. 2. Комплекс интенсивных источников нейтронов.
1-протонные пучки; 2-квазистационарный источник тепловых и холодных нейтронов; 3-импульсный источник тепловых и резонансных нейтронов; 4-нейтронные каналы с диберами; 5-тяжелый бетон.

5. Сечения деления и спектры вторичных нейтронов для атомной энергетики

Развитие перспективных направлений атомной энергетики (быстрые реакторы, установки электроядерного бридинга и термоядерного синтеза) требует проведения массовых оптимизационных расчетов-баланса нейтронов, критических размеров, тепловыделения, наработки новых изотопов, биологической защиты, радиационных дефектов в материалах. Подобные расчеты проводятся с использованием систем констант, создаваемых на основе экспериментально измеряемых сечений процессов и спектров вторичных нейтронов.

Интенсивные пучки протонов с энергией до 600 МэВ, импульсные источники нейтронов на основе сгустков протонов, сформированных в накопителе, микроструктуры пучка из ускорителя, позволят существенно повысить точность ключевых констант, необходимых для расчета, откроют возможность измерений сечений и спектров, ограниченных интенсивностью /20/

Для проблемы быстрых бридеров большое значение приобрели измерения сечений деления и спектров вторичных нейтронов для Pu240, 241, 242, накапливающихся в значительных количествах при многократном использовании плутония. Остаются актуальными прецизионные измерения сечений деления и α - отношения сечений захвата и деления для основных делящихся изотопов (U233, Th232, U235, U238, Pu239).

Величина α определяет коэффициент воспроизводства ядерного горючего в быстрых реакторах, и соответственно, их место в атомной энергетике. Соответствующие эксперименты в импульсных потоках нейтронов от замедлителей нейтронных линий в десятки и сотни раз превзойдут по светосиле проводимые в настоящее время.

Использование пучков протонов, пионов, потоков каскадно-испарительных нейтронов позволит провести детальные измерения сечений делений и спектров вторичных нейтронов при делении протонами и нейтронами с энергиями до 600 МэВ, π и μ - мезонами с энергиями до ~ 350 МэВ. Соответствующая информация, необходимая для проблемы электроядерного бридинга, пока еще ограничена.

Время-пролетный нейтронные спектрометры на основе микроструктуры протонного пучка позволит развить исследования деления, n,nf, $n,2n,f$, , - процессов в диапазоне энергий нейтронов до ~ 15 МэВ, представляющем интерес для проблемы термоядерного синтеза.

Литература

I. Ю.М. Ципенюк, Г.Н. Смиренкин и др. УФН, 1984, т.144, 6.I, 3.
2. В.М. Лобашев, А.Н. Тавхелидзе. Вестник АН СССР, 1983, № 2.
3. С.К. Есин, Г.Н. Вялов. Программа экспериментальных исследований на мезонной фабрике ИЯИ АН СССР, труды Ш-го Всесоюзного семинара, с.II, Москва, 1984 г.
4. М.И. Грачев, там же, с.17.
5. М.В. Казарновский, Ю.Я. Стависский и др., там же, с.87.
6. О.Бор. Международн. конф. по использ. ат. энергии, т.2, 175, Москва, 1955.
7. P.Fong,Phys.Rev.,1955,v 1o2,434.
8. W.Y.,Swiatecky Pyis.Rev,1955,v 102,434.
9. V.M.Strutinsky,Nucl.Phys,1967,A 95,420,A 112,1.
10. N.J.Pattenden,H.Postma,Nucl Phys,1971,A 167,225
II. Н.Н. Гонин и др., Письма в ЖЭТФ, 1982, 35, вып.4, 1976.
12. А.С. Ильинов, Ю.В. Рябов, там же где /3/,41, 299.
13. P.Grange,H.A.Weidemuller,Phys.Lett.,B,1980,v 96,26.
14. М.Н. Андроненко и др. Препринт, ЛИЯФ, 1976, № 237.
15. Ф.М. Сергеев, Поглощение пионов ядрами. Материалы 17-й Зимней школы ЛИЯФ, Ленинград, 1982.
16. С.М. Поликанов и др., Ядерная физика, 1976, т.24, в.2.
17. Д.Ф. Зарецкий и др., Ядерная физика, 1979, т.29, в.2, 306.
18. H.Marshak,A.Richardson,T.Tamura,Phys.Rev.,1966,v 150,996.
19. Г.В. Данилян, УФН, 1980, т.131, вып.3, 329.
20. Ю.Я. Стависский. Программа экспериментальных исследований на мезонной фабрике ИЯИ АН СССР. Труды Всесоюзных семинаров: Москва, 1977; Москва, 1982; Москва, 1984.

LINEAR MOMENTUM TRANSFER TO RESIDUAL NUCLEI LEADING TO FISSION

L.A. Andronenko, A.A. Kotov, L.A. Vaishnene
Leningrad Nuclear Physics Institute, 188350 Gatchina, U.S.S.R.

W. Neubert
Central Institute for Nuclear Research Rossendorf, 8051 Dresden, G.D.R.

Abstract

The angular correlations of coincident fragments emitted from U, Bi, Au, W, Yb, Ho, Sm, Sb, Ag and Ni targets bombarded with 1 GeV-protons were measured with a double-arm spectrometer including a position-sensitive parallel plate avalanche counter.
The forward momentum $\langle p_{\parallel} \rangle$ was deduced from the folding angles. $\langle p_{\parallel} \rangle$ as function of Z^2/A levels off below $Z^2/A \approx 25$ and indicates a limit of energy deposition in these nuclei.

Fission of heavy nuclei induced by relativistic protons is related to peripheral collisions which are characterized by both low momentum and energy transfer to the residual nuclei. However, the fission barrier increases considerably in medium weight residual nuclei and a large ammount of energy has to be deposited into these nuclei to undergo fission.
In intermediate energy collisions one cannot deposite momentum without depositing excitation energy E^*. The excited nuclei must have a forward velocity. The measurement of the transferred forward momentum is therefore a key to estimate the excitation energy of the system.
Two ways of experimentally determining this linear momentum transfer have been employed. On the one hand, the mean recoil properties of the produced individual radionuclides have been used to derive average values of $p_{\parallel}$ transferred to the target residue /1/. A more reliable method is the measurement of the angular correlation between coincident fission fragments where the deviation of the mean angle of the correlation function from collinearity is due to the transferred forward momentum. We used the last method to study momentum transfer to fissioning nuclei in a wide range of target masses.
The experiments were performed at the LNPI synchrocyclotron using the external beam of 1 GeV protons. The thickness of the targets was about 0.5 mg/cm^2 and they were mounted at 45° to the beam axis. The beam spot at the target had an elliptical shape of about 15 mm vertical height and 10 mm horizontal width. Coincident fragments were detected on both sides of the beam. One arm of the spectrometer consisted of a parallel plate avalanche counter (PPAC) and an array of 3 silicon surface barrier detectors. These detectors provided the time-of-flights and energies of the registered fission fragments. A position sensitive PPAC with delay-line read-out was installed on the opposite side. This detector covered an angular range of 48 degrees in the reaction plane. The out-of-plane acceptance was $\pm$ 4°. The set-up with the involved detectors and the following electronics was already described elsewhere /2/. Each of the strips of the position-sensitive parallel plate avalanche counter corresponds to an angular interval of 1.3 degrees in the reaction plane. After correction for target-detector geometry and strip efficiency we obtained the angular correlation directly from the well resolved peak areas of the induvidual strips. No corrections for the beam size have been carried out.
The average forward momentum $\langle p_{\parallel} \rangle$ is related to the folding angle $\langle \theta_1 + \theta_2 \rangle$ of the measured angular correlation by the equation

$$\langle p_{\parallel} \rangle = 2 \tan (180° - \langle \theta_1 + \theta_2 \rangle) \cdot p_F \cdot \left[4 + \tan^2 (180° - \langle \theta_1 + \theta_2 \rangle)\right]^{-1/2} \quad (1)$$

The experimental mean angles $\langle \theta_1 + \theta_2 \rangle$ for various targets are collected in table 1. Symmetric fission was assumed to calculate the momentum p_F of the fragments. The atomic and mass numbers of the residual nuclei undergoing fission were taken from the cascade-evaporation calculations, see ref. /3/.

The kinetic energies of the corresponding symmetric fragments were taken from the corrected values by using the Viola plot. The influence of asymmetric shapes of the fragment mass distribution on the accuracy of $\langle p_{//} \rangle$ was checked for the target nucleus Ag. An assumed flat fragment distribution within the interval 12 u. $\leq A \leq$ 66 u. yields $\langle p_{//} \rangle$ = 868 MeV/c whereas the experimental distribution within the same cut-offs gives 836 MeV/c. As seen in fig. 1, the accuracy of $\langle p_{//} \rangle$ for medium-weight target nuclei is decided by the event statistics. The statistical error exceeds the uncertainty due to the ignorance of the primordial mass distribution of the system undergoing fission. However, the obtained values $\langle p_{//} \rangle$ may be somewhat lowered because we have measured only the in-plane correlations. Both the present data $\langle p_{//} \rangle$ for 1 GeV and that of other authors for 660 MeV and 1 GeV incident proton energy are shwown in fig. 2. A nearly linear increase of the forward momentum with decreasing fissility parameter Z^2/A is observed in the range from heavy nuclei to the rare earths target nuclei. This behaviour was already observed in an earlier work /4/ and reflects the increasing role of non-peripheral collisions with decreasing target mass. Further, a leveling-off for the transferred forward momentum is observed for $Z^2/A < 25$ which implies also saturation in the deposited excitation nergy.

As already mentioned, the average excitation energy transferred to the residual nuclei is related to the longitudinal component $p_{//}$ of the imparted linear momentum. Firstly, such relationship was derived from Monte Carlo simulations of the collision process /5/. In this reference, a contour plot shows the correlation of both magnitudes. Although for a given value of $p_{//}$ only a range of corresponding excitation energies can be derived, an overall linear dependence between both average magnitudes can be established

$$\langle E^* \rangle / E_{max} \simeq 0.8 \ \langle p_{//} \rangle / p_{max} \qquad (2)$$

where E_{max} and p_{max} are the energy and momentum of the beam. Let us mention that a linear dependence of $\langle p_{//} \rangle$ on the excitation energy also comes out from the collective tube model /6/.

The excitation energies, calculated by using equation (2), are given in column 8 of table 1. They are in good agreement with the theoretical predictions of the cascade-evaporation model /3/.

The leveling off for $\langle p_{//} \rangle$ below $Z^2/A \leq 25$ corresponds to a nearly constant excitation energy for these medium weight nuclei. The striking fact is that only a maximum energy of about 4 MeV per nucleon can be deposited into these target residues. The analysis of heavy ion reactions at intermediate energies /7/ leads to nearly the same energy limit.

As follows from dynamical considerations, the observed behaviour of $\langle p_{//} \rangle$ as function of Z^2/A may be related to the onset of multifragmentation competition.

References:

/1/ J.B. Cumming, P.E. Haustein, H.-C. Hseuh, Phys. Rev. C24 (1981) 2162

/2/ W. Neubert, A.A. Kotov, L.N. Andronenko, A.I. Iljin, G.G. Kovshevny, L.A. Vaishnene and S.S. Volkov, Nucl. Instr. Methods 204 (1983) 453

/3/ L.N. Andronenko, A.A. Kotov, M.M. Nesterov, V.P. Petrov, N.A. Tarasov, L.A. Vaishnene, W. Neubert, Z. f. Physik A318 (1984) 97

/4/ A.A. Kotov, G.G. Semenchuk, L.N. Andronenko, M.N. Andronenko, B.L. Gorshkov, G.G. Kovshevny, V.R. Resnik and G.E. Solyakin, Yad. Fiz. 19 (1974) 756

/5/ N.T. Porile, Phys. Rev. 120 (1960) 572

/6/ J.B. Cumming, Phys. Rev. Letters 44 (1980) 17

/7/ C. Guet, Informal Workshop Phase Transitions, NBI Copenhagen, April 29-30, 1985

/8/ A.A. Kotov, Thesis, Leningrad 1976

/9/ F. Saint-Laurent, M. Conjeaud, R. Dayras, S. Harar, H. Oelscher and C. Volant, Nucl. Phys. A422 (1984) 307

/10/ G. Andersson, M. Areskoug, H.-A. Gustafsson, G. Hylten, B. Schrøder, Phys. Letters 71B (1977) 279

/11/ V.S. Bytchenkov, Thesis, Leningrad 1967

Table 1 Summary of the deduced mean momentum and energy transfers

target	Z^2/A	$\langle\theta_1+\theta_2\rangle$	A_f	Z_f	$\eta = \frac{\langle v_{\parallel}\rangle}{\langle v_f\rangle}$	$\langle p_{\parallel}\rangle$ [MeV/c]	$\langle E^*\rangle$ [MeV]	$\langle E^*_{calc}\rangle$ [MeV]
^{238}U	35.56	175.5 ± 0.3^x	226	90	0.03932 ± 0.00260	327 ± 21	154	-
^{209}Bi	32.96	172.4 ± 0.3^x	196	81	0.06657 ± 0.00260	481 ± 18	227	215
^{197}Au	31.68	170.7 ± 0.3^x	187	77	0.0816 ± 0.0026	556 ± 17	262	290
^{nat}W	29.76	167.8 ± 0.5^x	174	72	0.1075 ± 0.0045	675 ± 26	318	370
^{nat}Yb	28.3	165.5 ± 0.6^x	163	68	0.1282 ± 0.0054	751 ± 30	354	-
^{165}Ho	27.2	163.7 ± 1.0^x	155	65	0.1447 ± 0.0092	802 ± 52	378	-
^{nat}Sm	25.6	163.6 ± 0.5	140	60	0.1456 ± 0.0046	730 ± 21	344	385
^{nat}Sb	21.3	158.5 ± 1.5	112	49	0.1932 ± 0.014	767 ± 55	362	380
^{nat}Ag	20.5	153.0 ± 1.5	97	43.3	0.2469 ± 0.02	852 ± 50	402	380
^{nat}Ni	13.3	145.0 ± 1.5	48	25.5	0.3304 ± 0.03	635 ± 31	300	-

x) - independent measurement with a movable array of Si-detectors, ref. /4/, xx) see ref. /8/,
$\langle E^*_{calc}\rangle$ follows from cascade-evaporation calculations, ref. /3/,
the errors of η and $\langle p_{\parallel}\rangle$ include only uncertainties of the folding angles.

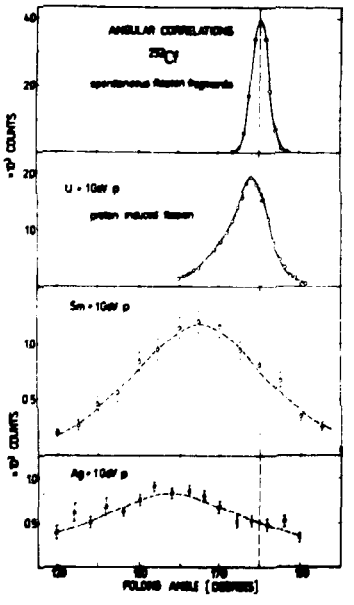

Fig. 1 Evolution of the angular correlations from spontaneous fission to induced fission with large longitudinal momentum transfer

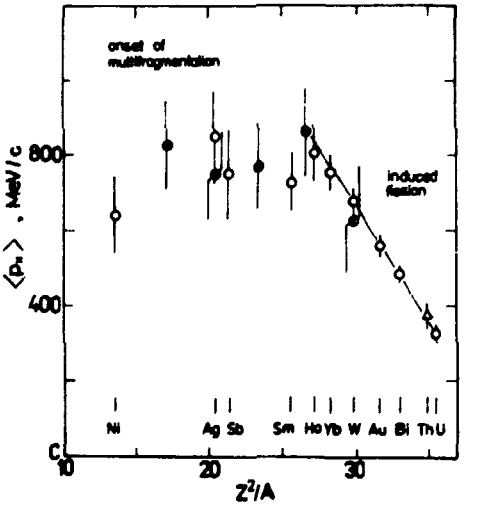

Fig. 2 The mean longitudinal momentum as function of Z^2/A.
ϕ - this work, ϕ - 1 GeV, ref. /9/
ϕ - 0.6 GeV, ref. /10/ ϕ - 0.66 GeV, ref. /11/.

CATAPULT MECHANISM FOR FAST PARTICLE EMISSION AFTER SCISSION

P. Mädler

Joint Institute for Nuclear Research, Dubna, USSR

Abstract: It is shown in TDHF approximation that the final disintegration of the prefragments is accompanied by a rapid snatching of the inner tails of the mean field including velocities of 0.1c or even larger. A nucleon moving towards the snatching ends with Fermi velocity becomes reflected, acquires additionally twice that velocity, and can escape with an energy of several tens MeV (preferentially along the scission axis). The proposed mechanism loses its purpose when neglecting self-consistency.

In a recent TDHF study of the fission of charged nuclear matter slabs[1] it has been found that the final disintegration of a slab ("snatching"), independently of the choice of the initial conditions used to boost the system beyond the saddle point, occurs on a time scale of a few 10^{-22}s. In [2] we have investigated the question whether the rapidly snatching inner ends of the mean field can act as a "catapult", i.e. push out fast nucleons, preferentially along the scission exis.

To get symmetric fission of a slab of thickness $2.15 fm^{-2}$, we have used a collective velocity field as initial conditions for the TDHF evolution [3]. Fig. 1 illustrates the response of the system for different strengths v_0 of the initial velocity field. While small v_0 values result in (enharmonic) density oscillations, we have found a transitional behaviour for v_0 =0.06c: The central density $\rho(z=0, t)$ comes close to zero but the two fragments do not yet separate. It is interesting to note that "snatching" occurs already for comparably small v_0 values: The "catapult" vecity" $v_{cat}(t)$, which we define to be the maximum velocity $v(z,t)$ in the "neck region" ($z \approx 0$) at given instant t, increases to substantial values if only the central density comes close to zero. In the present examples the return of matter into the $z \approx 0$ region prevents a further increase of v_{cat}.

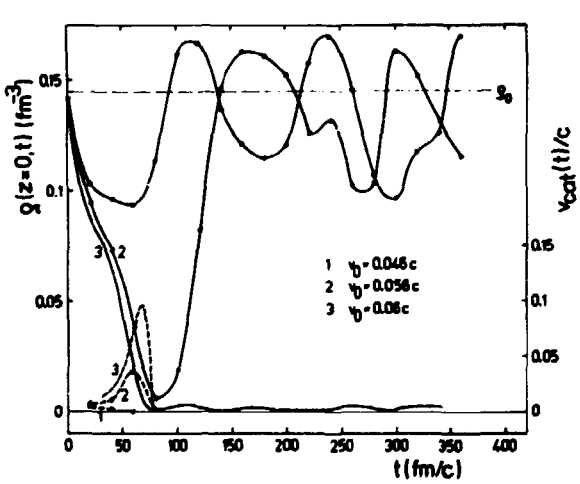

Fig.1. Time evolution of the density at z=0 (left-hand scale, full lines) for 3 different strengths vo of the initial collective velocity field. The "catapult velocity" in units of the velocity of light c is also shown (right-hand scale, dashed lines).

In Fig. 2 the peak values of $v_{cat}(t)$ are shown as a function of the strength v_0 of the initial velocity field. Due to the neglect of the Coulomb force in our calculations quite large v_0 values are needed to attain scission ($v_0 \gtrsim 0.062c$). Furthermore, in order to get final fragment

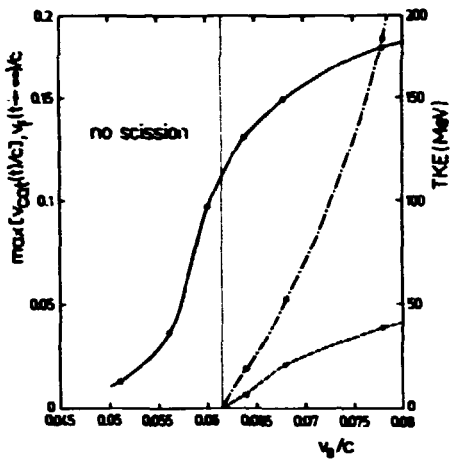

Fig.2. Maximum catapult velocity (solid line), final fragment velocity (dashed line), and the total kinetic energy of the corresponding realistic fragments of mass numbers A=126 (dash-dotted line, right-hand scale).

velocities of the order of the experimental ones, say for spontaneous fission of ^{252}Cf, one has to further increase v_0. Note, however, that even for $v_0 < 0.062c$ (no scission) already quite large values of v_{cat} result which cause the emission of "catapult particles" (cf. ref.[2]). Moreover, since the inclusion of the Coulomb force does not qualitatively influence the appearance of the fast snatching[1], we conclude that it is mainly an effect of the self-consistent nuclear single-particle potential.

We now analyse the case $v_0 = 0.078c$ in more detail. This is because with respect to both the mass number and TKE it resembles spontaneous fission of ^{252}Cf. At t=60fm/c v_{cat} reaches its maximum (velocity peak near z=0, Fig. 3).

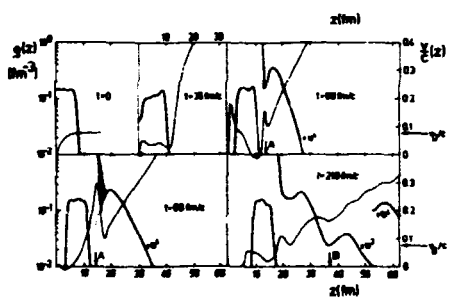

Fig.3. Time evolution of the density (thick lines) and the velocity field (thin lines, right-hand scale) for the case v_0=0.078c. The hatched region is identified with catapult particles.

At the same time a first portion of particles (low-density lump arround z=18fm) emerges. These particles are a consequence of our large v_0 values (omission of the Coulomb force) and a corresponding much too small saddle-to-scission time ($\approx 10^{-22}$s in the present example). Thus, we consider the first portion of particles emerging as a consequence of this artificially rapid process to be spurious. On the other hand, a second portion of particles appears in front of the fragment at t=80 fm/c in correlation with a peak in the velocity field around z=16fm. We identify it with catapult particles since a nucleon moving with Fermi velocity v_F towards the snatching end and being reflected at t =60fm/c acquires velocity $2v_{cat}+v_F$ and needs a characteristic time of about 20fm/c to cross the fragment. At later instants further particle decay of fragment compression modes (cf. t=210fm/c) takes place.

A further interesting feature of the density evolution can be seen in Fig.4: While in the necking-in stage the system becomes highly stretched, in the "catapult stage" the density profiles of the prefragments return to near-equilibrium shapes on a time scale of about 10^{-22}s with the positions of their mass centres remaining nearly unchanged.

We have evaluated energy spectra of emitted particles for the above example by recording all single-particle wave functions at a fixed "counter" position and then Fourier-analysing them [2]. The resulting spectra are shown in Fig. 5.

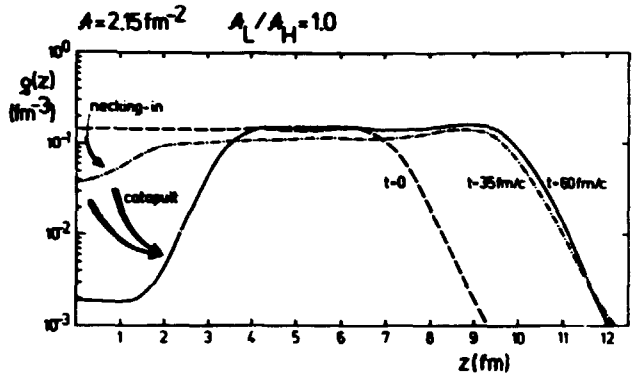

Fig. 4. Time evolution of the density for the same case as in Fig. 3.

The oscillating behaviour of the spectra is an artifact of the calculations since the time integration of the Fourier transformation has been extended only from t=0 up to a finite t (indicated in the figure) at which the considered signal has not yet sufficiently faded. To a less extent this concerns the spectrum from counter A taken at t= 60 fm/c. It describes the (spurious) contribution from the "necking-in particles" which for the given final t have almost completely passed counter A (cf. Fig. 3). At t=80fm/c counter A has registered both necking--in and catapult particles. However, there is a substantial contamination from the fragment, which is expected to cover preferentially the lower energy region.

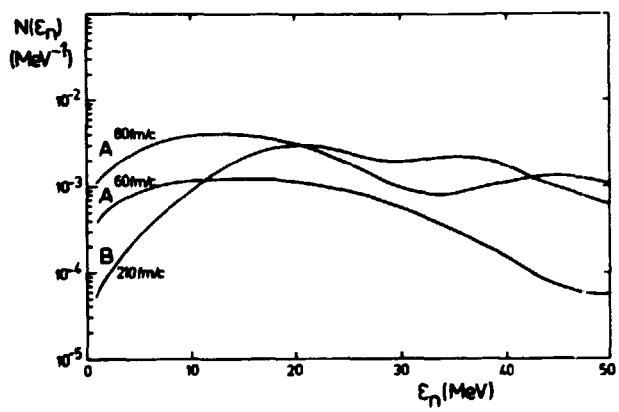

Fig.5. Neutron spectra for V_0=0.78c, taken at several instants with counters A and B (cf. Fig. 3) and normalized [2] to be comparable with the spectrum of prompt neutrons from spontaneous fission of ^{252}Cf.

To exclude it, we compare with a third spectrum taken at t= 210fm/c from counter B. Despite the described ambiguities Fig. 5 illustrates that in the energy range of 20-30 MeV catapult neutrons are emitted on a level of roughly 10^{-3}MeV^{-1} per fission event.

The recently obtained non-evaporative high-energy component in the inclusive spectrum of prompt fission neutrons from ^{252}Cf (s.f.)[4] possibly provides some evidence for catapult neutrons, the more since light charged particles from ^{252}Cf (s.f.) are found to be strongly peaked along the scission axis [5]. The latter is most pronounced for protons. However, alternative interpretations exist (cf.[5,6] and references cited therein). Our calculations overestimate the high-energy tail measured in [4] at least by two orders of magnitude. Obviously this deviation cannot be exclusively related to the difference between the dynamics in our effectively one-dimensional slab world and a realistic geometry [3]. Since we are concerned with very high momentum components in the prefragments, an inclusion of residual interactions (not inherent in TDHF) should substantially damp these components and, hence, lower the high-energy tail of the spectrum. In principle, the latter as well as pairing correlations could also lead to a stabilization of the shapes of fissioning nuclei and, consequently, lower the catapult velocity.

This, in turn, would soften the spectrum of catapult particles.

For the catapult effect to occur, one needs highly stretched fragments. Such events are probably as rare as cold fragmentation (nearly no deformation at scission). It is not excluded that our initial conditions somewhat favour large deformations. This could be a further reason for our overestimation with respect to the inclusive data. From these considerations we expect that the non-evaporative high-energy component would appear even more pronounced with respect to the evaporative "background" when detecting neutrons in coincidence only with smallest TKE. The latter would then correspond to a somewhat higher effective temperature, i.e. events where the large deformation energy is converted into heat. The ratio of non-evaporative to evaporative total multiplicities would be a measure of the probability that a large portion of the deformation energy is directly carried away be a single neutron. This ratio should not sensitively depend on the experimental cut in TKE provided the low-energy tail of the TKE distribution is concerned.

In [2] we have shown, that catapult particles can also appear in the final stage of heavy-ion reactions. To get rid of the ambiguities in extrapolating our one-dimensional TDHF results to reality, we consider a recent result of a realistic TDHF evolution[7,8] shown in Fig. 6. We observe: i) the return of the stretched configuration to near-spherical shapes really occurs on a time scale of 10^{-22}s, ii) from the density contours at $t_o + 5\cdot 10^{-23}$s and $t_o + 10^{-22}$s a catapult velocity of $v_{cat} \gtrsim 0.08c$ can be extracted (cf. Fig. 2), iii) during "snatching" the mass-centre positions of the fragments remain nearly unchanged (cf. Fig. 3).

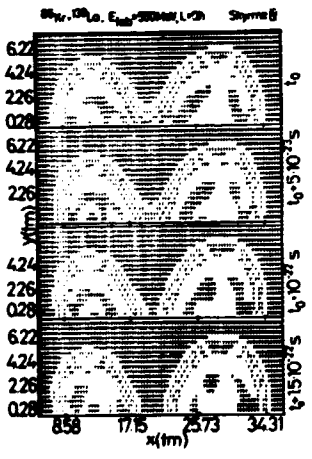

Fig.6. Density-contour plot for the final stage of a central Kr+La reaction. Results of an axially symmetric TDHF calculation [7,8].

Unfortunately, the linear density plot does not allow us to look for the low-density tails which correspond to emitted particles (cf. Fig.2) and which we expect to emerge at $t \gtrsim t_o + 1.5\ 10^{-22}$s. However, in this respect the given calculation does not contain the relevant information. A larger numerical box as well as a finer grid-point spacing have to be used to obtain numerically stable results in the tails of the density distribution (cf. ref.[3]). Nevertheless, from Fig.6 we conclude that the bulk properties of the mean-field dynamics (e.g. snatching) are qualitatively contained already in simple slab calculations and not artificially introduced by our initial conditions or the omission of the Coulomb force.

The author is grateful to J.A.Maruhn for providing him with more detailed informations concerning the series of calculations published in ref. [7].

References: 1. K.Dietrich and J.Nemeth.Z.Phys. A300 (1981) 183.
2. P.Mädler, Z.Phys. A321 (1985) 343.
3. P.Mädler, Z.Phys. A318 (1984) 87.
4. H.Marten and D.Seeliger, J.Phys. G10 (1984) 349.
5. A.J.Kordyasz et al., Nucl.Phys. A439 (1985) 28.
6. B.Milek, R.Reif and J.Revai, these proceedings.
7. J.A.Maruhn, et al. Phys.Rev. C31 (1985) 1289.
8. J.A.Maruhn, private communication.

POLAR PARTICLE EMISSION IN SPONTANEOUS FISSION

B. Milek, R. Reif
Technische Universität Dresden, Sektion Physik, Dresden, DDR
J. Revai
Central Research Institute for Physics, Budapest, Hungary

Emission and transfer of nucleons in heavy-ion collisions may be investigated by modelling the reaction dynamics as a particle in the field of two single-term separable potentials moving uniformly along straight-line trajectories. For this case in a Fadeev-like formulation the probabilities for the elastic, transfer, and breakup channel have been calculated in dependence on the basic reaction parameters /1, 2/.

This three-body model for the dynamics of heavy-ion collisions has been extended to simulate spontaneous fission. As an initial state two spherical mean fields, approximated as one-term separable potentials, have been located at a certain separation distance, with a neutron as a third particle being bound by 8 MeV with a two-center wave function, which goes asymptotically to two 1s-states in the separated wells. For a given trajectory for the relative motion of the fragments during the fission process, the single particle wave function is followed in time by solving the corresponding time-dependent Schrödinger equation. From the asymptotic wave function the escape probability can be calculated in dependence of the non-adiabatic features of the fission dynamics implied in the chosen trajectory. First calculations for ^{252}Cf, s.f. indicate the following results, rather independent from the details of the trajectory in the overlap region:

(1) The total emission probability is a few percent, increasing only very slightly with the mass asymmetry.
(2) The average energy of the emitted particles is in the range of a few MeV, with high-energetic particles of about 2o MeV being decreased by a factor of $1o^5$ - $1o^6$. The emission spectrum is hardened with increasing mass asymmetry.
(3) The particle is emitted preferentially in polar direction (fission axis), with the emission probability in perpendicular direction diminished by about two orders of magnitude for the case of symmetric fission.
(4) Concerning the correlation with the mass asymmetry, the particle emission along the direction of the light fragment is favoured by about one order of magnitude compared to the flight direction of the heavy fragment, if high-energetic particles are emitted.

The general trends expressed in these results are reflected in the experimental data on polar particle emission in fission /3, /.

References

/1/ J. Revai, Nucl. Phys. A438 (1985) 512
/2/ B. Milek, R. Reif, J. Revai, Phys. Letters 150B (1985) 65
/3/ A.J. Kordyasz et al., Nucl. Phys. A439 (1985) 28
/4/ J. Theobald, these proceedings

FRAGMENT MASS DISTRIBUTIONS IN HEAVY-ION REACTIONS LEADING TO COMPOSITE SYSTEMS WITH Z = 108

P. Gippner, K.D. Schilling, W. Seidel, F. Stary, E. Will
Central Institute of Nuclear Research, Rossendorf, GDR

H. Sodan, S.M. Lukyanov, G.G. Chubarian*), V.S. Salamatin and Yu.E. Penionzhkevich
Joint Institute of Nuclear Research, Dubna, USSR

Fragment mass distributions are presented obtained by investigating the heavy-ion reactions 22Ne + 249Cf, 32S + 238U, 40Ar + 232Th and 56Fe + 208Pb leading to composite systems with the nuclear charge Z = 108. The experiments were performed at the heavy-ion cyclotron U300 of the Laboratory of Nuclear Reactions in Dubna. The spectrometer DEMAS was used to measure the times of flight and the laboratory angles of correlated fragments. The shape of the mass distributions strongly depends on the mass asymmetry in the entrance channel. By variation of the bombarding energy it is shown that near to the Coulomb barrier the mass distribution of the reactions 32S + 238U and 40Ar +232Th exhibit relative maxima at M ≈ 205, interpreted as due to stabilizing effects of nuclear shells during the fragmentation.

For bombarding energies in the region up to 10 MeV/nucleon the following mechanisms can contribute to the total cross section of a heavy-ion reaction: elastic scattering; deep-inelastic scattering connected with multi-particle transfer and a considerable energy dissipation; fusionlike processes (fast fission and quasi-fission); compound nucleus formation followed by fission and/or emission of light particles; pre-compound emission of single nucleons or light fragments with high energy.

Investigating the contributions of these mechanisms one has to measure the distributions of masses and energies of the correlated reaction products as well as their angular correlations. In order to do this the double-arm time-of-flight spectrometer DEMAS was constructed [1]. It makes use of the fact that a binary reaction is fully characterized by determination of the times of flight TOF_3, TOF_4 and the laboratory angles Θ_3, Θ_4 of the correlated fragments [2,3]. As a result, pre-evaporation masses can be determined with good accuracy after verifying the conditions of colinearity and coplanarity [4].

The figure 1 shows the principle of our experimental equipment. The spectrometer DEMAS consists of a reaction chamber and two detector arms, which can be moved in steps of 15° between 30° and 150° in the middle plane. The fragments are detected after a flight path of 60 cm by position-sensitive ionization chambers. Fast timing signals for TOF-measurements are generated by microchannel-plate detectors(MCP) and parallel-plate avalanche counters(PPAC). A typical value for the time resolution is Δt_{α} = 350 ps. The PPAC has an active area of 18 x 5 cm^2, defining a solid angle of $\Delta\Omega$ = 18 msr for each detector arm. Besides microchannel-plate detectors a ΔE,E-semiconductor detector telescope for identification of light particles and a monitor detector are located inside the reaction chamber.

The acceptance in mass and angle of the spectrometer shows that for a fixed position of the first chamber the second one has to be moved in order to detect both the elastically scattered particles as well as the full mass region of the fission products [5]. The obtained results have then to be integrated in angle over the acceptance regions for different ionization chamber positions (see table 1). Further, colinearity and coplanarity tests were performed to distinguish between physical and unphysical events. In order to verify the colinearity only those

*) Yerevan Physics Institute, Yerevan, USSR

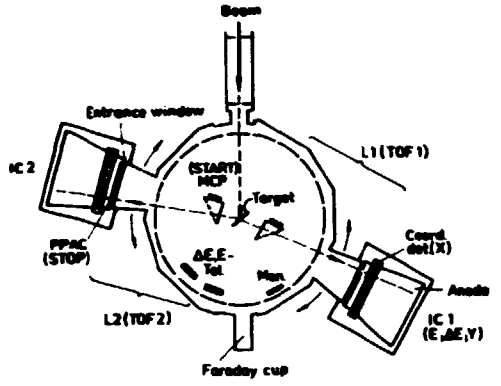

Fig. 1

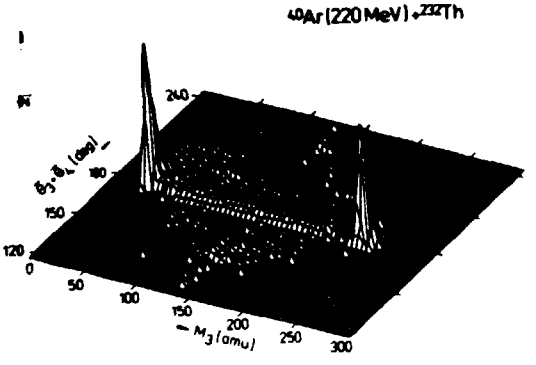

Fig. 2

events are accepted for data processing, for which the sum of angles $\bar{\Theta}_3 + \bar{\Theta}_4$ in the cm-system lies in the interval $180^\circ \pm 3^\circ$. Fig. 2 shows the intensity obtained by investigating the reaction $^{40}Ar(220\ MeV) + {}^{232}Th$ as a function of the parameters $\bar{\Theta}_3 + \bar{\Theta}_4$ and M_3. The plot demonstrates that the elastically scattered particles and most of the fission fragments fulfil the colinearity condition.

The present paper gives preliminary results obtained by investigating the reactions $^{22}Ne + {}^{249}Cf$ $^{32}S + {}^{238}U$, $^{40}Ar + {}^{232}Th$ and $^{56}Fe + {}^{208}Pb$. These combinations were chosen with the aim of producing composite systems with equal nuclear charge $Z_{comp} = 108$, assuming the influence of Z_{comp} on the results to be the same. Table 1 gives a survey on the entrance channel parameters and ionization chamber positions where the investigations have been done. The derived results are presented in the figures 3 - 7.

Table 1: Summary of the experimental conditions

Reaction	η_0	E_1 / MeV	$\bar{E}/V_{CB}$	E^* / MeV	IC-positions
$^{22}Ne + {}^{249}Cf$	0.84	174	1.47	97	$90^\circ - 60^\circ$
$^{32}S + {}^{238}U$	0.76	192	1.06	61	$60^\circ - 60^\circ$ $75^\circ - 60^\circ$ $90^\circ - 60^\circ$
$^{40}Ar + {}^{232}Th$	0.71	206 220 301	1.02 1.08 1.48	49 60 129	$75^\circ - 60^\circ$ $60^\circ - 60^\circ$ $75^\circ - 60^\circ$ $60^\circ - 60^\circ$ $75^\circ - 60^\circ$
$^{56}Fe + {}^{208}Pb$	0.58	354	1.24	78	$45^\circ - 60^\circ$ $60^\circ - 60^\circ$

E_1: bombarding energy; $\bar{E}$: energy in the cm-system; V_{CB}: Coulomb barrier; E^*: excitation energy of the composite system [6]

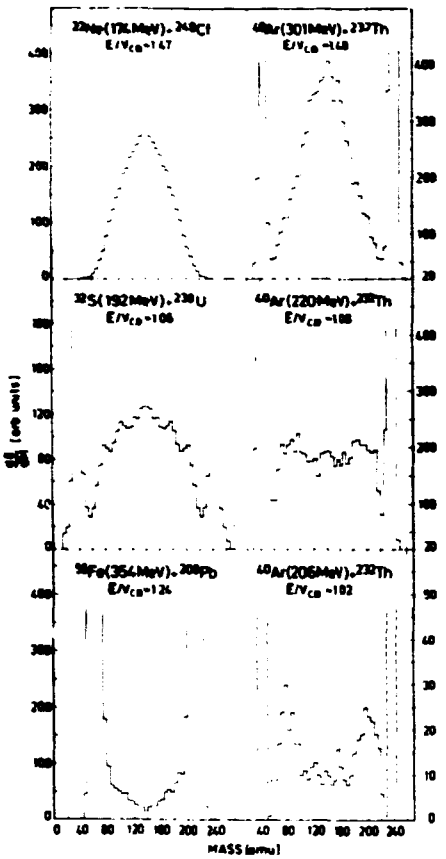

Fig. 3: Left-hand side: Fragment mass distributions for different parameters of mass asymmetry η_0 in the entrance channel. Right-hand side: Mass distributions of fragments obtained in the reaction $^{40}Ar + ^{232}Th$ at different bombarding energies

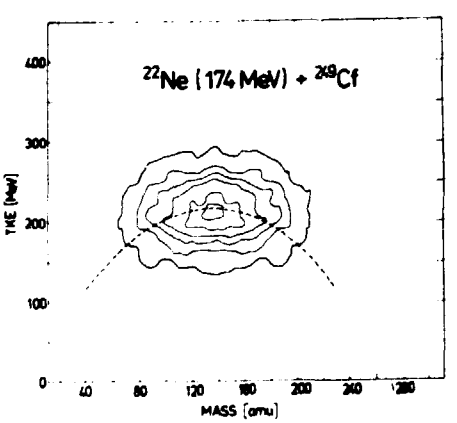

Fig. 4

The parabolic dashed lines in figs. 4-7 represent the expected TKE release in fission proportional to $M_3 \cdot M_4/(M_3^{1/3} + M_4^{1/3})$ according to refs. [3,10].

Three characteristic features of the results should be discussed:

(i) For an energy ratio $\bar{E}/V_{CB}$ higher than 1.4 the systems Ne + Cf and Ar + Th exhibit a symmetric mass distribution. The maximum yield of fragments has been observed at $M = (M_1 + M_2)/2$. The same was found for the system S + U studied at lower bombarding energies. Here the gaussian shows a superposition of relative maxima at $M \approx 205$ as well as the complementary mass value $M \approx 70$. For the combination Fe + Pb the yield of symmetric fragments sharply decreases compared with that of asymmetric products lying on the tails of the peaks due to elastic scattering. Concerning the diffusion model for heavy-ion reactions a symmetric mass distribution is expected for both fusion-fission and fast fission [7]. In order to distinguish between these mechanisms one has to account for the half-widths of the measured mass distributions. For fusion-fission the results of the Darmstadt-group [3] obtained for heavy collision systems allow to predict the full width at half maximum to be in the order of $\Gamma = 70$ amu for $Z_{comp} = 108$. Contrary to this one expects for fast fission broader mass distributions. Considering the value $\Gamma \approx 90$ amu obtained in our experiments for Ne + Cf, S + U and Ar + Th (see fig. 3) one may conclude that these systems undergo fast fission.

(ii) An other conclusion may be drawn from the mass distributions measured at different bombarding energies for the system Ar + Th. The figures 3 and 6 indicate that with decreasing incident energy the mass distributions become broader and the yield maximum at $M = (M_1 + M_2)/2$ vanishes. Instead of that appear relative maxima lying in the region of $M \approx 205$ and the complementary mass $M \approx 70$. The enhanced yield of fragments near the doubly magic nucleus ^{208}Pb can be interpreted as shell effects, which generate and/or stabilize components with closed nuclear

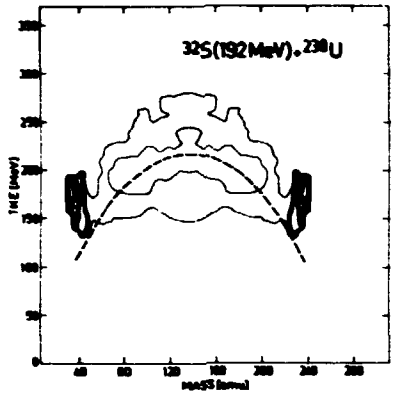

Fig. 5

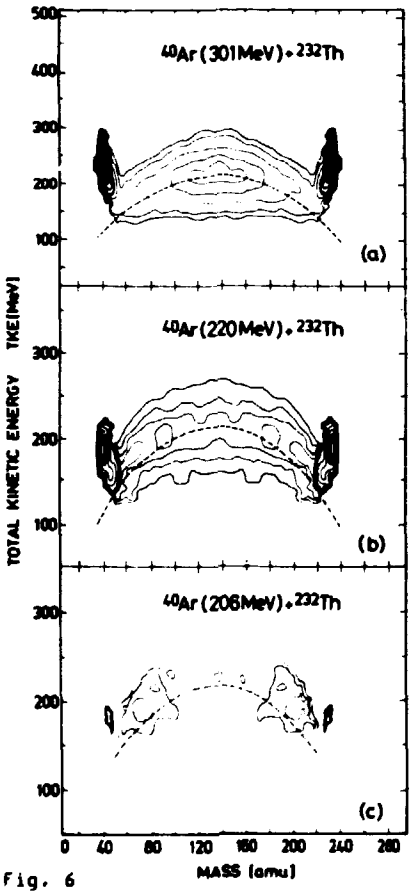

Fig. 6

shells during the diffusion phase of a heavy-ion reaction. Contributions of sequential fission should be negligible, since for low projectile energies only weakly excited fragments should appear [8]. The same interpretation may be valid for the system S + U, where a relative maximum of low intensity refers to an enhanced appearence of the doubly magic nucleus ^{208}Pb. A similar behaviour of the mass distributions has already been observed by investigating the reaction ^{40}Ar + ^{243}Am [9]. Including shell corrections in the ground state liquid drop energies of the interacting nuclei the authors found well pronounced minima in the driving potential corresponding to the nuclei ^{208}Pb and ^{132}Sn. For fast fission, the underlying assumption is that the systems are trapped by these minima on their way to mass symmetry. In this sence the presence of a minimum at a certain mass M leads to a maximum in the production cross section of this very mass.
For higher projectile energies leading to higher temperatures after the energy equlibration the minima will be washed out. Only the minimum for η = 0 remains in the driving potential preferring a symmetric mass distribution without additional maxima (see Ar + Th at E_1 = 301 MeV).
(iii) According to the diffusion model one expects that the collision system Fe + Pb undergoes fast fission leading to a mass drift towards symmetry. However, as can be seen from the figures 3 and 7 the yield of symmetric fragments is very low. Probably the system has no time for an evolution to mass symmetry during the contact phase and separates after a short rotationlike motion into two fragments, which are similar to the projectile and target nuclei. This behaviour may be connected with the fact that the system Fe + Pb exhibits an effective fissility $x_{eff} \gtrsim 0.8$ and needs an extra energy to overcome the saddle point after formation of a neck. When this formation is disturbed, a hindrance of the mass equilibration may be expected.
For the collision systems under investigation the yields of correlated fragments are displayed in the figures 4 - 7 as functions of the mass and the total kinetic energy. This twodimensional representation of the results is well suited to identify the peaks of elastically scattered particles as well as the region of fission fragments, which widely stretches out between these peaks. From fig. 6 the

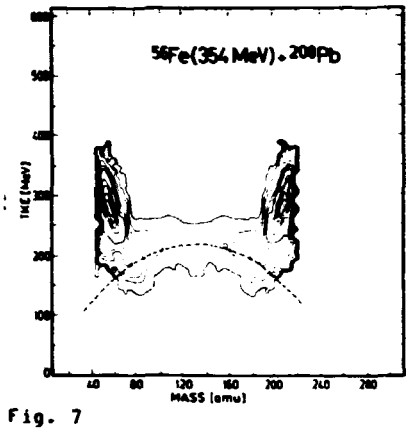

Fig. 7

mass drift to symmetry can easily be studied for the system ^{40}Ar (310 MeV) + ^{232}Th. Further, it can be deduced that the mean total kinetic energy of the observed fission products corresponds to the prediction of the Viola systematics for fragmentation of heavy nuclear systems [10]. Finally, it should be noticed that for the systems ^{22}Ne(174 MeV) + ^{249}Cf and ^{40}Ar(206 MeV) + ^{232}Th the peaks of elastic scattering could not be detected for kinematical reasons, since the data have been accumulated at ionisation chamber positions, where no elastically scattered particles are accepted (see table 1).

REFERENCES

1) H. Sodan, E. Will, S.M. Lukyanov, Yu.T. Oganessian, Yu.E. Penionzhkevich, G.G. Chubarian, P. Gippner, W. Seidel, K.D. Schilling: JINR Rapid Communications N4-84 (1984) p. 15
S.M. Lukyanov, Yu.Ts. Oganessian et al.: International Workshop on Gross Properties of Nuclei and Nuclear Excitations XIII, Hirschegg (Austria), 14.-19.1.1985, p. 123
P. Gippner, P. Manfraß et al.: Annual report ZfK-530 (1984) 115
P. Gippner, W. Seidel et al.: Meeting on experiments on heavy-ion beams, Varna (Bulgaria), 13.-19.9.1984, JINR D7 - 84 - 736, p. 75
2) G. Guarino, A. Gobbi et al.: Nucl. Phys. A424 (1984) 157
3) J. Töke, R. Bock et al.: Nucl. Phys. A440 (1985) 327
4) A. Gobbi, W. Nörenberg: Heavy ion collisions, Vol. 2, ed. by R. Bock, North Holland Publishing Company, 1980, p. 139
5) P. Gippner, K.D. Schilling et al.: ZfK-572 (1985)
6) K. Takahashi, H.v. Groote: Preprint Institut für Kernphysik, TH Darmstadt, IKDA 76/26
7) R. Schmidt, G. Wolschin: Z. Phys. A296 (1980) 215
R. Schmidt: Z. Phys. A320 (1985) 413
8) J. Töke, R. Bock et al.: Scientific report GSI 84-1, p. 11
9) R. Kalpakchieva, V.G. Kartavenko et al.: Nukleonika 24,4 (1979) 417
10) V.E. Viola, K. Kwiatkowski, M. Walker: Phys. Rev. C31,4 (1985) 1550

ALPHA-FRAGMENT CORRELATION MEASUREMENTS IN THE REACTION ^{12}C (85 MeV) + ^{232}Th

Nguyen Hoai Chau, W.Augustyniak, C.Borcea and M.Lewitowicz
Laboratory of Nuclear Reactions, Joint Institute for Nuclear Research, Dubna, USSR

The measurement of α-ff (fission fragment) correlations in heavy-ion reactions is an effective tool for obtaining information about the mechanism of the emission of high-energy nonequilibrium light particles. A measurement of the folding angle between fission fragments in coincidence with emitted light particles may also give information about the reaction time implied in the formation of these light particles[1]. From the study of the transferred linear momentum the authors ~~of work~~[2] draw some conclusions concerning the reaction mechanism. Correlation experiments also provide information about the residual nucleus and its fission properties[3,4].

~~In the present work,~~ some results of the study of α-ff correlation for the ^{12}C(85 MeV) + + ^{232}Th reaction are presented. In contrast to the earlier mentioned works, the present one studies the reaction near the Coulomb barrier ($E_{cm} - V_c = 15$ MeV), and this offers the possibility of obtaining information about the weakly excited systems formed after light particle emission.

The experiment has been performed at the U-200 cyclotron of the Laboratory of Nuclear Reactions, JINR. A ^{12}C beam, after being collimated, bombarded a self-supported 2 mg/cm^2 ^{232}Th target placed at 45° with respect to the beam. The emitted α-particles were detected in two ΔE-E semiconductor telescopes placed at 20° and 140°. The fission fragments were detected by two position-sensitive semiconductor detectors. A detailed description of the experimental set-up is given in [4], the difference being that in the present experiment the positive-sensitive detectors had dimensions of 3 x 50 mm^2 and that the telescopes were placed at different angles. The data aquisition system as well as off-line processing are described in [4,5]

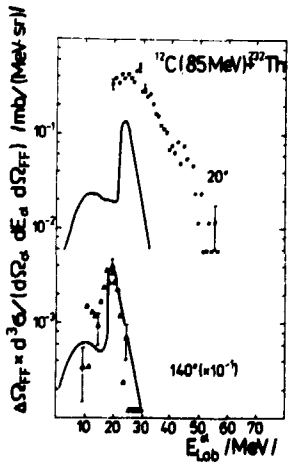

Fig.1. Energy spectra (in lab. system) of α particles measured in coincidence with fission fragments at angles of 20° and 140°. The points indicate experimental data, the lines show calculation using the program ELPHIC.

In fig.1 the energy spectra of α-particles emitted at angles of 20° and 140° are shown. The full curves present the Monte-Carlo calculation of evaporated - particles from the compound nucleus and fission fragments, performed using the ELPHIC program [6]. These curves were normalized in the maximum of the experimental spectra obtained at 140°. One can see that this calculation can not describe the observed forward - particle emission while the emission at 140° is reproduced rather well. The angular distribution of α-particles has also been measured. The large number of forward emitted α-particles and the shift toward high energy in the shape of the energy spectra of α-particles at small angles are signatures of formation of these particles at the early stage of the reaction. The similar shape of the α-particle energy spectra measured in and without coincidence with fission fragments (coincidence and inclusive spectra) indicate that they have the same nature i.e. they are both due to nonequilibrium process.

In Fig.2 there are shown distributions of the total transferred longitudinal momentum as a function of $(P^{\parallel}_{\alpha} + P^{\parallel}_{F1} + P^{\parallel}_{F2})/P_P$, measured in coincidence with α-particles at angles of 20° and 140°. Here $P^{\parallel}_{\alpha}$, $P^{\parallel}_{F1}$ and $P^{\parallel}_{F2}$ are projections on the beam axis of the linear momentum of an

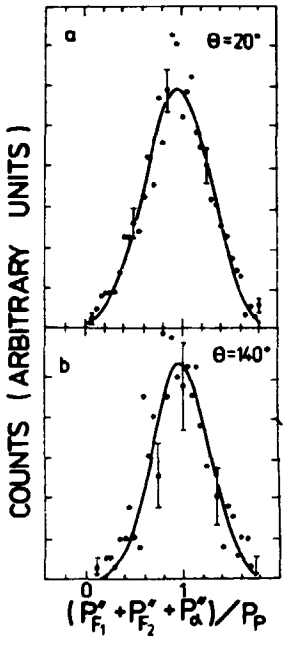

Fig.2. The distributions of the total transferred longitudinal momentum as functions of $(P''_{\alpha}+P''_{F1}+P''_{F2})$, measured in coincidence with α-particles. θ is the α-particle emission angle.

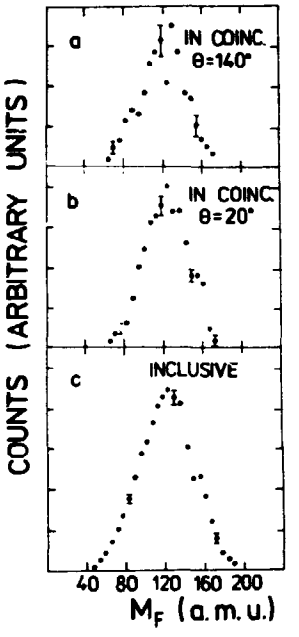

Fig.3. Mass distributions of fission fragments : (a) measured in coincidence with α particles emitted at 140°; (b) for the α emission angle of 20°; (c) without coincidence with α particles.

α-particle and two fission fragments respectively and P_P is the beam momentum. The points indicate experimental data and the curves are gaussian fits to the data. The mean values of $(P''_{F1}+P''_{F2})/P_P$ and $(P''_{\alpha}+P''_{F1}+P''_{F2})/P_P$ are 0.72 and 0.94 for the case (a) and 1.15 and 1.0 for the case (b). As to the obtained mean values one may say that if, as a result of a nonequilibrium process occurring inside the α-particles forward emitted from the compound system, another particle having a velocity close to that of the beam is emitted, then this can only be a neutron (for the proton the obtained energy is not enough to penetrate the barrier). One can observe that the measured distributions are broader than those calculated with the program ELPHIC. This discrepancy can be explained by the insufficient resolution in mass and angle determination and mainly by particle evaporation from the fission fragments (the contribution of all these factors is analysed in detail in [7]).

An important characteristic of the fission process is the fission fragment mass distribution. In the studied case, where almost all reaction products have been recorded it is possible to dstudy the dependence of the mass distribution on the excitation energy of the residual nuclei. In Fig.3 the mass distributions are shown for three cases:

(a) in coincidence with α-particles emitted at 140°;

(b) in coincidence with α-particles emitted at 20°;

(c) without coincidence with α-particles. For the case (b) in Fig.4 the mass distributions at three α-particle energy bins are shown. The width of the fragment mass distribution decreases with increasing α-particle energy (that is with decreasing excitation energy). For the most energetic α-particles (last bin) the excitation energy last for the residual fissioning nucleus is less than 30 MeV. One can see that despite this rather low excitation energy the fragment mass distribution does not show the expected two-humped structure. A possible explanation for this may be the fact that the residual fissioning nucleus has a sufficiently high angular momentum and correspondingly a deformation enough to wash out the shell effect.

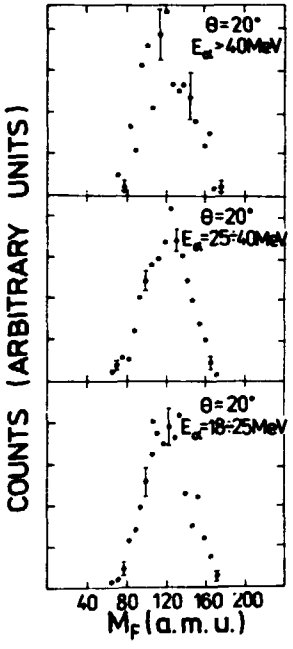

Fig.4. Fission fragment mass distributions measured with α-particles at an angle of 20°. E_{α} is the laboratory α particle energy.

Our main conclusions are as follows:

(1) The measurement of fission fragments in coincidence with light particles in heavy-ion reaction allows one to obtain interesting information about the fission process, in particular, one may study fission at very low excitation energies (a few MeV).

(2) At bombarding energies close to the Coulomb barrier in the studied reaction a substantial part of the emitted α-particles come from a nonequilibrium process.

(3) The process of α-particle formation and emission in the given reaction at an energy close to the Coulomb barrier is mainly a two-body one in which most of the α-particles are emitted in the forward direction and the remaining part of the projectile is absorbed by the target nucleus.

References

1. B.B.Back et al. Phys.Rev. C22 (1980) 1927.
2. T.Fukuda et al. Nucl.Phys., A429 (1984) 193
3. J.L.Laville et al. Phys.Letters B138 (1984) 35 and
   Phys.Letters B156 (1985) 42
4. M.Sowinski et al. Preprint JINR, P7-85-377, Dubna, 1985
5. Kupczak et al. JINR Communication, 10-84-87, Dubna, 1984
6. M.Lewitowicz JINR Communication, P11-84-280, Dubna 1984
7. G.Larana et al. Nucl.Phys. A407 (1983) 233

RECENT FISSION CROSS SECTION STANDARDS MEASUREMENTS

Oren A. Wasson
National Bureau of Standards, Gaithersburg, MD 20899, USA

Abstract

The $^{235}U(n,f)$ reaction is the standard by which most neutron induced fission cross sections are determined. Most of these cross sections are derived from relatively easy ratio measurements to ^{235}U. However, the more difficult $^{235}U(n,f)$ cross section measurements require the use of advanced neutron detectors for the determination of the incident neutron fluence. Examples of recent standard cross section measurements are discussed, various neturon detectors are described, and the status of the $^{235}U(n,f)$ cross section standard is assessed.

1. INTRODUCTION

The $^{235}U(n,f)$ reaction in the 0.1 to 20 MeV neutron energy interval has been accepted as the standard reaction to determine the neutron induced fission cross section of other nuclei. These cross sections are generally determined from the relatively simple measurement of the ratio of the fission yields from the nucleus to be measured to that from the ^{235}U reference deposit using multi-plated fission ionization chambers. The value of the determined cross section and its uncertainty thus are dependent upon the value and accuracy of the ^{235}U standard. Future improvements in the accuracy of the ^{235}U standard will thus produce improvements in the accuracy of many fission cross sections without the need for new measurements.

However, the more difficult determination of the standard cross section requires a measurement of the incident neutron fluence. This requires the use of state-of-the-art neutron detectors. These detectors include the proton recoil telescope, the hydrogen gas proportional counter, the thick plastic scintillator, thin plastic scintillators in various configurations, and ^{6}Li glass scintillators. The most accurate method is the time-correlated associated-particle technique which unfortunately is limited to a few neutron energies.

The requested uncertainty in the $^{235}U(n,f)$ standard cross section is 1% (one standard deviation) in the 0.1 to 20-MeV energy region. To date this level of accuracy has been achieved at only two energy regions; thermal and 14 MeV. The method of attack to solve this problem is to obtain accurate absolute cross sections at a few select neutron energies, use relative measurements to extend the energy region, and then normalize the relative measurements to the absolute measurements to determine the standard cross section throughout the full energy interval.

It is not the purpose of the present paper to give a complete listing of all measurements, since several excellent recent reviews exist. For example, an excellent review of the status of the measurements prior to 1984 was published by Carlson 1) and the IAEA sponsored an advisory group meeting on nuclear standard reference data in November 1984 at the Central Bureau for Nuclear Measurements (CBNM) in Geel Belgium. A complete description of the various measurements and references are included in these reports. In this paper we shall focus on several recent measurements as well as some earlier measurements which still strongly influence present evaluations of this important cross section standard.

2. $^{235}U(n,f)$ CROSS SECTION MEASUREMENTS

2.1 Thermal Energies. Although the thermal and low eV neutron energy region is not included in the standard energy region because of the large cross section changes due to the resonance

structure, this region is used for the normalization of relative measurements which extend into the standard energy region. (See, for example, Czirr and Sidhu 2), Wasson et al. 3), and Wagemans and Deruytter 4).) The most extensive measurements of the cross section in the thermal neutron energy region were published by Deruytter et al., in 1973 5). These measurements which extended over many years were performed at the neutron chopper at the BR2 reactor in Belgium. A large effort was performed to determine the properties of the ^{10}B and ^{235}U deposits used in the measurements. The absolute ^{10}B contents were determined from direct weighing in vacuum combined with careful chemical and isotopic analysis of many deposits. The relative ^{10}B contents of the standard boron deposits were checked by their neutron induced reaction rates in the geometry of the fission experiment.

The amount of uranium on the fissile deposits was determined by precise low geometry α-counting making use of uranium half-life values. The fission deposits were also checked by α- and fission fragment counting in the geometry of the experiment.

The fission cross section was determined in the energy range from 0.002 to 0.15 eV and the absolute value deduced at 2200 m/s was 587.6 ± 2.6 barn. The quality of this measurement is so good that no measurements have subsequently been reported. It is estimated that it would require a 5 to 10 man-year effort to reproduce the quality of this experiement. Thus, at this time it is a more efficient use of resources to concentrate on measurements at higher neutron energies where the cross section uncertainties are much larger.

2.2 The 7.8 to 11.0-eV Normalization Integral. Another useful energy region for the normalization of relative measurements is the 7.8 to 11.0-eV region. The most recent published results for this region are by Gwin et al. in 1984 6). This shape measurement extended from the thermal region to 30 keV using the 22-m flight path of the Oak Ridge Electron Linear Accelerator (ORELA). The fission events were recorded with multi-plate ionization chambers having ^{235}U deposit thicknesses of approximately 140 $\mu g/cm^2$ on 0.001-cm thick aluminum backings. The neutron fluence was measured with parallel-plate pulse ionization chambers filled with 75% argon and 25% BF_3 (enriched in ^{10}B). This chamber recorded the number of $^{10}B(n,\alpha)$ events. The shape measurements were normalized to the 2200 m/s $^{235}U(n,f)$ cross section of 587.6. The results of this Oak Ridge measurement are shown in Fig. 1 for the 0.5 to 14-eV energy region.

A comparison of the Gwin et al. measurements with other recent results for the fission cross section integral from 7.8 to 11.0 eV is shown in Table 1. These relative measurements, which are all normalized to a 2200-m/s value of 578.6 b., agree within 1%. This good agreement indicates that this normalization integral should soon be known with sufficient accuracy.

Table 1. Measured values of the secondary normalization integral I_1 (7.8 to 11.0 eV) for the $^{235}U(n,f)$ reaction based on a thermal cross section of 587.6 b.

Reference		I_1 (barn·eV)
Gwin 1984	(6)	248.0 ± 1.7
Czirr 1977	(2)	245.6 ± 1.7
Wagemans et al. 1979	(8)	246.2
Wagemans and Deruytter 1984	(7)	246.1

However, at higher neutron energies the ^{235}U cross sections measured with the $^{10}B(n,\alpha)$ fluence monitors differ from those measured with $^{6}Li(n,\alpha)$ monitors 7). Additional measurements in this energy region are in progress at CBNM in Geel and at the National Bureau of Standards (NBS) in the USA.

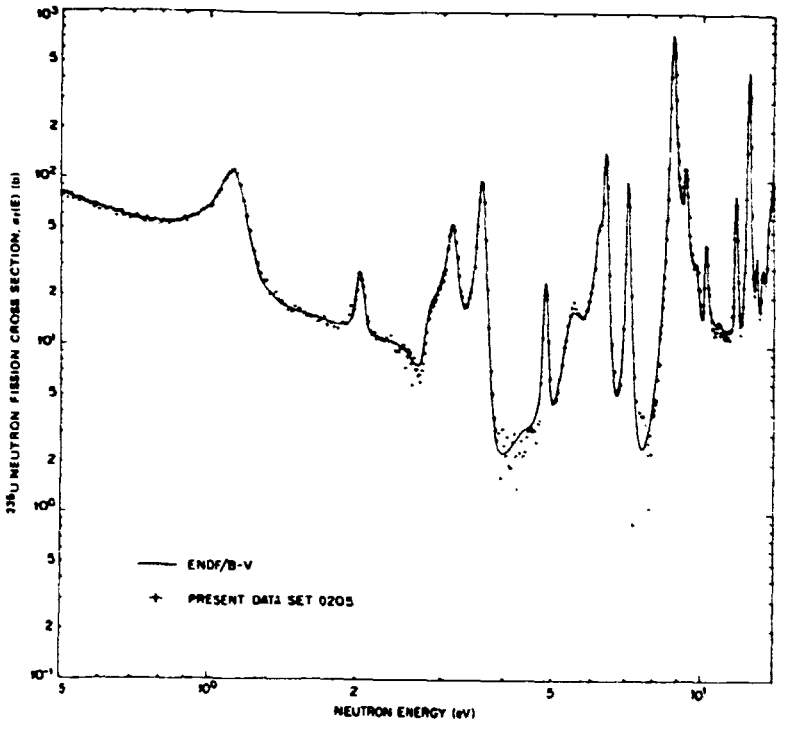

Fig. 1. $^{235}U(n,f)$ cross section in the 0.5 to 14-eV energy interval by Gwin et al. 6).

2.3 Absolute Measurements in the 0.3 to 6-MeV Range. Absolute measurements of the ^{235}U neutron fission cross section have been made at the NBS neutron time-of-flight facility. These are the first absolute measurements done with a linac neutron source. The neutron flux was measured at the 200-m end station with both a Black Neutron Detector 3) and the Dual Thin Scintillator (DTS) 9). The ^{235}U fission reaction rate was determined with a parallel plate fission ionization chamber located on the same beam line at 69 m from the neutron target. The Black Detector covered the 0.3 to 3.0-MeV region while the DTS detector was used in the 1 to 6-MeV region. The final data are shown in Figs. 2 and 3 for the Black Detector 10) and DTS detector 11), respectively. Extensive information on correlations and uncertainties is being used in the upcoming ENDF/B-VI evaluation of the neutron cross section standards. In the 0.3 to 1.2-MeV region the present measurements are generally in good agreement with two earlier NBS measurements using the linac and Van de Graaff facilities 3); however, the present data are systematically slightly lower than the previous measurements. All three NBS data sets are lower than the ENDF/B-V evaluation. The present Black Detector measurements are also lower than the evaluation in the higher end of the energy region (1-3 MeV).

Since the present measurement was intended primarily as a test of the DTS detector as a flux monitor, only moderate energy resolution (~10%) was planned. The statistical precision is 1.0% at 1.3 MeV and 2.1% at 6.0 MeV. In the region of overlap there is excellent agreement between the cross sections measured with the DTS and Black Detector (Fig. 3). While the overall agreement with ENDF/B-V is good the DTS data tend to be lower than the evaluation below 2.5 MeV and higher than the evaluation between 2.5 and 3.5 MeV.

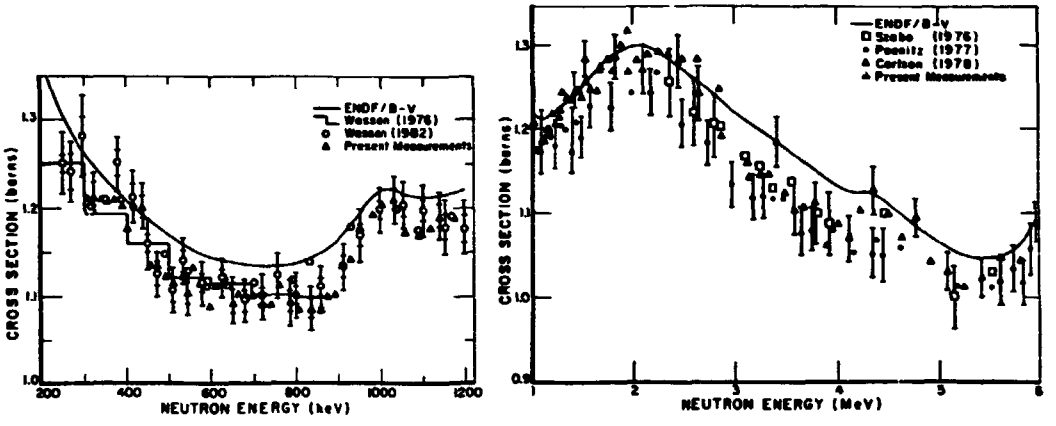

Fig. 2. Comparison of the present NBS Black Detector data with some of the previous absolute measurements for neutron energies from 0.3 to 2.1 MeV (left part of the figure) and for the higher neutron energies (right part of the figure). Also shown is the shape data of Carlson and Patrick normalized to the present measurements over the interval from 1.5 to 2.5 MeV.

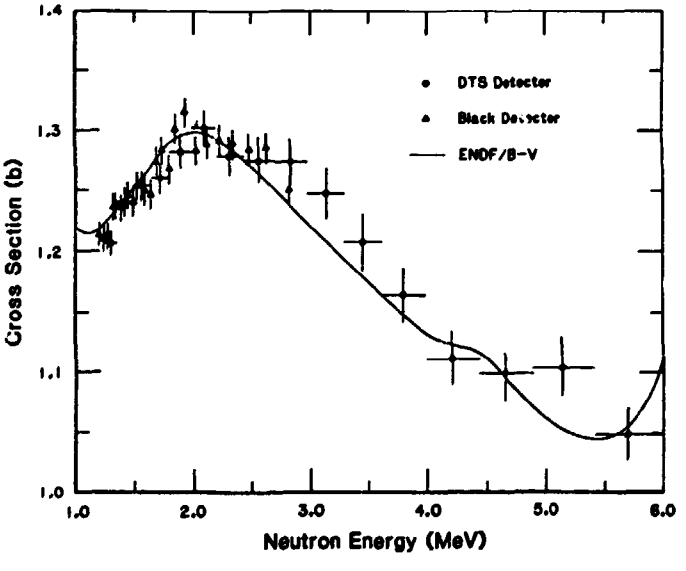

Fig. 3. The NBS $^{235}U(n,f)$ cross section in the 1 to 6 MeV range: circles, DTS detector as the flux monitor; solid line, ENDF/B-V evaluation. The vertical error bars represent statistical uncertainties only.

2.4. Measurement with the Time-Correlated Associated-Particle Technique (TCAP). The time-correlated associated-particle technique has demonstrated the best accuracy for neutron fluence measurements in the 14-MeV energy region. However, it is difficult to apply at other neutron energies. The application of this well-known technique in nuclear physics to the $^{235}U(n,f)$ cross section measurement at 14 MeV has been very successful 12)-15). The most difficult part of all neutron cross-section measurements is the measurement of the neutron flux incident on the sample. This method replaces the difficult neutron measurement with an easier alpha-particle measurement. Since the $^{3}H(d,\alpha)n$ is a two-body nuclear reaction with a Q value of 17.6 MeV, the kinematics of the reaction define the energy and angular relationship between the emitted 14-MeV neutron and a 3.6 MeV alpha particle.

A schematic diagram of the experimental method is shown in Fig. 4. At NBS a molecular ion beam D_2^+, with 500-keV energy is produced by the 3-MV Van de Graaff accelerator and is incident on a TiT target to provide the neutron source. The number of neutrons within the indicated cone, which are incident on the ^{235}U deposit, is determined by the number of associated alpha particles, Y_α. The fission events are detected in a parallel plate ionization chamber. The number of fission events produced by the incident neutrons is given by the number of time-coincident events between the alpha particle and fission events, $Y_{\alpha,f}$. The ^{235}U fission cross section is given by the simple relationship shown in the figure where n is the areal density of the ^{235}U deposit. The fission background produced by scattered neutrons, which is indicated by the dashed line in the figure, is eliminated by the coincidence requirement. This background is a major problem in most types of measurement which do not use the coincidence requirement.

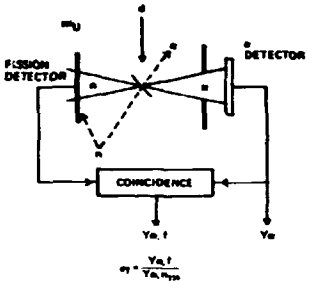

Fig. 4. Schematic diagram of the time-correlated associated-particle technique using the $^3H(d,\alpha)n$ reaction

The major source of background was produced by neutron interactions in the detector while a lesser background was produced by protons from the Ti(d,p) reaction in the target materials. Detailed measurements made at several detector angles with various absorbers demonstrated that there were no other significant background sources. The use of fresh targets eliminated the possible source of 3.5-MeV alpha particles from the $d(^3He,\alpha)p$ reaction on the tritium decay products. Also, protons from the $^2H(d,p)^3H$ reaction were not observed.

The application of this method to other neutron producing reactions is difficult because of the higher energy of the scattered incident beam. Only the group at the Technical University of Dresden 16) has been successful in measuring fission cross sections at 2.6 MeV using the $D(d,n)^3He$ reaction. They have also completed measurements near 4.4 and 8.2 MeV. The time-correlated associated-particle technique is thus an excellent neutron fluence measuring procedure for a few restricted neutron energies.

The measurements near 14 MeV using the TCAP method are shown in Fig. 5. These measurements, using four independent ^{235}U mass standards, are in excellent agreement (1%). This is the basis for the claim that the cross section at 14 MeV is known better than any other energy except thermal.

However, it has recently been suggested that some of these published measurements should be changed because of the effect of random events on the coincidence timing. Since the NBS conditions differed from those encountered in many other similar experiments, a detailed analysis of the NBS experiment and the electronic suppression of coincidence losses due to random events was performed. The unique combination of electronic components incorporated in the experiment eliminated the effect of losses due to random events in the timing analyzer. There is, thus, no correction to apply and no change in the published value of the NBS measurement 14) is warranted.

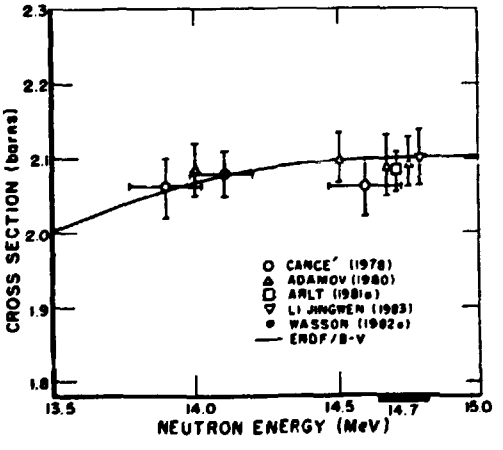

Fig. 5. Measurements of the $^{235}U(n,f)$ cross section near 14 MeV compared with the ENDF/B-V evaluation.

2.5 Absolute Measurement with ^{252}Cf Spontaneous Fission Neutrons. A series of experiments have been performed at NBS to measure the absolute fission cross sections of ^{235}U, ^{238}U, and ^{239}Pu for ^{252}Cf spontaneous fission neutrons 17). Results have also been obtained for the cross section ratios $^{238}U/^{235}U$ and $^{239}Pu/^{235}U$ which are independent of source strength. All of these experiments have been performed at the NBS ^{252}CF Irradiation Facility and employ the same mounting, fission chambers, ^{252}Cf source, and electronics. Computing procedures used to obtain the mean fission rate for each chamber were likewise the same. The ^{252}Cf source employed for the measurements has been calibrated repeatedly (5 times between 1979 and 1984) in the NBS Manganous Sulfate Bath Facility against the National Standard Ra-Be photoneutron source, NBS-I. The precision of the five measurements as determined by a least-squares fit to a 2.645-year half-life of ^{252}Cf is ± 0.5%. The presently assigned uncertainty of NBS-I is 0.85% leading to a total ^{252}Cf neutron source strength uncertainty of ± 1.1%. The cross sections are given in Table 2.

The importance of the $^{235}U(n,f)$ cross section averaged over the ^{252}Cf fission neutron spectrum lies in its insensitivity to the shape of the neutron spectrum. It is thus an important check on the ^{235}U fission cross section especially in the 100 keV to 5 MeV region which contains over 92% of the spectrum. The most recent measurements 17)-20) are listed in Table 3. The most recent NBS measurement of Schröder et al., 17) is a new measurement, which is independent of the earlier measurement of Heaton et al., 20). The mean of the four measurements is 1227 ± 12 mb which is in good agreement with the ENDF/B-V spectrum averaged value of 1231 mb. This requires that any changes in future evaluations from the ENDF/B-V values will be small in the energy region which contributes most to the ^{252}Cf spectrum average value.

Table 2 Absolute Fission Cross Section of ^{235}U, ^{238}U, and ^{239}Pu and the Fission Cross Section Ratios $^{238}U/^{235}U$ and $^{239}Pu/^{235}U$ Measured at NBS.

Nuclei	Cross Section
^{235}U	1234 ± 17 mb
^{238}U	332 ± 5 mb
^{239}Pu	1844 ± 24 mb
$^{238}U/^{235}U$	0.269 ± 1.2%
$^{239}Pu/^{235}U$	0.269 ± 1.2%

Table 3. Measurements of the ^{235}U fission cross section averaged over the ^{252}Cf fission neutron spectrum.

Reference	Cross Section, mb
Schröder et al., 17)	1234 ± 17
Davis and Knoll 18)	1215 ± 22
Adamov et al., 19)	1241 ± 18
Heaton et al., 20)	1216 ± 19
Mean	1227 ± 12

3. CROSS SECTION EVALUATION

3.1 Accuracy of Evaluated Data. In April 1983 the IAEA held a Consultants' Meeting on the ^{235}U Fast Fission Cross Section at Smolenice 21), Czechoslovakia. The conclusions and recommendations reached at that meeting are still appropriate since new evaluations have not been completed. The accuracy of the evaluated $^{235}U(n,f)$ cross section is shown in Table 4 for various neutron energies.

Table 4. Uncertainties in $^{235}U(n,f)$ cross section suggested by the IAEA Consultants' Meeting at Smolenice* in April 1983 (see IAEA(NDS)-146)

E_n (MeV)	$\frac{\Delta\sigma_{nf}}{\sigma_{nf}}$ (%)
0.1	2-3
1.0	2-3
3.0	2-3
5.0	3-4
8.0	3-4
13	4
14	1.0
15	2
20	6

*One participant felt that the cross section is known to 1-2% over much of the energy range below 13 MeV.

3.2 The U.S. Evaluated Nuclear Data File, ENDF/B-VI. This sixth evaluation effort of the neutron standards cross sections for the United States is being done by W. P. Poenitz (Argonne National Laboratory), G. M. Hale (Los Alamos National Laboratory), and R. W. Peelle (Oak Ridge National Laboratory), under the coordination of A. D. Carlson (NBS) 22). This effort with reduced manpower and funding is following a different process than that used for previous versions. The primary effort is concentrated on a simultaneous evaluation using generalized least squares, R-matrix evaluations and a procedure for combining the results of these evaluations. The simultaneous evaluation is important to this process since ratio measurements in addition to shape and absolute determinations are treated properly. Correlations within and among experimental data sets are also taken into account.

The R-matrix evaluations provide a method which allows charged-particle measurements involving the same compound nuclei (^7Li and ^{11}B) to be included in the evaluation process. These evaluations also provide a smooth meaningful expression for the energy dependence of the cross sections. Independent data bases are used in the simultaneous and R-matrix evaluations. The combining procedure is used to combine the information obtained from these analyses in a proper way to form the final evaluation and its variance-covariance matrix. The standards being evaluated are $^6Li(n,t)$, $^{10}B(n,\alpha_1)$, $^{10}B(n,\alpha)$, $^{197}Au(n,\gamma)$ and $^{235}U(n,f)$. Evaluations for the important reactions $^{238}U(n,\gamma)$, $^{238}U(n,f)$, and $^{239}Pu(n,f)$ are also being performed.

Preliminary results of the evaluation process with overlapping and non-overlapping data bases have been reported at recent nuclear data meetings 1). Efforts are now underway to further improve the grouping of the data bases for the simultaneous and R-matrix analyses. Also a new concept involving the thermal constants is being implemented. This will allow the relevant thermal constants to be evaluated simultaneously within the framework of the standards evaluation.

Efforts have been and continue to be made to handle the various parts of the evaluation process in a proper and defensible way. Significant progress has been made but the process is complicated and time consuming. It is anticipated that final combination results, i.e., adjusted R-matrix parameters for the lithium and boron cross sections and pointwise values for the $^{197}Au(n,\gamma)$ and $^{235}U(n,f)$ cross sections, will be available in 1986.

A detailed recent progress report was presented by Carlson at the International Conference on Nuclear Data for Basic and Applied Science at Santa Fe, New Mexico, USA in May 1985 22).

4. NEUTRON DETECTOR DEVELOPMENT

4.1 ^{3}He Gas Scintillator for Thermal to 3 MeV Neutrons. One of the most promising nuclear reactions for use as a neutron fluence detector in the energy region below 3 MeV is the ^{3}He(n,p)T reaction. This reaction has a positive Q value of 0.76 MeV. However, a useful detector with fast timing and adequate energy resolution to separate the (n,p) reaction from the ^{3}He recoils from neutron elastic scattering has not been developed. The use of this gas in the proportional counter mode has produced excellent energy resolution although the timing is too slow to permit use in MeV neutron time-of-flight measurements. A small high pressure gas scintillator with a resolution of 33% has been developed by Evans 23) for delayed neutron experiments.

Our group at NBS has pushed to establish the ^{3}He(n,p)T reaction as a useful neutron standard in the keV and MeV neutron energy regions. A prototype ^{3}He gas scintillator is shown in Fig. 6. The detector consists of a 2 atmosphere He-Xe gas mixture in a 11 cm diameter by 25 cm length cylindrical volume. The light is viewed through glass windows by two photomultiplier tubes positioned at opposite ends of the cylinder. A diphenylstilbene wavelength shifter was evaporated onto the inside of the windows to convert the ultraviolet light emitted by the scintillating gas into the visible region to which the photomultiplier tubes are sensitive. The response of the detector was measured with thermal neutron beams from the NBS reactor and higher energy neutrons from the linac facility. The light output increased a factor of two as the Xe gas fraction was increased from 5% to 32% in order to reduce the range of the product particles. The spectral resolution, which was nearly constant throughout the central 10 cm, was governed by the statistics of the number of summed photoelectrons from the two tubes (25 keV per photoelectron). The encouraging results obtained from these preliminary studies indicate the potential usefulness of this reaction as a neutron standard.

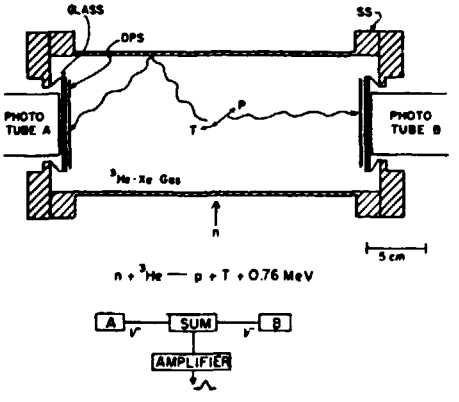

Fig. 6. ^{3}He-Xe gas scintillator.

4.2 Development of the Dual Thin Scintillator (DTS) in the Coincidence Configuration. The Dual Thin Scintillator (DTS) has been designed and built at the NBS for use as an absolute neutron flux monitor in the energy range of 1-20 MeV 9). The DTS detector consists of two thin, back-to-back plastic scintillators optically separated from each other and independently coupled to photomultiplier tubes as shown in Fig. 7. The efficiency of the detector is determined by the first scintillator while the function of the second scintillator is to measure the energy of the recoil protons which escape from the first scintillator. Because of the low multiple scattering and the spectrum discrimination, there is relatively little dependence of the detector efficiency on the carbon cross section and angular distributions. Therefore the detector efficiency is essentially dependent on the hydrogen cross section, on light tables, and on hydrogen areal density. These parameters are known well enough to determine the detector efficiency within an uncertainty of 1%.

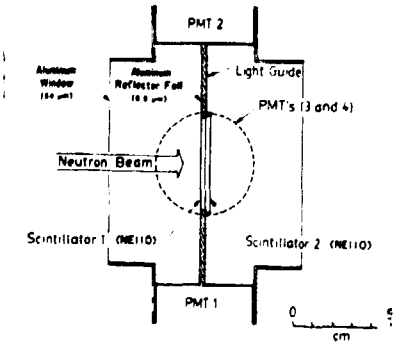

Fig. 7. Geometry of the dual-thin scintillator.

The proton recoil spectra and absolute detector efficiency were measured at 2.45 and 14.0 MeV neutron energy using the associated-particle technique with the NBS Positive-Ion Van de Graaff neutron source. The measured spectra for 14 MeV neutrons, as shown in Fig. 8, are in excellent agreement with those calculated using a Monte Carlo technique.

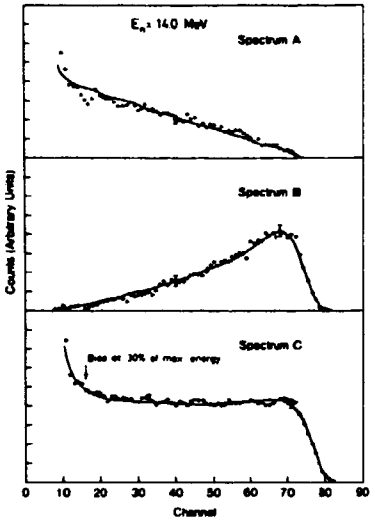

Fig. 8. Experimental proton recoil spectra obtained in an associated-particle experiment at 14 MeV. Spectrum A is from the first scintillator, Spectrum B is the sum coincidence of both scintillators. Spectrum C which is the sum of spectra A and B approximates the ideal thin scintillator response. The solid lines are Monte Carlo calculations.

The singles plus sum-coincidence mode of operation, shown in spectrum C, approximates the proton recoil energy spectrum. This mode was used for the $^{235}U(n,f)$ cross section measurement described earlier. However, it is observed that the more peaked response from the sum-coincidence mode, spectrum B, should provide an even better neutron flux monitor. Detailed calculations for this mode of operation are in progress at NBS.

ACKNOWLEDGMENTS

The author thanks his colleagues, A. D. Carlson, R. A. Schrack, R. G. Johnson, J. W. Behrens, K. C. Duvall, and M. S. Dias for their contributions to the NBS results reported in this paper.

REFERENCES

1) A. D. Carlson, Prog. Nucl. Ener. 13, 79-127 (1984); see also, Proc. Advisory Group Meeting on Nuclear Standard Reference Data (Geel) IAEA-TECDOC-335 (1984).
2) J. B. Czirr and G. S. Sidhu, Nucl. Sci. Eng. 58, 371 (1975); Nucl. Sci. Eng. 57, 18 (1975); and Nucl. Sci. Eng. 60, 383 (1976).
3) O. A. Wasson, M. M. Meier, and K. C. Duvall, Nucl. Sci. Eng. 81, 196-212 (1982).
4) C. Wagemans and A. Deruytter, Ann. Nucl. Eng. 3, 437 (1976).
5) A. J. Deruytter, J. Spaepen, and P. Pelfer, J. Nucl. Eng. 27, 546 (1973).
6) R. Gwin, R. R. Spencer, R. W. Ingle, J. H. Todd, and S. W. Scoles, Nucl. Sci. Eng. 88, 37 (1984).
7) C. Wagemans and A. Deruytter, Proc. Advisory Group Meeting on Nuclear Standard Reference Data (Geel) IAEA-TECDOC-335 (1984), p. 157.

8) C. Wagemans, G. Coddens, and A. J. Deruytter, Proc. Int. Conf. on Nuclear Cross Sections for Technology (Knoxville), NBS SP-594 (1979) p. 261.

9) M. S. Dias, R. G. Johnson, and O. A. Wasson, Nucl. Instrum. Methods 224, 532 (1984).

10) A. D. Carlson, J. W. Behrens, R. G. Johnson, and G. E. Cooper, Proc. Advisory Group Meetin on Nuclear Standard Reference Data (Geel) IAEA-TECDOC-335 (1984), p. 162.

11) M. S. Dias, A. D. Carlson, R. G. Johnson, and O. A. Wasson, Proc. Advisory Group Meeting on Nuclear Standard Reference Data (Geel) IAEA-TECDOC-335 (1984), p. 467.

12) R. Arlt, W. Meilung, G. Musiol, H. G. Ortlepp, R. Teichner, W. Wagner, I. D. Alkhazov, C. O. Kostochkin, S. S. Kovalenko. L. A. Petrzhak, and V. I. Shpakov, Kernenergie 24, 8 (1981).

13) M. Cancé and G. Grenier, Nucl. Sci. Eng. 68, 197 (1978).

14) O. A. Wasson, A. D. Carlson, and K. C. Duvall, Nucl. Sci. Eng. 80, 282 (1982).

15) Li Jingwen et al., Chinese Nucl. Phys. 5, 45 (1983).

16) R. Arlt, H. H. Heidrich, M. Josch, G. Musiol, H. G. Ortlepp, R. Teichner, and W. Wagner, Nucl. Instr. and Meth.

17) I. G. Schröder, Li Linpei, D. M. Gilliam, E. D. McGarry, and C. M. Eisenhauer, San Francisco Meeting of American Nuclear Society (to be published).

18) M. C. Davis and G. F. Knoll, Ann. Nucl. Eng. 5, 583 (1978).

19) V. M. Adamov, I. D. Alkhazov, S. E. Gusev, L. V. Drapchinsky, V. N. Dushin, A. V. Fomichev, S. S. Kovalenko, O. I. Kostochkin, L. Z. Malkin, K. A. Petrzhak, L. A. Pleskachevsky, V. I. Shpakov, R. Arlt, and G. Musiol, Proc. Int. Conf. on Nuclear Cross Sections for Technology, NBS Spec. Publ. 594 (1980) p. 995.

20) H. T. Heaton, D. M. Gilliam, V. Spiegel, C. Eisenhauer, and J. A. Grundl, ANL-76-90 (1976) p. 333; also J. A. Grundl and D. M. Gilliam, Trans. Am. Nucl. Soc. 44, 533 (1983).

21) IAEA Consultants' Meeting on the ^{235}U Fast-Neutron Fission Cross Section, and the ^{252}Cf Fission Neutron Spectrum, Smolenice, Czechoslovakia, INDC(NDS)-146 (1983).

22) A. D. Carlson, W. P. Poenitz, G. M. Hale, and R. W. Peelle, Radiation Effects (to be published).

23) A. E. Evans, Jr., Los Alamos National Laboratory Report LA-Q2TN-82-109 (1982).

ABSOLUTE MEASUREMENTS OF THE ^{235}U INDUCED FISSION CROSS SECTION AT THE NEUTRON ENERGY OF 1,88 MEV

I.D. Alkhazov, V.D. Dmitriev, V.A. Kalinin, S.S. Kovalenko, V.I. Kutuzov, V.N. Kuzmin, Yu.A. Nemilov, B.P. Petrov, L.M. Solin, V.I. Shpakov

V.G. Khlopin Radium Institute, Leningrad, USSR

The ^{235}U neutron induced fission cross section is one of the most important neutron standard, responcible for an accuracy and reliability of numerous nuclear data. However, according to the conclusions of the IAEA Consultant's Meeting, Smolenice, CSSR, 1983 /1/, the experimental data aviailable can not provide the required accuracy of the cross-section evaluation (~1 %) in the neutron energy interval of 100 KeV - 20 MeV. At the moment the most discrepant region is in neutron energy region from 1 MeV to 6 MeV (Fig. 1). As it can be seen the results obtained by different authors differ by a value exceeding 10 % and most of them are united into two groups one having higher values of the cross sections and a prominent shape and the other having lower values of the cross sections and a concave shape. Both groups essentially differ from the adopted evaluation ENDF/B-V.

Absolute cross-section measurements using the TCAPT were performed in collaboration of the Technical University of Dresden, GDR and the Khlopin Radium Institute, USSR at the 2,6 and 4,5 MeV neutron energy spot points. The results of these measurements are lower than the ENDF/B-V evaluation and well agree with the lower group and in particulary with the results obtained by Poenitz /8/ but are in discrepancy with the recent result obtained in the National Bureau of Standards, USA /3/. Therefore some more measurement has been performed using the TCAPT at the new neutron energy spot point of 1,88 MeV that is near the maximum of the fission neutron energy spectrum.

The measurement was carried out in the Khlopin Radium Institute using an experimental set up with the magnetic analysis in the associated particle channel. Both the set up and characteristics of the associated particle channel are described in detail in the other paper presented in this symposium.

Fission events were registrated by means of current pulse ionization chamber comprising 3 foils of the ^{235}U nuclide. The main features of both experimental set up and experimental conditions are presented in the table 1. The table 2 gives both the corrections introduced in the cross-section value and corresponding components of the result uncertainty. The correction for the background in the associated particle count was not introduced as the background value was lower than 0,1 %.

Fig. 2 shows the neutron cone profile in the plane of the $D(d,n)^3He$ reaction, and Fig. 3 shows that in the perpendicular plane.

The fission cross-section value is finally amounts 1,26 ± 0,03 barns.

Fig. 4 presents a comparison of the present work result with those obtained by other authors as well as with the ENDF/B-V evaluation value. It can be seen that the maximal discrepancy of the data at this point reaches the value of 8 % and the majority of data are grouped in the interval of 1,26 - 1,27 barns that is lower than the evaluation. The cross-section value obtained in the present work is in agreement with this group and particulary with the results of measurements of Dias /13/ and is higher than the value obtained by Poenitz /8/.

Table 1. The main features of the experimental conditions

Neutron energy	(1.88 ± 0.03) MeV
Deuteron beam energy	2.8 MeV
Neutron producing target	(0.9 ± 0.1) mg/cm^2 thick foil of (CD)n
Deuteron beam diameter at the target	2.1 mm
Angle of the ^{3}He flight out with respect to beam axis	(14.1 ± 0.4)^o
Flat angle of the ^{3}He registration	4°
^{3}He-particle counting rate	(1.5 - 1.7)$\cdot 10^3$ 1/sec
Associated particle SB detector	45 m depth of depleted zone (25 x 45)mm^2 large
Magnetic field	$5\cdot 10^3$ gs
^{3}He-particle trajectory radii	43 - 50 cm
Neutron emission angle with respect to beam axis	(141 ± 1)^o
Fission chamber	3 foils of ^{235}U, methane
Total areal density of the ^{235}U	(1297 ± 13) g/cm^2
Neutron cone	with at the level of 0.1 % of intensity 18° FWHM 6.5^o
Angular size of the most distant target	18°

Table 2. Corrections and uncertainty components of the ^{235}U fission cross-section measurements

Effect	Correction %	Uncertainty
Coincident statistics		± 1.95
Random coincidences	- 1.8	± 0.26
Extrapolation of the fragment pulse height spectrum to zero	+ 4	± 0.5
Fragment absorption in the target layers	+ 2.2	± 0.85
Neutron cone attenuation	+ 0.3	± 0.4
Target layer non-homogenity		± 0.7
Total uncertainty		± 2.5

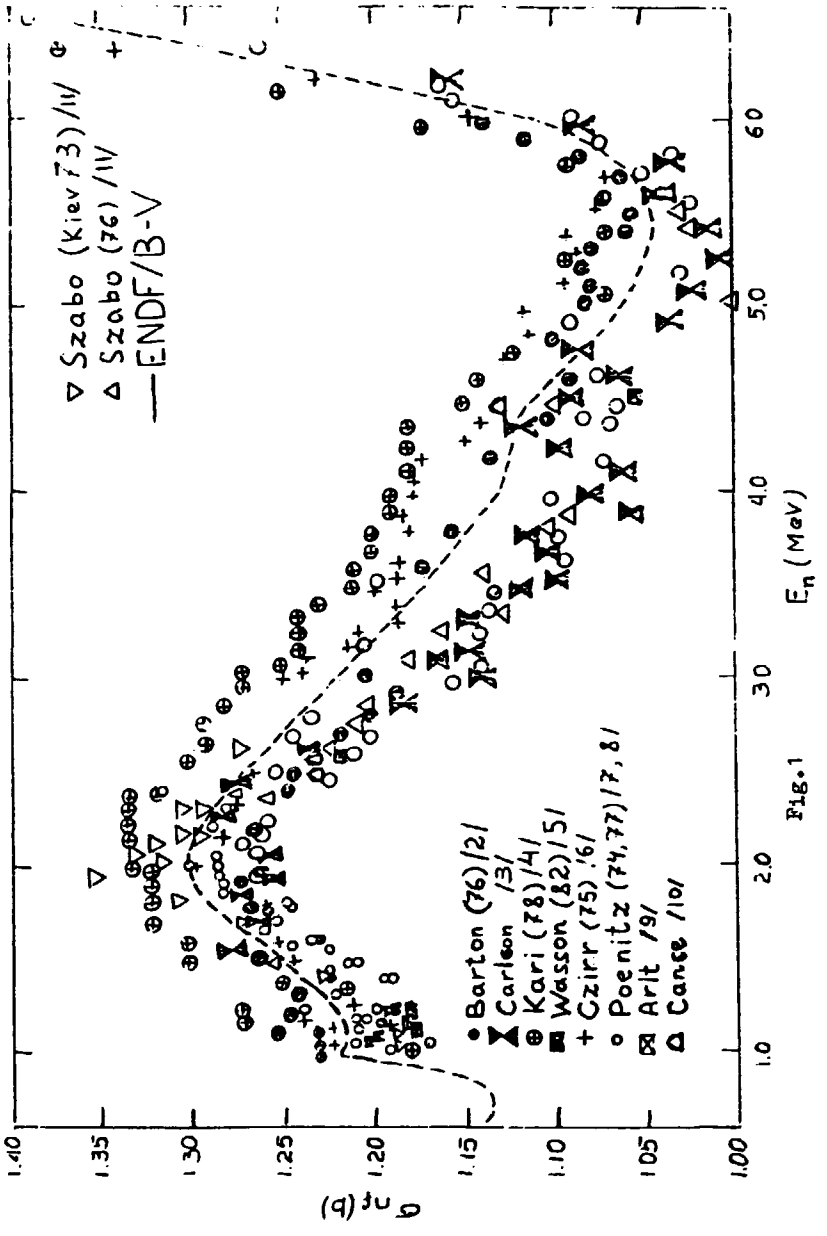

Fig.1

Fig. 1: Experimental data on the ^{235}U neutron induced fission cross sections in the neutron energy interval from 1 to 6 MeV.

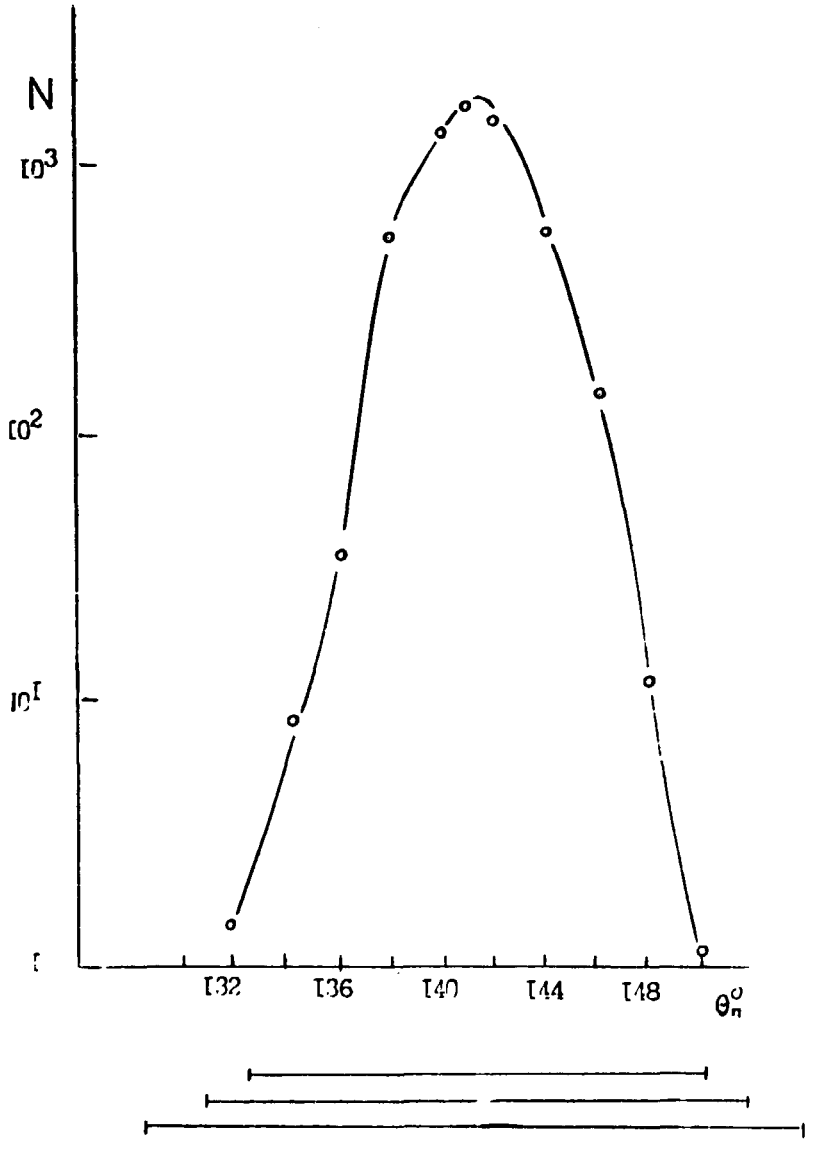

Fig. 2: Neutron cone profile in the plane of the reaction. (angular sizes of the targets are shown)

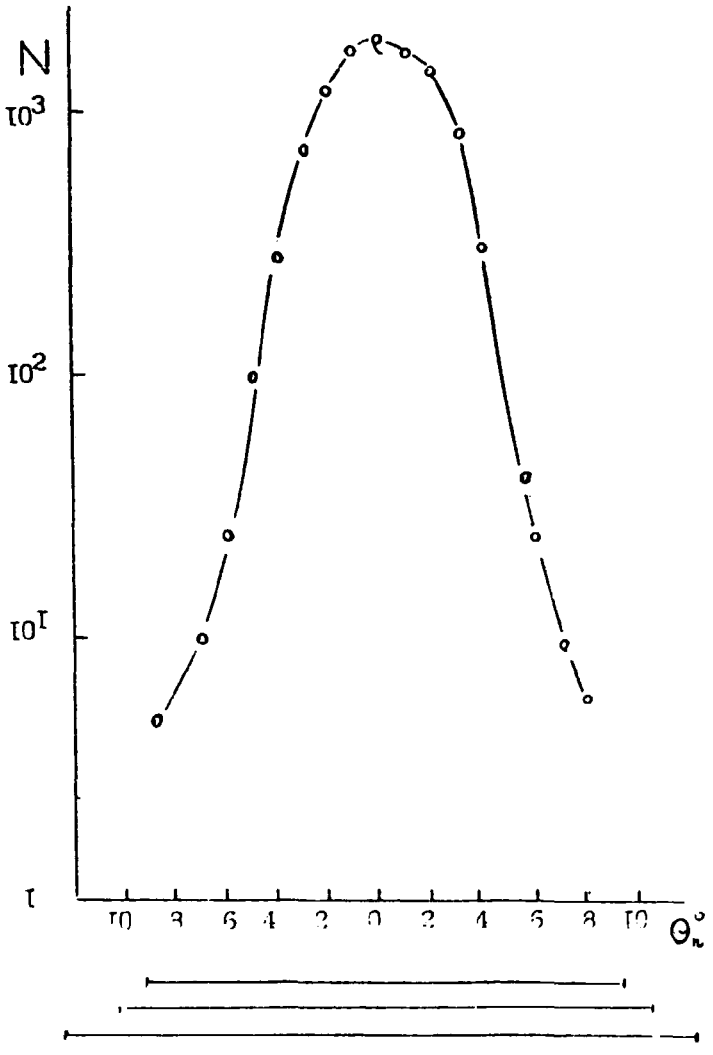

Fig. 3: Neutron cone profile in the vertical plane.
(angular sizes of the targets are shown)

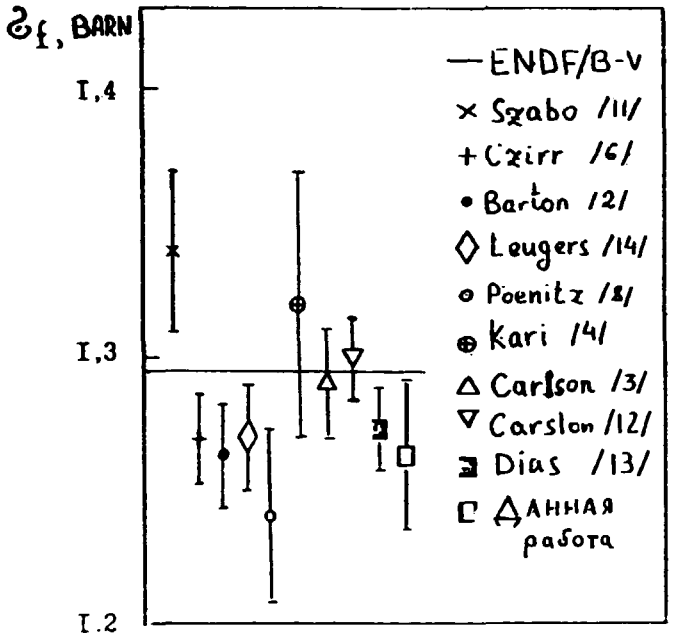

Fig. 4: Comparison of the results obtained in the present work with the data of other authors.

References

/ 1/ IAEA Consultant's Meeting on the U-235 Fast Neutron Cross-Section, Conclusions and Recomendations, Smolenice, CSSR, 1983, INDC (NDS)-146

/ 2/ Barton, D.M., Diven B.C., Hansen G.E. et al., Nucl. Sci. and Eng. 60, 369

/ 3/ Carlson A.D., Patrick B.H., Proc. of an Internat. Conf. on Neutron Physics and Nuclear Data for Reactors and Other Applied Purposes (1978), Harwell, p. 880

/ 4/ Kari K., Karlsruhe report (1978) KFK-2673

/ 5/ Wasson O.A., Meier M.M., Duvall K.C., Nucl. Sci. and Eng. 81, 196 (1982)

/ 6/ Czirr J.B., Sidhu G.S., Nucl. Sci. and Eng. 58, 371 (1975)

/ 7/ Poenitz W.P., Nucl. Sci. and Eng. 53, 370 (1974)

/ 8/ Poenitz W.P., Nucl. Sci. and Eng. 64, 894 (1977)

/ 9/ Arlt R., Josch M., Musiol G. et al., ZfK-459 (1981), p. 35

/10/ Canse M., Gimat D., Grenier G., Darisot D., CEA-N-2134 (INDC(FR)-38/L), 1980, p. 54

/11/ Szabo I., Marquette J.P., Proc. of the NEANDC/NEACRP Spec. Meeting on Fast Neutron Fission Cross Section, Argonne Nat. Lab. (1976), ANL-76-90, p. 208

/12/ Carlson A.D., Behrens J.W. Proc. of the 1982 Antwerp. Conf. on Nucl. Data for Science and Technology (1983), p. 456

/13/ Dias M.D., Johnson R.G., Wasson O.A., Proc. of the 1982 Antwerp. Conf. on Nucl. Data for Science and Technology (1983), p. 875

/14/ Leugers B., Cierjacks S., Brotz P. et al., Proc. of the NEANDC/NEACRP Spec. Meeting of Fast Neutron Fiss. Cross Section, Argonne Nat. Lab., ANL-76-90, p. 246

APPLICATION OF MAGNET ANALYSIS IN THE TIME CORRELATION ASSOCIATED PARTICLE METHOD

V.A. Kalinin, S.S. Kovalenko, V.N. Kuzmin, Yu.A. Nemilov, L.M. Solin, V.I. Shpakov, A.V. Fomichev,
V.G. Khlopin Radium Institute, Leningrad, USSR

The time correlated associated particle method (TCAPM) as applied for absolute measurements of neutron induced fission cross sections is well asknowledged at the moment and is regarded as an accurate and reliable one. The basic idea of the TCAPM is as follows. Either $^2D(d, n)^3He$ or $T(d,n)^4He$ reaction is used as a source of neutrons. The ^3He or ^4He particles associated with neutrons are detected by a detector within the cone fixed by the detector entrance apperture. The neutron cone corresponding to the associated particle cone irradiated a target of fissile nuclei. The fission events are registered in coincidence with ^3He associated particles. Provided the two main constrains are met:

i) the fission target is large enough to make the base of the neutron cone to lie completely inside the target,
ii) the fission target nonuniformity is negligible, the induced fission cross section is determined by the expression:

$$\sigma = \frac{N_c}{N_{ap} \cdot n}, \quad \text{where}$$

N_c is the number of coincidences registrated,
N_{ap} is the number of associated particles and
n is the number of fission nuclei per cm^2.

The TCAPM has the following advantages

i) determination of either neutron flux or total associated particle counts are not necessary
ii) fission events induced by background neutrons (scattered neutrons or neutrons from other reactions) are excluded
iii) there is no need to take the neutron flux anisotropy
iv) no geometical factors are to be taken into account in the first approach.

Exellent agreement (Within the limits of 1 %) of the results of five independent absolute fission cross-section measurements employing TCAPM at the neutron energy of 14-15 MeV /1-5/ is an example of the precision of this method. The IAEA Consultant's Meeting on the ^{235}U fission cross section (Smolenice, CSSR, 1983) has recommended to perform monoenergetic measurements using the TCAPM at as many energies as possible as the best way of improving the accuracy of the fission cross-section data /6/.

A practical realisation of the method in a wide interval of neutron energy is often connected with conciderable difficulties due to a high background of charged particles other than associated ones in the associated particle (AP)-channel. They are both scattered deutrons and charged particles produced in (d, p), (d,α), (n, p), (n, α) accompanying reactions. Specific AP-channels are to be designed for measurements at every neutron energy point.

Up to now two modifications of the TCAPM were developed.

i) <u>For measurements at neutron energies of 2.6 MeV and 14.5 MeV /1-5/.</u>

The $D(d, n)^3He$ and $T(d, n)^4He$-reactions and low energy deutron beams ($E_d \sim 150$ keV) were used to produce neutrons. As both reactions are exothermic and have rather high Q values ^3He and ^4He-particle energies exceed those of scattered deutrons. The latter therefore could be cut by means of thin aluminium foils of carefully chosen thickness.

ii) <u>For measurements at neutron energy of 8.5 /9/.</u>

The $D(d,n)^3He$-reaction and deutron beam with the energy of 9,5 MeV were used in this case and ^3He-particles were separated by means of a ΔE-E telescope consisting of two thin completely depleted silicon detectors.

This work describes an application of the TCAPM for neutron energy in the vicinity of the neutron spectrum maximum that is energy interval of 1.7-2.5 MeV. As it will be seen below in this case the experimental conditions force to apply a magnetic analysis in the AP-channel /10/. To produce neutrons the D(d, n)^{3}He-reaction and deutron beam with energy of 3 MeV were used. According to the reaction kinematics neutrons with the energy required were flying backward at the angle of about 130° with respect to the deutron beam (Fig. 1). Thin foils of deuterated polyethylene were used as neutron targets.

Fig. 2 shows the neutron energy spread as a function of the neutron emission angles with respect to the beam axis. It can be seen that both large angles of the neutron emission and low energy of the deutron beam are preferable for reducing the neutron energy spread. However, the beam energy decrease results in an increase of the number of scattered deutrons, in decrease of the ^{3}He-particle energy and, by the same way, makes worse the AP detection conditions. The advantage of utilization of large angles of the neutron emission is decrease of the cone of emission for the ^{3}He-particles relative to that for the neutrons. Correlation between both cones as a function of the neutron emission angle for different deutron energies is presented in Fig. 3. As it will be seen further, this advantage permits to facilitate the ^{3}He-particle registration in case of magnetic analysis. The choice of large angles of the neutron emission thus is necessary to obtain the neutron energy required and provides some advantages in experimental conditions.

However, the utilization of the large angles of the neutron emission corresponds to the AP-registration at the angles near the beam axis. In this case the background of scattered deutrons is very high due to a fast increase of coulomb scattering cross section. Therefore there is no possibility to use neither any telescope systems nor any shielding foils for absorption of background deuterons (as their ranges are lower than that of ^{3}He-particles).

To avoid this difficulty a separation of the particle trajectories in an uniform magnet field was applied. The field was produced by a sector magnet and had a value of $5 \cdot 10^3$ gauns. Fig. 4 shows a shematic drawing of the particle trajectories together with the border of the uniform field in its middle plane.

By this way the background connected with the D(d, p)T accompanied reaction products was completely eliminated beacause their radii are 2 times greater than those of the ^{3}He-particles. But as to scattered deutrons their radii are only 1.5 times greater and besides their energy spectrum has a low energy arising due to passing through the target foil. Magnetic analysis is not able therefore to eliminate scattered deutrons but enables never the less to reduce the corresponding background component by a factor of more than 10^2. Additional background components arise when deuterated polyethylene is used as a neutron target. They are protons produced by hydrogen in polyethylene and those from the ^{12}C(d,p) ^{13}C-reaction. Both groups can have radii roughly the same as those of ^{3}He-particles and can be registered due to a finite dimension ot the AP-detector. Thus the magnetic seperation itself can not reject completely the background and it is necessary additionaly to use a SB-detector with deepleted zone depth less than the proton ranges.

When magnetic separation is used a problem arises to provide sufficent AP-counting rate caused by a large size of the neutron one at the exit of magnetic field. This large size is due the following two factors:

- long flight path of AP through magnet
- energy and angular spread of the AP

because of traversing of the target foil which results in a corresponding spread in particle trajectories.

In the horizontal plane the former factors were compensated in the experimental conditions due the mentioned above kinematic narrowing of the AP-cone with respect to the neutron one. To diminish the neutron cone in vertical plane an additional focusing was introduced effected by the fringing magnetic field at the edge of the magnet, which focu-

sed all particles coming in direction not perpendicular the field border. The magnitude of this focusing is determinated by the expression $f = \frac{\rho}{tg\,\alpha}$, where f is focusing distance, α is the angle of AP direction with respect to normal, ρ is the AP-radius in uniform magnetic field. The focusing parameters used in the experimental setup provided the AP-ions size to be not exceeding the magnet gap width. As to the second factor an appropriate choice of the foil optimal thickness was made to increase the counting rate.
By this way a 45 mm - long and 25 mm - wide detector was large enough to provide the neutron flux of (2-3) $\cdot 10^3$ neutrons per second across fission target.
When a detector of such a large area was used, its large capacitance (which was about 10 nF) put special requirements on amplifying circuits.
As a fast current pulse amplifier was used to provide high time resolution current pulses must be integrated by input resistance and by the detector capacitance which results in both a decreese of pulse height and an increase of noise level. In the experimental set up a satisfactory signal to noise ratio was reached by employing an amplifier with four parallee input circuits.
The resulting pulse height spectrum obtained in the AP-channels is presented in Fig. 5. As can be seen, the background in the helion amplitude window was much less than 0.1 %, that was negligible. It proves an efficiency of magnetic separation in the TCAPM.

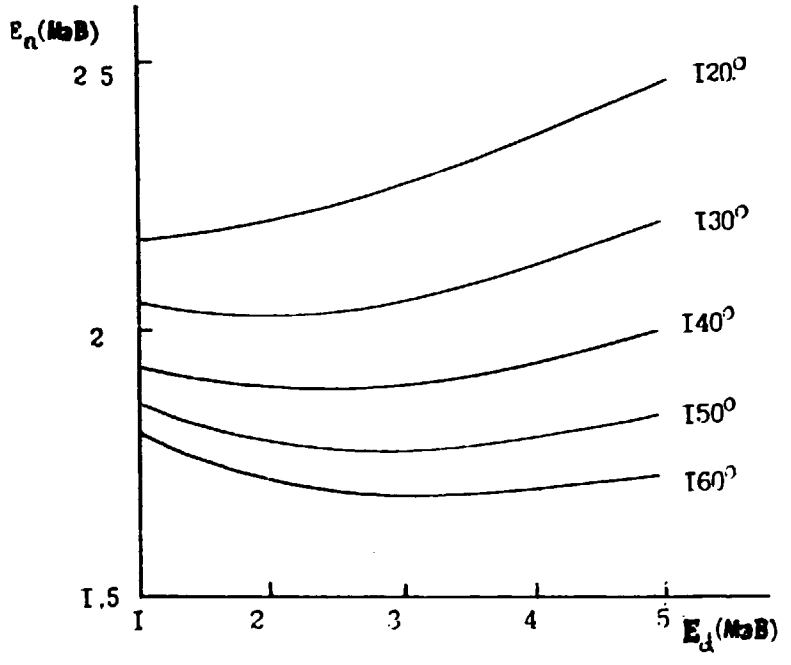

Fig. 1: Energy of neutrons E_n produced in the $D(d,n)^3He$-reaction as a function of the deuteron energy E_d for different angles of neutron emission with respect to the deuteron beam axis.

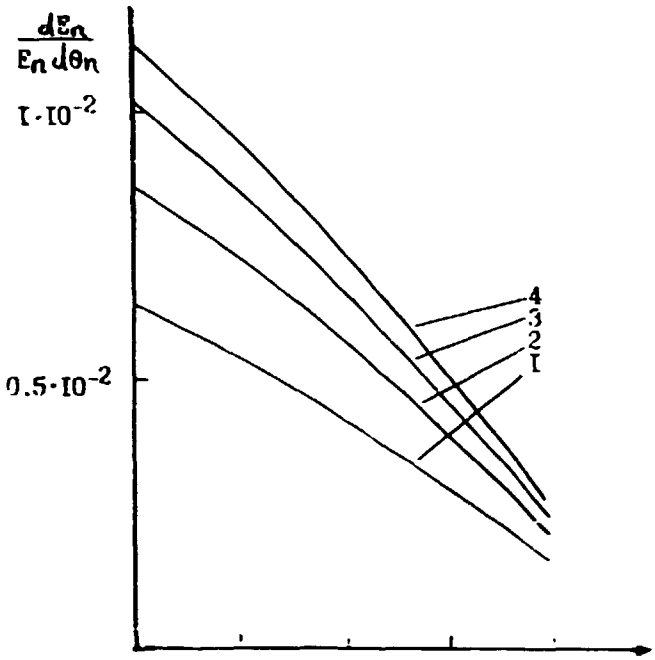

Fig. 2: Dependence of the energy spread of neutrons from the $D(d,n)^3He$-reaction on the angle of neutron emission. The figures show deuteron energies in MeV.

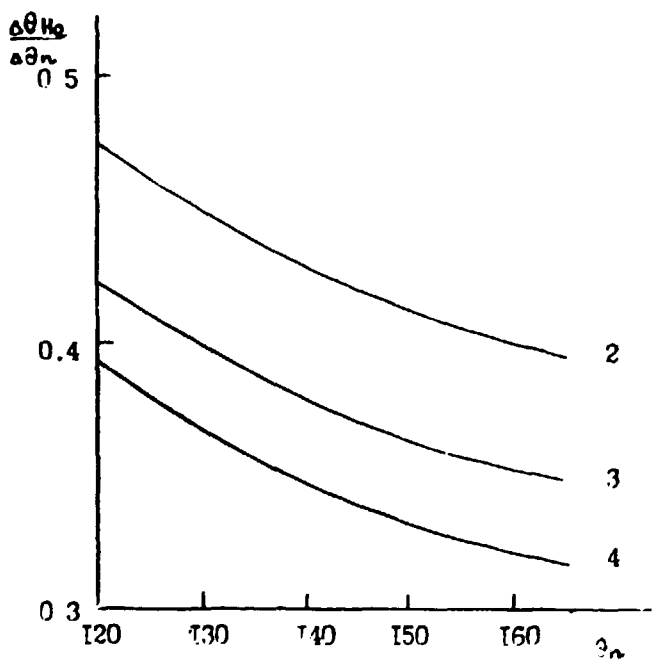

Fig. 3: Ratio of relative angular variations of helions and neutrons in the plane of the $D(d,n)^3He$-reaction as a function of the angle of neutron emission.

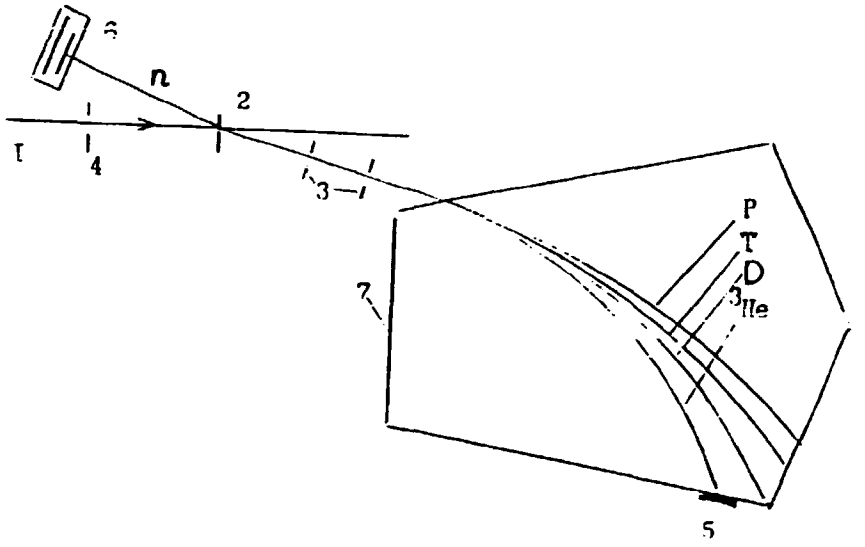

Fig. 4: Schematic drawing of the TCAPM using the magnetic analysis in the AP-channel.
1 - Deuteron beam, 2 - neutron producing foil of deuterated polyethylene, 3 - AP-collimators, 4 - beam collimators, 5 - AP-detector, 6 - fission chamber, 7 - border of the uniform magnetic field.

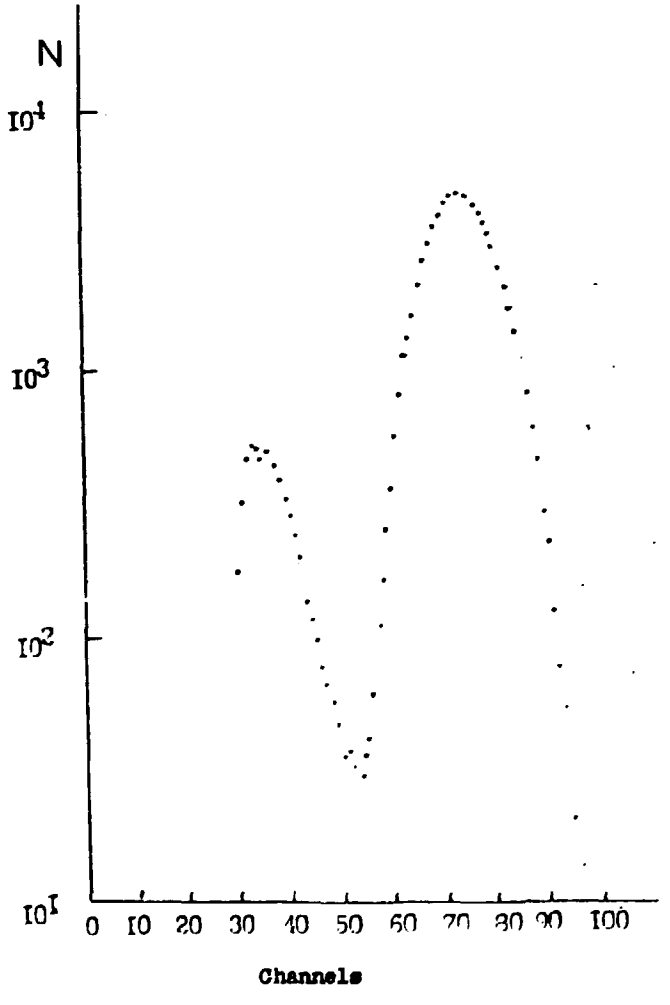

Fig. 5:
Pulse height spectrum in the AP-channel.
(the vertical line shows the discrimination threshold)

References

/ 1/ Arlt, R., Grimm, W., Josch, M. et al., Nucl. Cross. Sect. for Technology; Knoxwille, USA, 1979 (NBS Spec. Publ. 594, Washington, USA, 1980) p. 990

/ 2/ Wasson, O.A., Meier, M.M., Duvall, K.C., Nucl. Sci. and Eng., 80, 882 (1982)

/ 3/ Li Jiugwen, Li Anli, Rong Chaofan et al., Proc. of Int. Conf. on Nucl. Data for Sciens and Technology, Antwerpen, Belgium (1982)

/ 4/ Adamov V.M., Alkhazov I.D., Gusev S.E. et al., - Nucl. Cross Sect. for Technology, Knoxwille, USA, 1979 (NBS Spec. Publ. 594, Washington, USA, 1980) p. 995

/ 5/ Cause M., Grenier G. - Nucl. Sci. and Eng., 68, 197 (1978)

/ 6/ IAEA Consultant s Meeting on the U-235 Fast-Neutron Fission Cross-Section, Smolenice, CSSR, 1983, INDC(NDS) - 146, p. 20

/ 7/ Alkhazov I.D., Vitenko V.A., Dushin V.N. et al., Proc of the X-th Interu. Symp. on Selected Topics of Interact. of Fast Neutron with Nuclei, Gaussig, GDR, 1981 (ZfK-459, 1981) p. 40

/ 8/ Arlt R., Wagner W., Josch M. et al., ZfK-459, (1981), p. 44

/ 9/ Arlt, R., Josch M., Musiol G. et al., ZfK-459, (1981), p.35

/10/ Кузьмин В.Н., Калинин В.А., Солин Л.М., Шпаков В.И., Немилов Ю.А. - Ядерная спектроскопия и структура атомного ядра, тезисы докладов XXXV совещания, Ленинград, Наука, 1985, с. 375.

ABSOLUTE FISSION CROSS-SECTION MEASUREMENT OF PU-239 at 4.8, 8.65 AND 18.8 MEV AND OF U-235 AT 4.45 AND 18.8 MEV NEUTRON ENERGY

C.M. Herbach, K. Merla, G. Musiol, H G. Ortlepp [x)], G. Pausch
Technical University of Dresden, Dresden 8027, GDR; x) since 1984 CINR Rossendorf, GDR

I.L. Alkhazov, L.V. Drapchinsky, E.A. Gansa, S.S. Kovalenko,
O.I. Kostochkin, S.M. Solovjev, V.I. Shpakov
Khlopin Radium Institute, Leningrad 197022, USSR

Abstract: The results of new fast neutron fission cross-section measurements carried out in the 1983-85 years on Pu-239 and U-235 are presented. Using the 5 MV tandem accelerator of the CINR Rossendorf, the Time-Correlated Associated Particle Method (TCAPM) [1,2] was applicated to open new energy spot points for absolute measurements. Corrections, errors and the main experimental features are summarized. Special problems of the 18.8 MeV measurements are discussed.

1. Introduction

The presented work represents a continuation of the joint fission cross-section measurements program of the Khlopin Radium Institute Leningrad and the Technical University of Dresden [3)].

Besides the measurements of the standard fission cross-section on U-235, measurements on Pu-239 were performed because of the great importance of the Pu-239 data for the predetermination of the fast breeding reactor parameters. In addition to cross-section measurements relative to the U-235 standard, precise absolute measurements seem to be ingeniosly for improving the data accuracy from the reached value (5-10%) to the demanded (2-5%) in the 3-20 MeV neutron energy range [4)].

In this paper the main experimental conditions and the results of the measurements are summarized. Detailled informations about the used electronics and the data acquisition system are given in two other contributions [5,6)].

2. Neutron production and associated particle (AP) detection system

The principle of neutron production and AP detection [5)] was already developed for earlier measurements at about 8.4 MeV neutron energy [2,7)] and is based on a telescope of two completely depleted Si(SB) detectors. Measurements at neutron energies of about 4.5 MeV were carried out by means of the same system making another choice of the measuring geometry and the energy of the incident deuterons. By an optimization of the ΔE-detector parameters, especially the detector thickness, the pulse shaping in the spectroscopic AP channel and the measuring geometry, an important increase of the AP counting rate within the limited cone was achieved guaranteeing a small background portion. Main experimental parameters are listed in Tab.1.

In order to produce 18.8 MeV neutrons using the $T(d,n)^4He$ reaction, a 6 MeV deuteron beam was incident on a selfsupporting Ti-T foil. The experimental set-up is shown in Fig.1. The rotating target holder system allowed to work at deuteron beam currents of 800 nA without a noticeable escape of T out of the foil. By setting the CFD threshold of the fast ΔE-channel high enough above the amplitudes of the deuteron pulses, an effective discrimination of deuteron multiple pile ups was obtained.

The use of a computer-coupled two parameter unit with colour display was favourable to check the threshold conditions and to analyze the AP spectrum composition [8)].

Background events occur from (d,α) reactions at the Ti foil and the Al layer, but also from the $^{16}O(d,\alpha)$ reaction. Apparently, by producing the

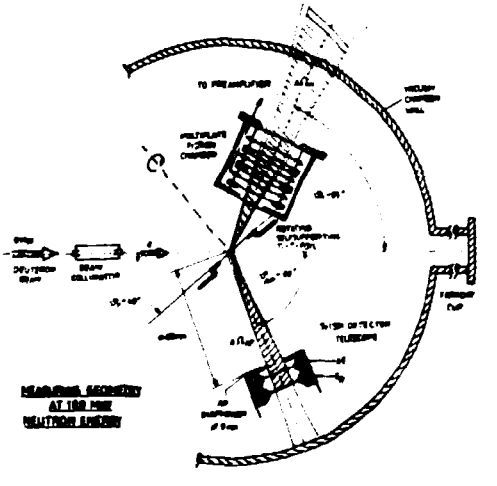

Fig.1: Experimental set-up of the measurements at 18.8 MeV

targets oxygen can be bound especially at the surface, but also in variuos properties within the whole target volume (Fig.2). The AP identification in the data taking runs was performed by single channel analysis of the total energy spectrum containing only events, which are identified as alpha particles within the window of the particle significant spectrum. The background correction procedure considereS (d,α) portions from Ti, Al and O individually and is based on measured spectra, which were obtained from several non-tritiated target foils (Fig.3). Employing various sets of background spectra obtained from different foils, the results correspond within ±(0.5-1)% [9]. Because of the T decay, an additional background portion due to the $^3He(d,p)^4He$ reaction has to be taken into account. To perform an experimental determination, a second ΔE-E_r semiconductor detector telescope was placed inside the vacuum chamber instead of the fission chamber. A 0.4 mm thick cupper foil was used to screen the detectors from the deuterons. Counting protons in coincidence with AP signals, the $^3He(d,p)^4He$ background portion within the AP window was determined to (0.35 ± 0.30)%.

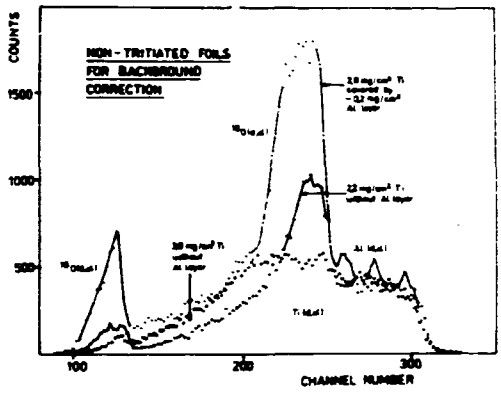

Fig.2: Background spectra of several non-tritiated Ti foils

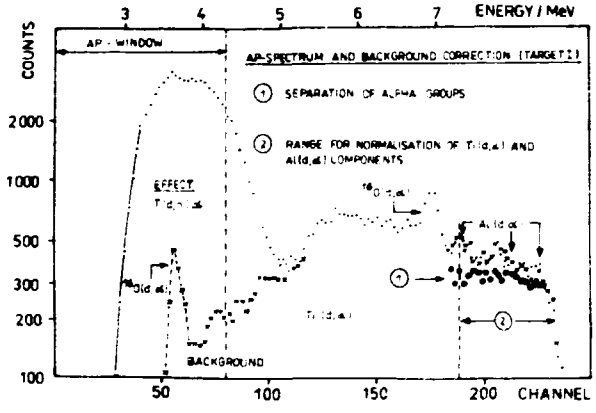

Fig.3: Spectrum of a Ti-T target foil and background correction

Calculated neutron energy				
- Averaged energy (MeV)	4.45 ± 0.2	4.8 ± 0.2	8.65 ± 0.2	18.8 ± 0.2
- FWHM of energy distr. (MeV)	0.23	0.25	0.40	0.60
Neutron production reaction		$D(d,n)^3He$		$T(d,n)^4He$
Deuteron beam				
- Energy (MeV)	5.00	5.80	9.50	6.00
- Current (nA)		400-600		300-800
Neutron producing target				
- Foil (used in a rotating target holder system)		deuterated polyethylene		selfsupporting Ti-T covered by 0.2mg/cm²Al layer
- Thickness (mg/cm²)	0.5-1.8	0.6-0.8	0.6-0.8	3.6 / 2.6
- Angle relative to the beam axis	52°	52°	75°	40°
AP detection				
- AP detection angle	38°	36.5°	42.5°	68°
- Solid angle of AP cone (msr)	1.05	1.40	1.40	8.05
- ΔE detector thickness (μm)	13 / 9	11	9	10
- LAR output pulse length (μs)		0.5		0.25
- Total energy resolution (keV)		70 - 80		100 - 120
- Scattered deuterons (s^{-1})	$1-1.5\cdot10^5$	$1-1.5\cdot10^5$	$6-8\cdot10^4$	$1.5-3\cdot10^5$
- Mean AP counting rate (s^{-1})	1500 / 2100	3600	3700	3300 / 2200
Neutron cone profile				
- Measured FWHM	4.5°	4.5°	5°	6.5° / 6°
- Measured 0.005M	11.5°	11.5°	12.5°	15° / 14°
- Angular extent of the fission foils	15.3°-20.5°	16.4°-25.2°	16.8°-26.3°	15.3°-21.6° (15.4°-22.8°)x)

Tab.1: Main experimental parameters of the neutron production and AP detection system
x) in the brackets are the values of the 18.8 MeV measurement on Pu-239

3. Neutron cone profile checking and analysis

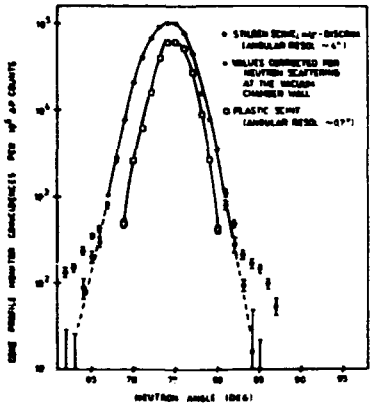

Fig.4: Neutron cone profile of the 4.45 MeV fission cross-section measurement on U-235

During the runs, the horizontal neutron cone profile was checked continuously using a scintillation detector, which was placed outside the vacuum chamber. Associated neutrons are identified by time-of-flight measurement refering to the AP timing signal. Small drifts of the cone maximum did not exeed 1°, and the fission chamber was always adjusted to the measured cone maximum.
To explain the neutron cone profile sides, a test measurement with an additional scatterer was performed and the effect of cone neutron scattering at the vacuum chamber wall (0.3 mm stainless steel) and the fission chamber material could be considered approximately.[10] (Fig.4)
Because of nearly the same reaction kinematics of the $T(d,n)^4He$ and $^3He(d,p)^4He$ reaction, corresponding conditions exist for the neutron and proton cone. By measuring the proton cone inside the vacuum chamber, it was possible to determine the true cone profile, including the effect of charged particle scattering within the neutron producing target and not falsified by neutron scattering (Fig.5). It was proved, that an exponential extrapolation of the measured cone sides considering the angular extent of the profile monitor should be a good approximation to calculate the neutron losses outside the angular extent of the fission foils.

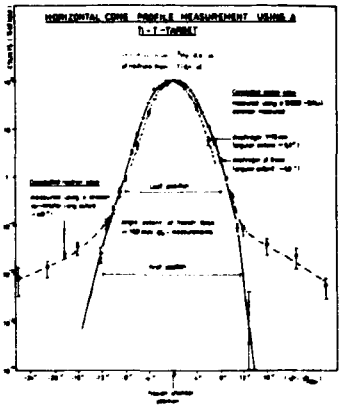

Fig.5: Comparision of proton and neutron cone profile measurements using a Ti-T foil

4. Fission fragment detection using a multiplate ionization fission chamber

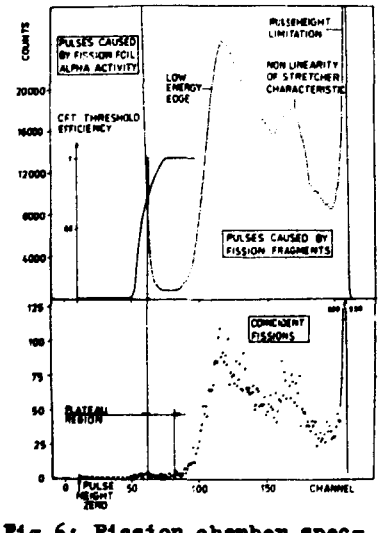

Fig.6: Fission chamber spectrum of a cross-section measurement on Pu-239

Thin fission foils (6 plates <300 $\mu g/cm^2$ Pu-239; 5 plates <500 $\mu g/cm^2$ U-235) were placed inside a parallel plate fission chamber. It was filled with methan at a pressure of 108 kPa and operated at a voltage of 400 V. The distance of 3 mm between electrodes and fission foils represents a compromise to reach a good separation of fission fragment pulses from alpha events under the restriction of a compact fission chamber design [11]. The short current pulses (30-40 ns) were analysed by means of a nanosecond stretcher. This method allowed a high fission fragment efficiency (>96%) also at high alpha activities of the fissile material (~ 9 MBq for 4 mg Pu-239). Within the fission chamber spectrum a broad "plateau" region was observed, indicating an excellent separation of fission fragments from alpha particles (Fig.6).
In the fission chamber channel at 18.8 MeV neutron energy an additional correction had to be introduced, which considers the $^{12}C(n,n')3\alpha$ reaction at the fission chamber gas CH_4.

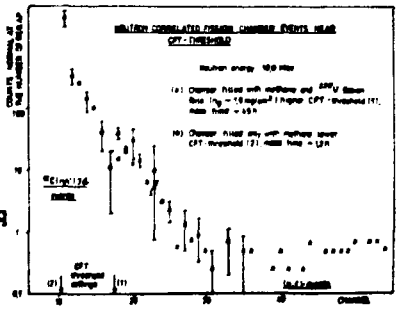

Fig.7: Experimental proof of reactions within the chamber gas caused by 18.8 MeV neutrons

This reaction is able to generate events within the coincident fission chamber spectrum above the CFT threshold (Fig.7).
The fission foils were produced at the KRI Leningrad using material of high isotopic purity >99.99% by HF- and thermo-sputtering of U-235 and Pu-239, respectively. Areal density measurements were performed by low geometry alpha counting.

5. Results

The Tab.2 gives a summary of the corrections, error contributions and results of the presented fission cross-section measurements. Most of the results are based on several measurements carried out under some different conditions at the same spot point [9,11].
The accuracy obtained for the neutron flux determination of the different energy spot points demonstrates the advantage of the used TCAPM.
The short test measurement on Pu-239 at 18.8 MeV will be completed by a further one.

Nuclide Neutron energy (MeV)	U-235 4.45		U-235 18.8		Pu-239 4.8		Pu-239 8.65		Pu-239 18.8	
	Corr. (%)	Error contr. (%)	Corr. (%)	Error contr. (%)	Corr. (%)	Error contr. (%)	Corr. (%)	Error contr. (%)	Corr. (%)	Error contr. (%)
Counting of coincidences										
- Statistics of effect	-	1.26	-	1.01	-	1.27	-	1.08	-	2.52
- Random coincidences	1.40	0.17	2.82	0.21	0.64	0.11	1.86	0.17	4.55	0.63
Fission chamber efficiency										
- Correlated background	-	-	1.72	0.04	-	-	-	-	0.34	0.13
- Extrapolation to zero	1.18	0.26	1.67	0.16	1.50	0.31	1.04	0.24	2.57	0.85
- Fragment absorption	2.00	0.85	1.73	0.78	1.21	0.46	1.20	0.43	1.30	0.39
AP counting										
- Background	2.32	0.67	5.62	1.35	2.30	0.36	1.62	0.32	5.92	1.74
Neutron cone										
- Neutron scattering	0.25	0.40	0.44	0.40	0.25	0.40	0.36	0.40	0.34	0.40
- Effective fission foil thickness due to the cone aperture	0.05	0.05	0.12	0.08	0.08	0.05	0.07	0.05	0.12	0.08
Fissile layer										
- Areal density	-	0.93	-	0.93	-	1.00	-	1.00	-	1.00
- Inhomogenoty	-	0.72	-	0.72	-	0.88	-	0.85	-	0.88
RESULT ($10^{-24}cm^2$) STANDARD DEVIATION (%)	1.057±0.022 2.10		1.999±0.045 2.25		1.740±0.035 2.00		2.350±0.044 1.85		2.487±0.088 3.55	

Tab.2: Results of the presented TCAPM fission cross-section measurements

At present there are investigations to improve the accuracy of the fission foil data and to obtain the correction values of fission fragment absorption experimentally.

REFERENCES

1) I.D. Alkhazov et al.; Proc. of the 2-nd Conf. on Neutron Physics, Kiev, USSR, Vol.4, p.13(1973)
2) R. Arlt et al.; Proc. Conf. Nucl. Cross-Sections and Technology, Knoxville, USA, 1979; NBS Spec. Publ., Vol.594, p.990 (1980)
3) R. Arlt et al.; Kernenergie 24(1981), p.48
4) H.D. Lemmel; Proc. X. Internat. Symp. on Selected Topics of the Interaction of Fast Neutron and Heavy Ions with Atomic Nuclei, Gaussig, GDR, 1980, ZfK-459(1981), p.27
5) H.G. Ortlepp et al.; "Identification of associated particles ...", contr. in this Vol.
6) G. Pausch et al.; "CAMAC data aquisition system ...", contr. in this Vol.
7) R. Arlt et al.; see ref.4, p.35
8) W.D. Fromm, M. Kahlenbach; ZfK-530(1984), p.131
9) C.M. Herbach et al.; report TU Dresden, 05-07-85 (1985)
10) R. Arlt et al.; Proc. of an Advisory Group Meeting on Nucl. Standard Reference Data, Geel, Belgium, 1984, IAEA-TECDOC-335, p.174, (1985)
11) C.M. Herbach et al.; report TU Dresden, 05-06-85 (1985)

IDENTIFICATION OF ASSOCIATED PARTICLES IN THE TCAPM FISSION CROSS SECTION MEASUREMENTS AT THE TANDEM ACCELERATOR OF THE CINR ROSSENDORF

H.-G. Ortlepp*, C.M. Herbach, K. Merla, G. Musiol, G. Pausch
Technical University Dresden, GDR

Abstract

The Time-Correlated Associated Particle Method was applicated to fission cross-section measurements in the neutron energy regions near 8.5, 4.5, and 19 MeV. The DD- and DT-reactions were used at a 5 - 10 MeV deuteron beam of the CINR tandem-van-de-Graaff-accelerator. To reach sufficient AP counting rates, neutron production targets of up to 3 mg cm^{-2} were used. Several problems connected with the high rate of scattered deuterons and with charged particles from other reactions could be solved with an especially developed equipment. A telescope of two Si-SB-detectors in connection with a fast timing, a high rate pulse height spectroscopy system and a specialized fast particle identification circuit was utilized. AP counting rates up to 5000 s^{-1} were obtained. Rates of scattered deuterons of 10^5 s^{-1} could be tolerated. The portion of not separated background events amounted to 2 - 6 %.

1. Introduction

The basic features of the Time-Correlated Associated Particle Method (TCAPM) are described in earlier papers (e.g. /1/). The application of this method to fission cross-section measurement at neutron energies in the 3 - 13 MeV ($D(d,n)^3He$) and 15 - 20 MeV ($T(d,n)^4He$) regions requires deuteron energies in the MeV region, and problems arise from the following facts:

i) It is not possible to screen the AP detector from scattered deuterons by means of absorber foils.

ii) The AP detector has to separate associated particles from background reaction products, especially from (d,α) reactions, depending on the target composition and the deuteron energy.

iii) To obtain sufficient statistics within a reasonable time under the restriction of a limited number of thin fission foils AP counting rates $> 10^3$ s^{-1} are necessary. Thereby the maximum diameter of the AP aperature is given by the fission chamber geometry which limits the possible neutron cone width. A neutron production rate high enough to meet the above requirement supposes then relatively thick target foils ($\sim$1 mg cm^{-2}). This increases the difficulties of the AP identification because of the energy spread of charged particles due to their different path length within the foil and the high rate of deuterons scattered into the AP cone ($\sim 10^5$ s^{-1}) leading to pile-up effects.

iv) The application of semiconductor detectors requires separate timing and pulse height channels. If the time and energy informations are treated utilizing a classical fast-slow coincidence scheme, difficulties occur from different partially correlated random coincidence background amounts in both channels as well as from dead-time effects in the timing spectra /2/.

To avoid all possible systematical error contributions arising from the above mentioned problems, a completely new scheme was developed utilizing a ΔE-E telescope in connection with a high rate pulse height spectroscopy system including efficient pile-up rejection and a "strobe coincidence" method in connection with a special fast particle identifier (fig. 1).

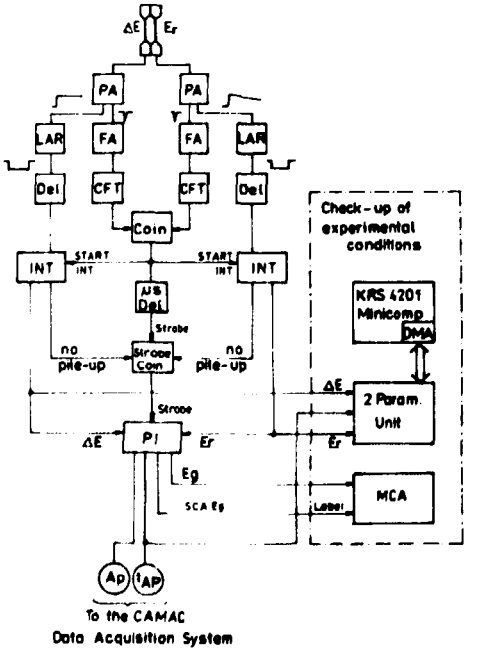

Fig. 1
Simplified block diagram of the AP identification system

2. The ΔE-E Telescope

If thin $(CD_2)_n$ targets are used (~100 µg cm^{-2}) the events corresponding to the ^3He's of the $D(d,n)^3He$ reaction from alphas of the (d,α) reaction can be spearated by single channel pulse height analysis /3/. At about 1 mg cm^{-2} however, ^3He and alpha peaks become overlapping (fig. 2) and must be separated by the ΔE-E technique. The experimental conditions, e.g. the beam energy and spot diameter, the angular position and solid angle of the AP telescope, the thickness of the ΔE detector, the fission chamber position and the target angle must be optimized at each neutron energy point taking into account contradicting requirements. The lower limit of the detectable ^3He energy of about 2 MeV is determined by the minimal thickness of the ΔE detector of about 8 µm Si necessary for sufficient ^3He-^4He separation. For kinematical conditions leading to ^3He energies higher than 5 MeV the neutron differential cross-section decreases but the elastical deuteron scattering into the AP cone increases. Considering the slowing-down in the $(CD_2)_n$ foil ^3He particles between 2 and 5 MeV must be expected. During the different measurements detectors of 9 - 13 µm thickness were used. Low energetic AP's were already stopped in the 13 µm detector. Tests with a 6 µm detector yielded unsufficient ^3He-^4He separation. The thickness of the E_r detector was chosen to stop the highest energetic alphas. The used 37 - 72 µm completely depleted Si SB detectors are passed by the scattered deuterons.

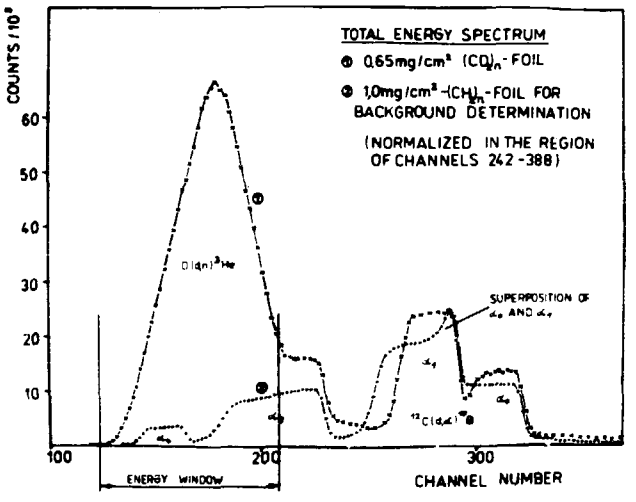

Fig. 2
Energy spectrum of charged particles

3. The High Rate Pulse Height Spectroscopy System

The preamplifiers have separate "energy" and "time" outputs. The "time" signals are used not only for fast timing but also to start the pulse height processing. The slow channels consist of a linear amplifier with delay line shaping which rectangular output pulses are integrated and checked for pile-up in a gated integrator unit /4,5/. Up to more than 10^5 pulses per second spectrum distortions due to pile-up remained neglectable /6/. The increasing pulser line width at the higher rates is tolerable, because the measured peaks of the particle spectra are much broader due to the target thickness and the kinematical acceptance. The resolution of the ΔE channel, important for the particle identification remains to be determined mainly by the energy straggeling.
The system was checked collecting a pulser peak in the presence of a high rate of reaction products. Varying the beam current different counting rates were obtained.

4. The Combination of the Pulse Height and Timing Informations

The "time" signals of the preamplifiers pass the timing filter amplifiers and are fed to constant fraction triggers. The timing threshold of the ΔE branch is set just above the deuteron pulses; in the E_r branch as low as possible. In this way deuteron events are suppressed. Several following shortly each other such events which would lead to multiple pile-up in the slow channels give separated short pulses in the timing channels and are suppressed also. A fast coincidence of the CFT output signals fires both gated integrators (fig. 1). The same signal but delayed by ~1 µs passes, conserving the timing information, a special "strobe coincidence" unit, if the unit has recieved the information "output signal valid" (no pile-up)

from both integrators. This inspection includes also pile-up by the small deuteron pulses. Then the signal passes, again conserving the timing information, a special particle identification unit, if the chosen energy and particle selection conditions are fulfilled. This signal then is used as "AP" in the basic TCAPM scheme. The delay of ~ 1 µs is realized in both the "AP" and the "f" branches by two identical cable units to avoid drift effects. Due to the minimal time interval between two AP signals determined by the dead time (~1 µs) of the particle identifier circuit, timing spectrum distortions are excluded.

5. The Principle of the Particle Identification

The above mentioned scheme requires fast analogue particle identification, but in a small dynamic range. The particle branches in a ΔE-E_r plot (fig. 3) can be approximated by straight lines in the energy interval of interest. Therefore the particle identification function can be realized by a simple linear combination of the ΔE and E_r pulse heights instead of a complicated nonlinear response. This is done by a weighted sum amplifier within some 10 ns. The sum of $\Delta E + E_r$ with equal weights represents the particle energy. The distributions of the energy and particle identification signals can be recorded as pulse height spectra.

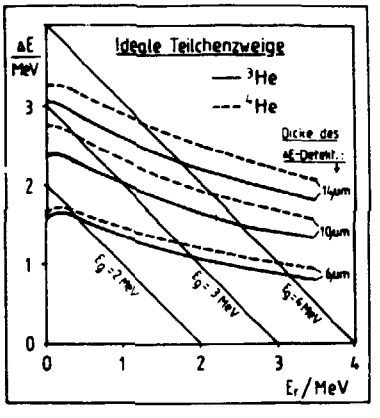

Fig. 3
Calculated ΔE-E_r plot for ^3He and ^4He

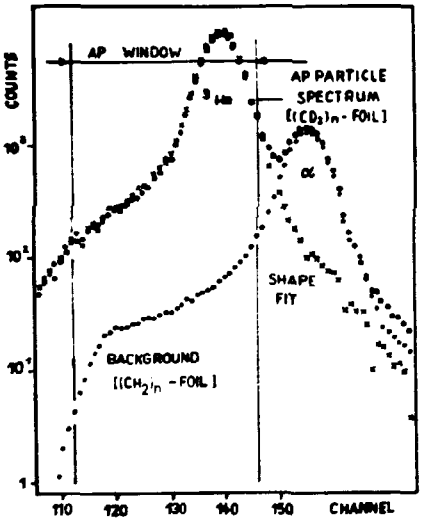

Fig. 4
Particle-significant spectrum of the AP telescope from a fission cross-section measurement at 8.65 MeV neutron energy /7/

The selection and background correction procedures are different for ^3He and ^4He AP's. At the 4.5 and 8.5 MeV experiments in a first step the energy range containing the ^3He peak is selected. For such events the particle identification signal is built-up showing characteristic ^3He and ^4He peaks. This spectrum (fig. 4) is collected during the whole measurement to determine the background underlying the ^3He peak within the ^3He window which is selected in the second step. The background is caused by the tail of the ^4He peak, and the normalization is performed with the help of spectra taken from $(CH_2)_n$ foils. At the 19 MeV experiments alpha events are selected with the help of the particle identification signal. The associated alpha particles are then selected by an energy window. The background correction procedure based on alpha spectra of different non-tritiated Ti foils is more complicated. Different components from (d,α) reactions on Al, O and Ti must be separated and then normalized and subtracted independently. All adjustments are performed with the help of a two-dimensional analyzer showing the ΔE-E_r distribution on a colour screen.

References

/1/ Arlt, R. et al., Kernenergie 24 (1981) 48

/2/ Poenitz, W., private communication

/3/ Schuster, D.G., Nucl. Instrum. Methods 76 (1969) 35

/4/ Andert, K. et al.,report JINR Dubna, USSR, P13-10110 (1976)

/5/ Ortlepp, H.-G., Proc. XII. Int. Symp. on Nucl. Physics, Gaussig, GDR, 1982: ZfK-491 (1982) 141

/6/ Ortlepp, H.-G., Proc. XI. Int. Symp. on Nucl. Electronics, Bratislava, Czechoslovakia, Sept. 1983; JINR Dubna D13-84-53, Dubna 1984, p. 113

/7/ Herbach, C.M. et al., Preprint TU Dresden 05-06-85, Dresden, GDR, 1985

CAMAC DATA ACQUISITION SYSTEM AND DATA ANALYSIS IN TCAPM FISSION CROSS-SECTION MEASUREMENTS AT THE TANDEM ACCELERATOR OF THE CINR ROSSENDORF

G. Pausch, W.D. Fromm[+], C.M. Herbach, K. Merla, G. Musiol, H.G. Ortlepp[+]
Technical University of Dresden, G.D.R.

[+] CINR Rossendorf, G.D.R.

ABSTRACT

A CAMAC data acquisition system, based on a ROBOTRON KRS 4201 minicomputer, was developed to record simultaneously all experimental data which are needed to determine precise fission cross-section values by means of the TCAP method. Hardware configuration and basic software components are described.

1. INTRODUCTION

Since 1977 precise absolute fission cross-section measurements, based on the Time-Correlated Associated Particle Method (TCAPM), have been performed at the Technical University of Dresden (TU) in close collaboration with the Khlopin Radium-Institute Leningrad (KRI). The principle scheme of a fission cross-section determination by means of the TCAP method is well known /1,2/ (fig. 1): A beam of accelerated deuterons is incident on a target containing deuterium or tritium, neutrons are produced together with charged associated particles (^3He, ^4He) using the reactions $D(d,n)^3He$ or $T(d,n)^4He$. An aperture selects a cone of associated particles (AP); the correlated neutrons form also a cone which is intercepted by homogeneous fission foils, placed inside an ionization fission chamber (FC). Energy and direction of correlated neutrons are given by the reaction kinematics and can be varied by changing the incidence energy of the deuterons or the AP detection angle relative to the beam axis. By simultaneously counting the selected associated particles (N_{AP}) and the fissions caused by correlated neutrons (N_f), the fission cross-section can be determined from the simple formula

$$\sigma_f = \frac{N_f}{N_{AP} \cdot n_T}$$

if the listed premises are fulfilled:

i) AP detection without background (correlated neutron for each AP pulse!);
ii) efficiency of 100 % for detection of fission events;
iii) foultless identification of fissions caused by correlated neutrons;
iv) homogeneous fission foil(s) with known number n_T of target nuclei per unit of area, great enough to cover the cone completely;
v) no neutron scattering out of the neutron cone, no AP scattering into the AP cone, no scattering of incident deuterons.

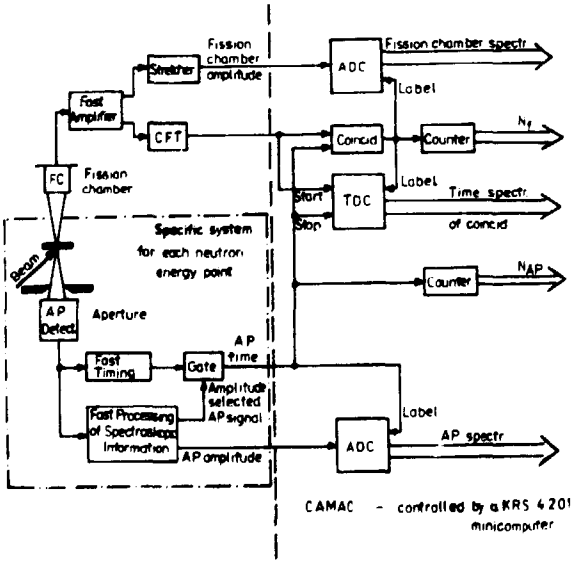

The total AP detection efficiency as well as geometrical factors are not required. Such an ideal arrangement - of course - is not possible in practice, and deviations from the listed requirements have to be measured or calculated carefully and to be considered in the analysis of the experimental data.

Fig. 1: Principle scheme of signal processing and data acquisition in TCAPM fission cross-section measurements at the tandem accelerator of the CINR Rossendorf

2. CAMAC DATA ACQUISITION SYSTEM

Within the last years, the activities at the TU Dresden within the joint programme /2/ have been concentrated on measurements at the 5 MV tandem van-de-Graaff accelerator of the CINR Rossendorf /3-5/. The scheme of signal processing and data acquisition applied in these measurements (fig. 1-2) was designed to record simultaneously all experimental data, which are needed to determine the cross-section value including corrections /6-8/:

1. AP detector pulses are caused not only by associated particles, but also by scattered incidence deuterons, protons and alphas from background reactions. To identify true AP events, the amplitude information of the AP detector is processed /6/; the portion of not suppressed background events can be determined by analyzing an amplitude spectrum, which is recorded during the run by means of a CAMAC analogue-to-digital converter (ADC 2). By labelling the amplitude signals of the AP channel (ATA) with the AP timing signals (t_{AT}), generated only for identified associated particles /6/, the AP window within the amplitude spectrum is manifested.

2. Counting losses in the FC channel occur from the energy loss of fission fragments in the target layer, leading to small pulse amplitudes or even a total absorption of both fragments, if the direction of fragment emission is nearly parallel to the target surface. The detection efficiency depends on the thickness of the target layers and on the electronic threshold, which is set by a constant fraction trigger (CFT in fig. 1). To calculate the portion of signals with pulse heights lower than the timing threshold, an amplitude spectrum is recorded (ADC 1).

3. Correlated fissions are identified by means of a fast coincidence circuit (Koinz.). The number of random coincidences can be derived from the timing spectrum, recorded by means of a time-to-digital converter (TDC). The fixed dead-time in the AP channel (~ 1 µs), which is greater than the conversion range of the TDC (T ~ 140 ns), guarantees a "white" spectrum for random events /6,8/.

The timing signals of the AP and FC channels as well as coincidences of both signals are counted by two independent sets of scalers. A timer is used as a real-time clock. The CAMAC data acquisition system is controlled by a ROBOTRON KRS 4201 minicomputer. FORTRAN codes for data acquisition and data analysis were developed in colleboration with the CINR Rossendorf /8-10/, using an extended FORTRAN LIBRARY which allows an easy programming of CAMAC operations and LAM interrupt handling /11,12/.

The experiment is divided into single runs, each of them having a complete set of spectra, scaler contents and other parameters, which are stored on a disc memory. A single run consists of measurements with presettable measuring time; the sequence of all actions is given by a computer code /8/.

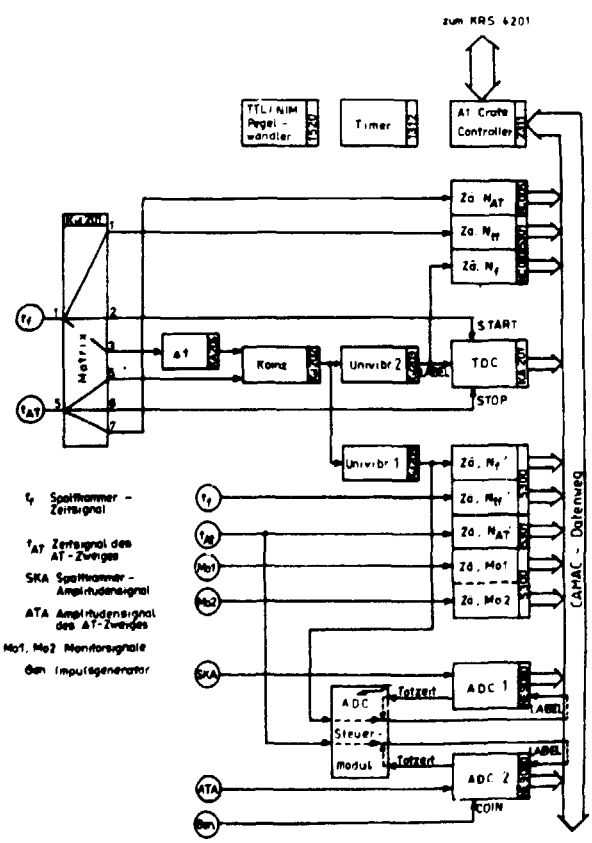

Fig. 2: Block scheme of the CAMAC data acquisition system
t_f, t_{AT}: FC and AP timing signals
SKA: FC amplitude signal
ATA: AP amplitude signal
Mo1, Mo2: Monitor signals
Gen: Pulse generator, used for reduction of the ATA rate
Zä.: Scalers

In the beginning of each single measurement, the AP input of the fast coincidence is switched off for 1 min to label the FC amplitude signals (SKA) with the corresponding timing signals (t_f). In this way, the efficiency curve of the CFT can be determined. This test phase is followed by the data acquisition phase (typically 20-30 min). Coincident events are labelled in the timing spectrum as well as in the FC spectrum. All spectra are built-up in the computer memory and can be inspected during the run on a display unit. The data inputs of all CAMAC modules are abled and enabled simultaneously by means of the INHIBIT signal; this includes a synchronous dead-time phase for all scalers, ADC, TDC, and the timer during any CAMAC interrupt handling and data transfer. Errors due to dead-time losses are excluded because of the fixed dead-time in the AP channel and the low counting rates for t_f signals ($\sim 10\ s^{-1}$) and t_f-t_{AT} coincidences ($50-100\ h^{-1}$). Nevertheless, a date test is performed at the end of each single measurement: The scaler contents of the independend scaler sets, as well as the numbers of coincident events recorded in the N_f scalers and the timing spectrum, must agree; and the measured fission cross-section is expected to be within given limits which are fare from possible statistical deviations. Any violation of this requirements indicates an incorrect work of the experimental set-up; therefore, the run is interrupted and the operator asked for a command. If all test conditions are fulfilled, the date of this measurement are included in the single run data, the result is transferred to the disc memory, and the next single measurement is started. At any time, the operator can terminate the single run. The computer protocol includes a protocol line for each single measurement (scaler contents and other parameters) as well as the summarized single run data and spectra, but also a note for each command of the operator.

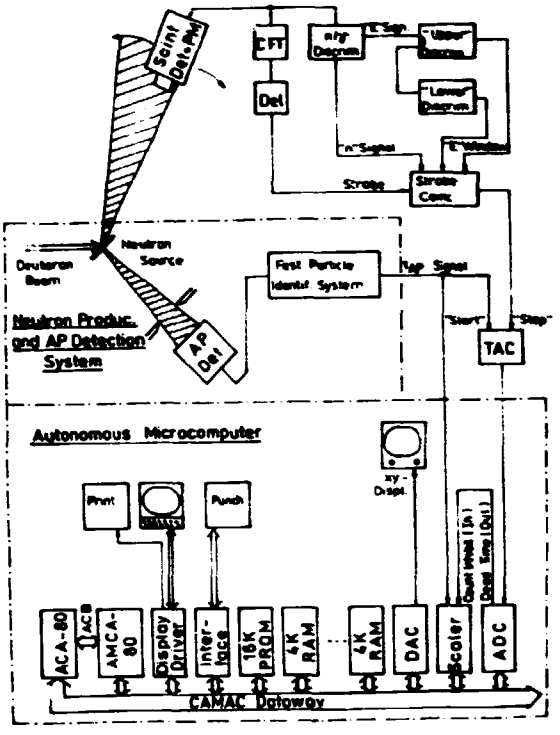

Fig. 3: Block scheme of the microcomputer controlled cone profile monitor

A seperate code operates the CAMAC system in a start-stop mode. It is used to record test- and background spectra and to store them on disc together with short comments.

A "disc administrator" allows to list the valid runs, to inspect any set of single runs and to include it in or to exclude it from the list of the valid ones, and to summarize any set of single runs. Various parameters are calculated from the single run spectra and included in the lists. This allows to check the stability of experimental conditions.

3. CONE PROFILE MONITOR

The cone profile monitor was designed as a seperate, microcomputer-controlled system (fig. 3) /4,13/ and allows a continuous test of neutron cone maximum and width during the life cross-section measurement. The monitor is based on a scintillation detector. Correlated neutrons are identified by the time-of-flight technique. The random background is reduced by neutron-gamma discrimination /14/ and by selecting the energy of recoil protons. The "strobe coincidence" method is applied to unify all information, conserving the time resolution /6/. Measurement and analysis of the TOF spectrum are controlled by a BASIC code /15/. As a result, the background-corrected number of correlated monitor signals,

related to 10^6 registered AP, is determined together with its statistical uncertainty.

4. DATA ANALYSIS

The corrections applied to the measured cross-section were briefly described in ref. /4, 5/. A more detailed discussion can be found in /8/ and will be published as a TU report in 1986. Therefore, only some notes to the "experimental" corrections, obtained from the recorded spectra, are given here.

The number of coincident events as well as the number of random coincidences are determined from the timing spectrum, summarized in general from a complete experiment. The correction for FC pulses below the timing threshold is also derived from the summarized coincident FC spectrum, using the corresponding summarized FC test spectra to calculate the CFT efficiency curve. Therefore, drifts of the CFT threshold are considered and cannot produce errors. The "zero" point is determined from several test spectra generated by means of a calibrated pulser.

The AP background correction is based only on experimental spectra, not on a mathematical description of peak shapes. The correction value is very sensitive to the detector properties, which can change during the run because of irradiation effects, and to parameters of the target foils. Therefore, in general only a few single runs are summarized, and the correction procedure is performed using corresponding background and "neutron-gated" effect spectra (coincidence with correlated neutrons /4,8 16/) which were recorded before starting and after terminating a single run. The uncertainty of the correction is mainly influenced by changes of the experimental conditions. The background calculation is carried out in a computer - operator dialogue; each step of the procedure can be inspected on a display.

5. CONCLUSIONS

A complete and careful documentation of the most important experimental parameters by means of a computer protocol, a computer-aided check of experimental conditions as stability of thresholds, background portions in the timing and AP spectra, plateau height in the FC spectrum and others, and a computer-aided analysis of the experimental data were introduced not only to get more convenience, but mainly to guarantee optimum experimental parameters and a high accuracy of the final result.

6. REFERENCES

/1/ I.D. Alkhazov et al., Proc. Third National Soviet Conf. Neutron Physics, Kiev, May 26-30, 1975, CONF-750555, Vol. 6, p. 9 (1976)

/2/ R. Arlt et al., Kernenergie 24 (1981), p. 48

/3/ C.M. Herbach et al., paper included in this volume

/4/ C.M. Herbach et al., report 05-07-85, TU Dresden, 1985

/5/ C.M. Herbach et al., report 05-06-85, TU Dresden, 1985

/6/ H.G. Ortlepp et al., paper included in this volume

/7/ H.G. Ortlepp, G. Pausch, ZfK-530 (1984), p. 118

/8/ G. Pausch, Dissertation, TU Dresden, 1986

/9/ G. Pausch, W.D. Fromm, ZfK-530 (1984), p. 148

/10/ G. Pausch, C.M. Herbach, ZfK-559 (1985), p. 23

/11/ W.D. Fromm, B. Tietze, ZfK-385 (1979), p. 260

/12/ W. D. Fromm, ZfK-443 (1981), p. 220

/13/ C.M. Herbach et al., ZfK-559 (1985), p. 24

/14/ R. Arlt et al., ZfK-408 (1980), p. 154

/15/ A. Schnalke, Dipl. work, TU Dresden, 1984

/16/ R. Arlt et al., Proc. of an Advisory Group Meeting on Nuclear Standard Reference Data, Geel (Belg.), 1984, IAEA-TECDOC-335, p. 174

^{6}Li GLASS SPECTROMETER FOR LOW ENERGY FISSION NEUTRONS

A. Lajtai, J. Kecskeméti
Central Research Institute for Physics, Budapest, Hungary and
P.P. Dyachenko, L.S. Kutsaeva, E.A. Seregina
Institute of Physics and Power Engineering, Obninsk, USSR

Abstract

Application of a 9.55 mm thick NE912 glass detector in a time of flight spectrometer is described for energy spectrum measurement of fission neutrons with energy of 20 keV - 1.2 MeV.

The measurement of low energy fission neutrons involves a great deal of difficulties in view of which there are many contradictory results in the experiments of the last 20 years.

Even measurements with ^{6}Li glass detectors have resulted in a 20-30 % neutron excess of energy spectrum from spontaneous fission of ^{252}Cf at energies lower than 1 MeV relative to Maxwell spectra with a T parameter of 1.42 MeV.

These results are assumed to be due to the lack of precise knowledge of neutron detection efficiency, the effects of neutron multiscattering, and the neglection of the various necessary corrections.

Thin (less than 1 mm) glass detectors are often used in time-of-flight (TOF) spectrometers to detect neutrons of energy below 100 keV, when detecting neutrons above 100 keV difficulties arise in determining the efficiency because of the resonances caused by Li, O, Si nuclei of the detector material.

Various Monte Carlo calculations have been performed in an attempt to assess the effects of these resonances |1,2|, i.e. the correction factors C(ε) for the thin glass detectors. These correction factors reflect the deviation of actual efficiencies from the efficiencies for the pure ^{6}Li (n,α) reaction.

Due to the low fission neutron yields at low energies one has to use detectors of higher efficiency. One such possibility is to increase the thickness of the Li glass detector, but the employment of thick detectors causes new problems requiring different corrections.

To obtain these corrections we first measured the efficiency of a thick (9.55 mm) NE912 detector at different neutron energies, relative to a thin one - the efficiency of which had been determined by Monte Carlo calculation 3-4 . The main results are shown in Fig. 1, where the different correction factors C(ε) are depicted, namely the ratios of efficiencies to corresponding pure ^{6}Li efficiencies of a thin (0.835 mm) ^{6}Li glass detector, the thick ^{6}Li glass detector, and that of the thick glass detector determined by Monte Carlo calculation.

Efficiency measurements of thick Li glass were carried out at two different photo multiplier positions, viz. in-beam and out-of-beam positions. These ratios are shown in Fig. 2, which demonstrates the effects of enhanced backscattering by Si and O of the photomultiplier glass.

Another important problem when evaluating the measured neutron spectra is the fact that the neutrons are scattered in the material of the thick glass detector so their flight-time distribution is modified.

If we take the original neutron spectrum as $\phi(E)$, then the measured time-of-flight spectrum can be expressed as

$$P(t)=\int F(E,t)\,\phi(E)\,dE,$$

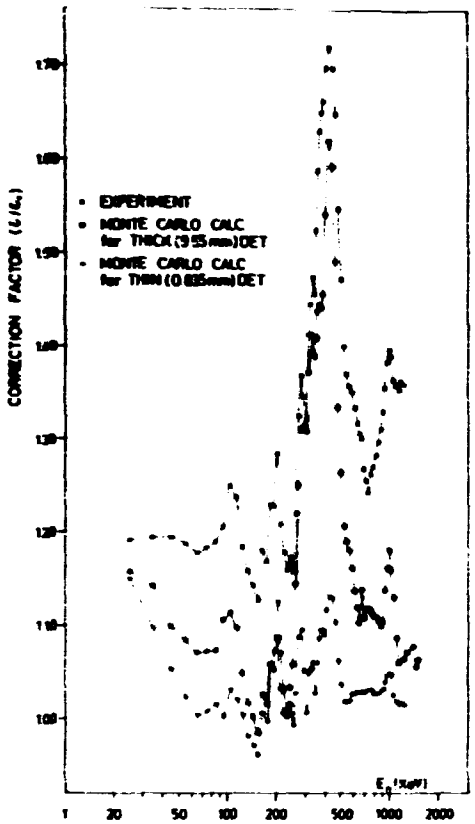

Fig. 1 Correction factors for the thin ^{6}Li glass detector (M.C. calc.) and for the thick detector (M.C. calc. and exp.).

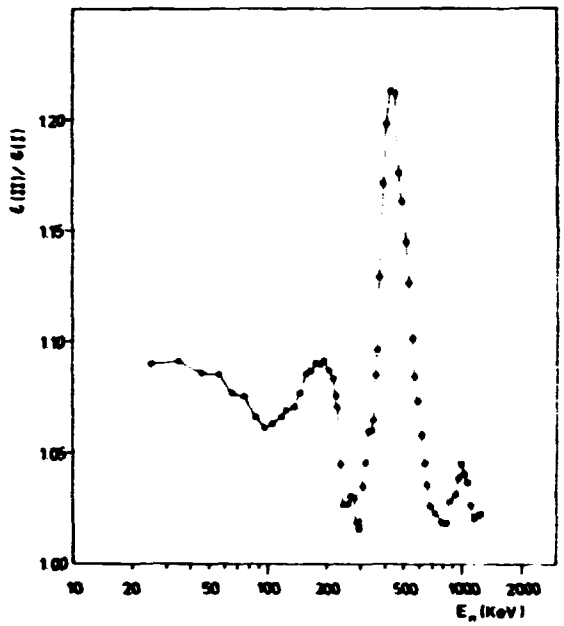

Fig. 2 Ratio of efficiencies in-beam and out-of-beam positions, the effect of the 56 AVP multiplier glass.

where F(E,t) is the response function of the detector system including the absolute efficiency of the neutron detector and the flight-time distribution of the scattered neutrons.

The F(E,t) function has been calculated by the Monte Carlo method at 200 values in the energy range of 20 keV-2 MeV, four of them are shown in Fig. 3.

Corresponding to the above mentioned components of F(E,t), we have two correction factors, one of which shows the ratio of the detection efficiency to that calculated from $^{6}Li(n,\alpha)$ cross sections (see Fig. 1). It agrees with that from the experiment within $\pm$ 10 %. This is a good agreement considering the ambiguities of the cross sections used in the calculation. This fact gives support to the reliability of the Monte Carlo calculation used to evaluate the flight-time distribution effects. Obviously when evaluating the neutron spectrum data the measured detection efficiency should be used.

The other correction factor C(t) from F(E,t), determines the distortion of the time--of-flight distribution due to multiple scattering of neutrons, i.e. the ratio of the number of neutrons registered at a given time to that of neutrons that arrived at the detector at the same time.

The C(t) correction factor which can be seen in Fig. 4 loses its importance with any increase in the flight path and for flight paths above 1 m it can be neglected. However, its neglection for smaller flight distances (less than 50 cm) causes an enhancement effect below 100 keV and oscillation in the 100 keV-1.2 MeV enerty range of the neutron spectrum.

A third problem of efficiency determination of thick glass detectors is their sensi-

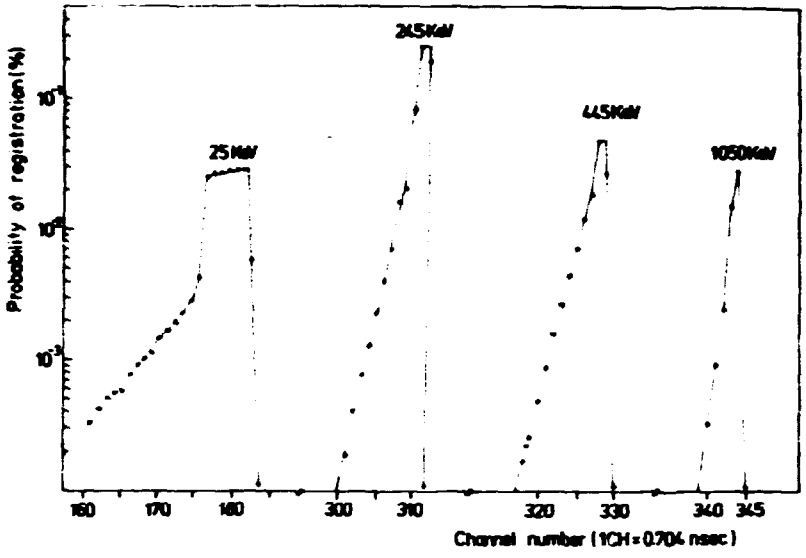

Fig. 3 Response functions of the thick ^{6}Li glass detector

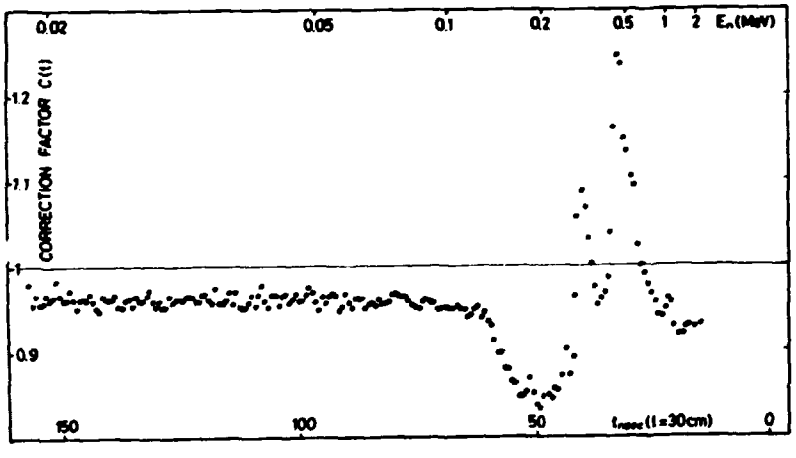

Fig. 4 Correction factor C(t)

tivity to γ rays of energy greater than 1.2 MeV. In case of fission neutron experiments, where the energy of a substantial part of delayed gammas is larger than 1.2 MeV, their detection falsifies the measured neutron spectrum.

These delayed gammas can be subtracted by their separate measurement using a ^{7}Li containing glass detector (NE913), which detects the delayed gammas only.

In summary the determination of a low energy fission neutron spectrum using a thick Li-glass detector spectrometer can be dealt with as follows:

1. measurement of the TOF spectrum by a NE912 glass detector - $P_1(t)$
2. measurement of the TOF spectrum with a NE912 glass detector with a shadow cone to measure the background neutrons only - $P_2(t)$
3. measurement of the TOF spectrum with a NE913 glass detector for delayed gammas - $P_3(t)$
4. measurement of the TOF spectrum with a NE913 glass detector for delayed gamma background - $P_4(t)$.

In this way we obtain the primary neutron TOF spectrum P(t):

$$P(t)=P_1(t)-P_2(t)-P_3(t)+P_4(t)$$

This spectrum is corrected f the systematic accident coincidences at high counting rates. The next step is to a the above discussed C(t) corrections

$$P'(t)=C(t)\cdot P(t)$$

The necessary time resolution corrections of TOF spectrometer must obviously be carried out. The minimum time resolution of a spectrometer with a NE912 glass detector is about 2 nsec. The P'(t) TOF spectrum corrected in this way can be transformed into the P(E) energy spectrum from which can we get the final neutron spectrum as

$$N(E)=\frac{P(E)}{N_f\Omega\varepsilon(E)},$$

where N_f is the number of detected fission events, Ω is the solid angle of the neutron detector, and $\varepsilon(E)$ is the measured neutron detection efficiency of the ^{6}Li glass detector.

References

1). B.J. Allen, R.L. Macklin, R.R. Winters and C.Y. Fu; Phys. Rec. C 8 (1973) 1504
2). G.P. Lamaze, R.A. Schrack and O.A. Wasson; Nucl. Sci. and Eng. 68 (1978) 183
3). V.N. Kononov et al.; Nucl. Instr. and Meth. A234 (1985) 361
4). A. Lajtai et al.; IAEA-TECDOC-335 (1985)

EMPLOYING OF GADOLINIUM LOADED LARGE LIQUID SCINTILLATION COUNTERS FOR RESEARCH OF NEUTRON MULTIPLICITY DISTRIBUTION IN SEPARATE CHANNELS OF REACTIONS

I.D. Alkhazov, A.V. Daniel, V.D. Dmitriev, V.N. Dushin, S.S. Kovalenko, K.A. Petrzhak, A.V. Kuznetsov, L.Z. Malkin, B.F. Petrov, V.I. Shpakov
V.G. Khlopin Radium Institute, Leningrad, USSR

Study of prompt neutron multiplicities permits to obtain an important information on the processes with essential alteration of nuclear matter (fission and fusion processes). The date of special interest are those obtained in multiparameter experiments in which measurements of neutron multiplicity are combined with simultaneous measurements of energy, mass and charge characteristics of the reaction products.

The two experimental set ups were designed in the Khlopin Radium Institute comprising gadolinium loaded large liquid scintillation counters of neutrons. Gadolinium was introduced into the scintillation in concentration of 1% what provided counting of 99% neutrons during the 25 μs time interval. Both counters allow to perform measurements either in a 4π-geometry, or in a 2π-geometry in case of their dividing into 2 halves (Fig. 1).

The first variant allows to measure a total neutron multiplicity for some fixed reaction channel. If any correlation exsists between the direction of neutron emission and the velocity of separated reaction products, as it is in case of fission fragments, the second variant gives a possibility to measure twodimensional multiplicity distributions of neutrons emitted by conjugate fragments. In the case of 2π-measurements that is when the counter performs as two separate independent halves the effect of its mutual influence must be taken into account occuring due to both scattering of neutrons from one tank into another and registration of gammas originating in one tank by the other one. To avoid this influence mutual shielding of both tanks must be provided. In the set ups described the 15 cm thick shield of polyethylene and lead was used installed between the tanks which reduced the mutual influence to the value of 5 %.

The counter design admitted employing of different detector systems and reaction chambers and permitted to study either spontaneous fission or reaction induced by accelerator beams.

The main principle of large liquid scintillation counters as well as their common characteristics are well known (for example /1,2/) and here we shall concern only two questions which are determination of the counting efficiency in the geometry of 2π and unfolding of initial multiplicity distributions proceedings from the experimentally measured ones.

The counting efficiency of large liquid scintillator with volume of 150 liters in case of 4π-geometry weakly depends on a reaction channel and can be determined by means of a source of spontaneous fission with a well known $\bar{\nu}$-value. The situation is much more complex when we deal with the 2π-measurements. In this case the efficiency value is to be replaced by an efficiency matrix

$$E = \begin{pmatrix} E_{11} & E_{12} \\ E_{21} & E_{22} \end{pmatrix}$$

where E_{11}, E_{12} are the efficiency of registration of correlated by the both halves of the counter, E_{12}, E_{21} take into account both the efficiency of registration of anticorrelated neutron and effects of the mutual influence of both halves. The elements of this efficiency matrix depend on the reaction kinematics, on the angular distributions and energy spectra of neutrons counted, on the counter shape and on the shielding characteristics.

To calculate the efficiency matrix a Monte-Carlo computer code was prepared in the Chlopin Radium Institute taking into account the geometry of both the counter and shield the scintillation composition, the reaction kinematics, the spectrum and the angular distri-

bution of neutrons. Following processes were considered in the computation. Slowing-down, diffusion and capture of neutrons by gadolinium, hydrogen, spread of gammas, emission of light and its collection by the photo multiplier tubes, leakage of neutrons and gammas out of the counter tanks and arising due to this leakage mutual influence of the counter halves. Verification of the computation results was performed by comparison of the results of measurements in the 2π and 4π geometry.

Another problem of great complexity arising at the neutron multiplicity measurements is unfolding of multiplicity distributions. Initial twodimensional distribution $P(\nu_1, \nu_2)$ are distorted in the measurement process due to the counting efficiency E, due to the presence of a background which has its own multiplicity distribution $P(n_1, n_2)$ and due the pulse pile-up which depends on the time resolution of the counting system τ and on the neutron pulse time distribution connected in turn with the $P(\nu_1, \nu_2)$ and $P(n_1, n_2)$ distributions. Transformation of the initial distribution $P(\nu_1, \nu_2)$ into the experimental one $Q(n_1, n_2)$ can be illustrated in the scheme

$$P(\nu_1, \nu_2) \xrightarrow{E} P'(n_1, n_2) \longrightarrow \tau \longrightarrow Q(n_1, n_2)$$

$$P^b(n_1, n_2) \nearrow \qquad \text{or}$$

in the matrix form

$$Q(n_1, n_2) = \sum_{\nu_1 \nu_2} A_{n_1, n_2, \nu_1, \nu_2}(E, P^b, \tau)\, P(\nu_1, \nu_2) \qquad (1)$$

where $A_{n_1, n_2, \nu_1, \nu_2}(E, P^b, \tau)$ is the operator of the transformation.

Reversion of the equation (1) belongs to a class of mathematicaly incorrect problems and direct methods of its solution lead to great oscillations in the unfolded distributions. In the work /4/ a variant of the method of statistical regularization was proposed for unfolding of onedimensional distributions, employing an aprior information on the solution smoothness. On our opinion the deficiency of this method consists in the complex and many-valued dependences of the momenta of the unfolded distributions on the regularization parameter especialy at low statistics. Our purpose was to study characteristics of mass and energy distributions of fission products for the case of fixed numbers of prompt neutrons what required unfolding of a large number of neutron multiplicity distributions. As a criterion of correct unfolding we chose a conservation of momenta of the partial multiplicity distributions and an equality of the total multiplicity distribution obtained to the known integral data /5/.

The employed method of unfolding was based on an approximation of the multiplicity distributions by convolutions of model probability distributions, whose parameters were selected from the conditions of the experimental momenta descriptions. The Poya generalized distribution was found to be the most advantageous and producing the best description of the experimental data. This distribution depending on the parameters values describes a large class of probability distributions.

The Poya distribution has the generating function of factorial momenta

$$\gamma(S) = (1 + \beta K(1 - S))^{-1/\beta} \qquad (2)$$

It is advantageously to describe the transformation of the initial distribution into experimental one in terms of factorial momenta. In this case the influence of the counting efficiency for onedimensional distributions is reduced to the replacement

$$A'_{[k]} = \varepsilon^k A_{[k]} \qquad (3)$$

where $A_{[k]}$ is the factorial momentum of the order k of the initial distribution, $A'_{[k]}$ is that of the unfolded distribution, ε is the counting efficiency.

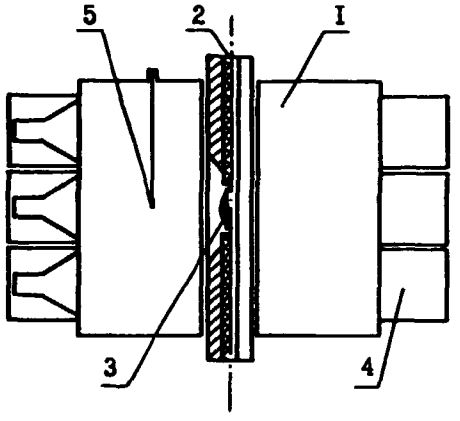

Fig. 1 Schematic drawing of the 2π- and 4π-neutron counters on the base of gadolinium loaded large liquid scintillator

1 - counter tank; 2 - shield at the 2 -measurements; 3 - fission chamber; 4 - PMT; 5 - source of light of the PMT stabilizatuion system.

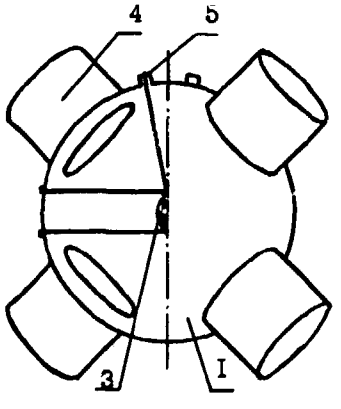

Indeed, let a generating function $\gamma(S)$ of the factorial momenta $A_{[k]}$ of the initial distribution $P(\nu)$ to be equal $\gamma(S) = \sum_{\nu} P(\nu) S^{\nu}$ then a generating function of the factorial momenta $A'_{[k]}$ of the unfolded distribution $P'(n)$ is determined by the expression

$$\gamma'(S) = \sum_{n} P'(n) S^{n} = \sum_{\nu n} C^{n} S^{n} \varepsilon^{n} (1-\varepsilon)^{\nu-n} P(\nu) =$$

$$= \sum_{\nu} (1+\varepsilon(S-1))^{\nu} P(\nu) = \gamma(1+\varepsilon(S-1)) \quad \text{and}$$

$$A'_{[k]} = \frac{d^k}{dS^k} \gamma(1+\varepsilon(S-1)) \Big|_{S=1} = \varepsilon^k A_{[k]} \tag{4}$$

In neglect of the effects of pulse pile-up ($\tau = 0$) factorial momenta of the experimental distribution $Q(n)$ are given by the expression

$$A^{g}_{[k]} = \sum_{i} C^{i}_{k} A'_{[i]} A^{b}_{[k-i]} \tag{5}$$

where $A^{b}_{[m]}$ are factorial momenta of the background distribution $P^{b}_{(n)}$.

In the first approach linear on τ the effect of pile-up is taken in to account by the expression

$$A^{g}_{[k]}(\tau) = C^{k}_{1}(\tau) \; A^{g}_{[k]}(\tau=0) - \tau C^{k}_{2}(\tau) \; A^{g}_{[k+1]}(\tau=0) \tag{6}$$

where $C_1^k(\tau)$ and $C_2^k(\tau)$ depend on the shape of the neutron life time curve in the scintillation and can be calculated numerically. Thus the factorial momenta of the initial distribution can be calculated on the basis of the equations (3), (4), (5), (6). It is advantageously to present the initial distribution by a convolution of model probability distributions in terms of semiinvariants

$$\chi_k = \frac{d^k}{ds^k} \ln \gamma(s) \quad S = 1$$

The expressions for the first there semiinvariants are:

$$\begin{aligned} \chi_1 &= A[1] = \bar{\nu} \\ \chi_2 &= A[2] - A^2[1] \\ \chi_3 &= A[3] - 3A[2]A[1] + 2A^3[1] \end{aligned} \tag{7}$$

The generating function of momenta of a convolution is a product of the partial generating functions. Hence semiinvariants of the resulting distribution are expressed via the sum of those of distributions forming the convolution.
For the Poya distribution the semiinvariants are given by the expression

$$\chi_i^p = (i-1)!\ \bar{k} \cdot \vartheta^{i-1} \tag{8}$$

where $\vartheta = \beta \bar{k}$

By comparing of model semiinvariants to the experimental ones a set of equations can be derived from which parameters of the theoretical model can be obtained

$$\begin{cases} \bar{K}_1 + \dots\dots\dots + \bar{K}_e = \chi_1 = \bar{\nu} \\ \vdots \\ \bar{K}_1 \vartheta_1^{2e-1} \dots\dots\dots + K_e \vartheta_e^{2e-1} = \chi_{2e}/(2l-1)! \end{cases} \tag{9}$$

The solution of this set of equations reduces to the solution of an algebraic equation of the pover e and of a set linear equations. After parameters of the approximating distributions are found the distributions themself can be calculated on the basis of the equations

$$\begin{aligned} P(0) &= (1+\vartheta)^{-1/\beta} \\ P(K) &= \left(\frac{\bar{K}}{1+\vartheta}\right)\left(\frac{1+\beta(K-1)}{K}\right) \cdot P(K-1) \end{aligned} \tag{10}$$

and the initial distribution is a convolution of the model distributions obtained.
The advantages of the methods employed was an automatic conservation of the momenta and realization of conditions of both smoothness and positivness. By this way a computer code has been prepared, produced an automatic selection of the number of fitting parameters depending on the both statistics and shape of the experimental distribution.

In the case of measurements in the 2π-geometry the unfolding procedure becomes much more cumbersome though the common approach does not changes. Corresponding program is now in progress.

References

/ 1/ H. Nifenecker et al., Report LBL-1950, Berkeley, USA, 1973

/ 2/ I.D. Alkhazov et al., Neutron Physics, Proc. of the 6-th All-union Conf. on Neutr. Physics, Kiev, 1983, M. 1984 v. 1, p. 329

/ 3/ A.V. Daniel et al., Preprint of the Khlopin Radium Inst., RI-170, L. 1983

/ 4/ Yu.A. Lazarev, Atomic Energy Review, 15, 75, (1973)
/ 5/ J.W. Boldeman, M.G. Hines, Nucl. Standard Ref. Data, Proc. of an Advisory Group Meeting on Nucl. Stand. Ref. Data IAEA - TECDOC - 335, Vienna, 1985, p. 242

ИЗОМЕРНОЕ ОТНОШЕНИЕ И СЕЧЕНИЕ РЕАКЦИИ ^{237}Np (n, 2n)

А.В.Игнатюк, Н.В.Корнилов, В.М.Маслов, А.Б.Пащенко

Физико-энергетический институт

Аннотация

В рамках последовательного оптико-статистического подхода рассчитаны изомерное отношение и сечение реакции ^{237}Np (n, 2n). Получено согласованное описание всей совокупности экспериментальных данных о сечениях деления и реакции (n, 2n). Результаты проведенных расчётов могут служить основой для оценки сечений реакции ^{237}Np(n, 2n) в диапазоне энергий от порога до 20 МэВ.

Введение

Интерес к сечениям реакции ^{237}Np (n, 2n) определяется в первую очередь, практическими потребностями ядерной энергетики. Реакция (n, 2n) с возбуждением короткоживущего состояния $^{236}Np^{m}$ является одним из главных источников накопления в быстрых реакторах изотопа ^{232}U, сильно осложняющего переработку ядерного топлива. Эта же реакция является нежелательным конкурентом при производстве в реакторах изотопа ^{238}Pu, используемого в качестве интенсивного α-источника /I/.

К ранее имевшимся экспериментальным данным о реакции ^{237}Np (n, 2n) $^{236}Np^{m}$ при энергии нейтронов около I4 МэВ /2-6/ и одной точке при энергии 9,6 МэВ /6/ в последние годы добавились измерения сечений в области энергий от 7 до I0 МэВ /7/. Эти данные не охватывают, однако, весь диапазон энергий от порога до 20 МэВ, важный для прикладных задач, и необходимость надежного определения сечений во всем диапазоне по прежнему остается актуальной.

Значительный интерес представляет и вторая ветвь реакции ^{237}Np (n, 2n), в которой образуется долгоживущее состояние $^{236}Np^{1}$. В этом состоянии нептуний обладает столь высоким сечением деления для тепловых нейтронов 2500 ± I50 б /8/, что накопление данного изотопа при длительной работе реактора может существенно отражаться на балансе нейтронов. Получение прямых экспериментальных данных об этой реакции, а, следовательно, и о полном сечении (n, 2n)-реакции крайне затруднено. Поэтому сколь-либо надёжная оценка сечений в настоящее время может быть осуществлена лишь с помощью теоретических расчётов. Проведение таких расчётов в рамках достаточно последовательных и согласованных с экспериментом на близлежащих ядрах теоретических моделях является целью настоящей работы.

I. Схема низколежащих уровней ядра ^{236}Np

Экспериментальному исследованию спинов нижайших состояний ^{236}Np посвящен целый ряд работ /9-I7/. Для долгоживущего состояния $^{236}Np^{1}$ с периодом полураспада $I,I5 \cdot I0^{5}$ лет показано, что при его β^{-}-распаде образуется изотоп ^{236}Pu в состоянии со спином 6^{+}, а при е-захвате в аналогичном состоянии образуется

^{236}U /II,I2/. Столь полное в пределах экспериментальных погрешностей заселение уровней 6^+, подтверждаемое расчетами величин $\lg f$, служит весьма веским аргументом для идентификации спина и четности 6^- долгоживущего состояния $^{236}Np^1$. Исследования короткоживущего состояния $^{236}Np^s$ с периодом полураспада 22,5 часа показали, что при его β^- - распаде заселяются основное состояние 0^+ и первый возбужденный уровень 2^+ изотопа ^{236}Pu, а при е-захвате - уровни $0^+, 2^+$ и 2^- изотопа ^{236}U /II-I6/. Это позволяет приписать состоянию $^{236}Np^s$ спин I, но вопрос о четности этого состояния остается открытым.

Таким образом спины образующихся в реакции ^{237}Np (n, 2n) долгоживущего и короткоживущего состояний можно считать достаточно надежно определенными. Какое из этих состояний является основным и какое изомерным, какова энергия возбуждения изомерного состояния, а также какова схема других низколежащих уровней ядра ^{236}Np еще не установлено. Известно лишь присутствие уровня 3^-, для которого в работе /I6/ при изучении α- распада ^{240}Am был продемонстрирован облегченный характер α- перехода, свидетельствующий о подобии структуры образующегося состояния ядра ^{236}Np со структурой 3^-($5/2^-[523]p$, $1/2^+[631]n$) основного состояния ^{240}Am. Это подобие структур, так же спектры нижайших одночастичных уровней соседних нечетных ядер можно использовать для теоретического моделирования низколежащих уровней ^{236}Np. В работе /I6/ для этой цели были взяты два первых нейтронных одночастичных состояний $7/2^-$/743/ и $1/2^+$/631/ ядер ^{235}U и ^{237}Pu, а также первые протонные состояния $5/2^+$ /642/ и $5/2^-$/523/, наблюдаемые в ядрах ^{235}Np и ^{237}Np. Полученный спектр нижайших протон-нейтронных состояний ^{236}Np показан на рис.Iа. В работе /I7/ использовались те же исходные конфигурации нуклонов, но несколько иначе было выбрано остаточное взаимодействие нуклонов в рассматриваемых состояниях. Полученный спектр состояний приведен на рис.Iб. Для построения полной схемы уровней представленные на рис.I состояния были дополнены ротационными полосами с энергиями

$$E_{JK} = E_K + A\,[J(J+1) - K(K+1)]\,, \qquad (I)$$

где параметр A=5,5 кэВ определен на систематики ротационных полос близлежащих нечетных изотопов урана и нептуния /I8/.

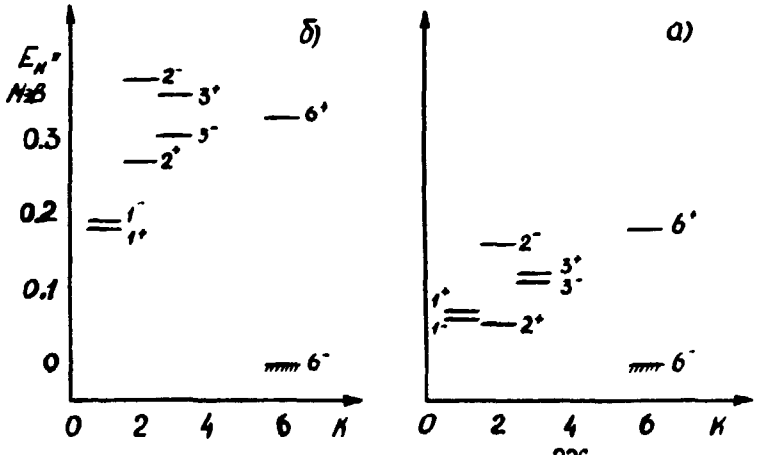

Рис.I. Схема нижайших квазичастичных уровней ^{236}Np по данным работ /II/ - а) и /I6/ - б).

Ни одна из рассмотренных выше схем , естественно, не претендует на высокую точность. Расхождения между этими схемами фактически отражают существующие неопределенности моделирования низколежащих уровней ядра ^{236}Np . Согласно соотношению (I) в диапазоне энергий возбуждения до I МэВ должны присутствовать уровни с угловым моментом до ~ I5 и полное число уровней, построенных на нижайших квазичастичных основаниях ротационных полос (рис.I), достигает ~ I20.
С другой стороны, в работе /I9/ при систематике полного числа наблюдаемых низколежащих уровней актинидов показано, что число уровней с энергией возбуждения ниже заданной U можно достаточно хорошо описать соотношениями модели постоянной температуры

$$\mathcal{N}(U) = \exp(\delta/T)\left[\exp(U/T) - 1\right] , \qquad (2)$$

где $\delta = 0$, Δ_0 и $2\Delta_0$ для четно-четных, нечетных и нечетно-нечетных ядер, соответственно. Для всех актинидов можно принять среднее значение температуры T = = 0,388 МэВ и величину $\Delta_0 = I2/\sqrt{A}$ МэВ. На основе данной систематики следует ожидать до I50 уровней ниже энергии 0,5 МэВ и примерно 700 уровней ниже энергии I МэВ. Эти цифры весьма существенно превышают число рассмотренных выше дискретных уровней, и это указывает на важную роль корректного совмещения верхней границы дискретных уровней с нижней границей статистического описания уровней.

2. Расчёты сечений и изомерного отношения

Для расчётов сечений реакций, протекающих при взаимодействии нейтронов с ядром-мишенью ^{237}Np , использовалась статистическая модель, учитывающая законы сохранения углового момента и четности на всех этапах распада возбужденных ядер. Совместно с компаундным механизмом распада в модели учитывалось также предравновесное испускание нейтронов. Необходимые для статистических расчетов коэффициенты прилипания нейтронов были получены в рамках обобщенной оптической модели,описывающей совокупность нейтронных сечений детального изученного близлежайшего изотопа ^{238}U /20/. Для вычисления плотности уровней нейтронного и делительного каналов использовались соотношения сверхтекучей модели ядра с феноменологическим учетом оболочечных и коллективных эффектов /I9/. При этом параметры плотности уровней делительного канала, а также барьеры деления рассматриваемых ядер были получены согласованным образом из анализа сечений деления в области первого "плато" /2I/. Параметры предравновесной модели были выбраны из условий оптимального описания спектров неупругого рассеяния нейтронов изотопом ^{238}U /22/. Совместный анализ сечений деления и сечений (n ,2n)-реакций для изотопов ^{235}U и ^{238}U, имеющих наиболее полную экспериментальную информацию об энергетической зависимости рассматриваемых сечений, позволяет сделать вывод, что выбранная статистическая модель хорошо описывает всю совокупность экспериментальных данных и, следовательно, она является оптимальной для расчётов интересующих нас сечений реакций ^{237}Np (n ,2n).
Для расчётов изомерного отношения первостепенное значение имеет выбор схемы низколежащих дискретных уровней остаточного ядра ^{236}Np и определение вероятностей гамма-переходов между этими уровнями. Выше уже отмечалось, что необходимые для этого экспериментальные данные почти полностью отсутствуют. Поэтому в расчёты была заложена наиболее простая схема развития гамма-каскада: статистическое описание вероятности E I, E 2 и M I переходов в области непрерывного спектра и переходы только внутри ротационных полос для дискретных уровней.

Такое рассмотрение позволяет рассчитать заселенность нижайших двухквазичастичных состояний, показанных на рис.I. Далее использовалось предложение, что переход в основное 6^- или изомерное I^- состояния определяется условиями минимальной мультипольности гамма-квантов. Согласно такому предложению все состояния со спинами $J \leqslant 3$ должны заселять изомерное состояние, тогда как состояния с более высокими спинами - основное. Варьируя схему низколежащих состояний и границу дискретного и статистического описания спектра низколежащих уровней, мы добивались согласия расчетов изомерного отношения с имеющимися экспериментальными данными.

Учитывая неопределенности теоретического моделирования дискретных уровней и вероятностей переходов между ними, мы не должны надеяться на корректность расчетов абсолютной величины изомерного отношения. Однако, статистический подход позволяет проследить изменения заселенностей состояний с различными спинами при изменении энергии налетающих частиц и, добившись описания экспериментальных в одной точке, можно достаточно надежно воспроизвести энергетические изменения изомерного отношения.

3. Обсуждения результатов расчётов.

На рис.2 представлены результаты расчета изомерного отношения $r = \sigma^{1}_{n,2n}/\sigma^{s}_{n,2n}$ для различных схем низколежащих состояний ^{236}Np. Можно видеть, что даже сравнительно небольшие изменения относительного положения ряда уровней существенно влияют на абсолютную величину изомерного отношения. При этом, однако, практически не изменяется характер энергетической зависимости этого отношения. Схема уровней рис.Iа позволяет с хорошей точностью описать единственное экспериментальное значение изомерного отношения /I0/.

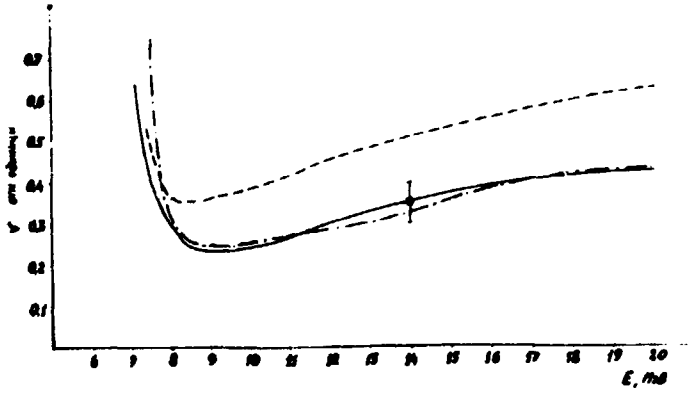

Рис.2. Энергетическая зависимость изомерного отношения в реакции ^{237}Np (n ,2 n), сплошная кривая - расчеты со схемой уровней рис.Iа), пунктир - со схемой рис.Iб), штрихпунктир- результаты расчётов /23/, ♦ - экспериментальное значение изомерного отношения /I0/.

Вместе с результатами настоящей работы на рис.2 приведены также расчеты работы /23/, в которых моделировались 720 дискретных уровней в интервале энергий возбуждения до I,5 МэВ. К сожалению, мы не имеем полного описания этой схемы

уровней и вероятностей переходов между дискретными уровнями. Следует, однако, отметить, что даже столь большое число уровней остается еще в 3 раза меньшим, чем следует из статистического описания (2). Поэтому, необходимость нормировки на экспериментальное значение изомерного отношения не снимается и при большом числе дискретных уровней. В то же время, близкое согласие расчетов /23/ с нашими расчетами, привязанными к наблюдаемому изомерному отношению, позволяет считать полученную энергетическую зависимость изомерного отношения достаточно надежной оценкой.

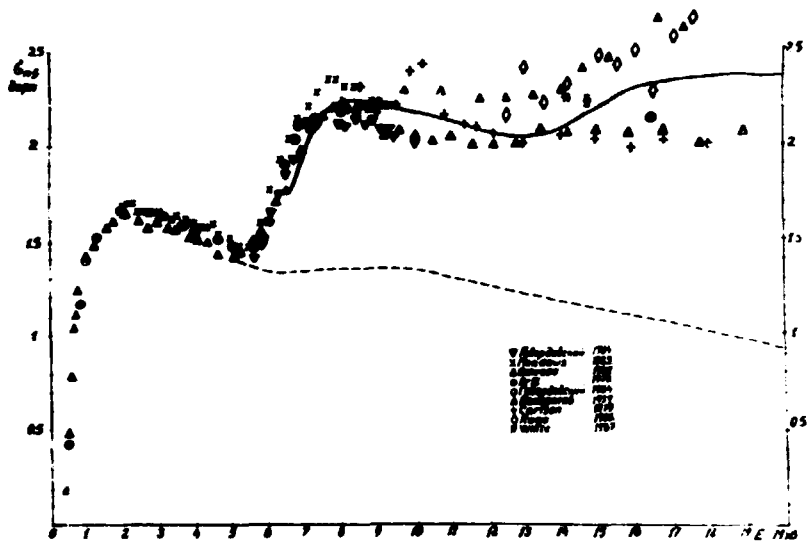

Рис. 3. Экспериментальные данные о сечении деления и результат теоретического расчета (сплошная линия).
Пунктиром показан расчет первого шанса деления.

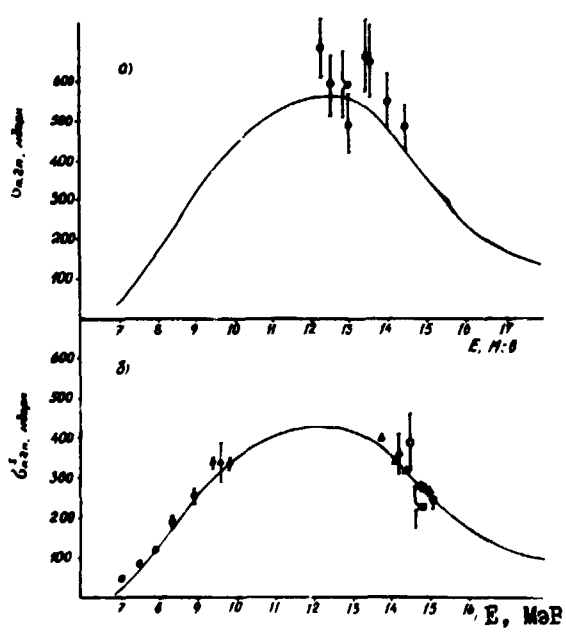

Рис.4.а)Полное сечение реакции (n,2n):
ϕ -экспериментальные данные из работы /24/, сплошная линия - результаты теоретического расчёта.
б)Сечение реакции (n,2n) с образованием короткоживущего состояния.Экспериментальные значения работ: △ -/2/, ■ -/3/, ▽ -/4/, □ -/5/, ▲ -/6/, ● -/7/. Сплошной линией показана величина $\sigma_{n,2r}/(1+r)$.

На рис.3 и 4 показаны совместно с имеющимися экспериментальными данными результаты теоретических расчетов сечения деления и полного сечения (n,2n). Необходимо подчеркнуть, что прямые данные о сечении реакции ^{237}Np (n, 2 n) отсутствуют на рис.4 использованы косвенные данные, полученные из реакций (t,2 n). (α, 2 n) и обладающие значительной погрешностью /24/. Ввиду этого, более информативным оказывается сопоставление расчетов с имеющимися данными о сечении образования короткоживущего состояния. Результаты, приведенные на рис.4б показывают, что рассчитанная величина $\sigma/(1+r)$ достаточно хорошо описывает экспериментальные значения $\sigma^{*}_{n,2n}$. Некоторые расхождения расчетов с экспериментом имеются при энергиях ниже 7 МэВ. В этой области возбуждение остаточного ядра ^{236}Np столь мало, что закономерности статистического моделирования вероятности гамма-переходов становятся мало оправданными. Однако, при имеющихся неопределенностях схем уровней добиваться описания околопорогового поведения изомерного отношения в реакции (n,2 n) нецелесообразно.

Следует отметить, что согласованное описание экспериментальных данных об изомерном отношении и сечении реакции ^{237}Np (n,2 n) ^{236}Np* на основе выбранного оптического потенциала и соответствующего ему сечения образования составного ядра достигается, если сечение деления при энергиях выше 14 МэВ проходит ближе к данным /30/ и оказывается на 200 ÷ 300 mb выше результатов работ /31,32/. Снижение сечения деления до уровня данных /31,32/ потребует увеличения изомерного отношения до ~ 0,8 или соответствующего изменения сечения образования составного ядра. Таким образом, полученные результаты в области энергий 8 ÷ 15 МэВ адэкватны всему набору экспериментальных данных о сечениях деления, образования короткоживущего изомера и изомерного отношения.

Энергетическая зависимость полного сечения реакции (n,2 n) полученная в настоящей работе существенно отличается от ранее выполненных оценок (рис.5).

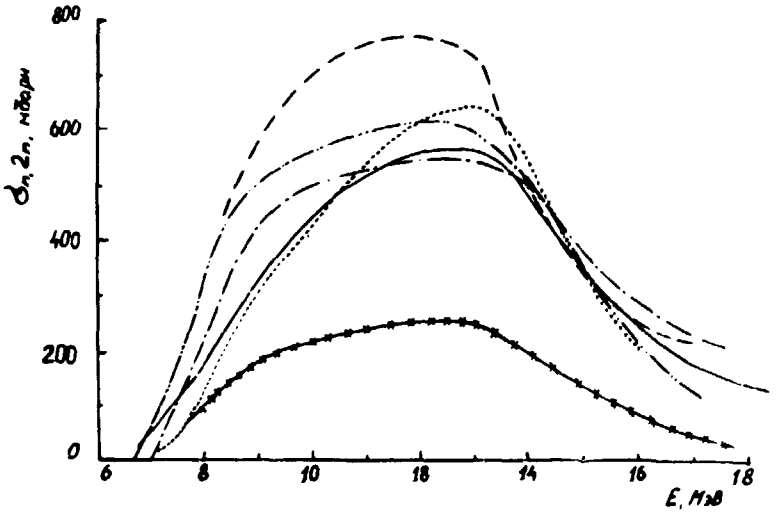

Рис.5. Полное сечение (n,2 n) по данным различных работ:
——— - настоящая работа, -·· - /25/, - - - /26/,
- · - /27/, ... - /28/, - ж - /29/.

Наибольшее согласие наблюдается с данными работы /28/, однако при $E_n < 9$ МэВ результаты работы /28/ проходят ниже нашей зависимости и экспериментальных данных о сечении образования короткоживущего изомера. Результаты настоящей работы слабо чувствительны к неопределенности сечения деления, поскольку главным критерием проверки теоретических расчетов являлось описание экспериментальных данных об изомерном отношении и сечении $\sigma^{*}_{n,2n}$. Поэтому погрешность оцененного сечения (n ,2n) в основном определяется точностью экспериментальных данных $\Delta r/r$ (I4 МэВ) = I4%, $\Delta\sigma/\sigma^{*}_{n,2n}$ =5÷20%. Следует, однако отнестись осторожно к рекомендуемым сечениям (n ,2n)-реакции, так как наиболее существенная для расчетов величина-изомерное отношение-изомерно только в одной работе.

Заключение

На основе теоретических расчетов в рамках теории Хаузера-Фешбаха с учетом закона сохранения моментов удается расчитать изомерное отношение в реакции ^{237}Np(n , 2n). Неопределенность моделирования схемы уровней ^{236}Np по всей видимости слабо влияет на энергетическую зависимость изомерного отношения.
Погрешность расчитанного сечения реакции (n ,2n) главным образом определяется погрешностью экспериментальных данных об изомерном отношении и сечении образования короткоживущего состояния. Однозначная оценка погрешности затруднена малочисленностью экспериментальных данных об изомерном отношении.
Проведенные теоретические расчёты могут быть полезны в практической деятельности при оценке сечений и создании полного файла нейтронных сечений ^{237}Np . Учет теоретических расчетов при проведении оценки в значительной мере может компенсировать скудность и неопределенность экспериментальных данных.

Литература

1. Круглов А.К.,Рудик А.П. Реакторное производство радиоактивных изотопов.М.: Энергоатомиздат,1985.
2. Landrum I., Nagle R., Lindner M.- Phys. Rev., 1970, v.C8, p.1938.
3. Громова Е.А.,Коваленко С.С.,Немилов Ю.А. и др.-Атомная энергия.1983,т.54, с.108.
4. Lindeke K., Spect S., Born H.J. - Phys. Rev., 1975, v. C12, p. 1507.
5. Perkin J.L., Coleman R.F. - J.Nucl. Energy A/B, 1961, v.14, p.69.
6. Nishi T., Fujiwava I., Imanishi N. INDC(JAP) - 28 "L", 1975.
7. Корнилов Н.В.,Барыба Е.Я.,Балицкий А.В. и др.-Атомная энергия,1985,т.58, с.117.
8. Mughabghab S.F. Neutron Cross Sections, v.1, part B. N.Y.: Academic, 1984.
9. Schmorak M. - Nuclear Data Sheets, 1982, v. 36, p. 367.
10. Myers W.,Lindner M.,Newbury R. - J. Inorg.Nucl.Chem, 1975, v.37, p. 637.
11. Lindner M. et al. - J. Inorg Nucl. Chem., 1981, v. 43, p. 3071.
12. Ahmad I., Hines J., Gindler J. - Phys. Rev., 1983, v. C27, p. 2239.
13. Gray P.H. - Phys. Rev. 1956, 101, p. 306.
14. Gindler J., Sjoblom R. - J. Inorg. Nucl. Chem., 1959, v. 12, p. 8.
15. Liderer C.M. et al. - Nucl. Phys., 1969, v. A135, p. 36.
16. Gorman D.J., Asaro F. - Phys. Rev., 1970, v. C22, p. 2406.
17. Sood P.C. - Z. Phys., 1983, v. A318, p. 111.
18. Бор О.,Моттельсон Б.Структура атомного ядра.М.:Мир,1977,т.2.
19. Анципов Г.В.,Коньшин В.А.,Маслов В.М.- In: Proc. of IAEA Consult. Meeting, Vienna, INDC-129/G7, 1981, p. 329.
20. Lagrange Ch. Report INDC(FR)-56/L, 1982.
21. Игнатюк А.В. и др.-Ядерная физика,1985, т.42,с.569.
22. Груздевич О.Т. и др.-В кн:Нейтронная физика.М.:ЦНИИАтоминформ,1984,т.2,с.318.
23. Gardner D.G., Gardner M.A., Hoff R.W. Report UCAR-10062-83/1, p. 51.
24. Андреев М.Ф.,Серов В.И.-В кн.:Нейтронная физика.М.:ЦНИИАтоминформ,1980.ч.3,301.
25. Seger M., Caner M. - Ann. Nucl. Energy, 1978, v. 5, p. 239.
26. ENDL-76, UKRL-50014, v. 15, part D, rev 1, 1978
27. Бычков В.М.,Пляскин В.И.-Ядерная физика,1984,т.39,с.684.
28. Fort E.,Derrien H.,Doat J.-In:Nucl.Data for Science and Technology.Antwerpen,1982.
29. ENDF/B-V, Actinide File, MAT - 1337.
30. Arlt R. et al. - ZFK-382, 1979, p. 180.
31. Behrens J.W.,Brown J.A. et al.- Nucl. Sci. and Ergin., 1982, v. 80, p. 393.
32. Carlson A.D., Patrick B.N. - In: Proc. Inter. Conf. on Nuclear Data. Knoxvill, 1979, NBS, 1980, v. 1, p. 971.

MEASUREMENT OF THE TOTAL PROTON EMISSION CROSS SECTION OF NEUTRON INDUCED REACTION ON ^{60}Ni AT 18.5 MeV.

A.Korman, B.Mariański, J.Rondio, K.Czerski

Institute for Nuclear Studies, 00-681 Warsaw, Hoża 69, Poland.

The experimental data for proton emission cross sections neutron induced reactions are very scarce especially at neutron energies different than 14-15 MeV. The growth of interest in studying of these reactions can be noticed in the connection with assessing radiation damage of materials for future fussion reactors [1].

We have measured the differential proton emission cross section of ^{60}Ni(n,p) ^{60}Co reaction at 18.5 MeV. The study of this reaction in 3-30 MeV neutron energy range is also significant in dosimetry [2].

The angular distribution of protons from this reaction was measured in the range 0°-170°, with a 10° step.

The experiment was carried out with the help of an eight-telescope chamber [3]. Neutrons were produced in the ^{3}T(d,n)^{4}He reaction, the deuterons being accelerated to 2.3 MeV in a Van de Graaff accelerator. The neutron energy spread due to deuteron energy loss in T-Ti target and the geometrical conditions was about ± 150 keV. The target used was ^{60}Ni deposited electrolytically on 1mm tantalum backing. Its dimensions were 12÷15mm and its thickness was 20 mg/cm^2. The background was measured by replacing the target with the backing. The absolute normalization of the cross sections was provided by measuring the protons recoiled from the polyethylene target.

The angle integrated proton spectrum was obtained according to the following formula

$$\sigma_T(E_i) = \frac{4\pi \sum_k \sigma_k(E_i) \sin\theta_k}{\sum \sin\theta_k}$$

where $\sigma_k(E_i)$ is a differential cross section measured at angle θ_k.

This spectrum is shown in figure 1 and is compared with the results of the combined pre-equilibrium hybrid model and multi-stage nuclear reaction Hauser-Feshbach calculations. The calculations were made with the help of code EMPIRE [4] and included the contributions from (n,p) and (n,np) reactions, and the pre-equilibrium contribution in the first step of the reaction. The calculated (n,p) spectrum includes all the reactions in which the proton is emitted as a first particle. The optical-model parameters used in this calculation were those proposed by Becchetti and Greenless [5] for protons and neutrons and by Mc Fadden and Satchler [6] for α particles. Level density parameters were taken from Gilbert and Cameron [7]. We see that, in general, there is agreement between our data and the EMPIRE results, although the EMPIRE data exceeded experimental ones, especially in the high-energy region of the spectrum. This suggests that the contribution due to pre-equilibrium is overestimated.

The experimental total cross section value integrated in the proton energy range from 3 MeV to 17 MeV is 420 mb, the calculated value is 450 mb.

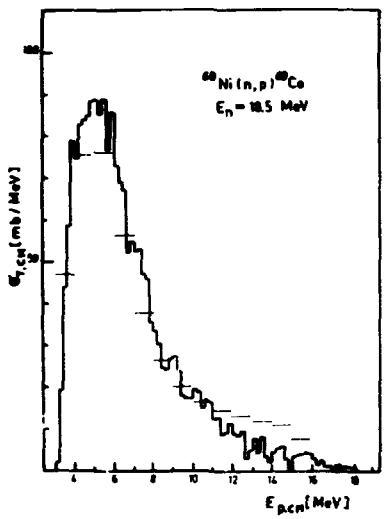

Fig.1. The angle integrated spectrum of protons from the neutron induced reaction on ^{60}Ni at 18.5 MeV. The horizontal bars represent the results of combined pre-equilibrium multi-stage Hauser-Feshbach calculations.

In spite of differences between the shapes of experimental and calculated spectra the obtained values agree very well.

The angle integrated experimental spectrum was fitted by the sum of (n,p) and (n,np) compound spectra the ratio $\sigma(n,p)/\sigma(n,np)$ being suitable adjusted. The calculation was performed with the approximate formulae. The method of calculation is fully described elsewhere [8]. The dotted line in figure 2. is a result of this fitting. Some structure is seen above the calculated compound continuum. The cross section of noncompound processes (structure above the calculated continuum) is 60 mb. The EMPIRE calculated compound cross section is 330 mb what agrees with the experimental value 360 mb obtained after the subtraction of noncompound processes. There are suggestions that the noncompound processes are due to multistep proton emission from GDR doorway states [9].

Total proton emission cross section has been measured only at 14.8 MeV neutron energy [10]. The obtained value was 325 mb. The cross sections of the (n,p), (n,np) and (n,pn) reactions change in different way with neutron energy. The (n,p) reaction cross section was measured by activation method and the obtained value was 112 mb and 70 mb at 14.8 MeV and 18.5 MeV neutron energy, respectively [11].

Any data about (n,pn) + (n,np) reactions cross sections at 18.5 MeV are not available. Evaluation maid by P.Guenther et al. [11] gives a rapid increase of the cross section to a value of 310 mb at 18.5 MeV. The sum of the measured (n,p) reaction cross section and the evaluated (n,np) + (n,pn) one is in reasonable agreement with the value obtained by us. The error of the measured cross section was estimated to be about 10%.

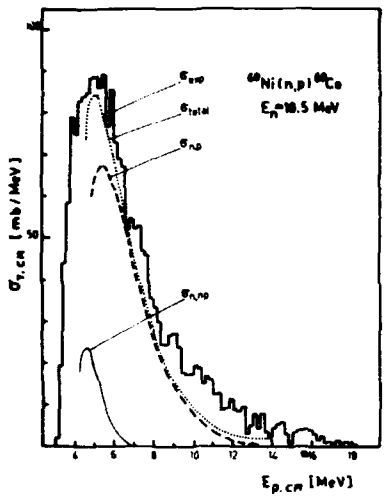

Fig.2. The angle integrated spectrum of protons from the neutron induced reaction on ^{60}Ni at 18.5 MeV. The dashed and full lines represent compound proton spectra of (n,p) and (n,np) reactions calculated according to the approximate formulae. The resulting continuum (dotted line) also includes a small pre-equilibrium contribution.

References:

1. R.C.Haight, S.M.Grimes and R.G.Johnson, H.H.Barschall, Phys. Rev. C. 23 1981 700.
2. Symp. of Neutron Cross-sections from 10 to 40 MeV, 1977, ed. M.R.Bhat and S.Pearlstein BNL-NSC-50681 p.30 .
3. B.Mariański, J.Rondio, A.Korman, Nucl. Instr. Methods 206 1983 421.
4. M.Herman, A.Marcinkowski, K.Stankiewicz, Comput. Phys. Commun.33 1984 373.
5. F.D. jr Becchetti and G.W.Greenlee, Phys. Rev. 182 1969 1190.
6. W.R. Mc Faden and G.R.Satchler, Nucl. Phys. A84 1966 177.
7. A.Gilbert and A.G.W.Cameron, Can. J. Phys. 43 1965 1146.
8. J.Rondio, B.Mariański, A.Korman, J. Phys. G: Nucl. Phys. 11 1985 549.
9. J.Rondio, B.Mariański, A.Korman, K.Czerski, Proceedings of the 17th Mikołajki Summer School on Nuclear Physics. Mikołajki, September, 1985.
10. S.M.Grimes, R.C.Haight, K.R.Alvar, H.H.Barschall and R.R.Borchers, Phys. Rev. C 19 1979 2127.
11. P.Guenther, A.Smith, D.Smith, J.Whalen, R.Howerton, Argonne National Laboratory Report No. ANL/NDM-11.

TWO TARGET DSAM FOLLOWING THE (n,n'γ) REACTION WITH FAST REACTOR NEUTRONS

M. Georgieva, D. Elenkov, G. Toumbev
Institute of Nuclear Research and Nuclear Energy
1184-Sofia, Bulgaria

A version of the Doppler Shift Attenuation Method (DSAM) has been applied for the first time to measure lifetimes of nuclear states excited in the (n,n') reaction with reactor fast neutrons simultaneously in two targets. The experimental arrangement and the procedure of experimental data treatment are briefly described.

I. Experimental arrangement

The applicability of the (n,n'γ) reaction, i.e. inelastic neutron scattering, to mean lifetime measurements of excited nuclear states was originally pointed out by Nichol and Kennett in the early seventies [1]. On the other hand, Warburton et al. [2] suggested and Antilla et al. [3] applied to DSAM the idea of the two-target method using charched particles reactions.

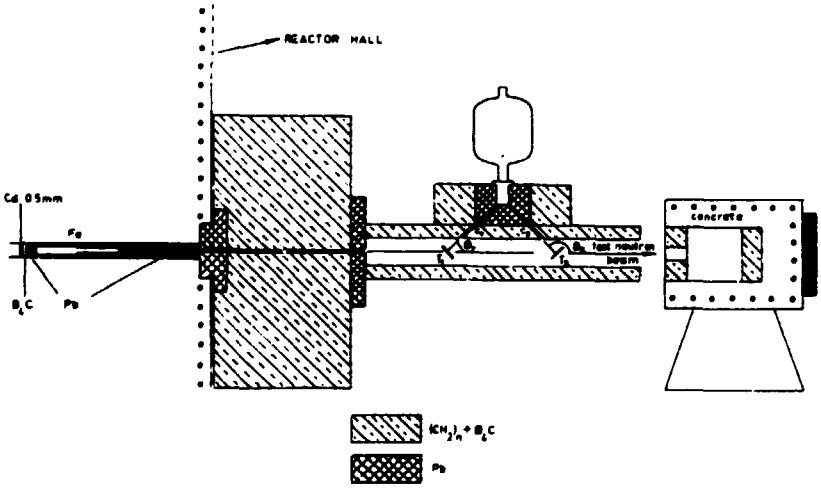

Fig. 1. Two-target experimental arrangement for DSAM after a (n,n'γ) reaction with reactor fast neutrons.

In the way, shown in fig.1 we developed and applied this method to the reaction (n,n'γ) with reactor fast neutrons which, in our opinion, has the following advantages:

i) during the simultaneous measurement of the γ-peaks from the two targets, the electronic drift is unidirectional and it affects the two Doppler-shifted γ-peaks in the same way. For this reason, the distance between their barycenters ΔE (measured in DSAM) does not depend on the drift

ii) the neutron beam is more effectively used - actually the beam is used approximately twice

iii) due to the fixed geometry, the background conditions remain the same

during the whole time of the measurement.

In our experiments Ge(Li)-detectors of effective volume 28, 60 and 75 cm^3 are usually used. The resolution is about 2.5 keV at 1.33 MeV. Targets of approximate size of 100 x 60 x 8 mm are used, $\Theta_1 = 45^\circ$, $\Theta_2 = 135^\circ$, the distance between the targets being about 70 cm. To ensure the same beam intensity on the two targets, if necessary the target M_1 accepts special geometry - it is made thinner or slits are made in it. Some experimental spectra, obtained in the above described way of measurement, are shown in fig.2.

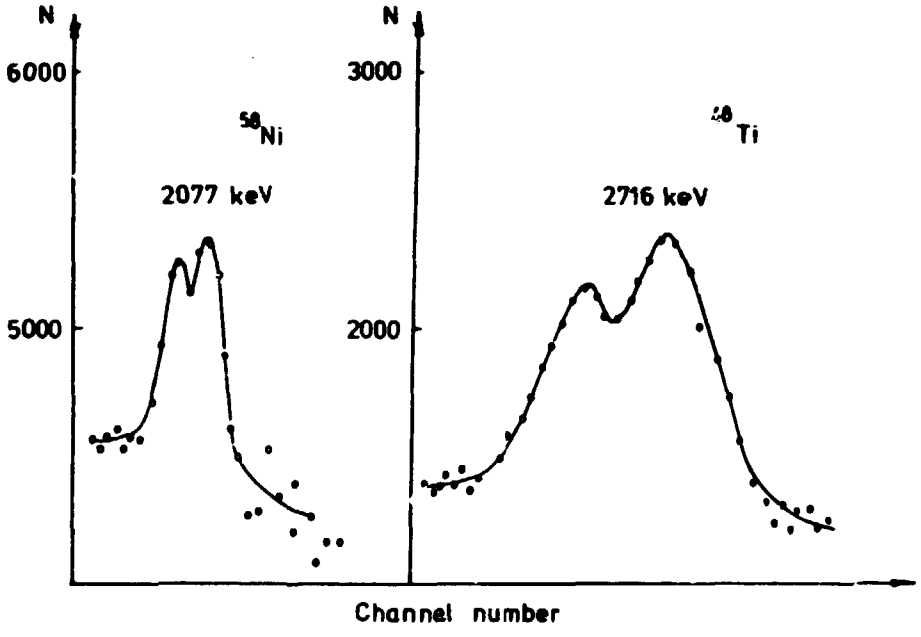

Fig. 2. Typical experimental spectra of Doppler-shifted energies of γ-transitions.

II. Processing of the experimental data. Results.

To obtain the mean lifetime of a given excited state, the experimentally measured Doppler shift ΔE is used to find the so-called attenuation factor F^{exp}

$$F^{exp} = \frac{\Delta E}{E_\gamma^0 \beta_0 (\cos\Theta_1 - \cos\Theta_2)}$$

where E_γ^0 is the energy of the unshifted γ-ray and β_0 is a measure of the recoiling nucleus velocity. On the other hand, $F^{th}(\tau)$ is calculated according to standard Blaugrund's theory /4/ from the expressions

$$F^{th}(\tau) = \frac{1.62 \cdot 10^{-16} A Z^{2/3}}{\tau \beta_0 d} \int_{\varepsilon_0}^{0} \frac{0.29 + \varepsilon}{\sqrt{\varepsilon}(K\varepsilon + B)} \langle \cos\Phi \rangle e^{-\mu} d\varepsilon$$

for homogeneous and

$$F^{th}(\tau) = \frac{T}{\tau}\sqrt{\frac{M}{2}} \int_{\varepsilon_0}^{0} \left(\frac{d_e\varepsilon + d_n}{d_e\varepsilon_0 + d_n}\right)^{\lambda} \left(\frac{d_e\varepsilon_0\varepsilon + d_n\varepsilon}{d_e\varepsilon_0\varepsilon + d_n\varepsilon_0}\right)^{\mu} \left(\frac{\varepsilon}{\varepsilon_0}\right)^{1/2} \frac{d\varepsilon}{d_e\varepsilon + d_n}$$

for heterogeneous stopping medium. The notation is as Blaugrund's one.

The mean lifetime τ is derived from the position of F^{exp} on the slope of the curve $F^{th}(\tau)$ as it is shown in fig.3. For full details see ref./5/. To illustrate the method some results are presented in the table below.

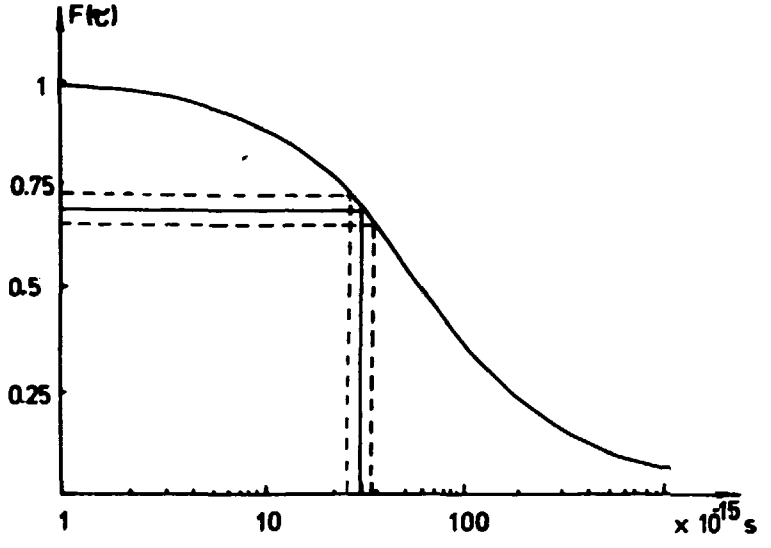

Fig. 3. Theoretically calculated $F^{th}(\tau)$ and finding τ from F^{exp}.

Table 1
Examples of mean lifetimes obtained by DSAM following the $(n,n'\gamma)$ reaction.

Nucleus	E_γ(keV)	$\tau.10^{-14}$ sec	Other's (quoted in /5/
B^{11}	2124	0.62 ± 0.22	0.60 ± 0.22
	4442	0.14 ± 0.10	0.12 ± 0.05
Mg^{24}	4124	5.6 ± 1.9	5.5 ± 1.0
	4239	10.5 ± 0.5	10.0 ± 1.0
	6011	11.5 ± 2.0	8.5 ± 2.0
S^{32}	4281	4.0 ± 1.4	3.6 ± 0.8
	4461	12.7 ± 3.0	13.0 ± 3.0
Cl^{35}	2694	5.2 ± 0.8	6.2 ± 1.6
	3002	7.2 ± 1.2	3.1 ± 1.3
K^{39}	2523	9.2 ± 0.9	9.0 ± 3.0
	3883	2.6 ± 1.0	2.0 ± 0.7
	4127	8.5 ± 5.0	8.5 ± 2.0
Ca^{40}	3904	5.2 ± 2.0	5.4 ± 0.6
V^{51}	3614	8.6 ± 2.8	8.0 ± 4.0
	3632	2.0 ± 0.6	1.8 ± 2.0

III. Conclusion

The above described DSAM version has been used, up to now, for the determination of the mean lifetimes of excited nuclear states of more than 20 nuclei in the mass region A~10 - 60. The results, shown in the table, lead to the conclusion that the (n,n'γ) reaction could be successfully used in DSAM with two targets simultaneously with quite satisfactory accuracy.

REFERENCES:

1) L. Nichol, T.J. Kennett, Can.J.Phys., 49 (1971) 1461
2) E.K. Warburton et al., Phys.Rev., 129 (1963) 2180
3) A.Antilla et al., Nucl.Instr.Meth., 124 (1975) 605
4) A.E. Blaugrund, Nucl.Phys., 88 (1966) 501
5) D. Elenkov et al., Nucl.Instr.Meth., 228 (1984) 62

LOW BACKGROUND TELESCOPIC SYSTEM FOR STUDY OF (n,α) REACTIONS ON LIGHT NUCLEI.

A.Trzciński, S.Burzyński, K.M.Rusek, I.M.Turkiewicz.

Institute for Nuclear Studies, Warsaw, Poland.

I. INTRODUCTION

Since 1950 high fluxes of 14 MeV neutrons became available from $T(d,n)\alpha$ reactions with low energy deuteron beams. Nuclear (n,α) reactions on various nuclei at this neutron energy soon became one of nuclear physics fields to be investigated using such neutron sources. Recently also other energy neutrons, 12-18 MeV, produce using higher energy deuteron beams have been utilized.

A usual way to measure (n,α) cross sections is to place behind the target one or two proportional counters followed by a thick silicon detector - a system called a telescope. Everything is placed in the sealed container filled up with the gas appropriate for proportional counters, so α-particles do not have to pass foil windows separating gas cells on their way from the target to detector. Proportional gas counters enable the separation of α-particles produced in the target from the products of the reactions induced by incident neutrons in the walls of the telescope and especially in the silicon detector. In the $^{28}Si(n,\alpha)$ reaction having the considerably large cross section σ =270 mb and Q-value equal to -2.62 MeV the α-particles are produced which can simulate the events from the target. The problem is especially serious for the backward angles when the silicon detector is nearer to the neutron source than the target under study. The hyperbola ΔE-E is smeared-out and can hardly be distinguished from the background. To eliminat this background it is necessary to perform separate no-target runs which requires additional beam hours. Even subtracting background, backward parts of an angular distributions of (n,α) reactions are normally measured with rather poor accuracy. For the reaction with negative Q-value as for example $^{12}C(n,\alpha)^{9}Be$ (Q=-5.702 MeV) the measurements at the angles larger than 100° are simply not possible.

In order to measure differential cross sections of $^{12}C(n,\alpha)^{9}Be$ g.s. reaction with sufficient accuracy in a full angular range, we developed a more complex system. In our design we use a self-supporting carbon target, behind which is placed an additional proportional gas counter to detect ^{9}Be recoil nuclei associated with a-particles registered in the telescope. For all the angles above 50° energy and direction of ^{9}Be ions is such that they can be detected in an additional counter with full efficiency. This method allowed us to obtain backgroundless data for large part of angular distribution normally difficult to measure.

II. TARGET - DETECTOR ASSEMBLY

The whole system is placed in a cylindrical chamber which has at one side an extension to house a silicon detector (Fig. 1). Target, proportional counters and slits are all mounted on the cover and are easily accesible for mechanical reparations and modifications. All internal parts of the chamber are made of tantalum. Each proportional counter has as the anode three 20 μm in diameter wires electrically connected and placed between two parallel grounded walls. This way all the charge produced by α-particles in the gas between the target and silicon detector is used for ΔE pulses. The proportional gas counter for ^{9}Be ions consists of 13 source wires (20μm) and 14 grounded wires (50μm). Both groups of wires are parallel to the target plane and subtend enough space that all ^{9}Be of interest have to pass active volume of the counter. Pulses from all the detectors pass charge sensitive preamplifiers and spectroscopy amplifiers to be recorded as four-dimentional events in ND-4420 computer. The processing of the data was carried out off-line on SM-4 computer. For reaction angles above 50° all four detectors were working and at smaller angles the ^{9}Be counter was not used.

Our proportional counters are filled up with the hydrogen gas instead of commonly used argon + dioxycarbon or isobutane mixture. Hydrogen gas is advantageous because neutron flux does not produce unwanted α-particles from its nuclei. Initially we used a sealed gas system for runs lasting for one or two weeks but we had problems because pulses from proportional counters diminished slowly in time as air admixture in hydrogen gas increased. We solved this problem by developing a simple and reliable hydrogen gas flow system to exchange gas continously. Gas pressure in our telescope have been set to 200 mmHg, such that ^{9}Be nuclei had sufficiennt range to be detected with full efficiency. The hydrogen gas before it entered detector volume, had to pass through palladium tube walls heated to appropriate temperature by a tungsten spirale. Gas outlet from the telescope was through a thin glass tube dipped in mercury, contained in a thick tube with a closed bottom end. Internal volume of the thick tube has been continously pumped out by a mechanical pump. When hydrogen pressure in the detector volume exceeded slightly 200 mmHg mercury was push out from the thin tube and small bubbles of the gas left a system.

III. ANALYSIS OF RESULTS.

Application of the presented method requires carefull examination of the investigated reaction kinematics. With this purpose we have written a Monte Carlo code to calculate the distribution of the directions and energies of the ^{9}Be nuclei associated with the α-particles emitted at a given laboratory angle θ. Results of such calculations are given in Fig. 2. At backward angles positions of the telescope the ^{9}Be are emitted almost perpendiculary to the target plane and with energies large enough that the expected pulse-hight distribution from E_R counter is relatively narrow. At forward angles the pulse height decreases and its distribution spreads out. In the case illustrated in the Fig 2 this effect limits the application of the method to the angles larger 50°. In fact

the two-dimensional spectrum of $E_R \times E$ obtained from the measurements of $^{12}C(n,\alpha)^9Be$ reaction at 50° lab angle (Fig 3c) shows the group of events corresponding to the ground state transition with the well defined α-energy and the energy of ^9Be recoils spread over many channels. For the position of the telescope at 145° (Fig 4a) the same transition is seen as well defined group. At 50° we have performed two measurements of the energy distribution of the particles from $^{12}C(n,\alpha)^9Be$ reaction. One was done with our conventional telescope using three-dimensional analysis (ΔE_1, ΔE_2, E) and another with ^9Be recoils counter added and the four-dimensional analysis (E_R, ΔE_1, ΔE_2, E). Two-dimensional plot (3a) of ΔE_2 pulse height versus α-particle energy contains events coming from various sources: α-particles produced in the target form a hyperbola like curve, α-particles from the silicon detector give a continuum widely spread arround the hyperbola and a large number of light particles, mostly protons, which are grouped in the left corner. Energy spectrum for events from the hyperbola (3b) is continuous and the peak corresponding to $^{12}C(n,\alpha)^9Be$ g.s. reaction can hardly be identified. The application of the ^9Be recoil counter has permitted to reduce the background in a very effective way as is illustrated in Figs 3d and 3e. In the α-spectrum (Fig 3e) are also seen peaks corresponding to the excited states of ^9Be but registration efficiency for this case is difficult to calculate because these states are particle-unstable, and we have limited our analysis to the ground state transition.

The method presented here allows also to separate α-particles coming from the reactions induced on the target contaminents. For example in the case of $^{12}C(n,\alpha)^9Be$ reaction even small admixture of oxygen in the carbon target produces the substantial effect in the observed α-energy spectrum, especially at backward angles. Detection of ^{13}C recoil nucleus which produced in E_R counter pulses higher than ^9Be nucleus has helped us to identify these events and to separate them from the investigated peak. In Fig. 4a the two dimensional $E - E_R$ spectrum is shown taken at 145°. Two well separated groups of events are coming from two different reactions: $^{12}C(n,\alpha)^9Be$ lying in the lower E_R window and $^{16}O(n,\alpha)^{13}C$ in the upper one. The corresponding α-energy spectra are shown below.

IV. REMARKS.

The method described in this paper allows us to measure an angular distribution of $^{12}C(n,\alpha)^9Be$ g.s. reaction with high accuracy in a full angular range. The application of this method is however rather limited. Only reactions on very light nuclei can be investigated this way because in these cases recoil nucleus is light enough to leave the target. Also two reaction products have to be of comparable masses because otherwise, like for example in (n,p) reaction, a recoil nucleus gets a very small energy. The recoil nucleus has also to be a particle stable system. For neutron energy about 14 MeV (n,α) reactions on ^6Li, ^9Be, ^{10}B, ^{12}C, ^{14}N, ^{15}N, ^{16}O, ^{17}O, ^{18}O targets can be investigated. For heavier of these nuclei also transitions to excited states can be measured because such nuclei decay by gamma rays emission. Also (n,t) reactions on such light targets as ^6Li, ^7Li, ^9Be, ^{10}B, ^{11}B for which exist stable final nuclei can be investigated using presented method. For higher neutron energy application of this method would of course increase considerably.

FIGURE CAPTIONS

Fig 1. Lay-out of the experimental assembly

D - deuterium beam

Tr - tritium target

C - carbon target

E_R, ΔE_1, ΔE_2 - proportional counters

G - grounded wires

E - semiconductor detector

S - tantalum sheets

N - neutron flux

Fig 2. Solid lines -

the estimated pulse height limits from E_R counter for ^{9}Be recoil from $^{12}C(n,\alpha)^9Be$ reaction at 14.3 MeV for different position of the telescope

Dashed line -

the direction of the emission of ^{9}Be recoils relative to the normal to the target.

Fig 3. The spectra taken at 50° lab. angle with ^{12}C target bombarded by 14.3 MeV neutrons.

a/ E_2 x E spectrum measured using the triple coincidence ΔE_1, ΔE_2, E

b/ alpha - energy spectrum obtained by projecting the events from the hyperbola in Fig a/.

c/ E_R x E spectrum measured using the four fold coincidence E_R, ΔE_1, ΔE_2, E .

d/ ΔE_2 x E spectrum obtained by setting the window on E_R indicated in Fig c/.

e/ alpha - energy spectrum obtained by projecting the events from the hyperbola in Fig d/.

Fig 4. The spectra from $^{12}C(n,\alpha)^9Be$ reactions measured at 145° using the four fold coincidences E_R, ΔE_1, ΔE_2, E .

a/ E_R x E spectrum

b/ alpha - energy spectrum obtained with lower window on E_R, corresponding to the $^{12}C(n,\alpha)^9Be$ reaction.

c/ alpha - energy spectrum for upper window, corresponding to the $^{16}O(n,\alpha)^{13}C$ reaction.

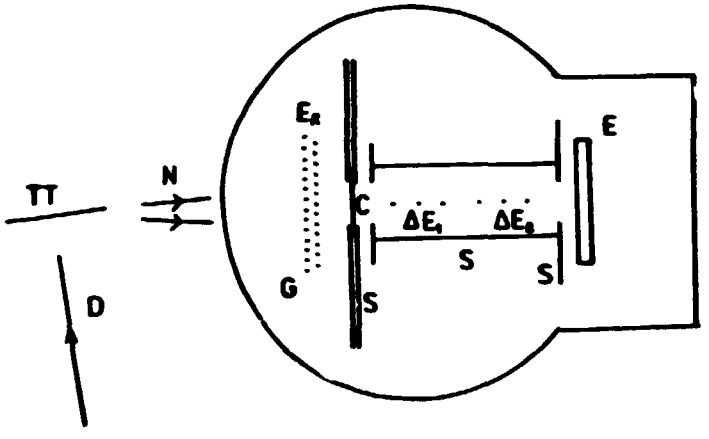
TT
N
D
G
C
S
S
S
E

Fig. 1

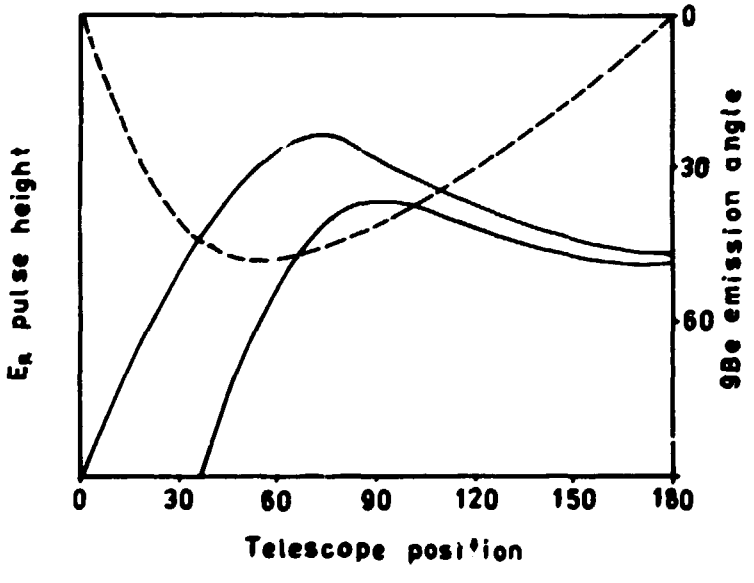
0
30
60
90
120
150
180
Telescope position
0
30
60
9Be emission angle

Fig. 2

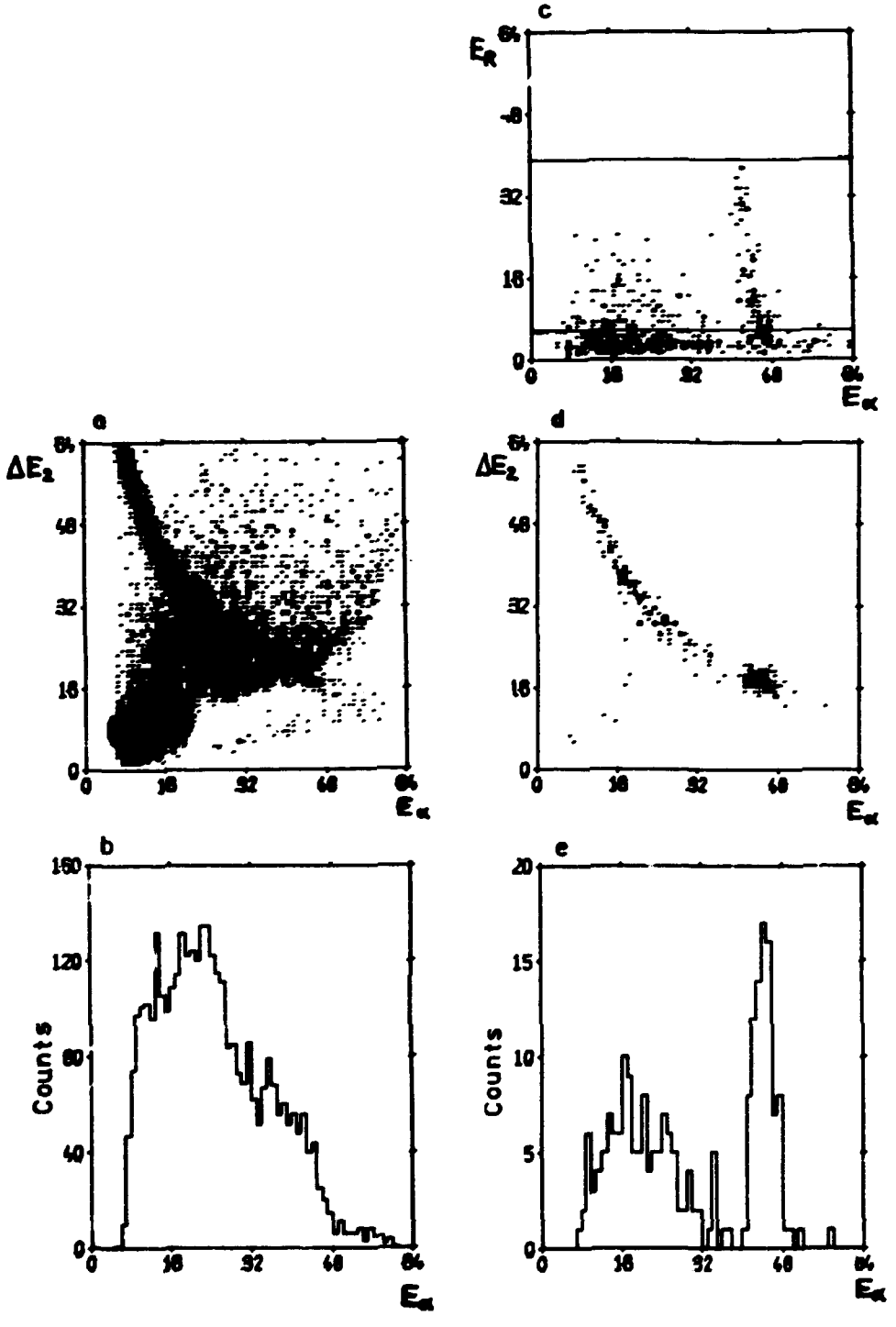
c
E_R
64
48
32
16
0
0
16
32
48
64
E_α
a
ΔE_2
64
48
32
16
0
0
16
32
48
64
E_α
d
ΔE_2
64
48
32
16
0
0
16
32
48
64
E_α
b
160
120
80
40
0
Counts
0
16
32
48
64
E_α
e
20
15
10
5
0
Counts
0
16
32
48
64
E_α

Fig.3

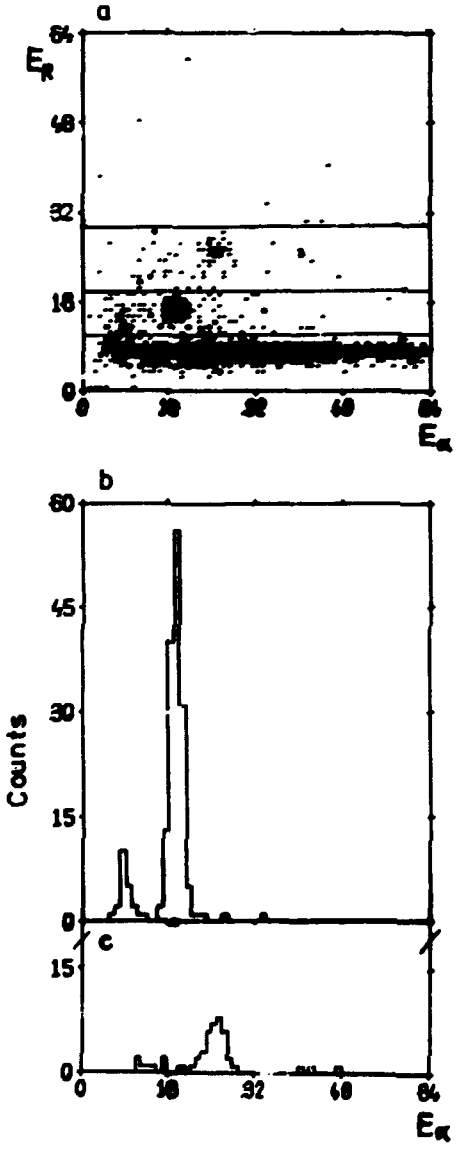
a
E_R
64
48
32
16
0
0
16
32
48
64
E_α
b
60
45
30
15
0
Counts
c
15
0
0
16
32
48
64
E_α

Fig. 4